GEODYNAMICS & TECTONOPHYSICS

PUBLISHED BY THE INSTITUTE OF THE EARTH'S CRUST
SIBERIAN BRANCH OF RUSSIAN ACADEMY OF SCIENCES

2015 VOLUME 6 ISSUE 3 PAGES 275–287 ISSN 2078-502X

http://dx.doi.org/10.5800/GT-2015-6-3-0182

Recent Geodynamics

A SEISMOTECTONIC MAP OF EASTERN SIBERIA

V. S. Imaev[1], L. P. Imaeva[1], O. P. Smekalin[1], B. M. Koz'min[2], N. N. Grib[3], A. V. Chipizubov[1]

[1] *Institute of the Earth's Crust, Siberian Branch of RAS, Irkutsk, Russia*
[2] *Institute of Diamond and Precious Metals Geology, Siberian Branch of RAS, Yakutsk, Russia*
[3] *Technical Institute (branch) of M.K. Ammosov North-Eastern Federal University, Neryungri, Russia*

Abstract: The paper reviews goals and objectives, stages and the content of seismotectonic studies conducted in Eastern Siberia. Such studies are based on a comprehensive analysis of geological and geophysical data and provide for establishing whether the local earthquakes are of tectonic origin and revealing their relationships with recent geodynamic processes in the area under study. Seismic hazard assessment and evaluation of tectonic processes are the two major, closely interrelated aspects of seismotectonic studies. The latter are generally conducted in combination with seismic studies prior to the stage of detailed seismic zonation (DSZ) which is followed by seismic micro-zonation (SMZ). In three stages of seismotectonic studies, we analyse specific geological structures, reveal the regional dynamics of seismotectonic processes, clarify details of potential seismic hazard locations and identify sites of the potential instantaneous deformation of the crust which may take place due to active faulting. Based on results of the long-term studies conducted by the authors, a seismotectonic map of Eastern Siberia is compiled. The paper briefly reviews the methods of mapping and refers to data on active faults and neotectonic structures revealed in the area under study, which are closely related to regional earthquake sources.

Key words: seismotectonic studies, seismic hazard, active faults, geological and geomorphological methods, trenching, seismic source zones, seismic belts and their segments, seismotectonic map of Eastern Siberia.

Recommended by S.I. Sherman

For citation: *Imaev V.S., Imaeva L.P., Smekalin O.P., Koz'min B.M., Grib N.N., Chipizubov A.V.* 2015. A seismotectonic map of Eastern Siberia. *Geodynamics & Tectonophysics* 6 (3), 275–287. doi:10.5800/GT-2015-6-3-0182.

КАРТА СЕЙСМОТЕКТОНИКИ ВОСТОЧНОЙ СИБИРИ

В. С. Имаев[1], Л. П. Имаева[1], О. П. Смекалин[1], Б. М. Козьмин[2], Н. Н. Гриб[3], А. В. Чипизубов[1]

[1] *Институт земной коры СО РАН, Иркутск, Россия*
[2] *Институт геологии алмаза и благородных металлов СО РАН, Якутск, Россия*
[3] *Технический институт (филиал) Северо-Восточного федерального университета им. М.К. Аммосова, Нерюнгри, Россия*

Аннотация: В статье рассматриваются задачи, стадийность проведения и содержание сейсмотектонических исследований как отдельного вида анализа комплексных геолого-геофизических материалов, используемых для установления тектонической природы проявлений местных землетрясений и их связи с современными геодинамическими процессами, протекающими на исследуемой территории. В задачи сейсмотектонических исследований входят два тесно взаимосвязанных направления: оценка опасности сейсмических явлений и оценка тектонических процессов. Сейсмотектонические исследования, совместно с сейсмологическими, всегда предваряют стадию детального сейсмического районирования (ДСР) и в последующем – сейсмического микрорайонирования (СМР). Сами сейсмотектонические исследования проводятся в три этапа и позволяют на региональном уровне изучения конкретных геологических структур определить геодинамику сейсмотектонических процессов, провести детальную локализацию сейсмической опасности и выявить места возможного проявления мгновенных деформаций земной поверхности, связанных с активными разломами. Результаты многолетних авторских исследований обобщены в карте сейсмотектоники Восточной Сибири, для которой дается краткое описание принципов и методов ее построения, приводятся наглядные примеры выделенных активных разломов и неотектонических структур, тесно связанных с региональными эпицентрами землетрясений.

Ключевые слова: сейсмотектонические исследования, сейсмическая опасность, активные разломы, геолого-геоморфологические методы, тренчинг, зоны ВОЗ, сейсмические пояса и их сегменты, карта сейсмотектоники Восточной Сибири.

1. Введение

При проведении многолетних работ по установлению вероятных связей разновозрастных и разнообразных по своей позиции и структурному стилю элементов геологических и тектонических структур горно-складчатых областей территории Восточной Сибири с сейсмической опасностью удалось установить некоторые закономерности в проявлении развития разрывных структур и сейсмичности территории. Исследования подобного рода известны в российской и англоязычной научной литературе как самостоятельные сейсмотектонические исследования, главной целью которых является «…установление или изучение связи проявлений сейсмичности и тектоники регионов…» [*Geological Dictionary, 1973*].

Другое, более развернутое, определение сейсмотектоники приводится американскими учеными, которые утверждают, что сейсмотектоника «является научной дисциплиной, изучающей взаимосвязь между землетрясениями, активной тектоникой и отдельными разломами региона. Стремится понять, какие данные несут ответственность за сейсмическую активность в конкретном районе путем анализа региональной тектоники, последних инструментально записанных сейсмических событий, исследования исторических и палеоземлетрясений, а также неотектонических и геоморфологических данных. Эта информация в дальнейшем может быть использована для количественной оценки сейсмической опасности того или иного региона. При проведении сейсмотектонического анализа территории требуется интеграция большого количества разнородных геолого-геофизических данных…» (по [*Allen, 1975; Wallace, 1977; Yeats et al., 1997; McCalpin, 2009*]).

Согласно практике проведения исследований подобного рода, сейсмические показатели используются для характеристики степени устойчивости геотектонического режима, определения зон контрастных тектонических движений, выявления доминирующих направлений подвижек. По глубине расположения очагов землетрясений, группирующихся в линии определенного простирания, судят о глубине заложения разрывов. Динамические параметры очагов дают сведения о величине и направлении сил, которые деформируют и разрушают горные породы. Результаты сейсмотектонических исследований выражаются обычно в виде сейсмотектонических карт, на которые наносятся данные о формах развития неотектонических структур и эпицентральные зоны землетрясений, что позволяет установить связь этих землетрясений с особенностями тектонического (неотектонического) строения местности и использовать эту связь для прогноза места, силы и частоты землетрясений, а также для составления карт сейсмического районирования [*Gorshkov, 1984; Nikolaev et al., 1982; Imaev et al., 1990, 2000; Rogozhin, Platonova, 2002; Rogozhin, 2012*].

Отсутствие единого подхода и четкой регламентирующей базы используемых геолого-геофизических характеристик среды часто не позволяет успешно провести такие сейсмотектонические исследования и ставит под сомнение результаты оценки уровня сейсмической опасности, полученные только методом инструментальных наблюдений и не подкрепленные определенными обязательными в настоящее время сейсмотектоническими исследованиями. В настоящей статье суммируется многолетний опыт проведения сейсмотектонических исследований в разнообразных сегментах сейсмоактивных структур территорий

Якутии, Алтая, Саян, Тувы и области Байкальской рифтовой зоны, приводятся методические указания и обоснования целесообразности использования выбранных геолого-геофизических показателей для целей создания карты сейсмотектоники Восточной Сибири. Как и во всех остальных исследованиях подобного рода, эффективность и достоверность результатов сейсмотектонических исследований во многом обеспечиваются соблюдением стадийности наблюдений, которые проводятся в три этапа.

2. Стадийность исследований

На первом этапе проводится сбор исходного материала. Собственно исследования включают в себя совместный анализ всех имеющихся материалов по геологическому строению, сейсмическому режиму, неотектонике, истории развития рельефа, глубинному строению, напряженному состоянию и современным движениям земной коры. Также проводится дешифрирование материалов дистанционного зондирования Земли (ДЗЗ). Иными словами, создается и анализируется материал, являющийся региональной сейсмотектонической базой данных.

Второй этап включает более конкретные исследования применительно к проектируемым народнохозяйственным объектам и связан с непосредственным полевым изучением активных разломов. Методика установления и изучения активных разломов основана на комплексе дистанционных и полевых методов, позволяющих по рельефу и составу молодых отложений выявить активные разломы, закартировать зоны связанных с ними деформаций и определить тип, амплитуду и среднюю скорость смещений. Следует особо подчеркнуть, что без реальных структурно-геологических и геоморфологических наблюдений непосредственно в полевых условиях все дальнейшие обобщения и построения будут неполноценными и недостоверными.

Третий этап (камеральный) подразумевает общую обработку результатов как полевых, так и фондовых и литературных материалов. Результаты обязательного тренчинга используются при этом не только для установления мест пересечения проектируемых объектов с активными разломами, но и для построения сейсмотектонической модели.

3. Задачи и методика сейсмотектонических исследований

Основными элементами сейсмотектонической модели (карты зон возможных очагов землетрясений (ВОЗ)) являются источники сейсмических воздействий – площадные (домены), характеризующие рассеянную (фоновую) сейсмичность, и линейные, отражающие сосредоточенную сейсмичность, т.е. потенциальные очаги сильных землетрясений (сейсмолинеаменты по [*Ulomov, Shumilina, 1999*]). Согласно сложившейся сейсмологической практике, в качестве линейных источников рассматриваются активные разломы. Для объяснения доменной сейсмичности предложен новый критерий – геодинамически активные неотектонические зоны (ГАНЗ) [*Gusev*, *Imaeva, 2014*].

ГАНЗ, с позиции системного анализа, рассматривается как пространственно-локализованный целостный объект с многофакторным взаимодействием его основных компонентов в разрезе земной коры и верхней мантии (литосфере) – коровомантийный вариант; в разрезе литосферы и нижней мантии – суперглобальный вариант. Классификация ГАНЗ представляет собой систему, состоящую из десяти классов. Каждый из них характеризуется набором признаков: геодинамической обстановкой формирования геологических структур, скоростями горизонтального (по данным GPS и геологическим и геоморфологическим данным) и вертикального движения геологических тел (мм/год), размерами их пластических (пликативных) и разрывных деформаций, направлениями силовых тектонических полей, морфоструктурными типами эндогенного рельефа суши и морей, их высотами и значениями контрастности, геофизическими данными (величины теплового потока и поля силы тяжести), сейсмической томографии, глубинного строения (мощности земной коры, глубины залегания поверхности Мохоровичича и астеносферного слоя, мощности верхней и нижней мантии) [*Gusev*, *Imaeva, 2014*].

Примером построения карты ГАНЗ территории Восточной Сибири является рис. 1, на котором показано распределение зон с отдельной интенсивностью на исследуемой территории. Поскольку построение геолого-геофизических критериев сейсмичности производилось при помощи геоинформационных технологий, ставших доступными сравнительно недавно (ГИС-программы ArcView, ArcInfo), изображение отдельного информационного слоя не представляет большой проблемы, но позволяет лучше понять распространение отдельных частей слоя в пространстве.

Необходимость анализа новейшей позднекайнозойской (позднеплиоценовой-четвертичной) структуры изучаемой территории определялась тем, что новейшая тектоника представляет собой тот структурный каркас, в который вписываются активные разломы и другие проявления современной тектонической активности, напрямую

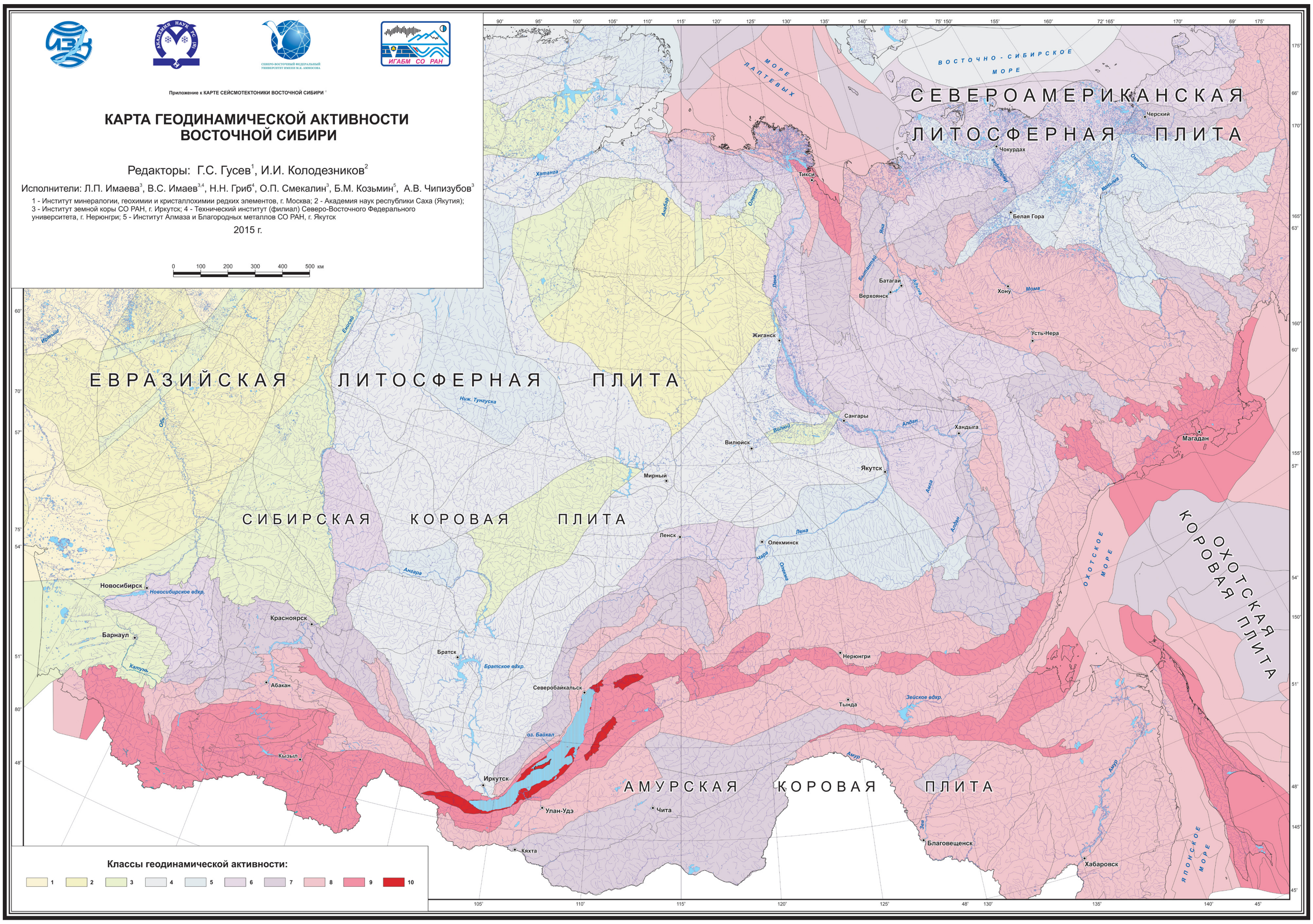

Рис. 1. Распределение геодинамически активных неотектонических зон (ГАНЗ) в пределах Восточной Сибири. Интенсивность окраски соответствует классу структур.

Fig. 1. Geodynamically active neotectonic zones (GANZ) in Eastern Siberia. The colour intensity range correlates with classes of structures.

связанные с региональной сейсмичностью. Плановое распределение элементов ГАНЗ в пределах Восточной Сибири показывает, что наиболее высокие показатели активности характерны для южной границы Сибирской платформы и ее северо-восточного обрамления (Верхояно-Колымская складчатая область), хотя линейность простирания структур на востоке от платформы выражена не так четко, как вдоль южной границы. Вместе с тем, для всей территории к востоку от р. Лены характерны также весьма высокие значения ГАНЗ, впрочем некоторая линейность прослеживается и на о-ве Сахалин. Для центральных областей Сибирской платформы характерны невысокие, но в то же время и не нулевые значения активности. Разумеется, все это связано с разными режимами неотектонической жизни структур.

Следует отметить, что впервые интегральные оценки геодинамической активности тех или иных районов Азии были предложены в работах сибирских исследователей, успешно обьединивших их в геодинамическую активность литосферы Азии (ГАЛА) [*Logatchev et al., 1987, 1991*]. Такой же интегральный показатель (внерегиональный) использовался Г.И. Рейснером с коллегами в работах по установлению сейсмической опасности различных районов Евразии [*Reisner et al., 1993*].

Важнейшей составляющей сейсмотектонической модели являются прогнозные магнитуды землетрясений. Оценка максимально возможных магнитуд ожидаемых землетрясений производится по комплексу геолого-геофизических, сейсмологических и сейсмотектонических данных. Оценка магнитуды по комплексу сейсмотектонических данных основывается на глобальных статистических соотношениях между магнитудой землетрясения, протяженностью разрыва и величиной подвижки по нему [*Strom*, *1993*; *McCalpin*, *2011*].

Конечным итогом сейсмотектонических исследований является создание сейсмотектонической модели региона и построение карты зон ВОЗ в крупных масштабах – 1:1000000, 1:500000 и 1:200000, что позволяет перейти к картам ДСР и в результате решить проблему определения уровня сейсмической опасности конкретных народнохозяйственных объектов. В ряде случаев такие исследования приводят к существенному сокращению участков с высокой (8–9 баллов) сейсмической опасностью по сравнению с картами общего сейсмического районирования (ОСР), что соответственно удешевляет будущее строительство. В других случаях могут быть найдены новые, ранее неизвестные источники сейсмических воздействий. Тогда уровень сейсмической опасности может быть повышен на локальных участках по сравнению с данными ОСР.

При проведении исследований очень важно соблюдение стадийности. Нарушение стадийности иногда может создать видимость сокращения сроков, но всегда отрицательно сказывается на результате. С учетом нестандартного характера исследований, а также особенностей их выполнения, работы по сейсмотектонике целесообразны только при непосредственном участии специализированных научных организаций, имеющих опыт в изучении активных разломов и высокую квалификацию исполнителей.

Сейсмотектоническое районирование предусматривает разделение территории на области, где ожидаемые местные землетрясения будут настолько слабы, что не окажут воздействия на население и систему его жизнеобеспечения, включая инженерные сооружения. Такие области считаются неспособными генерировать землетрясения и могут испытывать лишь сейсмические воздействия от удаленных сильных землетрясений. Другие области способны генерировать коровые землетрясения и потому называются зонами возникновения очагов землетрясений. Они подразделяются по их максимально возможной магнитуде и частоте возникновения. Выделение и параметризация, т.е. оценка сейсмического потенциала зон ВОЗ производятся путем комплексного применения двух равнозначных групп критериев: сейсмологической и геолого-геофизической.

Сейсмологическая группа включает в себя каталоги произошедших землетрясений: инструментальных, исторических и голоценовых палеособытий, выявляемых по геологическим и геоархеологическим данным, а также инструментальные и макросейсмические показатели распределения интенсивности сотрясений от ощутимых сейсмических событий, которые и служат основой всех дальнейших картографических построений. Кроме того, исследования планового распределения эпицентров землетрясений, помимо оценки самих сейсмических воздействий, позволяют очертить очаговые области сильных землетрясений и тем самым уточнить геометрию зон ВОЗ.

Приведенная карта планового распределения эпицентров землетрясений Восточной Сибири была построена при компиляции данных, полученных региональными отделениями геофизической службы РАН и СО РАН, а также с использованием каталогов местных землетрясений, которые доступны по литературным источникам и на интернет-ресурсах [*Mackey et al., 2010*; *Ulomov, 2015*].

Анализ планового распределения эпицентров землетрясений на территории исследований показывает приуроченность Южно-Сибирского сейсмического пояса к южной границе Сибирской платформы в области развития горно-складчатых орогенных структур Алтая, Саян, Тувы. Далее, пространственно тяготея к области Байкальской рифтовой зоны, проявления сейсмичности образуют эпицентральные поля Олекмо-Становой области и соединяются с сейсмичностью побережья Охотского моря. Другой, Арктико-Азиатский, сейсмический пояс прослеживается от побережья моря Лаптевых через систему структур Верхояно-Колымской горно-складчатой области на юго-восток, соединяясь с сейсмичностью побережья Охотского моря и п-ва Камчатка (рис. 2).

Другим немаловажным фактором проявления сильных землетрясений определенных районов служат механизмы очагов сильных землетрясений, сводный анализ которых позволяет установить напряженно-деформированное состояние среды в тех или иных элементах геологической и неотектонической структур. Фокальные механизмы очагов землетрясений, произошедших на территории Восточной Сибири, приводятся на рис. 3. Факты приводимых решений механизмов очагов землетрясений были скомпилированы из многочисленных работ разных авторов и интернет-ресурсов, находящихся в свободном доступе на соответствующих сайтах американской геологической службы [*Mel'nikova, 2008; Radziminovich et al., 2012; Starovoit et al., 2003; Emanov et al., 2012; Koz'min, 1984; Imaeva et al., 2011, 2015; USGS Earthquake Hazards Program, 2015*].

Одним из главных выводов, следующих из планового распределения эпицентров землетрясений и решений фокальных механизмов их очагов, является то, что вся наблюдаемая современная сейсмичность и древние палеоземлетрясения группируются в протяженные сейсмические пояса, пространственно тяготеющие к южной и восточ-

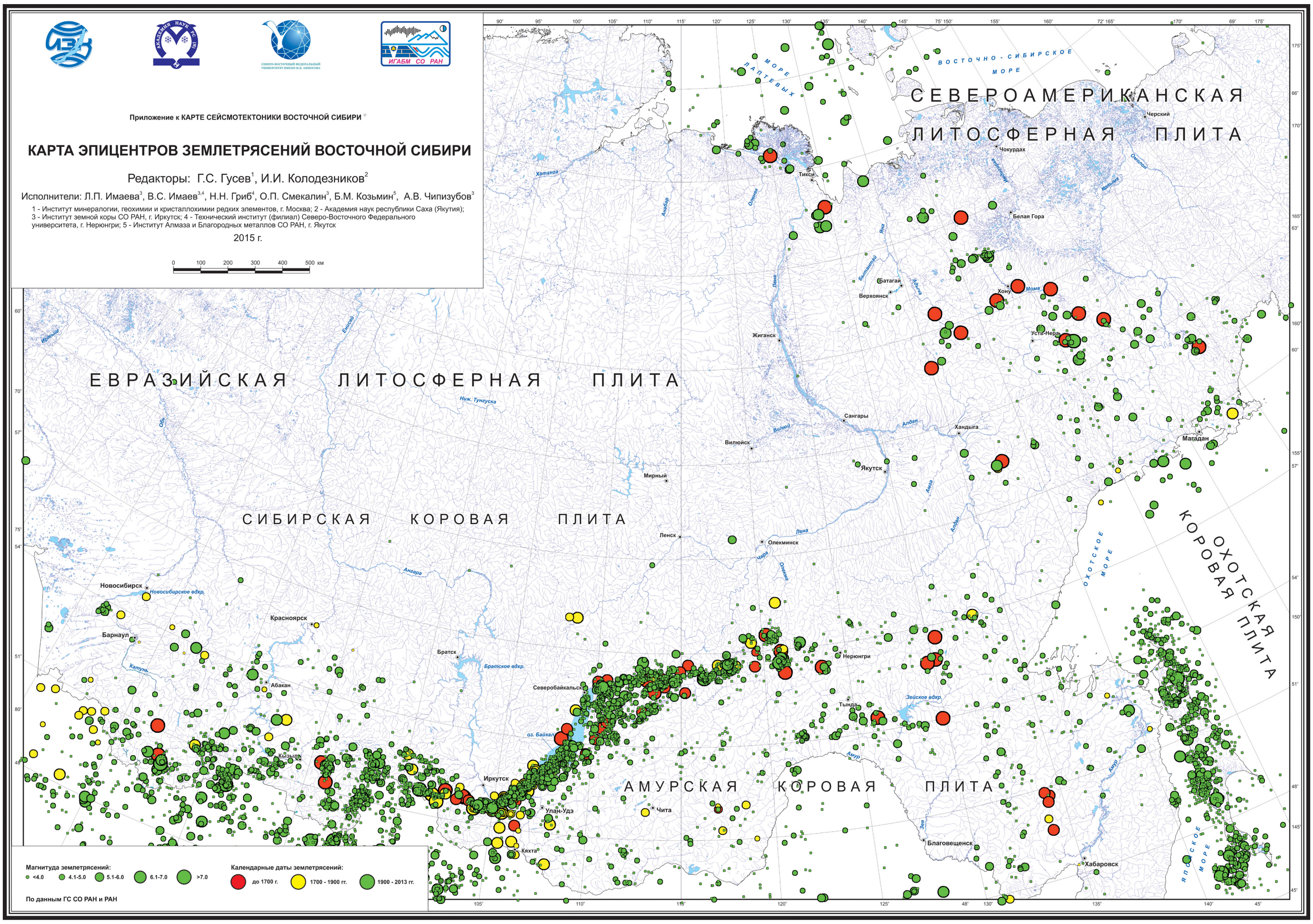

Рис. 2. Карта эпицентров Восточной Сибири (составлена по компиляционным данным геофизической службы РАН и СО РАН, а также литературным данным и из интернет-ресурсов [*Mackey et al., 2010*; *Ulomov, 2015*].

Fig. 2. Earthquake epicentres in Eastern Siberia. The map is based on data consolidated by RAS Geophysical Survey and Siberian Branch of RAS, published records and data available in the internet resources [*Mackey et al., 2010*; *Ulomov, 2015*].

ной границе Евразийской литосферной плиты. А тип напряженно-деформированного состояния земной коры указывает на превалирование процессов горизонтального сжатия вдоль всей континентальной части этой границы (за исключением Байкальской рифтовой области) и фрагментирование по геодинамическому принципу на отдельные сегменты Южно-Сибирского и Арктико-Азиатского сейсмических поясов.

Применение геолого-геофизической группы критериев зон ВОЗ в настоящее время состоит в выделении и параметризации активных геологических структур, в которых землетрясения определенной магнитуды и частоты возникали в недавнем прошлом и могут ожидаться в близком будущем, к которому относятся оценки сейсмической опасности. Материалы детального изучения активных разломов и вторичных эффектов древних землетрясений, наряду с другими сейсмотектоническими и сейсмологическими данными, ложатся в основу карты зон возможных очагов землетрясений, что представляется едва ли не главной целью сейсмотектонических исследований [*Trifonov et al., 1993, 1997; Rogozhin, 2012; Imaev et al., 2000; Yeats et al., 1997*]. Поскольку активные разломы, как правило, соответствуют главным зонам ВОЗ региона, даже качественный анализ рисунка и параметров разломов позволяет оконтурить такие зоны и выполнить их предварительное ранжирование. Численные характеристики зон ВОЗ, среди которых определяющими являются максимальная ожидаемая магнитуда землетрясений (M_{max}) и период повторяемости таких землетрясений, в основном опираются на сейсмологические данные.

Детальное изучение активных разломов дает возможность составить представление о структуре

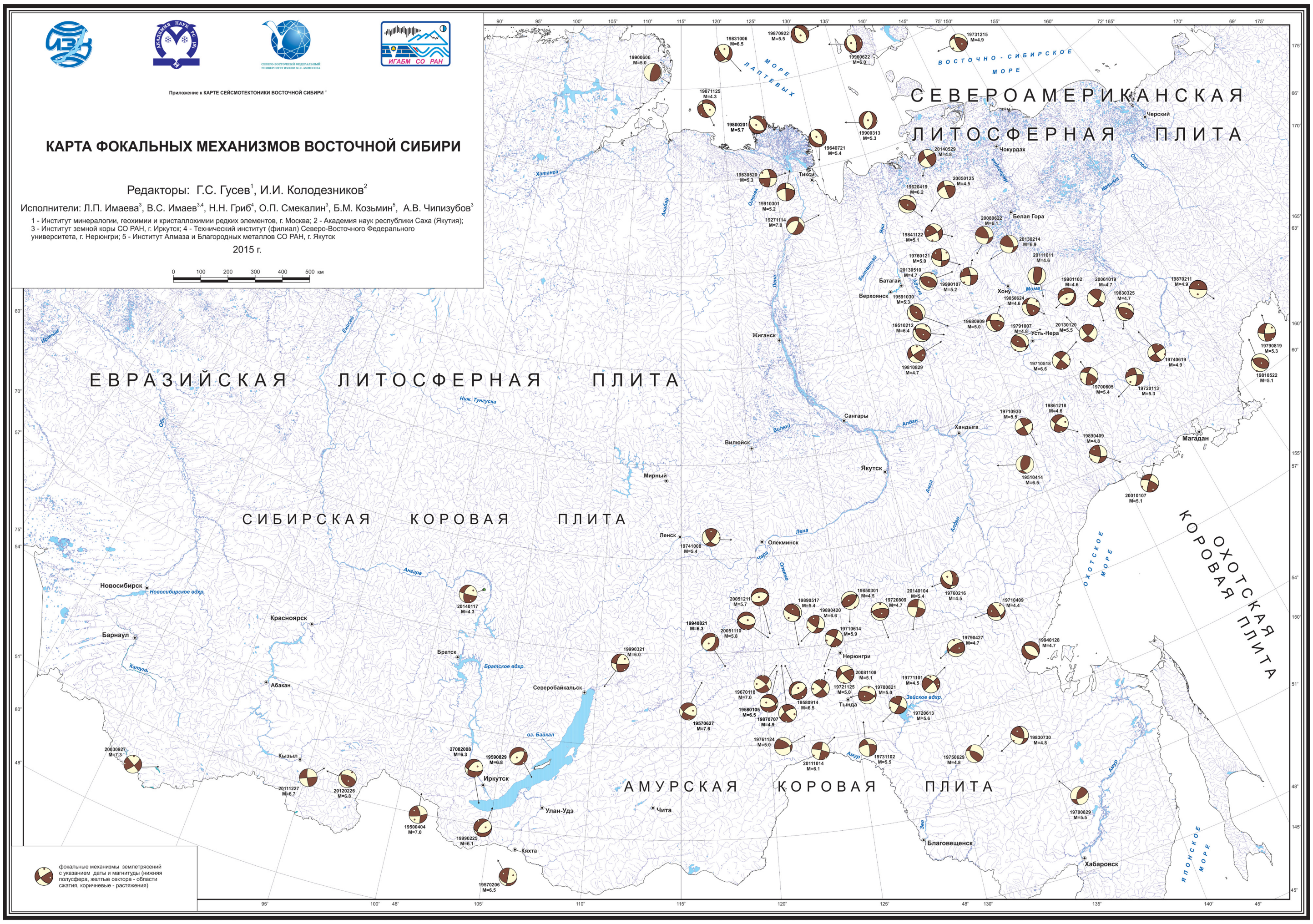

Рис. 3. Карта фокальных механизмов очагов землетрясений Восточной Сибири [*Centroid Moment Tensor Catalog, 2015*].

Fig. 3. Earthquake focal mechanisms map of Eastern Siberia [*Centroid Moment Tensor Catalog, 2015*].

очага и древних, доисторических, сейсмических событиях, произошедших в этих же очаговых зонах. Очаги сильных и сильнейших землетрясений представляют собой устойчивые структуры в геологической среде (активные разломы), положение которых определено особым сочетанием геолого-геофизических условий, причем кинематика подвижки от раза к разу может изменяться.

В большинстве случаев выходы очагов сильных современных землетрясений на поверхность образуют некую область – зону сейсморазрывов. Ширина ее может достигать нескольких сотен метров и даже первых километров, в зависимости от конкретных геолого-геоморфологических условий и силы землетрясения. При этом разрывы могут появляться на поверхности на разных участках зоны разлома, т.е. менять свое положение от одного землетрясения к другому. Суммарное смещение в очаге в приповерхностных условиях может рассеиваться в виде множества разрывов и связных деформаций, однако все они образуют характерные структурные рисунки, свойственные тектоническим деформациям в целом. Обычно они приурочены к определенным геологическим структурам и формам рельефа, сформированным предыдущими сейсмическими подвижками. Эти древние события находят отражение не только в смещениях молодых отложений и форм рельефа, но и в развитии древних вторичных нарушений (палеосейсмодислокаций).

Палеосейсмологические исследования решают две основные задачи, имеющие важное практическое и теоретическое значение. Одна из них, направленная на установление величины самих палеособытий, касается выделения одноактных и приблизительно одновозрастных палеосейсмодислокаций (ПСД). Вторая связана с определением морфокинематических типов активных разломов, по которым происходили эти разрывообразующие палеоземлетрясения [*Arzhannikov, 2000; Solonenko,*

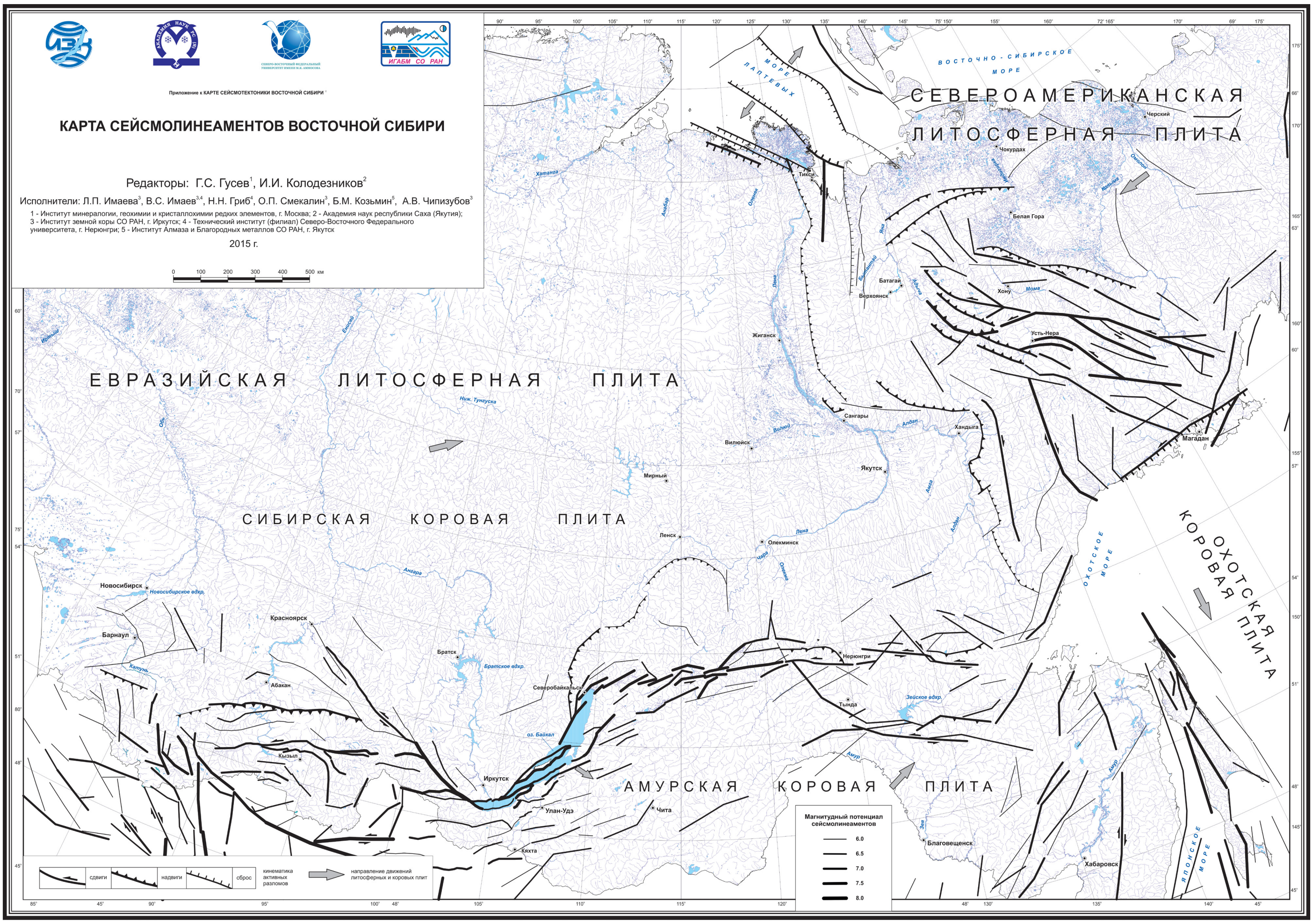

Рис. 4. Карта сейсмолинеаментов Восточной Сибири с предполагаемой магнитудой возможных землетрясений и установленной кинематикой смещения по ним.

Fig. 4. Seismic lineaments map of Eastern Siberia. It shows potential earthquake magnitudes and the kinematics of shearing.

1977; Smekalin et al., 2011; Strom, Nikonov, 1997; Rogozhin, Platonova, 2002]. В результате проведенных многолетних исследований все установленные активные разломы были вынесены нами на соответствующую топографическую основу территории Восточной Сибири с установленной магнитудой генерируемых ими землетрясений (рис. 4).

Обращает на себя внимание распространение активных разломов вдоль южной границы Евразийской литосферной плиты, в области взаимодействия ее с Амурской (Китайской) плитой, и формирование пояса активных разломов вдоль восточной границы Евразийской плиты, в пределах Верхояно-Колымской складчатой системы, которая формирует западную границу Североамериканской литосферной плиты. Для планового распределения разломов характерно наличие крупных сейсмолинеаментов, способных генерировать самые сильные землетрясения с магнитудой M=7.5–8.0, развитых в осевых частях выделенных сейсмических поясов и тяготеющих к самым активным частям геодинамически активных неотектонических зон.

4. Карта сейсмотектоники и динамика формирования сейсмогенерирующих структур Восточной Сибири

Комплексный анализ геолого-геофизических, геоморфологических и неотектонических данных, систем позднекайнозойских активных разломов, сейсмичности, результатов тектонофизических исследований позволил выявить на юге Восточной Сибири протяженный сейсмический пояс – Южно-Сибирский, состоящий из нескольких крупных отдельных сегментов: Алтай-Саяно-Тувинского, Байкальской рифтовой области и Олекмо-Становой зоны, соединяющих собой проявления сейсмич-

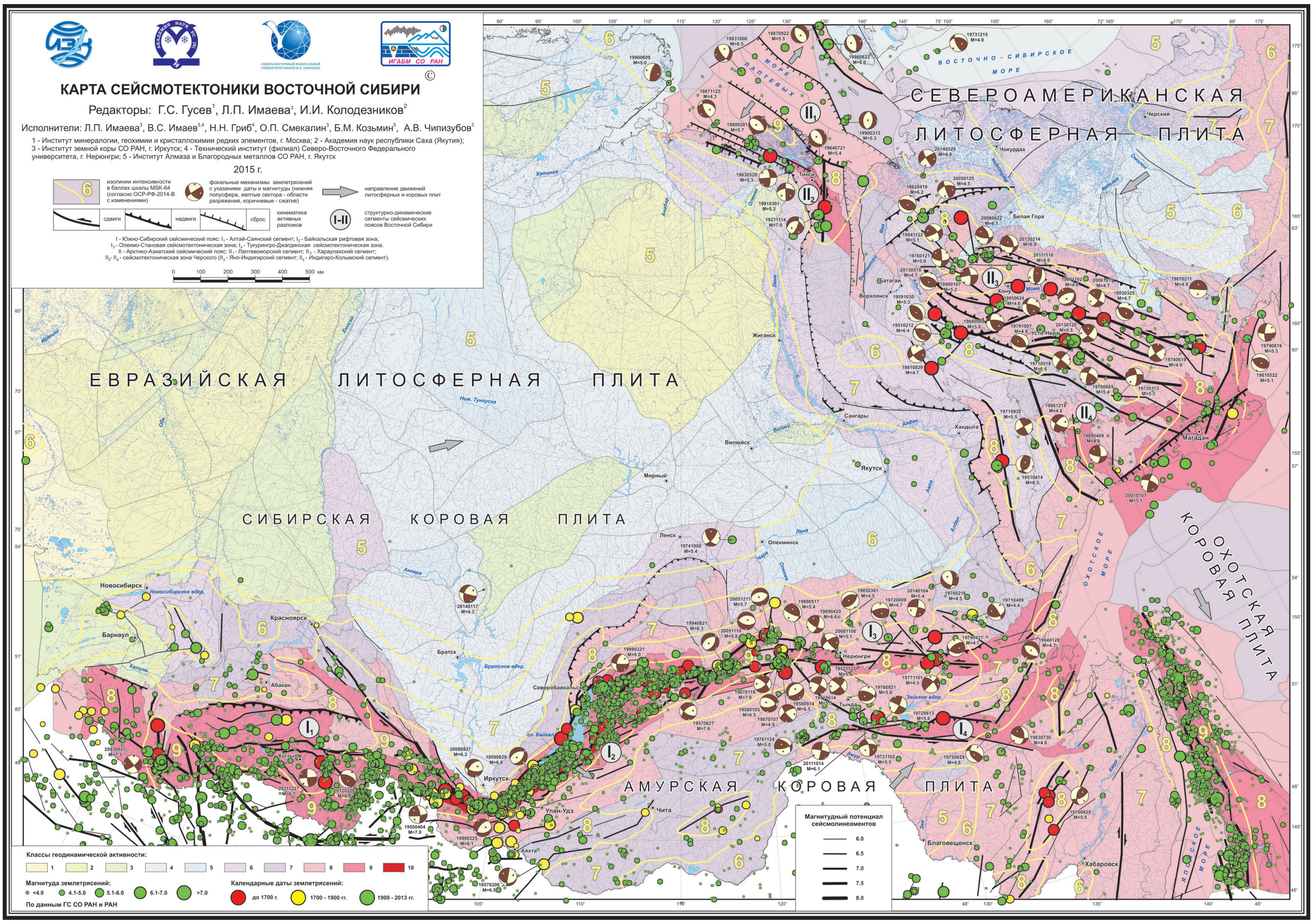

Рис. 5. Карта сейсмотектоники Восточной Сибири с нанесенными на нее изолиниями балльности возможных интенсивностей сейсмических сотрясений (по шкале MSK-64), соответствующих карте ОСР-2014-В (с повторяемостью 1000 лет), с добавлениями и исправлениями.

Fig. 5. Seismotectonic map of Eastern Siberia. Isolines show potential intensity of seismic events (MSK-64 scale), which correspond to OSR-2014-V Map (repeatability period of 1000 years) with additions and amendments.

ности сдвиговых структур Алтая, Саянской и Тувинской горно-складчатых областей, растяжения Байкальской рифтовой зоны, транспрессионные сдвигово-надвиговые перемещения Олекмо-Становой зоны и сейсмичность Охотского моря. Другой крупный сейсмический пояс – Арктико-Азиатский – прослеживается вдоль границы между Евразийской и Североамериканской литосферными плитами и соединяет сейсмичность побережья Арктического океана, связанную с растяжением земной коры, далее через сдвигово-надвиговые структуры, развитые на континентальном отрезке границы плит, соединяется с сейсмогенными структурами побережья Охотского моря и п-ова Камчатка.

Обобщенные материалы по сейсмотектонике и новейшей геодинамике сейсмических поясов на северо-востоке Азии дают возможность весьма успешно вести прогноз сценариев поведения сейсмической активности территории, с определением места и предельной величины возможной сейсмической катастрофы. Определение структурной позиции позволяет предполагать наиболее опасные направления выделения сейсмической энергии и снижать степень риска расположения потенциальных народнохозяйственных объектов. Построенная карта сейсмотектоники Восточной Сибири представляет собой комплексную многослойную модель развития сейсмотектонических процессов, протекающих на исследуемой территории. Карта для этой территории впервые составлена с использованием геоинформационных технологий. Применение новых технологий позволило при построении оперировать целостной картой, как совокупностью нескольких информационных слоев, содержащих определенную заданную информацию, характеризующую сейсмотектонические процессы территории Восточной Сибири (рис. 5).

Дополнительно на карту была вынесена интенсивность возможных сейсмических сотрясений в баллах (по шкале MSK-64), согласно новой карте Общего сейсмического районирования РФ (ОСР-2014–B), соответствующая расчетным событиям с периодичностью 1 в 1000 лет. Именно такой диапазон будущих толчков соответствует интересам народнохозяйственного освоения территории. Вместе с тем следует учесть, что рассматриваемая территория (особенно территория Якутии) все еще представляет собой весьма сложный и малоосвоенный (недостаточно изученный) регион России, где происходят активные деформации между несколькими тектоническими плитами, что, конечно, требует дальнейшего детального изучения отдельных частей этих сейсмических поясов. Это, прежде всего, относится к прибрежно-шельфовым областям арктических морей Восточной Сибири, с активным освоением которых связана ближайшая стратегия развития РФ и, в конечном итоге, экономическая и социальная безопасность нашей страны.

5. Заключение

Подводя итог сейсмотектоническим исследованиям, можно констатировать:

1. Карта сейсмотектоники Восточной Сибири является первым наглядным примером построения карты нового поколения (электронная база данных сейсмотектонических параметров), которая объединяет элементы геолого-геофизических параметров и сейсмичности и объясняет особенности современной геодинамики (а соответственно и сейсмическую опасность) региона.

2. Построение таких карт позволяет перейти к созданию карт детального сейсмического районирования отдельных частей активно промышленно осваиваемых районов Восточной Сибири и обоснованно установить уровень сейсмической угрозы тех или иных районов проживания коренного населения Сибири. Данный подход позволит приступить к новому этапу исследований проблемы сейсмобезопасности, а созданные региональные сейсмогеодинамические модели будут способствовать уточнению исходного сейсмического балла существующих нормативных карт общего и детального сейсмического районирования.

3. Карта должна использоваться органами исполнительной власти отдельных районов, комитетами по чрезвычайным ситуациям с целью владения информацией о возможном негативном влиянии сильных местных землетрясений, определения балла сейсмической угрозы конкретных населенных пунктов.

6. Благодарности

Данное научное исследование выполнено при поддержке интеграционного проекта СО РАН и гранта Министерства науки и образования РФ (Гос. задание № 5.1771.2014/К), а также гранта РНФ № 15-17-20000 (работы, выполненные в рамках анализа арктической территории РФ). Особую благодарность хотелось бы выразить д.г.-м.н. С.И. Шерману, д.г.-м.н. Г.С. Гусеву (ИМГРЭ, г. Москва) и д.г.-м.н И.И. Колодезникову (АН РС(Я), г. Якутск) за постоянное внимание и поддержку этих непривычных пока еще для большого круга сейсмологов исследований.

7. Литература / References

Allen C.R., 1975. Geological criteria for evaluating seismicity. *Geological Society of America Bulletin* 86 (8), 1041–1057. http://dx.doi.org/10.1130/0016-7606(1975)86<1041:GCFES>2.0.CO;2.

Arzhannikov S.G., 2000. Paleoseismodislocations in the Ottugtaiginsk-Azassky fault zone (Eastern Tuva). *Geologiya i Geofizika* (*Russian Geology and Geophysics*) 41 (11), 1499–1504.

Centroid Moment Tensor Catalog, 2015. Available from: http://www.globalcmt.org/CMTsearch.html (last accessed 08.09.2015)

Emanov A.F., Emanov A.A., Leskova E.V., Seleznev V.S., Filina A.G., 2012. Earthquake in Tuva (27.12.2011, ML=6.7) and aftershocks. *Vestnik Otdelenia nauk o Zemle RAN* 4, NZ2002 (in Russian) [*Еманов А.Ф., Еманов А.А., Лескова Е.В., Селезнев В.С., Филина Е.Г.* Тувинское землетрясение 27.12.2011 г. ML=6.7 и его афтершоки // *Вестник ОНЗ РАН*. 2012. Т. 4. NZ2002]. http://dx.doi.org/10.2205/2012NZ000112.

Geological Dictionary, 1973. Two volumes. Nedra, Moscow, 986 p. (in Russian) [Геологический словарь. В двух томах. М.: Недра, 1973. 986 с.].

Gorshkov G.P., 1984. Regional Seismotectonics of the Southern Territory of the USSR. Alpine Belt. Nauka, Moscow, 272 p. (in Russian) [*Горшков Г.П.* Региональная сейсмотектоника территории юга СССР. Альпийский пояс. М.: Наука, 1984. 272 с.].

Gusev G.S., Imaeva L.P., 2014. Recent and current tectonic (geodynamic) activity of the territory of Russia. *Razvedka i Okhrana Nedr* (*Subsoil Prospecting and Protection*) (12), 23–29 (in Russian) [*Гусев Г.С., Имаева Л.П.* Новейшая и современная тектоническая (геодинамическая) активность территории России // *Разведка и охрана недр.* 2014. № 12. С. 23–29].

Imaev V.S., Imaeva L.P., Koz'min B.M., 1990. Active Faults and Seismotectonics of North-Eastern Yakutia. Yakutia Scientific Centre, Siberian Branch of the USSR Acad. Sci., Yakutsk, 138 p. (in Russian) [*Имаев В.С., Имаева Л.П., Козьмин Б.М.* Активные разломы и сейсмотектоника Северо-Восточной Якутии. Якутск: ЯНЦ СО АН СССР, 1990. 138 с.].

Imaev V.S., Imaeva L.P., Koz'min B.M., 2000. Seismotectonics of Yakutia. GEOS, Moscow, 227 p. (in Russian) [*Имаев В.С., Имаева Л.П., Козьмин Б.М.* Сейсмотектоника Якутии. М.: ГЕОС, 2000. 227 с.].

Imaeva L.P., Imaev V.S., Koz'min B.M., 2011. Seismotectonic analysis of the Yana-Indigirka segment of the Chersky zone. *Izvestiya, Physics of the Solid Earth* 47 (12), 1045–1057. http://dx.doi.org/10.1134/S1069351311120056.

Imaeva L.P., Koz'min B.M., Imaev V.S., Mackey K.G., 2015. Structural dynamic analysis of the epicentral zone of the Ilin-Tas earthquake (Feb 14, 2013, Ms=6.9). *Journal of Seismology* 19 (2), 341–353. http://dx.doi.org/10.1007/s10950-014-9469-5.

Koz'min B.M., 1984. Seismic Belts of Yakutia and Earthquake Focal Mechanisms. Nauka, Moscow, 125 p. (in Russian) [*Козьмин Б.М.* Сейсмические пояса Якутии и механизмы очагов их землетрясений. М.: Наука, 1984. 125 с.].

Logatchev N.A., Sherman S.I., Levi K.G., 1987. Geodynamic activity of the lithosphere in Siberia in the Cenozoic. *Geologiya i Geofizika* (*Russian Geology and Geophysics*) (8), 3–10 (in Russian) [*Логачев Н.А., Шерман С.И., Леви К.Г.* Геодинамическая активность литосферы Сибири в кайнозое // *Геология и геофизика.* 1987. № 8. С. 3–10].

Logatchev N.A., Sherman S.I., Levi K.G., 1991. Geodynamic activity of the lithosphere in Asia: bases for analysis and principles of mapping. In: Geodynamics and Development of Tectonosphere. Proceedings of ITC Tectonic Meeting. Nauka, Moscow, p. 31–39 (in Russian) [*Логачев Н.А., Шерман С.И., Леви К.Г.* Геодинамическая активность литосферы Азии: основы анализа и принципы картирования // Геодинамика и развитие тектоносферы: Труды Тектонического совещания МТК. М.: Наука, 1991. С. 31–39].

Mackey K.G., Fujita K., Hartse H.E., Stead R.J., Steck L.K., Gunbina L.V., Leyshuk N., Shibaev S.V., Koz'min B.M., Imaev V.S., Gordeev E.I., Chebrov V.N., Masal'ski O.K., Gileva N.A., Bormatov V.A., Voitenok A.A., Levin Y.N., Fokina T.A., 2010. Seismicity Map of Eastern Russia, 1960–2010. *Seismological Research Letters* 81 (5), 761–768. http://dx.doi.org/10.1785/gssrl.81.5.761.

McCalpin J.P. (Ed.), 2009. Paleoseismology. Second Edition. Academic Press, Amsterdam–London, 615 p.

McCalpin J.P. (Ed.), 2011. Paleoseismology. Two volumes. Nauchny Mir, Moscow, 878 p. (in Russian) [Палеосейсмология. В 2-х томах / Ред. Дж.П. МакКалпин. М.: Научный мир, 2011. 878 с.].

Mel'nikova V.I., 2008. Crustal Deformation Parameters of the Baikal Rift Zone from Seismological Data. Synopsis of the Ph.D. Thesis. Institute of the Earth's crust, Irkutsk, 38 p. (in Russian) [*Мельникова В.И.* Деформационные параметры земной коры Байкальской рифтовой зоны по сейсмологическим данным: Автореф. дис. … докт. геол.-мин. наук. Иркутск: ИЗК СО РАН, 2008. 38 с.].

Nikolaev V.V., Semenov R.F., Semenova V.G., Solonenko V.P., 1982. Seismotectonics, Volcanoes and Seismic Zonation of the Stanovoy Ridge. Nauka, Novosibirsk, 150 p. (in Russian) [*Николаев В.В., Семенов Р.Ф., Семенова В.Г., Солоненко В.П.* Сейсмотектоника, вулканы и сейсмическое районирование хребта Станового. Новосибирск: Наука, 1982. 150 с.].

Radziminovich Ya.B., Mel'nikova V.I., Seredkina A.I., Gileva A.I., Radziminovich N.A., Papkova A.A., 2012. The Balei earthquake of 6 January 2006 (Mw=4.5): a rare case of seismic activity in eastern Transbaikalia. *Russian Geology and Geophysics* 53 (10), 1100–1110. http://dx.doi.org/doi:10.1016/j.rgg.2012.08.010.

Reisner G.I., Ioganson L.I., Reisner M.G., Baranov Yu.E., 1993. Typification of the Earth's Crust and Recent Geological Processes. UIFE RAS, Moscow, 208 p. (in Russian) [*Рейснер Г.И., Иогансон Л.И., Рейснер М.Г., Баранов Ю.Е.* Типизация земной коры и современные геологические процессы. М.: ОИФЗ РАН, 1993. 208 с.].

Rogozhin E.A., 2012. Features of Regional Seismotectonics. IPE RAS, Moscow, 340 p. (in Russian) [*Рогожин Е.А.* Очерки региональной сейсмотектоники. М.: ИФЗ РАН, 2012. 340 с.].

Rogozhin E.A., Platonova S.G., 2002. Focal Zones of Strong Earthquakes in Mountainous Altai in the Holocene. UIFE RAS, Moscow, 130 p. (in Russian) [*Рогожин Е.А., Платонова С.Г.* Очаговые зоны сильных землетрясений Горного Алтая в голоцене. М.: ОИФЗ РАН, 2002. 130 с.].

Smekalin O.P., Imaev V.S., Chipizubov A.V., 2011. Paleoseismology of Eastern Siberia (Applied Practice). IEC SB RAS, Irkutsk, 99 p. (in Russian) [*Смекалин О.П., Имаев В.С., Чипизубов А.В.* Палеосейсмология Восточной Сибири (некоторый опыт практического применения). Иркутск: ИЗК СО РАН, 2011. 99 с.].

Solonenko V.P. (Ed.), 1977. Seismic zoning of Eastern Siberia and its geological and geophysical base. Nauka, Novosibirsk, 301 p. (in Russian) [Сейсмическое районирование Восточной Сибири и его геолого-геофизические основы / Ред. В.П. Солоненко. Новосибирск: Наука, 1977. 301 с.]

Starovoit O.E., Chepkunas L.S., Gabsatarova I.P., 2003. Parameters of 27 September 2003 earthquake in Altai according to instrumental data. *Vestnik Otdelenia nauk o Zemle RAN* 1 (21), 1–12 (in Russian) [*Старовойт О.Е., Чепкунас Л.С., Габсатарова И.П.* Параметры землетрясения 27 сентября 2003 года на Алтае по инструментальным данным // *Вестник Отделения наук о Земле.* 2003. № 1 (21). С. 1–12].

Strom A.L., 1993. Comparison of parameters of recent and paleoseismotectionic structures. *Fizika Zemli* (9), 38–42 (in Russian) [*Стром А.Л.* Сопоставление параметров современных и палеосейсмотектонических дислокаций // *Физика Земли.* 1993. № 9. С. 38–42].

Strom A.L., Nikonov A.A., 1997. Relations between the seismogenic fault parameters and earthquake magnitude. *Izvestiya, Physics of the Solid Earth* 33 (12), 1011–1022.

Trifonov V.G., Kozhurin A.I., Lukina N.V., 1993. Studies and mapping of active faults. In: Seismicity and seismic zonation of North Eurasia. Vol. 1. UIFE RAS, Moscow, p. 196–206 (in Russian) [*Трифонов В.Г., Кожурин А.И., Лукина Н.В.* Изучение и картирование активных разломов // Сейсмичность и сейсмическое районирование Северной Евразии. М.: ОИФЗ РАН, 1993. Т. 1. С. 196–206].

Trifonov V.G., Vostrikov G.A., Trifonov R.V., Soboleva O.V., 1997. Active faults in Eurasia: geodynamic aspect. In: Tectonic and geodynamic phenomena. Nauka, Moscow, p. 174–195 (in Russian) [*Трифонов В.Г., Востриков Г.А., Трифонов Р.В., Соболева О.В.* Активные разломы Евразии: геодинамический аспект // Тектонические и геодинамические феномены. М.: Наука, 1997. С. 174–195].

Ulomov V.I., 2015. Attention! Earthquake! (in Russian) [*Уломов В.И.* Внимание! Землетрясение!]. Available from: http://seismos-u.ifz.ru/ (last accessed 14.08.2015).

Ulomov V.I., Shumilina L.S., 1999. The Set of General Seismic Zonation Maps of the Territory of the Russian Federation – OSR-97. Scale 1:8000000. Explanatory Note. UIFE RAS, Moscow, 57 p. (in Russian) [*Уломов В.И., Шумилина Л.С.* Комплект карт общего сейсмического районирования территории Российской Федерации – ОСР-97. Масштаб 1:8000000. Объяснительная записка. М.: ОИФЗ РАН, 1999. 57 с.].

USGS Earthquake Hazards Program, 2015. Available from: http://earthquake.usgs.gov/earthquakes/ (last accessed 14.08.2015).

Wallace R.E., 1977. Profiles and ages of young fault scarps, north-central Nevada. *Geological Society of America Bulletin* 88 (9), 1267–1281. http://dx.doi.org/10.1130/0016-7606(1977)88<1267:PAAOYF>2.0.CO;2.

Yeats R.S., Sieh K., Allen C.R., 1997. The Geology of Earthquakes. Oxford University Press, New York, 568 p.

Имаев Валерий Сулейманович, докт. геол.-мин. наук, г.н.с.
Институт земной коры СО РАН
664033, Иркутск, ул. Лермонтова, 128, Россия
e-mail: imaev@crust.irk.ru

Imaev, Valery S., Doctor of Geology and Mineralogy, Chief Researcher
Institute of the Earth's Crust, Siberian Branch of RAS
128 Lermontov street, Irkutsk 664033, Russia
e-mail: imaev@crust.irk.ru

Имаева Людмила Петровна, канд. геол.-мин. наук, с.н.с
Институт земной коры СО РАН
664033, Иркутск, ул. Лермонтова, 128, Россия
e-mail: imaeva@crust.irk.ru

Imaeva, Lyudmila P., Candidate of Geology and Mineralogy, Senior Researcher
Institute of the Earth's Crust, Siberian Branch of RAS
128 Lermontov street, Irkutsk 664033, Russia
e-mail: imaeva@crust.irk.ru

Смекалин Олег Петрович, канд. геол.-мин. наук, с.н.с.
Институт земной коры СО РАН
664033, Иркутск, ул. Лермонтова, 128, Россия
e-mail: smekalin@crust.irk.ru

Smekalin, Oleg P., Candidate of Geology and Mineralogy, Senior Researcher
Institute of the Earth's Crust, Siberian Branch of RAS
128 Lermontov street, Irkutsk 664033, Russia
e-mail: smekalin@crust.irk.ru

Козьмин Борис Михайлович, канд. геол.-мин. наук, в.н.с.
Институт геологии алмаза и благородных металлов СО РАН
677007, Республика Саха (Якутия), Якутск, пр. Ленина, 39, Россия
e-mail: b.m.kozmin@diamond.ysn.ru

Koz'min, Boris M., Candidate of Geology and Mineralogy, Leading Researcher
Institute of Diamond and Precious Metals Geology, Siberian Branch of RAS
39 Lenin avenue, Sakha (Yakutia) Republic, Yakutsk 677007, Russia
e-mail: b.m.kozmin@diamond.ysn.ru

Гриб Николай Николаевич, докт. техн. наук, профессор, заместитель директора
Технический институт (филиал) Северо-Восточного федерального университета им. М.К. Аммосова
678960, Республика Саха (Якутия), Нерюнгри, ул. Кравченко, 16, Россия
e-mail: grib@nfygu.ru

Grib, Nikolai N., Doctor of Technical Sciences, Professor, Deputy Director
Technical Institute (branch) of M.K. Ammosov North-Eastern Federal University
16 Kravchenko street, Sakha (Yakutia) Republic, Neryungri 678960, Russia
e-mail: grib@nfygu.ru

Чипизубов Анатолий Васильевич, докт. геол.-мин. наук, с.н.с.
Институт земной коры СО РАН
664033, Иркутск, ул. Лермонтова, 128, Россия
e-mail: chipizub@crust.irk.ru

Chipizubov, Anatoly V., Doctor of Geology and Mineralogy, Senior Researcher
Institute of the Earth's Crust, Siberian Branch of RAS
128 Lermontov street, Irkutsk 664033, Russia
e-mail: chipizub@crust.irk.ru

GEODYNAMICS & TECTONOPHYSICS

PUBLISHED BY THE INSTITUTE OF THE EARTH'S CRUST
SIBERIAN BRANCH OF RUSSIAN ACADEMY OF SCIENCES

2015 VOLUME 6 ISSUE 3 PAGES 289–310 ISSN 2078-502X

http://dx.doi.org/10.5800/GT-2015-6-3-0183

Paleogeodynamics

TECTONIC POSITION OF MINGLING DYKES IN ACCRETION-COLLISION SYSTEM OF EARLY CALEDONIDES OF WEST SANGILEN (SOUTH-EAST TUVA, RUSSIA)

I. V. Karmysheva[1, 2], V. G. Vladimirov[1, 2], A. G. Vladimirov[1, 2, 3], R. A. Shelepaev[1, 2], V. A. Yakovlev[2], E. A. Vasyukova[1, 2]

[1] *V.S. Sobolev Institute of Geology and Mineralogy, Siberian Branch of RAS, Novosibirsk, Russia*
[2] *Novosibirsk State University, Novosibirsk, Russia*
[3] *Tomsk State University, Tomsk, Russia*

Abstract: Dykes composed of basic rocks and granite are formed due to interactions between melts in a wide range of conditions, from contrasting compositions and fluid saturation rates to various tectonic settings and processes at different depths. Textures and petrochemical characteristics of the dykes are thus widely variable. This paper is focused on composite dykes observed in the West Sangilen region in South-East Tuva, Russia.

The Sangilen wedge is a fragment of the Early Caledonian orogenic structure of the Tuva-Mongolia Massif which evolved in a succession of geodynamic settings, from collision (transpression, 570–480 Ma) to transform faulting (transtension, 480–430 Ma). Intensive tectonic deformation facilitated massive basic-rock and granite magmatism at various layers of the crust and associated heating and metamorphism of the rocks (510–460 Ma). Basic-rock–granite composite dykes were formed in the above-mentioned period in various tectonic settings that controlled conditions of dyke intrusions and their compositions.

We distinguish two groups of composite dykes observed on two sites, in the area between the Erzin and Naryn rivers and on the right bank of the Erzin river (Strelka and Erzin Sites, respectively) (Fig. 1). The dykes in both groups originated from one and the same basic-rock melt source. However, mingling of the contrasting melts was carried out by different mechanisms as suggested by the proposed intrusion models.

In the area between the Erzin and Naryn rivers (Strelka Site), the host rock of the composite dykes is granite of the Nizhneerzin massif. The mingling dykes are composed of amphibole gabbro and monzogabbro, granosyenite and two-feldspar granite. Contacts between basic and felsic rocks vary from smooth contrasting to complex 'lacerated' flame-shaped, and gradual transition zones are present (Fig. 6).

The dykes were formed at mesoabyssal or abyssal depths, and the subliquidus heat regime was thus maintained for a long time, and even the smallest portions of the basic-rock melt were consolidated through quite a long period of time. As a consequence, indicators of deformation are lacking in the composite dykes, while transition zones and hybridization are present.

On the right bank of the Erzin river (Ersin Site), the dykes cut through migmatite-granite of the Erzin formation in the same-name tectonic zone. Contacts with host rocks are transverse. Melanocratic rocks are represented by small-grained diorite and quartz diorite, and the felsic composite dykes are composed of medium- and small-grained two-feldspar granite and leukogranite. Transition zones, hornfelsing and contact alterations are absent at contacts of all the types (Fig. 8).

The composite dykes of this type intruded and emplaced when the shear zone was subject to extension and fragmentation, which predetermined active intrusion of basic and, possibly, felsic melts through conjugated faults. Crystallization of the melts was rapid, and their potential heat impact on the adjoining rocks was thus excluded, as evidenced by the presence of oxygonal chips of igneous and host metamorphic rocks, vein pegmatoid intrusions, and composite dykes of the reticulate-cuspate texture with the dominant basic-rock component.

The mingling dykes classified in the first group intruded when the Erzin and Kokmolgarga shear zones were formed at the early stage of the tectonic-magmatic evolution of the Sangilen orogen (510–490 Ma). Intrusions of the basic-rock melts were accompanied by the formation of relatively large massifs of the basic composition, i.e. the Erzin and Bayankol gabbro-monzodiorite massifs, as well as by the occurrence of composite dykes that are abundant in the area between the Erzin and Naryn rivers. In the second stage (460–430 Ma), the composite dykes occurred when the orogen was subject to extension along the system of tectonic zones, the Bashkymugur gabbro-monzodiorite massif was emplaced, and fracture-vein structures, including the dykes, were formed.

Key words: mingling, composite dykes, net-veined complexes, shear zone, tectonic and magmatic evolution, Sangilen, South-East Tuva.

Recommended by E.V. Sklyarov

For citation: *Karmysheva I.V., Vladimirov V.G., Vladimirov A.G., Shelepaev R.A., Yakovlev V.A., Vasyukova E.A.* 2015. Tectonic position of mingling dykes in accretion-collision system of early Caledonides of West Sangilen (South-East Tuva, Russia). *Geodynamics & Tectonophysics* 6 (3), 289–310. doi:10.5800/GT-2015-6-3-0183.

Тектоническая позиция минглинг-даек в аккреционно-коллизионной системе ранних каледонид Западного Сангилена (Юго-Восточная Тува)

И. В. Кармышева[1, 2], В. Г. Владимиров[1, 2], А. Г. Владимиров[1, 2, 3], Р. А. Шелепаев[1, 2], В. А. Яковлев[2], Е. А. Васюкова[1, 2]

[1] *Институт геологии и минералогии им. В.С. Соболева СО РАН, Новосибирск, Россия*
[2] *Новосибирский государственный университет, Новосибирск, Россия*
[3] *Томский государственный университет, Томск, Россия*

Аннотация: Формирование базит-гранитных комбинированных даек происходит в широком спектре условий и обстановок взаимодействия контрастных по составу расплавов, начиная от специфики состава и флюидонасыщенности расплавов и заканчивая тектоническими обстановками и глубинностью процессов. Все эти факторы отражаются на структурно-текстурных и петрогеохимических характеристиках даек. В настоящей работе данные вопросы рассмотрены на примере комбинированных (минглинг) даек Западного Сангилена (Юго-Восточная Тува).

Сангиленский выступ представляет собой фрагмент раннекаледонской орогенной структуры Тувино-Монгольского массива, тектоническая эволюция которой отражает смену геодинамических обстановок – от коллизионной (режим сжатия, 570–480 млн лет) до сдвиговой (режим растяжения, 480–430 млн лет). Интенсивные тектонические деформации способствовали проявлению масштабного базитового и гранитоидного магматизма на различных уровнях земной коры и связанного с ним теплового прогрева и метаморфизма пород в период 510–460 млн лет. С этим же периодом связано проявление базит-гранитных комбинированных даек, формирование которых происходило в различных тектонических обстановках, контролирующих условия их внедрения и становления.

В статье рассматривается две группы минглинг-даек, изученных в междуречье Эрзина и Нарына и на правобережье р. Эрзин (рис. 1). В обоих случаях их происхождение связано с одним источником базитового расплава. Однако, механизмы смешения контрастных расплавов отвечают различным моделям внедрения.

В междуречье Эрзина и Нарына вмещающими породами комбинированных даек являются гранитоиды Нижнеэрзинского массива. Минглинг-дайки сложены амфиболовыми габбро и монцогаббро, граносиенитами и двуполевошпатовыми гранитами. Контакты между основными и кислыми породами различны и изменяются от ровных и контрастных до пламеневидных и микрофестончатых с образованием зон постепенных переходов (рис. 6).

Формирование даек этого типа происходило на мезоабиссальных либо абиссальных уровнях глубинности, что обеспечило при их становлении сохранность длительного субликвидусного теплового режима и относительно продолжительный период консолидации даже мелких порций базитового расплава. Как следствие, в комбинированных дайках отсутствуют признаки деформаций, но наблюдаются переходные зоны и гибридизация.

Дайки на правобережье р. Эрзин прорывают мигматит-граниты эрзинского комплекса в одноименной тектонической зоне. Контакты с вмещающими породами секущие. Меланократовые породы представлены мелкозернистыми диоритами и кварцевыми диоритами, кислая часть комбинированных даек сложена средне-, мелкозернистыми двуполевошпатовыми гранитами и лейкогранитами. Для всех типов контактов характерно отсутствие зон перехода, ороговикования и контактовых изменений (рис. 8).

Внедрение и становление комбинированных даек данного типа происходило в условиях обстановок растяжения и фрагментации сдвиговой зоны, что обусловило как активное внедрение базитовых и, возможно, кислых расплавов по сопряженным трещинам, так и их быструю кристаллизацию. Наличие остроугольных обломков магматических и вмещающих метаморфических пород, существование жильных пегматоидных образований, сетчато-фестончатый характер минглинг-даек с преобладанием базитовой составляющей прямо указывают на быструю кристаллизацию базитовых расплавов без возможности их последующего теплового воздействия на окружающие породы.

Внедрение первой группы минглинг-даек связывается с заложением Эрзинской и Кокмолгаргинской тектонических зон и отвечает раннему этапу тектономагматической эволюции Сангиленского орогена на рубеже 510–490 млн лет. Данный этап сопровождался как внедрением базитовых расплавов с формированием относительно крупных массивов основного состава (Эрзинский и Баянкольский габбро-монцодиоритовые массивы), так и появлением комбинированных даек, распространенных в междуречье Эрзина и Нарына. Второй этап формирования минглинг-даек связывается с тектономагматической активностью в регионе на рубеже 460–430 млн лет, когда происходило активное растяжение орогенной структуры по системе тектонических зон, внедрение и становление Башкымугурского массива габбро-монцодиоритов и развитие трещинно-жильных образований, в том числе комбинированных даек.

Ключевые слова: минглинг, комбинированные дайки, сетчатые интрузии, тектоническая зона, тектономагматическая эволюция, Сангилен, Юго-Восточная Тува.

1. Introduction

In case of interaction between basic-rock magma and granitoid magma, chemical and mechanical processes, i.e. mixing and mingling, take place simultaneously. Resultant structures are called composite / mingling dykes and net-veined complexes.

The problem of mingling has been discussed in many publications, including [*Wiebe, 1973; Gambler, 1979; Marshall, Sparks, 1984; Furman, Spera, 1985; Frost, Mahood, 1987; Cook, 1988; Huppert, Sparks, 1988; Didier, Barbarin, 1991; Litvinovsky et al., 1995; Nardi, de Lima, 2000; Fedorovsky et al., 2003; Perugini, Poli, 2005; Dokukina, Vladimirov, 2005; Sklyarov, Fedorovskii, 2006*], and numerous models have been proposed to describe and clarify the textures and structures of composite dykes.

Dykes can occur in a wide range of conditions predetermining interactions between melts of contrasting compositions. Such conditions include – but not limited to – tectonic processes, crustal depths and structures, duration of melt consolidation, composition and fluid saturation of interacting melts. Mingling dykes of various patterns and textures may be observed in one and the same region due to the presence of shear faults that differ in age and origin and control movements of basic-rock and granitoid melts. In our study, we review composite dykes located in West Sangilen, analyse petrogeochemical compositions at micro- and macroscopic levels and attempt at establishing relationships between the compositions and regional tectonic and magmatic events.

2. Geological setting

West Sangilen, a part of the Sangilen upland, is located at the border of Tuva, Mongolia and Buryatia in the Tuva-Mongolia Massif (hereafter TMM) in the Central Asian folded belt that is traditionally viewed as a collage of island arcs, continental blocks and oceanic crust fragments attached to the Siberian craton during the Neoproterozoic and Paleozoic [*Kovalenko et al., 2004, Kuzmichev et al., 2001*]. TMM is bordered by deep faults, and its structure differs from that of the neighbouring blocks. In its current coordinates, the Sangilen wedge is located in the north-western TMM (Fig. 1). It is bordered from the north-west by the Agardag ofiolite zone that is also viewed as the TMM boundary [*Kuzmichev, 2004*].

The Sangilen wedge is a fragment of the Early Caledonian orogenic structure of TMM which evolved in a succession of geodynamic settings, from collision (transpression, 570–480 Ma) to transform faulting (transtension, 480–430 Ma) [*Vladimirov et al., 2005*]. Intensive shearing facilitated massive basic-rock and granitoid magmatism at various layers of the crust and associated heating and metamorphism of the rocks (510–460 Ma) [*Vladimirov et al., 2005; Egorova et al., 2006; Karmysheva, 2012*].

The current West Sangilen structure includes the Muguro-Chinchilig and Erzin-Naryn metamorphic blocks separated by the Erzin shear zone (Fig. 1). The Muguro-Chinchilig block is mainly composed of a Moren metamorphic complex (medium temperature and high pressure). The Erzin-Naryn block's texture is inhomogeneous as it is composed of a variety of rocks from epidote-amphibolite to granulite facies of metamorphism, such as garnet-biotite, cordierite and spinel-cordierite schists and gneisses. Amphibolite and granulite are related to the Erzin metamorphic complex at the boundaries of the blocks which follow the tectonic boundaries, i.e. the Erzin and Kokmolgarga shear zones (Fig. 1).

The time periods when magmatism occurred in the Muguro-Chinchilig and Erzin-Naryn blocks are different. The Erzin-Naryn block includes the Bayankol gabbro-monzodiorite-granodiorite-granite, Nizhneerzin gabbro-monzodiorite-granosyenite-granite, Teskhem granosyenite-granite, and Ukhadag granosyenite-granite massifs (490±10 Ma). The Erzin shear zone includes the Nizhneulor granite massif (475±5 Ma) and the Matut gneiss-granite massif (510–490 Ma, according to the geological data). Mingling dykes composed of basic rocks and granite (i.e. the subject of our study) are observed in migmatite-granite of the Erzin complex

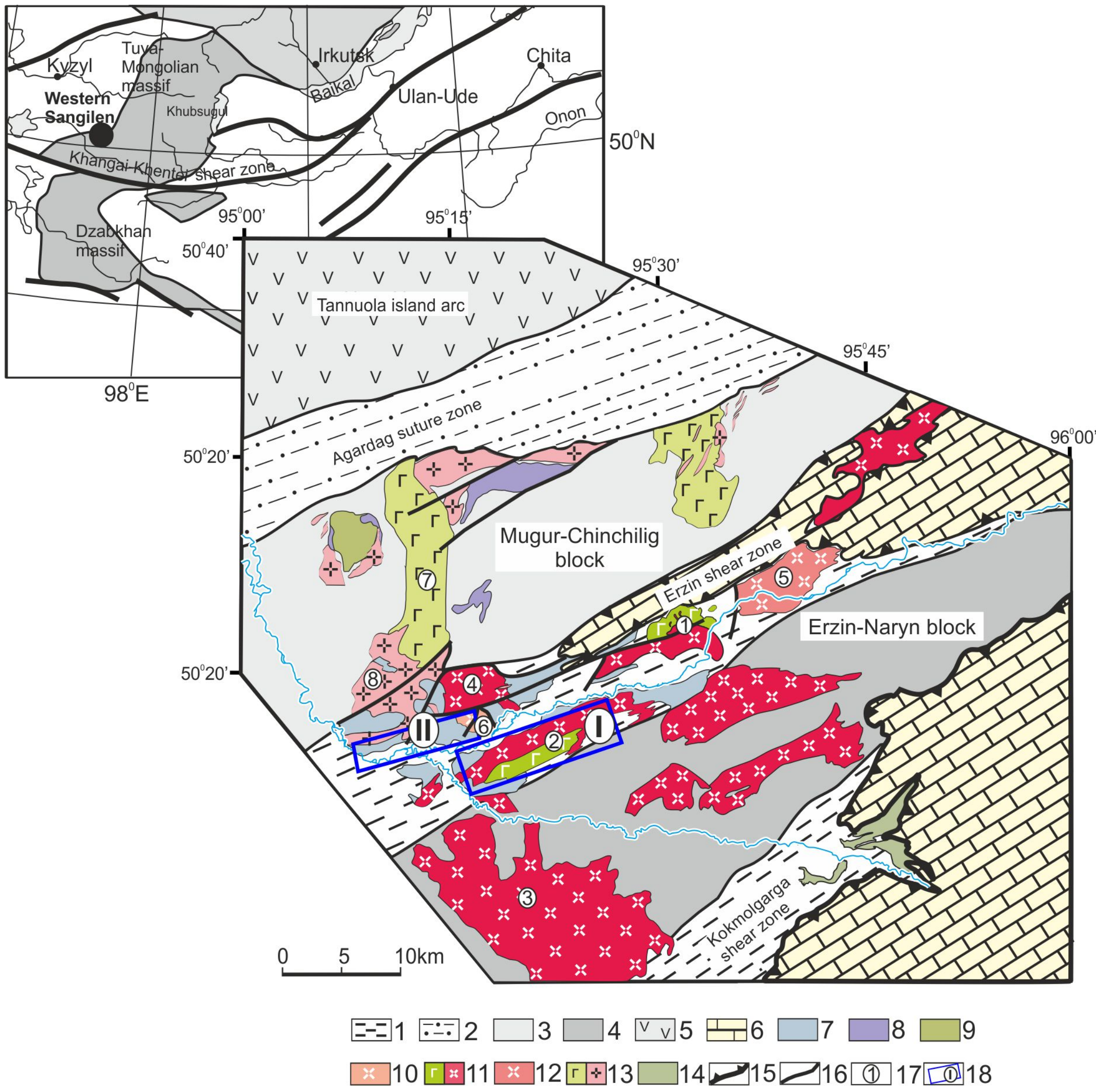

Fig. 1. The structural-tectonic scheme of West Sangilen (South-East Tuva, Russia). The inset shows the West Sangilen position at the southern margin of the Siberian craton (according to [*Kuzmichev, 2004*]).

1 – Erzin and Kokmolgarga shear zones (Є$_{1-2}$); *2* – Agardag ophiolitic belt (V-Є$_1$); *3* – Moren metamorphic complex (R$_3$); *4* – Nizhneerzin metamorphic complex (R$_3$); *5* – Tannuola island arc (V-Є$_1$); *6* – carbonate-terrigenous cover of the Tuva-Mongolia microcontinent (V$_1$); *7* – Erzin granulitic migmatite-granite complex (Є$_3$-O$_1$); *8* – Aktovrak dunite-harzburgite complex (V); *9* – Pravotarlashkin anortosite-gabbronorite complex (Є$_1$); *10* – Matut gneiss-granite massif (O$_1$); *11* – Bayankol gabbro-monzodiorite-granosyenite (granodiorite)-granite-leukogranite series (O$_1$); *12* – Nizhneulor granite massif (O$_1$); *13* – Bashkymugur gabbro-monzodiorite-granite-leukogranite series (O$_{1-2}$); *14* – gabbroids of the Kokmolgarga massif; *15* – nappe boundaries; *16* – faults; *17* – intrusive massifs: 1 – Bayankol gabbro-monzodiorite-granodiorite-granite, 2 – Nizhneerzin gabbro-monzodiorite-granosyenite-granite, 3 – Teskhem granosyenite-granite, 4 – Ukhadag granosyenite-granite, 5 – Nizhneulor granite, 6 – Matut gneiss-granite, 7 – Bashkymugur gabbro-monzodiorite, 8 – Baidag granite-leukogranite; *18* (I and II) – Strelka and Erzin Sites, respectively, where mingling dykes were studied in detail.

Рис. 1. Структурно-вещественная схема Западного Сангилена (Юго-Восточная Тува). На врезке – положение Западного Сангилена в структурах южного обрамления Сибирской платформы по [*Kuzmichev, 2004*].

1 – Эрзинская и Кокмолгаргинская тектонические зоны (Є$_{1-2}$); *2* – Агардагский офиолитовый пояс (V-Є$_1$); *3* – моренский метаморфический комплекс (R$_3$); *4* – нижнеэрзинский метаморфический комплекс (R$_3$); *5* – Таннуольская островная дуга (V-Є$_1$); *6* – карбонатно-терригенный чехол Тувино-Монгольского микроконтинента (V$_1$); *7* – эрзинский гранулитовый мигматит-гранитный комплекс (Є$_3$-O$_1$); *8* – актовракский дунит-гарцбургитовый комплекс (V); *9* – правотарлашкинский анортозит-габброноритовый комплекс (Є$_1$); *10* – Матутский гнейсогранитный массив (O$_1$); *11* – баянкольская габбро-монцодиорит-граносиенит (гранодиорит)-гранит-лейкогранитная серия (O$_1$); *12* – Нижнеулорский гранитный массив (O$_1$); *13* – башкымугурская габбро-монцодиорит-гранит-лейкогранитная серия (O$_{1-2}$); *14* – габброиды Кокмолгаргинского массива; *15* –границы покровов; *16* – разломы; *17* – интрузивные массивы: 1 – Баянкольский габбро-монцодиорит-гранодиорит-гранитный, 2 – Нижнеэрзинский габбро-монцодиорит-граносиенит-гранитный, 3 – Тесхемский граносиенит-гранитный, 4 – Ухадагский граносиенит-гранитный, 5 – Нижнеулорский гранитный, 6 – Матутский гнейсогранитный, 7 – Башкымугурский габбро-монцодиоритовый, 8 – Байдагский – гранит-лейкогранитный; *18* – участки детального исследования минглинг-даек: I – участок «Стрелка»; II – участок «Эрзинский».

and granosyenite-granite of the Nizhneerzin massif. Results of the isotope geochoronology suggest that the dykes are not younger than 462.5 Ma as shown by the following data: 471.2±1.9 Ma – Ar/Ar, amphibole from basic rocks; 462.5±1.0 Ma – Ar/Ar, biotite from basic rocks [*Vladimirov et al., 2005*], and 467±21 Ma – Rb/Sr, rocks in gross [*Petrova, 2001*].

The Muguro-Chingilig metamorphic block contains younger igneous rocks (460±10 Ma). The Bashkymugur gabbro-monzodiorite and Baidag granite-leukogranite (alaskaite) massifs are of the same age.

In our study, we focus on mingling dykes composed of basic rocks and granite which are observed on Strelka and Erzin Sites, i.e. in the area between the Erzin and Naryn rivers and on the right bank of the Erzin river, respectively (Fig. 1).

3. Composite dyke structure and texture

In the area between the Erzin and Naryn rivers, the host rock of the composite dykes is granite of the Nizhneerzin massif. Visible segments of the dykes are traceable for several tens to hundreds meters, and their depth varies from 0.15 to 3.5 m (Fig. 2 and 3). It is not always possible to clearly define the positions of the endo- and exocontact zones, and the contacts with the host rocks are not clarified. Separate nodules of basic rocks penetrating into the host matrix can be observed in the marginal exocontact zones of the composite dykes (Fig 2, II). Typically, a large basic-rock body is either surrounded by a leucocratic rim or cut by a system of granite veins (Fig. 2, III and 3, IV). It is noteworthy that contacts of the granite veins are almost always flame-shaped and never linear (Fig. 2, III and 3, IV).

Basic-rock bodies of patchy shapes with flame-shaped contacts are cut by veins of large-grained granites (Fig. 3, II). In some cases, basic rocks in the granitoid matrix compose tree-shaped elongated bodies with elements of viscous boudinage and separate nodules (Fig. 3, I). However, such cases are not numerous, and composite dykes containing irregularly distributed fragments of basic rocks are dominating (Fig. 3, II and 3, III).

On Strelka Site, two generations of composite dykes are distinguished: (1) early sub-horizontal dykes composed by basic rocks, strongly boudinaged and cut by granite, and (2) later subvertical dykes composed by basic rocks, which cut the dykes of the first generation, have chill zones and are cut by aplite that cuts both the dykes and the host granite [*Izokh et al., 2004; Vasyukova et al., 2008*].

On Erzin Site, the dykes cut through migmatite-granite of the Erzin formation in the same-name shear zone. Clusters of composite dykes form linear zones which strike is similar to that of the Erzin shear zone. Depth of some dykes vary from 0.5 to 2.5 m. Contacts with host rocks are transverse (Fig. 4 and 5). In the leucogranitic component of the mingling dykes, oxygonal xenoliths of the host rocks (which maintain their original structure) are combined with separate angulated inclusions of diorite (Fig. 4, I). A contact acid rim is lacking around the dykes. Pegmatoid inclusions are common at the boundary between granites and host rocks and inside conjugated fractures (Fig. 4, II). The texture of such dykes is complex, reticulate-cuspate or patchy (see Fig. 5, I–III). Transition zones, hornfelsing and contact alterations are absent at contacts of all the types.

4. Composition of basic rocks and granites of mingling dykes

In the area between the Erzin and Naryn rivers (Strelka Site), the basic-rock component of the composite dykes is variable in composition from amphibole gabbro to monzogabbro and amphibole monzogabbro with gabbro and porphiric-like structures: Hbl (45–60 %), Kfs (20–35 %), Pl (10–15 %), Bt (5 %), and Qtz (>5 %). Accessory minerals are fine-grained sphene and apatite. Coarse-grained amphibole rims and plagioclase are absent in the contact zones.

The felsic dykes are composed of coarse-grained granosyenite: Kfs (40–65 %), Qtz (20–25 %), Pl (10–15 %), and Bt+Hbl (3–5 %), and two-feldspar granite: Kfs (35–40 %), Qtz (25–35 %), Pl (15–20 %), and Bt+Hbl (up to 3 %). Accessory minerals are sphene and ortite. Rocks vary from evenly grained to glomeroporphyric. Porphyric inclusions contain large aggregates of K-Na feldspar and, rarely, quartz. Small veins and fractures in the basic rocks are filled with the most coarsely grained rocks.

Contacts of basic and acid rocks are variable in shapes, from smooth to contrasting (Fig. 6, I), flame-shaped to micro-cuspate, with zones of transition from granites to basic rocks (Fig. 6, II–V). In microsections, changes in the composition and grain size of the rocks are clearly evidenced by 'bay-shaped' contours. The inner structure is changed near the contact from the side of basic rocks due to the occurrence of poikilitic grains of quartz with inclusions of idiomorphic small crystals of biotite and amphibole. Patchy aggregates with flame-shaped contacts, which are quite common, may be cut by acidic veins.

In the contact zone, basic rocks vary from gabbrodiotite to amphibole monzogabbro. Transitions from one rock to another are abrupt and clearly detected at the meso- and micro-levels. In several microsections and rock slices, amphibole gabbro and monzogabbro are rimmed by coarse-grained amphibole (see Fig. 6, III).

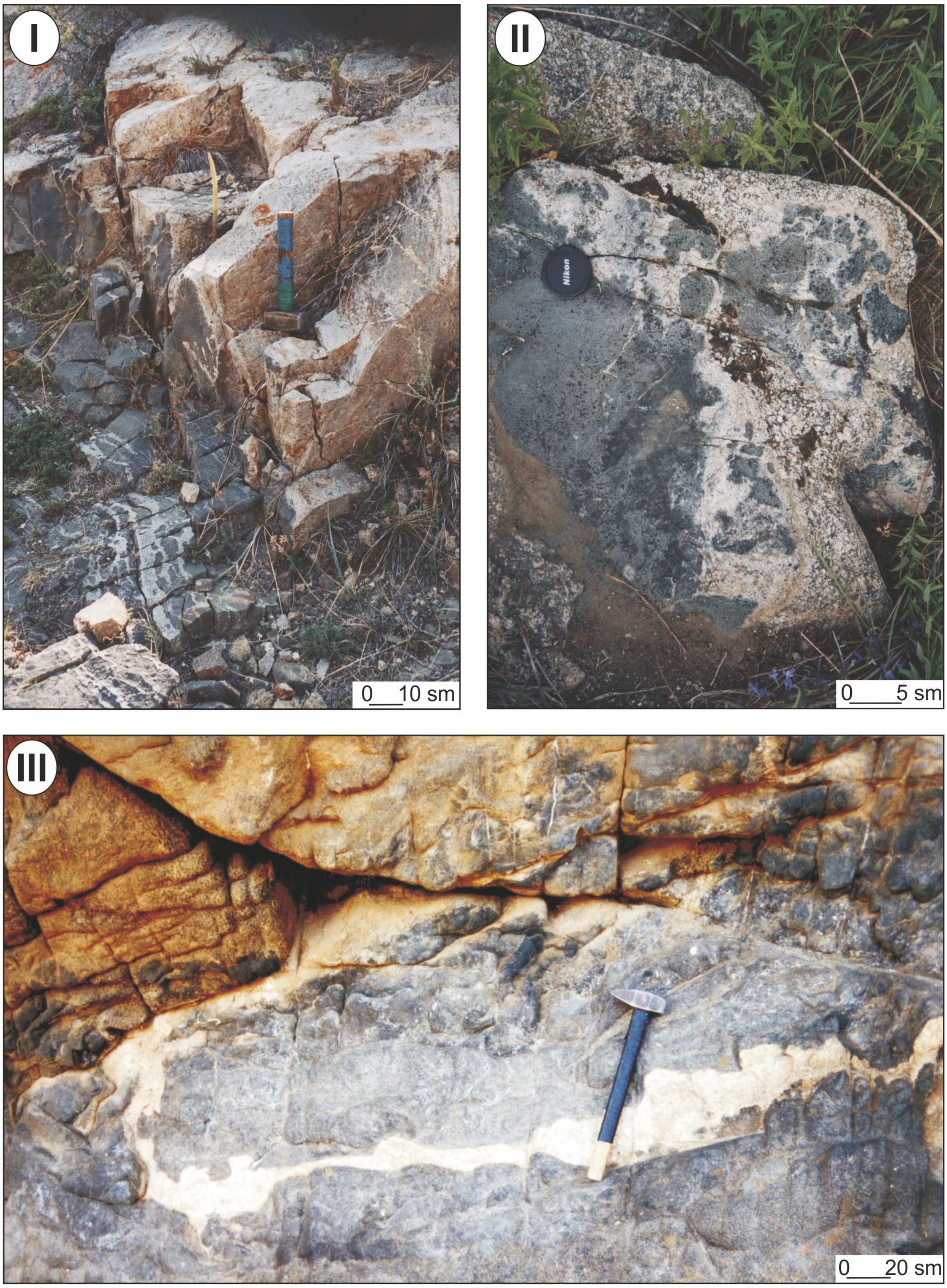

Fig. 2. Contacts between mingling dykes and host granite of the Nizhneerzin massif in the area between the Erzin and Naryn rivers (Strelka Site).

I – linear composite dyke composed of basic rocks and leucogranites in host parautochthonous granite; II – flame-shaped contact between basic rocks and host mega-porphyric granosyenite and basic-rock nodules in granite; III – cuspate sinuous contacts of the granite vein that cuts basic rocks in the interior zone of the mingling dyke.

Рис. 2. Контакты минглинг-даек с вмещающими гранитоидами Нижнеэрзинского массива в междуречье Эрзина и Нарына (участок «Стрелка»).

I – линейная комбинированная дайка, сложенная базитами и лейкогранитами, в параавтохтонных гранитах; II – пламеневидный контакт базитов с вмещающими крупнопорфировыми граносиенитами с формированием в гранитоидах нодулей основного состава; III – фестончатые, извилистые контакты гранитной жилы, пересекающей базиты, во внутренней зоне минглинг-дайки.

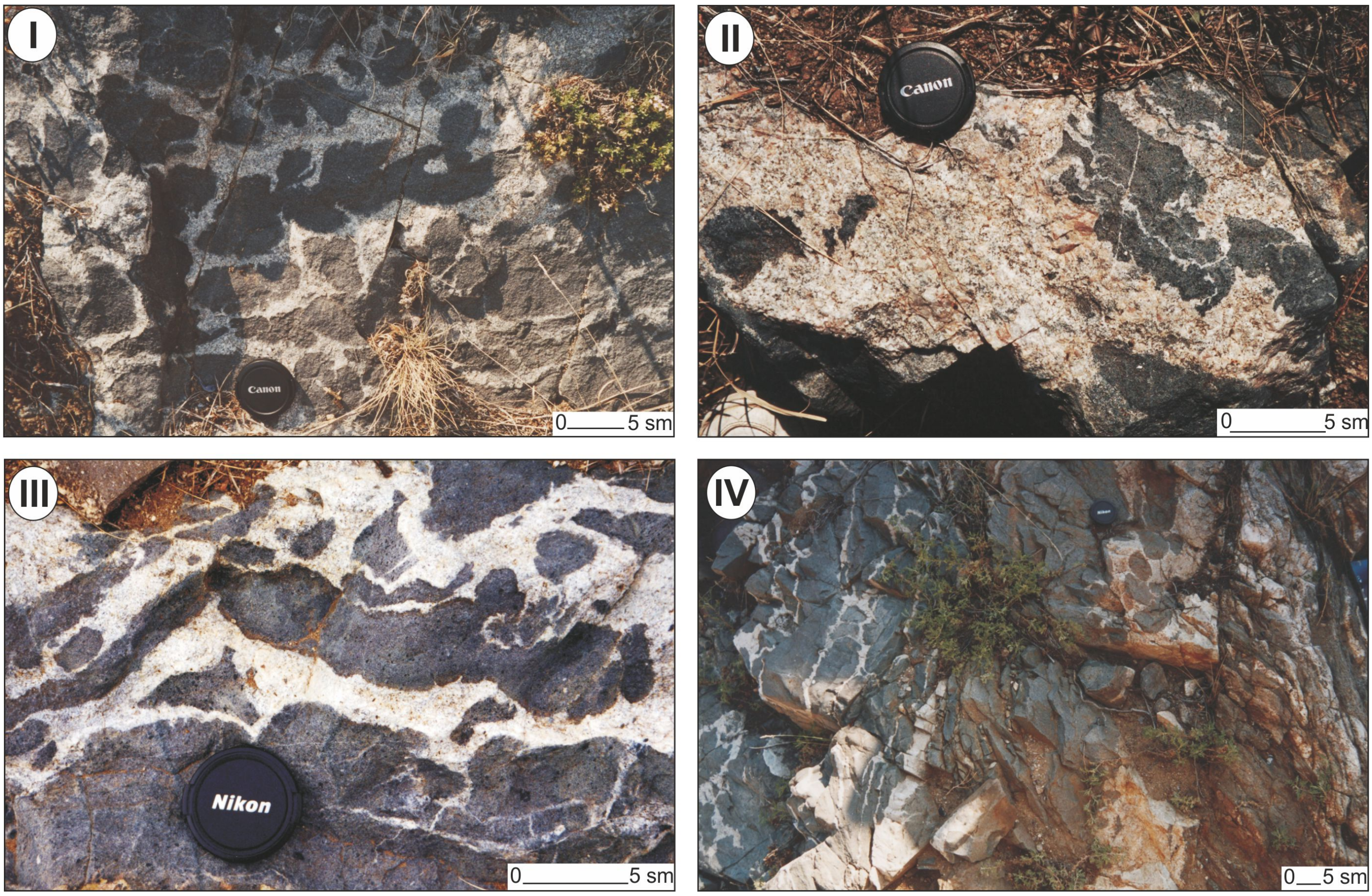

Fig. 3. The interior structure of mingling dykes in the area between Erzin and Naryn rivers (Strelka Site).

I – tree-shaped, reticulate-cuspate and nodule structure of basic rocks in the felsic matrix; II – patchy basic-rock bodies with flame-shaped contacts and thin leukogranite veins in the porphyric granosyenite matrix; III – reticulate-nodule texture of the composite dyke; IV – reticulate-cuspate inner texture of the composite dyke with the dominant basic-rock component.

Рис. 3. Внутренняя структура минглинг-даек в междуречье Эрзина и Нарына (участок «Стрелка»).

I – дендроидная, сетчато-фестончатая и нодульная структура обособлений базитов, заключенных в матрикс кислого состава; II – кляксообразные тела базитов с пламеневидными контактами и маломощными жилами лейкогранитов в матриксе порфировидных граносиенитов; III – сетчато-нодульная структура комбинированной дайки; IV – сетчато-фестончатая внутренняя структура комбинированной дайки с доминированием базитовой составляющей.

Contact zones may differ in width, and their patterns may be complex. The contact zones contain small nodules of basic rocks, fine-grained transitional rocks with evenly scattered melanocratic minerals and porphyric inclusions of K-Na feldspar, medium-grained transitional rocks with unevenly scattered melanocratic and leucocratic minerals, and sporadic coarse-grained aggregates of biotite and hornblende in granosyenite.

The transitional zones are composed of amphibole (10–60 %), biotite (10 %), K-Na feldspar (15–40 %), plagioclase (5–10 %) and quartz (>5 %) (Fig. 7). K-Na feldspar can form poikilite structures containing inclusions of fine-grained prismatic crystals of amphibole and biotite. Recrystallization of individual grains of quartz and plagioclase is typical of the marginal parts. Besides, a high content of sphene is noted in the transition zones, and sphene grains (up to 1 mm) are larger than those in monzogabbro and granosyenite.

Composite dykes on the right bank of the Erzin river (*Erzin Site*). Melanocratic rocks are represented by fine-grained diorite and quartz diorite: Amf (45–50 %), Pl (40–45 %), Qtz (10–15 %), and Bt (5 %). The rock texture is gabbro-ophite and porphyric. Porphyric inclusions are agglomerates of amphibole with a cribrose texture.

Felsic dykes are composed of medium- and fine-grained two-feldspar granite and leucogranite: Kfs (25–30 %), Pl (20–40 %), Otz (25–40 %), and Bt (1–3 %). The granite and porphyric textures are evenly grained. Porphyric inclusions are composed of K-Na feldspar. Deformation twins are observed in plagioclase grains.

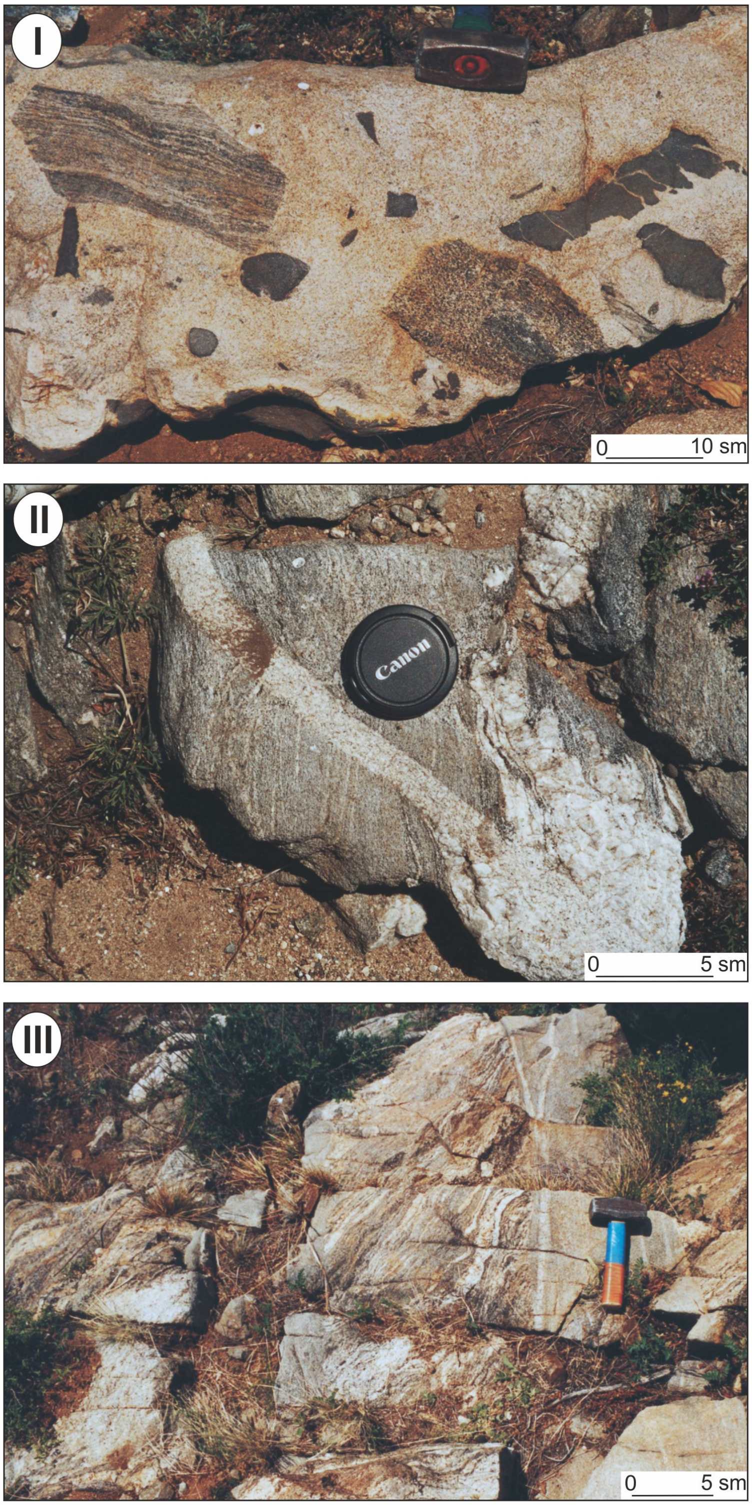

Fig. 4. The morphology of mingling dykes in migmatite of the Erzin metamorphic complex on the right bank of Erzin river (Erzin Site).

I – combination of oxygonal xenolithes of host rocks and angular diorite inclusions in leukogranite of mingling dykes; II – migmatite of the Erzin complex which is cut by leukogranite of composite dykes with pegmatoid inclusion in the contact zone of extension; III – transverse 'cold' contacts between granite in mingling dykes and host garnet-biotite-cordierite schist.

Рис. 4. Морфология минглинг-даек в мигматитах эрзинского метаморфического комплекса на правобережье р. Эрзин («Эрзинский» участок).

I – сочетание остроугольных ксенолитов вмещающих пород и угловатых обособлений диоритов в лейкогранитовой составляющей минглинг-даек; II – мигматиты эрзинского комплекса, прорванные лейкогранитами комбинированных даек с пегматоидным обособлением в приконтактовой зоне растяжения; III – секущие «холодные» контакты гранитоидов минглинг-даек с вмещающими гранат-биотит-кордиеритовыми сланцами.

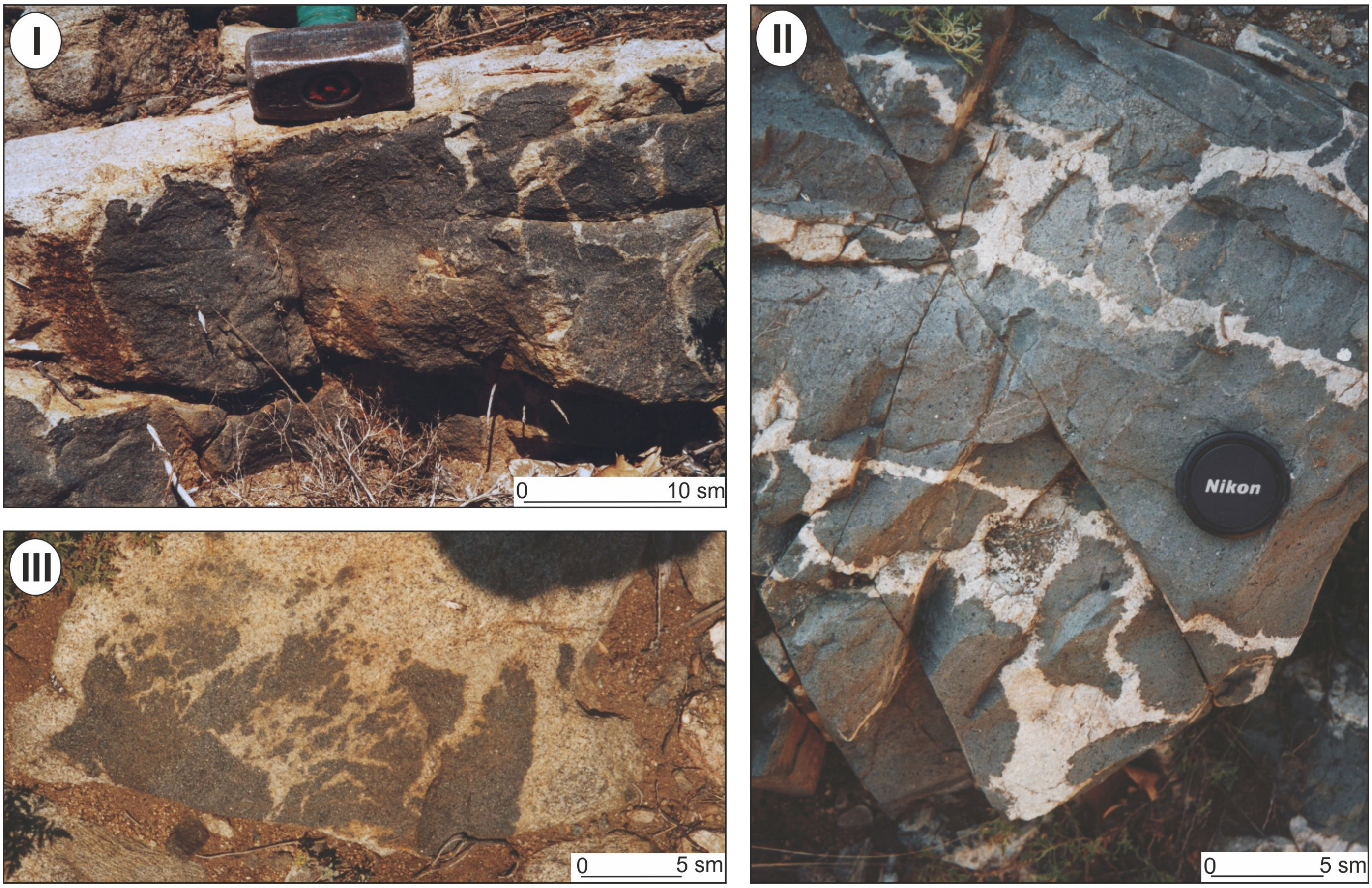

Fig. 5. The inner textute of mingling dykes on the right bank of the Erzin river (Erzin Site).

I-II – reticulate-cuspate contacts between granite and diorite in composite dykes with dominatant basic-rock component; III – complex patchy morphology of the mingling dyke.

Рис. 5. Внутренняя структура минглинг-даек на правобережье р. Эрзин («Эрзинский» участок).

I-II – сетчато-фестончатый контакт гранитов и диоритов в комбинированных дайках с резким преобладанием базитовой составляющей; III – сложнопятнистая морфология минглинг-дайки.

The diorite-granite contact is marked by smooth contours without any transitional zone as clearly evidenced by grain sizes and compositions of the rocks in the microsections and rock slices (Fig. 8). In the endocontact of diorites, observed are glomero-clusters of leust-biotite and a poikilite structure composed by quartz aggregates with inclusions of fine-grained idiomorphic crystals of biotite and amphibole (Fig. 8, II). In the contact zone, granites are characterized by porphyric inclusions of quartz and xenomorphic 'blurred' fine-grained aggregates of quartz, plagioclase and K-Na feldspar. Boundaries between the minerals are indistinct and patchy. Round-shaped porphyric grains of quartz are attenuated by cloud in crossed polars of a microscope.

The smooth contrasting contacts without any indicators of shifting of the original composition give evidence of the rapid crystallization of the basic-rock and granite melts, and the 'gradual' transition zones observed at the macro- and micro-levels may suggest that the lowest-melt-point minerals of granite and diorite were subject to recrystallization, or elements (K, Na, Ca, and Ti) were exchanged by diffusion between the rocks of contrasting compositions, or the rocks have not consolidated yet.

5. Petro- and geochemical characteristics of composite dykes

In the area between the Erzin and Naryn rivers (*Strelka Site*), granites are represented by midalkaline peraluminous (A/CNK=0.94–1.14) granosyenites and two-feldspar granites (Fig. 9). Average contents of petrogenic elements are given in Table 1. Rare-earth-element (REE) scatter diagrams and spider diagrams show that granite and granosyenite are characterised by negative slopes of the spectrum and high contents

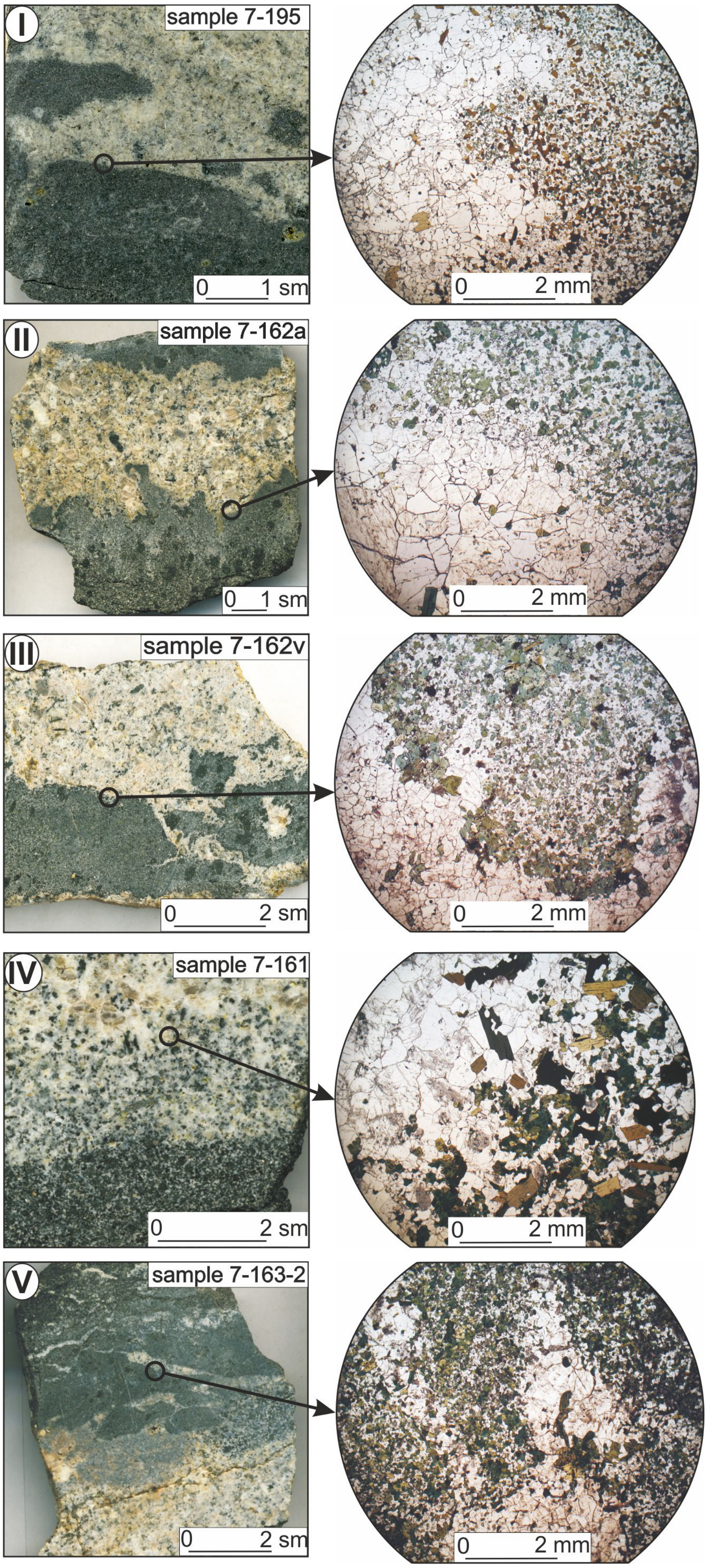

Fig. 6. Microtextures of contacts between basic rocks and granite in composite dykes in the area between the Erzin and Naryn rivers (Strelka Site). Left – rock slice texture; right – fragment in the corresponding transparent microsection (translucent light).

I – smooth contrasting contact between basic rocks and granite in the rock plate; in the microsection, it is sinuous; II – smooth flame-shaped contact between basic rocks and granite in the rock slice; a small transition zone is noted in the microsection; III – complex 'lacerated' flame-shaped contact between basic rocks and granite; it is clearly visible in both the rock slice and the microsection that the basic rocks become more melanocratic towards the contact; IV – gradual assimilation of the gabbro vein in granite; granosyenite and rocks in the transition zone are clearly distinguished in the microsection; V – complex contact between basic rocks and granite; the transition zone is composed of coarse- to fine-grained rocks with small nodules of basic rocks and contains; fractures are filled with rocks of the transitional composition and granite.

Рис. 6. Микроструктурная характеристика контактов и взаимоотношений базитов и гранитоидов в комбинированных дайках междуречья Эрзина и Нарына (участок «Стрелка»). Ряд слева – структурно-текстурная характеристика в пластинке, ряд справа – соответствующий фрагмент структуры в прозрачном петрографическом шлифе (проходящий свет).

I – контрастный ровный контакт базитов и гранитоидов в пластинке на микроуровне образует «заливообразный» контур; II – пламеневидный контакт базитов с гранитоидами в пластинке характеризуется ровной границей между базитами и гранитоидами с узкой переходной зоной; III – сложный «рваный», пламеневидный контакт базитов и гранитоидов. В шлифе и пластинке отчетливо видно увеличение меланократовости базитов в приближении к контакту; IV – постепенная ассимиляция габброидной жилы в гранитоидах. На микроуровне отчетливо различаются граносиениты и породы переходной зоны; V – сложный контакт базитов и гранитоидов с образованием переходной зоны, сложенной породами разной зернистости, мелкими нодульными агрегатами базитов и трещинами, заполненными породой переходного состава и гранитоидами.

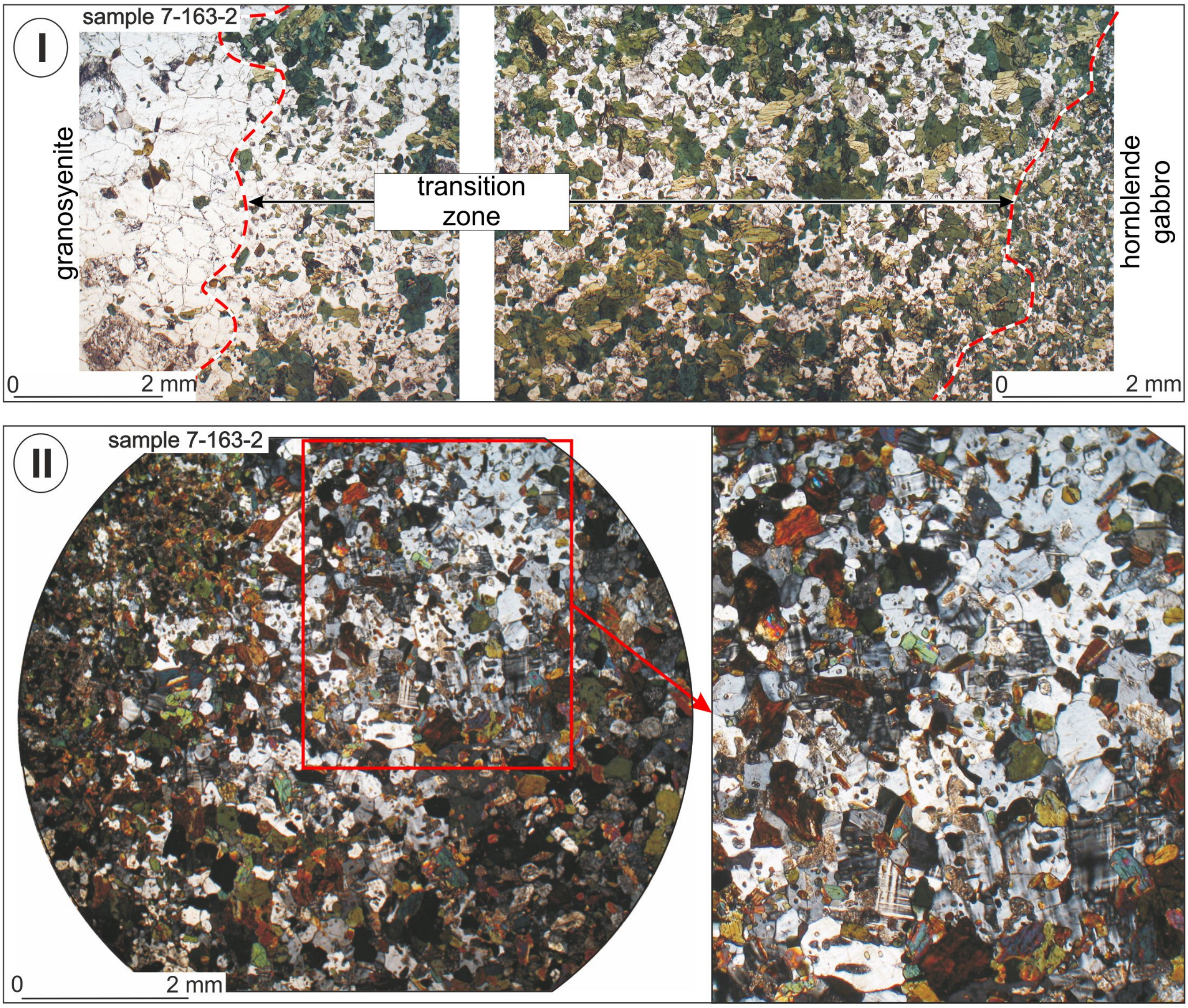

Fig. 7. Petrography of rocks in the zone of transition from basic rocks to granites in mingling dikes in the area between Erzin and Naryn rivers (Strelka Site).

I – transition zone at the contact between granosyenite and hornblende gabbro (translucent-light photos); II – poikilitic texture of potassium feldspar in the transition zone (crossed-nicols photos).

Рис. 7. Петрографический состав пород переходной зоны между базитами и гранитоидами в комбинированных дайках междуречья рек Эрзин и Нарын (участок «Стрелка»).

I – строение переходной зоны в контакте граносиенитов и роговообманковых габбро (снимки сделаны в проходящем свете); II – пойкилитовая структура калиевого полевого шпата в породах переходной зоны (снимки сделаны в скрещенных николях).

of REE. Light REE dominate over heavy REE: (La/Yb)n=8.37–16.04. A negative Eu anomaly is poorly expressed (Eu/Eu*=0.56–0.64). Multi-element spectra show negative slopes, large-ion lithophile elements (LILE) enrichment, and sharp minimums of Nb, Ti and Sr, as well as maximums of Zr and Hf (Table 2, and Fig. 10).

The REE scatter in gabbroids composing the mingling dykes on Strelka Site (see Table 1) is characterized by a sloping negative spectrum with a weak positive Eu anomaly (Eu/Eu*=1.15). The content of REE is high, and light REE dominate over heavy REE: (La/Yb)n=5.87–6.77. Multi-element spectra show LILE enrichment, sharp minimums of Nb and Sr, and insignificant values of Ti (Table 2, and Fig. 10).

On the right bank of the Erzin river (*Erzin Site*), the salic mingling dykes are composed of normal- and medium-alcaline, high- and medium-potassium, peraluminous (A/CNK=0.97–1.20) granite and leucogranite (see Table 1 and Fig. 9). According to the REE

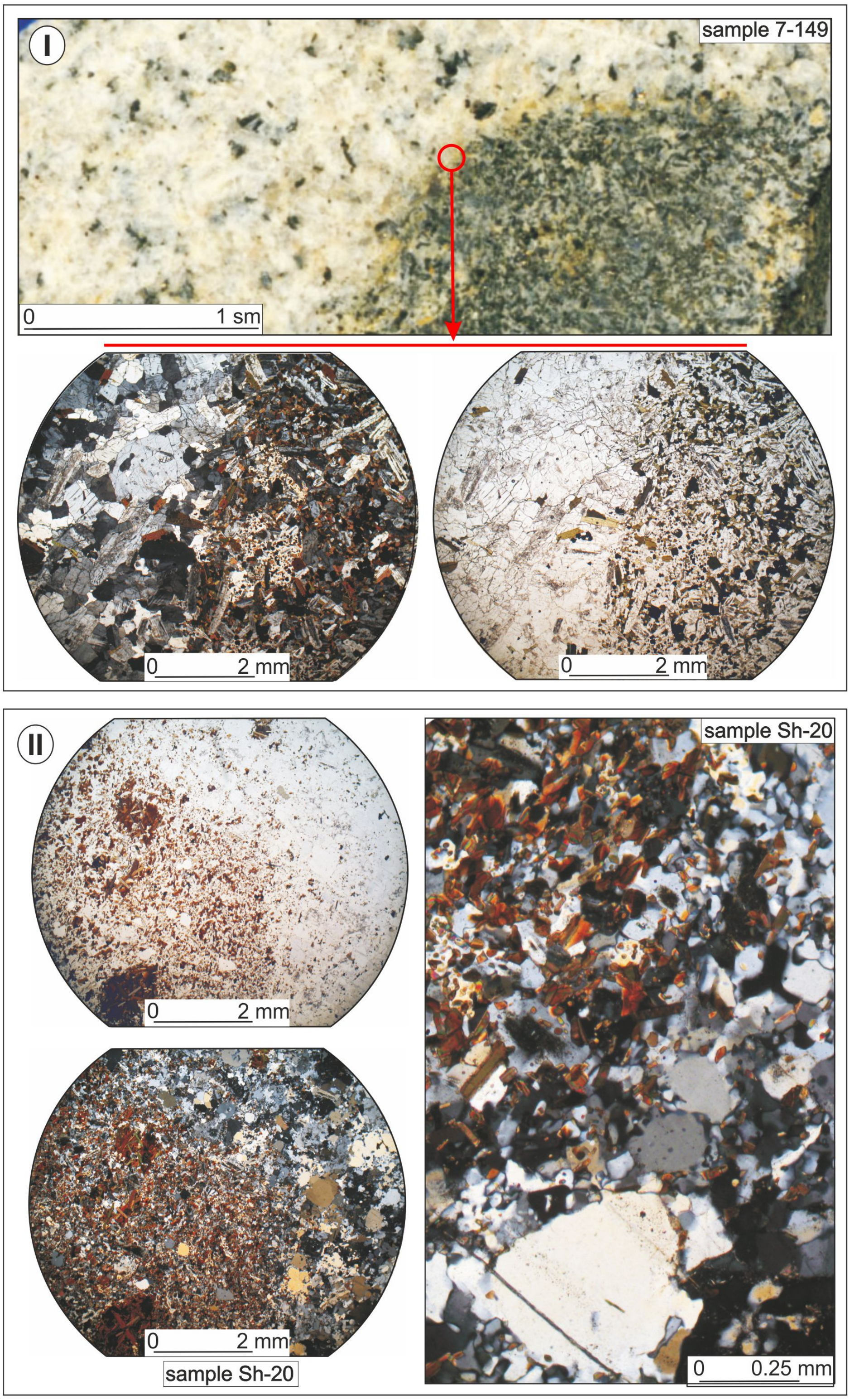

Fig. 8. Typical contacts and relations between basic rocks and granite in mingling dykes on the right bank of the Erzin river (Erzin Site).

I – smooth contact between basic rocks and granite; a poikilitic structure is observed in diorite (translucent-light and crossed-nicols photos); II – biotite glomero-clusters; a poikilitic structure and porphyric-quarts inclusions at the contact between diorite and leukogranite.

Рис. 8. Характерные контакты и взаимоотношения базитов и гранитоидов в минглинг-дайках на правобережье р. Эрзин («Эрзинский» участок).

I – ровный контакт базитов и гранитоидов; в шлифе со стороны диоритов наблюдается пойкилитовая структура (фотографии шлифов сделаны в проходящем свете и скрещенных николях); II – гломероскопления биотита. Пойкилитовая структура и порфировидные вкрапленники кварца в контакте диоритов и лейкогранитов.

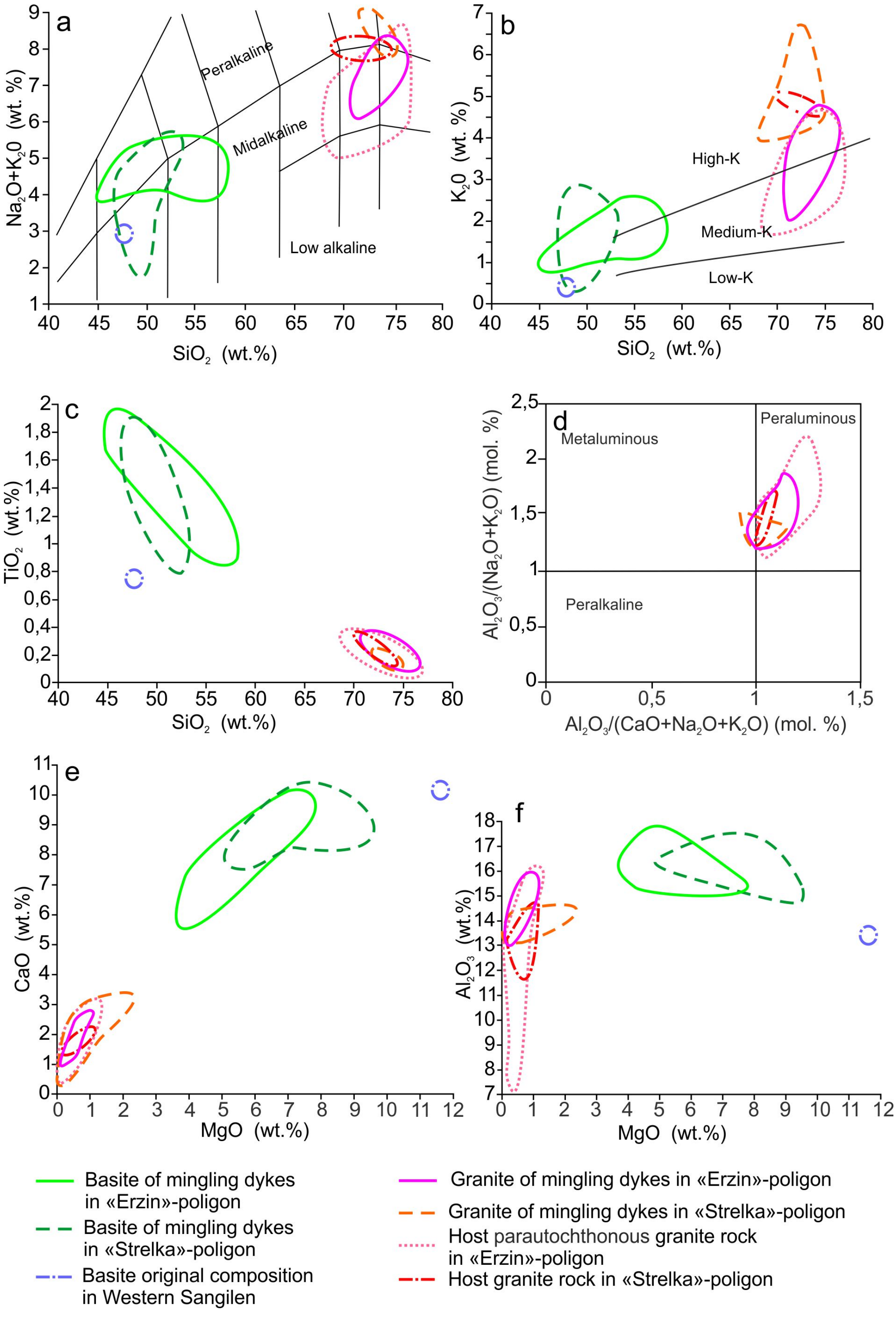

Fig. 9. Petrochemical diagrams. Comparison of compositions of the original basic rocks and host granite of the Nizhneerzin massif, and parautochtonous granite of the Erzin migmatite-granite complex and rocks in composite dykes.

Fig. 9a and b – classification boundaries according to [*Petrographic Code*.., *2009*] and [*Le Maitre et al*., *1989*], respectively. Fig. 9c – Harker's diagram SiO_2–TiO_2. Fig. 9d – Shand's diagram [*Maniar, Piccoli*, *1989*]. Fig. 9e and f – binary diagrams MgO–CaO и MgO–Al_2O_3, respectively.

Рис. 9. Петрохимические графики сравнения состава исходного базитового расплава и вмещающих гранитоидов Нижнеэрзинского массива и параавтохтонных гранитов эрзинского мигматит-гранитного комплекса с составами комбинированных даек.

Рис. 9a – классификационные границы [*Petrographic Code*.., *2009*]; рис. 9b – классификационные границы [*Le Maitre et al*., *1989*]; рис. 9c – диаграмма Харкера SiO_2–TiO_2; рис. 9d – диаграмма Шенда [*Maniar, Piccoli*, *1989*]; рис. 9e–f – бинарные диаграммы MgO–CaO и MgO–Al_2O_3.

Table 1. **Content of petrogenic oxides (wt %) in mingling dykes of West Sangilen**

Таблица 1. **Содержание петрогенных оксидов (мас. %) в минглинг-дайках Западного Сангилена**

Component	Rocks of mingling dykes on Strelka Site		Rocks of mingling dykes on Erzin Site		Source melt
	Mafic dykes (n=27)	Salic dykes (n=8)	Mafic dykes (n=21)	Salic dykes (n=12)	
SiO_2	47.45 – 52.9 / 49.22	62.76 – 74.52 / 71.56	45.48 – 57.76 / 53.57	66.31 – 76.01 / 73.13	47.84
TiO_2	0.79 – 1.89 / 1.4	0.12 – 0.93 / 0.38	0.88 – 1.93 / 1.30	0.13 – 0.78 / 0.28	0.75
Al_2O_3	14.86 – 17.09 / 16.24	13.21 – 14.43 / 13.37	15.40 – 17.61 / 16.57	13.19 – 15.86 / 14.10	13.42
Fe_2O_3*	7.69 – 12.79 / 10.96	1.27 – 7.35 / 2.96	8.07 – 12.38 / 9.80	1.36 – 4.34 / 2.50	11.52*
MnO	0.11 – 0.18 / 0.17	<0.01 – 0.09 / 0.03	0.12 – 0.23 / 0.17	<0.01 – 0.12 / 0.05	-
MgO	5.09 – 9.40 / 7.73	0.14 – 2.26 / 0.64	3.84 – 7.66 / 4.92	0.19 – 1.00 / 0.50	11.62
CaO	7.59 – 10.29 / 9.22	1.13 – 3.24 / 1.61	5.61 – 10.00 / 7.46	1.21 – 2.63 / 1.74	10.16
Na_2O	1.41 – 3.75 / 2.52	2.23 – 3.64 / 3.14	2.28 – 3.73 / 2.91	2.89 – 4.64 / 3.50	2.51
K_2O	0.41 – 2.66 / 1.15	3.40 – 6.65 / 4.92	0.88 – 2.46 / 1.80	1.59 – 4.65 / 3.71	0.41
P_2O_5	0.16 – 0.66 / 0.32	<0.01 – 0.32 / 08.11	0.27 – 0.58 / 0.39	0.04 – 0.25 / 0.10	-
Alum slate index	-	0.94 – 1.14 / 1.03	-	0.97 – 1.20 / 1.09	

Note. Above the line – variations of contents of petrogenic components; under the line – average content; n – number of samples; Fe_2O_3* – total content of Fe in Fe_2O_3; the Fe content in the source melt is given in FeO; the alum slate index is $Al_2O_3/(CaO+K_2O+Na_2O)$ (mol. %) [*Maniar, Piccoli*, *1989*]. Contents of petrogenic elements were analysed by the 'wet' chemical method (Assayer N.N. Ukhova, IEC SB RAS, Irkutsk) and the X-ray fluorescence analysis method using SRM-25 installation (Assayer A.D. Kireev, V.S. Sobolev IGM SB RAS, Novosibirsk).

Примечание. Над чертой – вариации содержаний петрогенных компонентов, под чертой – среднее содержание; n – число проб; Fe_2O_3* – суммарное железо в форме Fe_2O_3, для исходного расплава содержание железа указано в форме FeO; индекс глиноземистости – $Al_2O_3/(CaO+K_2O+Na_2O)$ (мол. %) [*Maniar, Piccoli*, *1989*]. Анализ содержания петрогенных элементов выполнен методом «мокрой» химии (аналитик – Н.Н. Ухова, ИЗК СО РАН, г. Иркутск) и методом РФА на установке СРМ-25 (аналитик – А.Д. Киреев, ИГМ им. В.С. Соболева СО РАН, г. Новосибирск).

scatter diagrams, granite is characterized by a sharp domination of light REE over heavy REE: $(La/Yb)_n$= =7.42–13.10. A Eu anomaly is absent (Eu/Eu*=0.96–1.06). Multi-element spectra show negative slopes, LILE enrichment, and low contents of HFSE. Sharp minimums are noted for Ti and Nb (Table 2, and Fig. 10).

The melanocratic composite dykes located on Erzin Site are composed of diorite and quartz diorite (see Table 1, and Fig. 9). The REE scatter shows a sloping negative spectrum and a high content of REE (381 g/t), and a Eu anomaly is absent (Eu/Eu*=0.94–1.17). There is an insignificant domination of light REE over heavy REE: $(La/Yb)_n$=4.62–7.99. In spider diagrams, minimums are noted for Ti and Nb (Table 2, and Fig. 10).

6. Correlation between compositions of composite dykes and igneous complexes of West Sangilen

In West Sangilen, the largest basic-rock massifs are Bashkymugur, Erzin and Bayankol (490–460 Ma) that are composed of gabbro-monzodiorite originating from source magmas of similar compositions, as suggested by results of mineralogical, petrographical and petrochemical studies of the basic rocks [*Shelepaev, 2006*].

Т a b l e 2. **Contents of petrogenic elements (wt %), rare and rare-earth elements (g/t) in representative samples of basic rocks and granite from mingling dykes of West Sangilen**

Т а б л и ц а 2. **Содержания петрогенных элементов (мас. %), редких и редкоземельных элементов (г/т) в представительных пробах базитов и гранитов из минглинг-даек Западного Сангилена**

Component	Rocks of mingling dykes on Strelka Site					Rocks of mingling dykes on Erzin Site					
	Mafic dykes		Salic dykes			Mafic dykes				Salic dykes	
	7-158-2	7-192-3	7-159	7-160	7-163-2	7-149-3	7-153-1	7-153-2	BC-402	7-149	7-150
SiO_2	52.24	51.25	73.24	62.76	72.30	57.11	45.48	46.05	48.45	73.35	66.31
TiO_2	0.79	1.23	0.20	0.93	0.22	1.12	1.64	1.93	1.83	0.18	0.78
Al_2O_3	15.91	16.36	14.01	14.43	13.21	16.00	15.40	15.68	16.69	14.01	15.86
Fe_2O_3*	7.69	9.82	1.54	7.37	1.77	8.07	12.17	12.38	11.41	2.05	4.34
MnO	0.11	0.18	0.01	0.06	0.01	0.12	0.15	0.16	0.17	0.03	0.11
MgO	6.24	5.66	0.22	2.26	0.55	3.84	7.66	7.05	6.05	0.38	1.00
CaO	9.44	7.59	1.35	3.24	1.19	5.61	9.36	10.00	8.41	1.71	2.63
Na_2O	3.37	3.69	3.64	3.55	2.23	3.17	2.87	3.06	3.73	3.75	4.64
K_2O	1.53	1.75	4.96	3.40	6.65	2.27	1.05	0.88	1.39	4.08	3.63
P_2O_5	0.17	0.32	0.05	0.32	0.05	0.33	0.27	0.27	0.42	0.07	0.25
Loss on ignition (LOI)	2.12	2.09	0.38	1.47	0.66	2.22	1.81	1.84	1.67	0.22	0.71
Total	**100.24**	**99.63**	**99.83**	**99.96**	**98.96**	**99.57**	**99.58**	**99.87**	**99.80**	**99.98**	**100.20**
Rb	47	50	117	111	145	61	19.1	11.6	28	70	77
Sr	657	497	179	263	506	525	439	459	619	308	438
Y	18.5	27	32	51	13.1	30	24	25	31	10	44
Zr	72	130	115	331	76	170	133	142	137	161	432
Nb	4.5	7.1	8.2	7.9	8.0	9.9	13.3	12.8	6.5	4.9	17.0
Cs	0.29	0.79	1.87	1.36	1.10	0.32	1.11	0.54	0.25	1.44	1.54
Ba	156	369	901	1029	1141	601	173	181	505	1077	1262
La	15.9	19.2	35	46	27	31	13.3	13.8	26	24	43
Ce	35	43	67	93	45	63	29	31	57	41	91
Pr	4.9	6.2	7.8	13.8	4.9	8.6	4.3	4.5	8.5	5.0	12.8
Nd	19.8	25	27	55	16.1	32	17.9	19.5	34	16.2	48
Sm	4.0	4.9	4.7	11.5	2.5	5.9	4.2	4.5	6.6	2.4	9.6
Eu	1.46	1.90	0.84	2.3	0.50	1.85	1.59	1.67	2.6	0.71	3.2
Gd	3.6	5.1	4.3	11.1	2.3	5.9	4.5	4.9	6.9	1.99	8.5
Tb	0.53	0.75	0.73	1.61	0.35	0.86	0.67	0.73	0.92	0.30	0.86
Dy	2.8	4.3	4.2	8.4	2.0	4.6	3.9	4.1	5.2	1.38	6.6
Ho	0.54	0.83	0.89	1.61	0.40	0.91	0.78	0.81	0.97	0.28	1.34
Er	1.59	2.3	2.8	4.5	1.15	2.6	2.1	2.2	2.8	0.92	3.9
Tm	0.24	0.35	0.46	0.62	0.18	0.40	0.30	0.32	0.41	0.18	0.62
Yb	1.59	2.2	2.8	3.6	1.15	2.6	1.94	1.99	2.5	1.21	3.9
Lu	0.24	0.35	0.42	0.51	0.18	0.40	0.28	0.30	0.37	0.19	0.59
Hf	2.2	3.2	3.9	8.4	2.5	4.5	3.3	3.5	3.2	4.2	9.5
Ta	0.38	0.43	0.92	0.38	0.80	0.73	0.78	0.78	0.32	0.43	1.10
Th	2.8	3.0	19.5	3.0	16.4	7.9	1.08	1.17	1.17	7.6	9.0
U	1.37	1.32	2.7	0.78	0.83	3.4	0.36	0.33	0.63	0.99	3.6

N o t e. Fe_2O_3* – total Fe in Fe_2O_3. Contents of petrogenic elements (wt %) were analysed by the 'wet' chemical method (Assayer N.N. Ukhova, IEC SB RAS, Irkutsk). Contents of rare elements (g/t) were analysed by the ICP-MS method (Assayer I.V. Nikolaeva, V.S. Sobolev IGM SB RAS, Novosibirsk).

П р и м е ч а н и е. Fe_2O_3* – суммарное железо в форме Fe_2O_3. Анализ содержания петрогенных элементов выполнен методом «мокрой» химии (аналитик – Н.Н. Ухова, ИЗК СО РАН, г. Иркутск), содержание компонентов приведено в мас. %. Анализы редких элементов выполнены методом ICP-MS (аналитик И.В. Николаева, ИГМ им. В.С. Соболева СО РАН, г. Новосибирск), содержание компонентов приведено в г/т.

It is assumed that the source magma corresponds by its composition to olivine basalt or olivine gabbronorite [*Egorova, 2005*] (see Table 1 and Fig. 9).

The mingling dykes located on Erzin and Strelka Sites have similar compositions of the basic rocks which differ from the source magma composition by contents of TiO2 and MgO. An insignificant difference is noted between contents of alkalies in the source melt and in the basic rocks from the dykes. The REE scatter diagrams and the spider diagrams (see Fig. 10) show similar spectra and similar absolute values. Minimums are noted for Nb, Th, Hf, and Ti.

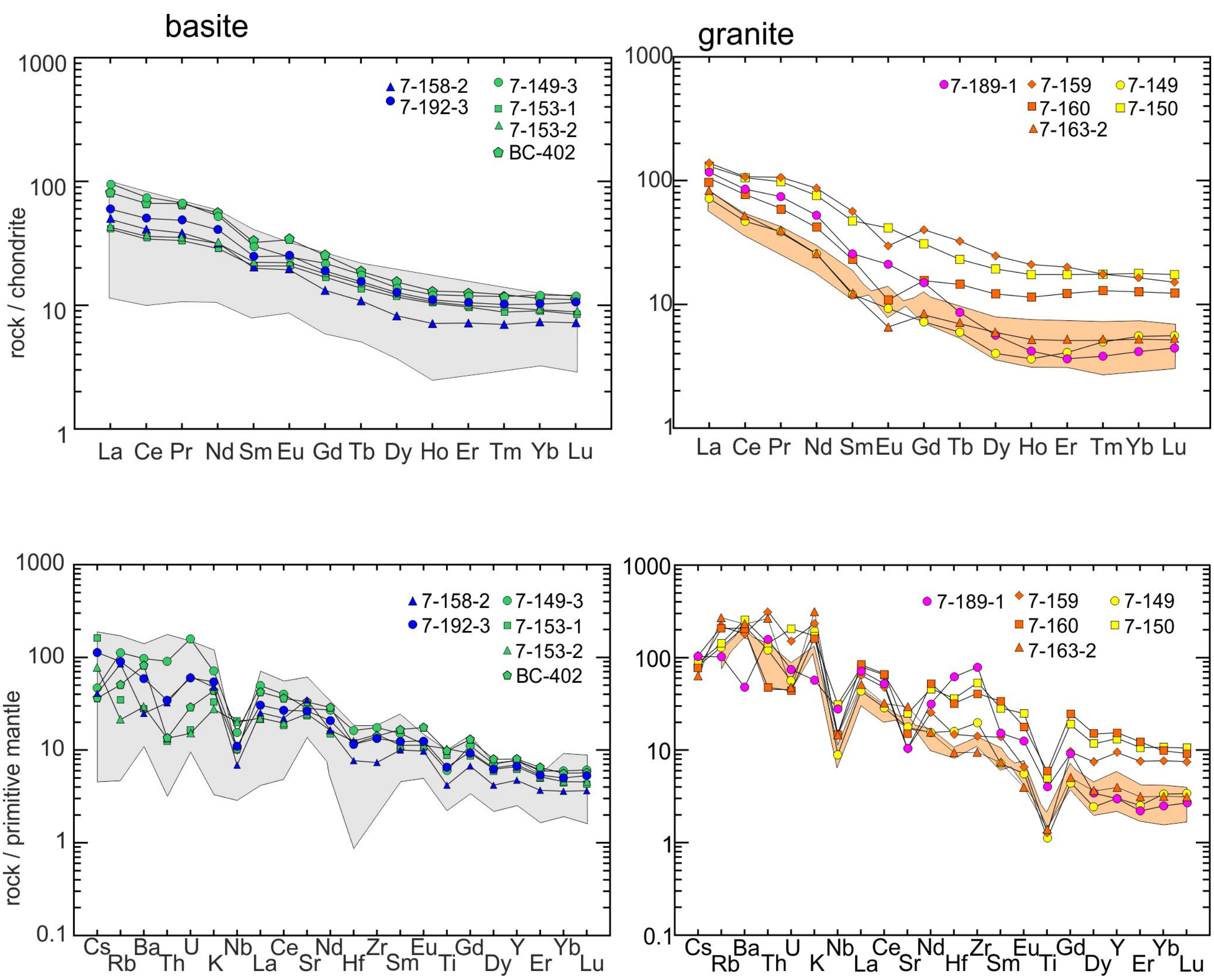

Fig. 10. REE scatter diagrams and spider diagrams for basic rocks and granite from mingling dykes and magmatic complexes of West Sangilen.

Basic rocks: 7-158-2, 7-192-3 – Strelka Site; 7-149-3, 7-153-1, 7-153-2, and BC-402 – Erzin Site; area in grey – olivine gabbronorite of the Bashkymugur massif [*Egorova*, *2005*]. Granite: 7-189-1 – host granite on Strelka Site; 7-159, 7-160, and 7-163-2 – Strelka Site; 7-149, and 7-150 – Erzin Site; area in orange – host parautochtonous granite on Erzin Site [*Karmysheva*, *2012*]. The REE contents are normalized to CI contents in chondrite [*Boynton*, *1983*]. In the spider diagrams, normalization is done to CI contents in the primitive mantle [*Taylor*, *McLennan*, *1985*].

Рис. 10. Спектры распределения РЗЭ и спайдер-диаграммы для базитов и гранитов минглинг-даек и магматических комплексов Западного Сангилена.

Базиты: 7-158-2, 7-192-3 – участок «Стрелка»; 7-149-3, 7-153-1, 7-153-2, BC-402 – участок «Эрзинский»; серое поле – оливиновый габбронорит Башкымугурского массива [*Egorova*, *2005*]. Граниты: 7-189-1 – вмещающие гранитоиды на участке «Стрелка»; 7-159, 7-160, 7-163-2 – участок «Стрелка»; 7-149, 7-150 – участок «Эрзинский»; оранжевое поле – параавтохтонные вмещающие граниты на участке «Эрзинский» [*Karmysheva*, *2012*]. Содержания РЗЭ нормированы по содержанию в хондрите CI [*Boynton*, *1983*]. На спайдер-диаграммах содержания нормированы к таковым в примитивной мантии [*Taylor, McLennan*, *1985*].

Considering the similarity of the petrochemical composition of the basic rocks from the mingling dykes and the composition of the source basic rocks, it can be suggested that the mafic dykes originated from the same upper mantle or intruded from the same magma chamber as the large gabbro-monzodiorite massifs of West Sangilen. Figure 9 shows an insignificant difference between compositions of the basic rocks of the mingling dykes located on the different sites. The composition of the basic rocks from the dykes on Strelka Site are closer to the composition of the source basic-rock melt, while the basic rocks from the dykes on Erzin Site are more felsic, which may suggest hybridization with either host rocks or granite of the dykes proper.

In samples from the different sites, compositions of granite from the mingling dykes are practically similar, with insignificantly different contents of potassium.

The Nizhneerzin massif (486+10 Ma – Rb-Sr) [*Petrova, 2001*]; 491.6+9.5 Ma – U-Pb [*Kozakov et al., 1999*]) is composed of porphyric granosyenite (see Fig. 9). Lines in the REE scatter diagrams and the multi-element spectra of granite from the mingling dykes on Strelka Site and the host porphyric granite from the Nizhneerzin massif are practically coincident. Minimums are noted for Nb, Sr, and Ti. A noticeable difference is the lacking Eu minimum in granite from the Nizhneerzin massif, while the Eu minimum is expressed in granite of the composite dykes, and the Zr maximum is evident in the host rocks (see Fig. 10).

On Erzin Site, parautochthonous granite of the Erzin complex (which is the host rock for the composite dykes) is represented by peraluminous, medium-fine-grained, poorly foliated, garnet-containing biotite granite [*Karmysheva, 2012*]. In the REE scatter diagrams and the spider diagrams, the spectra of the host granite and granite from the mingling dykes are coincident, and typical minimums for Nb and Ti and maximums for K and Zr are noted (see Fig. 10).

7. Discussion of results

Based on the available geological data, the composite/mingling dykes of West Sangilen are classified into two types. Their textures are studied at the macro- and micro-levels, and the petrochemical characteristics are subject to comparative analyses. Results of our studies give grounds to conclude that specific features of the mingling dykes are predetermined by geological settings of their formation, depths and duration of tectonic and magmatic processes.

Composite dykes in the area between the Erzin and Naryn (*Strelka Site*). By its texture, granite from the mingling dykes located on Strelka Site does not differ much from the host porphyric granite from the Nizhneerzin massif containing the rocks that are either not deformed or show rare traces of flow in the fine-grained rock samples. In felsic composite dykes, traces of deformation are absent, while indicators of recrystallization of K-Na feldspar, plagioclase, quartz and biotite are present.

The model proposed in [*Huppert, Sparks, 1988*] can provide an explanation of the similarity between the petrochemical compositions of granite from the Nizhneerzin massif and granite from the mingling dykes [*Vasyukova et al., 2008*]. According to the above-mentioned model, the host granite is partially melted due to the intrusion of the basic rocks which leads to mechanical mixing of the melts contrasting in composition and rheologial properties. Consequently, the chemical composition is inherited, and specific mingling textures and structures, such as reticulate-cuspate structures and round-shaped basic-rock bodies cut by thin veins of granite, are formed. Using the model, it is possible to explain specific petrogeochemical properties of the composite dykes and the local reomorphism of granite in the Nizhneerzin massif, which took place when the basic rocks intruded into granite. However, the model fails to explain the tectonic position of the composite dykes on Strelka Site.

The intrusion of granite of the Nizhneerzin massif took place at the post-collisional stage of the orogen's evolution in conditions when the compression regime was replaced by the extension regime (480–490 Ma) [*Vladimirov et al., 2005*]. As of the time of the Nizhneerzin massif emplacement, the crust was locally disturbed and thinned due to developing extension of the Erzin metamorphic block along the Erzin and Kokmolgarga shear faults, and the basic-rock melts were uplifted and intruded into the extension zones.

As of the time of the basic-rock intrusions, granite of the Nizhneerzin massif was only partially consolidated, as evidenced by structures and textures of the composite dykes, such as non-linear 'patchy' outlets of the mingling dykes in the massif's body, their vague contacts with the host granite, lacking indicators of deformation, the presence of zones with mixed basic rocks and granite, and diffusional smoothing of the compositions in high-temperature conditions.

The absence of active penetrating tectonic deformation is also evidenced by the similar petrochemical compositions and similar scatter of LILE and HFSE in the host granite and granite of the mingling dykes, i.e. melting and recrystallization of the source granite took place practically in a closed system.

It is most likely that the dykes were formed at mesoabyssal or abyssal depths, and the subliquidus heat regime was thus maintained for a long time, and even the smallest portions of the basic-rock melt were consolidated through quite a long period of time. Indicators of deformation are thus absent in the composite dykes, and transition zones and hybridization are observed.

The composite dykes on the right bank of the Erzin river (*Erzin Site*) were formed in the period of active extension of the Sangilen fragment of the orogen which took place along the systems of shear zones (460–430 Ma) [*Vladimirov et al., 2005*] and was accompanied by the intrusion of the Bashkymugur gabbro-monzodiorite massif (464.6±5.7 Ma – U-Pb [*Kozakov et al., 1999*], 465±1.2 Ma – Ar-Ar [*Izokh et al., 2001*], 464±5 Ma – Rb-Sr [*Petrova, 2001*]). In the same period, the Erzin shear zone was active; later on, its integrity was disturbed by fractures, faults and veins, and it was fragmented [*Vladimirov et al., 2005*]. The occurrence of conjugated fault systems facilitated the formation of local extension zones, provided favourable conditions for intrusions of felsic melts and basic-rock melts and predetermined positions of the composite dykes.

Our assumption that the dykes intruded and emplaced in conditions of the tectonically active zone is supported by many indicators, including positions of the composite dykes in the Erzin shear zone, abrupt transversal contacts with the host rocks, pegmatoids in the decompression zones, the presence of oxygon xenoliths in the composite dykes etc. Besides, due to low temperatures, the main melts were efficiently chilled and consolidated, as evidenced by textures of the mingling dykes which show contrasting contacts with both the host rocks and between the basic rocks and granite, lacking zones of hybridization, the presence of chill zones and indicators of recrystallization of the minerals.

The observed difference between the basic rocks in the first group of mingling dykes from the source composition of the basic rocks in West Sangilen may suggest potential contamination and/or differentiation of the mafic melt during its assent to the upper crustal layers.

Our model showing the intrusion of the melts of contrasting compositions on Erzin Site in the same-name shear zone takes into account the structural and textural characteristics of the rocks, positions of fine-grained granites (mainly in the marginal parts of the mingling dykes), melting of granites (evidenced by the thin rock samples), and petrochemical compositions of the rock samples.

The composite dykes of this type intruded and emplaced when the shear zone was subject to extension and fragmentation, which predetermined active intrusion of basic and, possibly, felsic melts through conjugated faults and rapid crystallization of the melts. Crystallization of the melts was rapid, and their potential heat impact on the adjoining rocks was thus excluded, as evidenced by the presence of oxygonal chips of igneous and host metamorphic rocks, vein pegmatoid intrusions, and composite dykes of the reticulate-cuspate texture with the dominating basic rock component.

8. Main conclusions

Two groups of mingling dykes are distinguished in the Sangilen upland. The dykes in both groups originated from one and the same basic melt source. However, mingling of the contrasting melts was carried out by different mechanisms as suggested by two intrusion models.

In the first model, the basic-rock melts intrude into the non-consolidated granite melt and mix with it. In the second model, the felsic melt occurs due to heating by the mafic magmas, the melts are mechanically mixed, and mingling is controlled by tectonic processes, specifically extension and faulting.

According to the first model, the mingling dykes are related to the emplacement of the Erzin and Kokmolgarga shear zones at the early stage when the compression regime was replaced by the extension regime in the Sangilen fragment of the orogen (510–490 Ma). Intrusions of the basic-rock melts were accompanied by the formation of relatively large massifs of the basic composition, i.e. the Erzin and Bayankol gabbro-monzodiorite massifs, as well as by the occurrence of composite dykes that are abundant in the area between the Erzin and Naryn rivers.

The second stage (460–430 Ma) of the formation of composite dykes took place when the orogenic structure was subject to extension along the system of shear zones, and the Bashkymugur gabbro-monzodiorite massif was intruded and emplaced, and fracture-vein structures (including the composite dykes) were formed.

Isotope geochonological dating of the regional tectonic and magmatic events have yielded the ages that support the above conclusions.

9. Aknowledgments

The authors are grateful to A.E. Izokh (IGM SB RAS, Novosibirsk), A.A. Tsygankov (GI SB RAS, Ulan-Ude), G.N. Burmakina (GI SB RAS, Ulan-Ude), E.V. Sklyarov (IEC SB RAS, Irkutsk) for valuable discussions, T.V. Donskaya (IEC SB RAS, Irkutsk) for supporting our analytical studies, and I.V. Nikolaeva (IGM SB RAS, Novosibirsk) and N.N. Ukhova (IEC SB RAS, Irkutsk) for their analytical studies.

The study was supported by Joint Project of the Siberian and Ural Branches of RAS No. IP – Magmatism, Metamorphism and Ore-Generating Potential of Altaides and Uralides, RBRF Projects Nos. 13-05-01132, 14-05-00747 and 14-05-00498, RSF Project No. 15-17-10010, and Competitive Growth Programmes of the Tomsk and Novosibirsk State Universities.

10. References

Boynton W.V., 1983. Cosmochemistry of the rare earth elements: meteorite studies. In: P. Henderson (Ed.), Rare Earth Element Geochemistry. Elsevier, Amsterdam, p. 63–114. http://dx.doi.org/10.1016/B978-0-444-42148-7.50008-3.

Cook N.D.J., 1988. Diorites and associated rocks in the Anglem complex at the Neck, northeastern Stewart Island, New Zealand: an example of magma mingling. *Lithos* 21 (4), 247–262. http://dx.doi.org/10.1016/0024-4937(88)90031-X.

Didier J., Barbarin B., 1991. Enclaves and granite petrology. In: Developments in Petrology. V. 13. Elsevier, Amsterdam – Oxford – New York – Tokio, p. 545–549.

Dokukina K.A., Vladimirov V.G., 2005. Tectonic fragmentation of basaltic melt. *Doklady Earth Sciences* 401 (2), 182–186.

Egorova V.V., 2005. The Basic-Rock Melt Crystallization in Deep Magmatic Chambers for Example Gabbro Xenolites and Intrusions of Western Sangilen. Author's PhD thesis (Geology and Mineralogy). Novosibirsk, 20 p. (in Russian) [*Егорова В.В.* Кристаллизация базитового расплава в глубинных магматических камерах на примере габброидных ксенолитов и интрузий Западного Сангилена: Автореф. дис. … канд. геол.-мин. наук. Новосибирск, 2005. 20 с.].

Egorova V.V., Volkova N.I., Shelepaev R.A., Izokh A.E., 2006. The lithosphere beneath the Sangilen Plateau, Siberia: evidence from peridotite, pyroxenite and gabbro xenoliths from alkaline basalts. *Mineralogy and Petrology* 88 (3–4), 419–441. http://dx.doi.org/10.1007/s00710-006-0121-0.

Fedorovsky V.S., Khromykh S.V., Sukhorukov V.P., Kuibida M.L., Vladimirov A.G,. Sklyarov E.V., Dokukina K.A., Chamov S.N., 2003. Metamorphic mingling (a new type of mingling structure). In: Tectonics and geodynamics of continental crust: Proceedings of the XXXVI Tectonic Conference, vol. II. GEOS, Moscow, p. 255–259 (in Russian). [*Федоровский В.С., Хромых С.В., Сухоруков В.П., Куйбида М.Л., Владимиров А.Г., Скляров Е.В., Докукина К.А., Чамов С.Н.* Метаморфический минглинг (новый тип минглинг-структур) // Тектоника и геодинамика континентальной литосферы: Материалы XXXVI Тектонического совещания. М.: ГЕОС, 2003. Т. II. С. 255–259].

Frost T.P., Mahood G.A., 1987. Field, chemical, and physical constraints on mafic-felsic magma interaction the Lamarck granodiorite, Sierra Nevada, California, USA. *Geological Society of America Bulletin* 99 (2), 272–291. http://dx.doi.org/10.1130/0016-7606(1987)99<272:FCAPCO>2.0.CO;2.

Furman T., Spera F.J., 1985. Co-mingling of acid and basic magma with the implications for the origin of mafic I-type xenoliths: field and petrochemical ralations of an unusual dike complex at Eagle Lake, Sequoia National Park, California, USA. *Journal of Volcanology and Geothermal Research* 24 (1–2), 151–178. http://dx.doi.org/10.1016/0377-0273(85)90031-9.

Gambler J.A., 1979. Some relationships between coexisting granitic and basaltic magmas and the genesis of hubrid rocks in the Tertiary central complex of Slieve Gullion, northeast Ireland. *Journal of Volcanology and Geothermal Research* 5 (3–4), 297–316. http://dx.doi.org/10.1016/0377-0273(79)90021-0.

Huppert H.E., Sparks S.J., 1988. The generation of granitic magmas by intrusion of basalt into continental crust. *Journal of Petrology* 29 (3), 599–624. http://dx.doi.org/10.1093/petrology/29.3.599.

Izokh A.E., Kargopolov S.A., Shelepaev R.A., Travin A.V., Egorova V.V., 2001. Cambrian-Ordivician basic magmatism of Altai-Sayan region and associated HT/LP-type metamorphism. In: Actual problems of geology and minerageny of Southern Siberia: Conference Proceedings. Novosibirsk, p. 68–72 (in Russian) [*Изох А.Э., Каргополов С.А., Шелепаев Р.А., Травин А.В., Егорова В.В.* Базитовый магматизм кембро-ордовикского этапа Алтае-Саянской складчатой области и связь с ним метаморфизма высоких температур и низких давлений // Актуальные вопросы геологии и минерагении юга Сибири: Материалы научно-практической конференции. Новосибирск, 2001. С. 68–72].

Izokh A.E., Lavrenchuk A.V., Vasuykova E.A., 2004. The West Sangilen dyke complex as an Ordovician mantle magmatism result. In: Geodynamic evolution of the lithosphere of the Central Asian mobile belt (from ocean to continent). Issue 2, vol. 1. Institute of Geography SB RAS Publishing House, Irkutsk, p. 143–144 (in Russian). [*Изох А.Э., Лавренчук А.В., Васюкова Е.А.* Дайковый комплекс Западного Сангилена – проявление ордовикского мантийного магматизма // Геодинамическая эволюция литосферы Центрально-Азиатского подвижного пояса (от океана к континенту). Вып. 2. Иркутск: Изд-во Ин-та географии СО РАН, 2004. Т. 1. С. 143–144].

Karmysheva I.V., 2012. Synkinematic Granite and Collision-Shear Deformation in West Sangilen (South-East Tuva). Author's PhD thesis (Geology and Mineralogy). Novosibirsk, 16 p. (in Russian) [*Кармышева И.В.* Синкинематические граниты и коллизионно-сдвиговые деформации Западного Сангилена (ЮВ Тува): Автореф. дис. … канд. геол.-мин. наук. Новосибирск, 2012. 16 с.].

Kovalenko V.I., Yarmolyuk V.V., Kovach V.P., Kotov A.B., Kozakov I.K., Salnikova E.B., Larin A.M., 2004. Isotope provinces, mechanisms of generation and sources of the continental crust in the Central Asian mobile belt: geological and isotopic evidence. *Journal of Asian Earth Sciences* 23 (5), 605–627. http://dx.doi.org/10.1016/S1367-9120(03)00130-5.

Kozakov I.K., Sal'nikova E.B., Bibikova E.V., Kirnozova T.I., Kotov A.B., Kovach V.P., 1999. Polychronous evolution of the paleozoic granitoid magmatism in the Tuva-Mongolia Massif: U-Pb geochronological data. *Petrology* 7 (6), 592–601.

Kuzmichev A., 2004. Tectonic History of the Tuva-Mongolia Massif: Early Baikalian, Late Baikalian and Early Caledonian Stages. PROBEL-2000, Moscow, 192 p.

Kuzmichev A.B., Bibikova E.V., Zhuravlev D.Z., 2001. Neoproterozoic (similar to 800 Ma) orogeny in the Tuva-Mongolia Massif (Siberia): island arc-continent collision at the northeast Rodinia margin. *Precambrian Research* 110 (1–4), 109–126. http://dx.doi.org/10.1016/S0301-9268(01)00183-8.

Le Maitre R.W., Bateman P., Dudek A., Keller J., Lameyre M., Le Bas M.J., Sabine P.A., Schmid R., Sorensen H., Streckeisen A., Wooley A.R., Zanettin B., 1989. A Classification of Igneous Rocks and a Glossary of Terms. Blackwell Scientific Publications, Oxford, 193 p.

Litvinovsky B.A., Zanvilevich A.N., Lyapunov S.M., Bindeman I.N., Devis A.M., Kalmanovich M.A., 1995. Conditions for formation of composite basic-rock–granite dykes (Shaluta pluton, Transbaikalia). *Geologiya i Geofizika* (*Russian Geology and Geophysics*) 36 (7), 3–22 (in Russian) [*Литвиновский Б.А., Занвилевич А.Н., Ляпунов С.М., Биндеман И.Н., Дэвис А.М., Калманович М.А.* Условия образования комбинированных базит-гранитных даек (Шалутинский массив, Забайкалье) // *Геология и геофизика*. 1995. Т. 36. № 7. С. 3–22].

Maniar P.D., Piccoli P.M., 1989. Tectonic discrimination of granitoids. *Geological Society of America Bulletin* 101 (5), 635–643. http://dx.doi.org/10.1130/0016-7606(1989)101<0635:TDOG>2.3.CO;2.

Marshall L.A., Sparks R.S.J., 1984. Origin of same mixed-magma and net-veined ring intrusions. *Journal of the Geological Society*, *London* 141 (1), 171–182. http://dx.doi.org/10.1144/gsjgs.141.1.0171.

Nardi L.V.S., de Lima E.F., 2000. Hybridisation of mafic microgranular enclaves in the Lavras granite complex, Southern Brazil. *Journal of South American Earth Sciences* 13 (1–2), 67–78. http://dx.doi.org/10.1016/S0895-9811(00)00006-7.

Perugini D., Poli G., 2005. Viscous fingering during replenishment of felsic magma chambers by continuous input of mafic magmas: Field evidence and fluid-mechanics experiment. *Geology* 33 (1), 5–8. http://dx.doi.org/10.1130/G21075.1.

Petrographic Code of Russia, 2009. Magmatic, Metamorphic, Metasomatic, and Impact Formations. Third edition, corrected and supplemented. VSEGEI Press, Saint-Petersburg, 200 p.

Petrova A.Yu., 2001. Rb-Sr Isotop System of Metamorphic and Magmatic Rocks in West Sangilen (South-East Tuva). Author's PhD thesis (Geology and Mineralogy). Moscow, 26 p. (in Russian) [*Петрова А.Ю.* Rb-Sr изотопная система метаморфических и магматических пород Западного Сангилена (Юго-Восточная Тува): Автореф. дис. … канд. геол.-мин. наук. М., 2001. 26 с.].

Shelepaev R.A., 2006. Evolution of Basic Magmatism of West Sangilen (South-East Tuva). Author's PhD thesis (Geology and Mineralogy). Novosibirsk, 16 p. (in Russian) [*Шелепаев Р.А.* Эволюция базитового магматизма Западного Сангилена (Юго-Восточная Тува): Автореф. дис. … канд. геол.-мин. наук. Новосибирск, 2006. 16 с.].

Sklyarov E.V., Fedorovskii V.S., 2006. Magma mingling: tectonic and geodynamic implications. *Geotectonics* 40 (2), 120–134. http://dx.doi.org/10.1134/S001685210602004X.

Taylor S.R., McLennan S.M., 1985. The Continental Crust: Its Evolution and Composition. Blackwell, London, 312 p.

Vasyukova E.A., Izokh A.E., Lavrenchuk A.V., 2008. Petrology of syngranite Ordovician dikes (West Sangilen, South-East Tuva). In: Geodynamic evolution of the lithosphere of the Central Asian mobile belt (from ocean to continent). Issue 6, vol. 1. IEC SB RAS, Irkutsk, p. 56–58 (in Russian) [*Васюкова Е.А., Изох А.Э., Лавренчук А.В.* Петрология сингранитных ордовикских даек (Западный Сангилен, Юго-Восточная Тува) // Геодинамическая эволюция литосферы Центрально-Азиатского подвижного пояса (от океана к континенту). Вып. 6. Иркутск: ИЗК СО РАН, 2008. Т. 1. С. 56–58].

Vladimirov V.G., Vladimirov A.G., Gibsher A.S., Travin A.V., Rudnev S.N., Shemelina I.V., Barabash N.V., Savinykh Ya.V., 2005. Model of the tectonometamorphic evolution for the Sangilen block (Southeastern Tuva, Central Asia) as a reflection of the early Caledonian accretion–collision tectogenesis. *Doklady Earth Sciences* 405 (8), 1159–1165.

Wiebe R.A., 1973. Relations between coexisting basaltic and granitic magmas in a composite dike. *American Journal of Science* 273 (2), 130–151. http://dx.doi.org/10.2475/ajs.273.2.130.

Karmysheva, Irina V., Candidate of Geology and Mineralogy, Researcher
V.S. Sobolev Institute of Geology and Mineralogy, Siberian Branch of RAS
3 Ac. Koptyug ave, Novosibirsk 630090, Russia
Novosibirsk State University
2 Pirogov street, Novosibirsk 630090, Russia
✉ e-mail: iri@igm.nsc.ru, karmysheva.irina@gmail.com

Кармышева Ирина Владимировна, канд. геол.-мин. наук, н.с.
Институт геологии и минералогии им. В.С. Соболева СО РАН
630090, Новосибирск, просп. Коптюга, 3, Россия
Новосибирский государственный университет
630090, Новосибирск, ул. Пирогова, 2, Россия
✉ e-mail: iri@igm.nsc.ru, karmysheva.irina@gmail.com

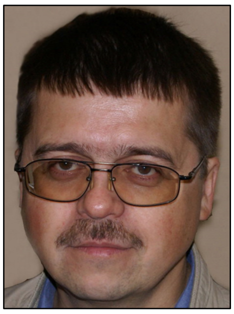

Vladimirov, Vladimir G., Candidate of Geology and Mineralogy, Senior Researcher
V.S. Sobolev Institute of Geology and Mineralogy, Siberian Branch of RAS
3 Ac. Koptyug ave, Novosibirsk 630090, Russia
Novosibirsk State University
2 Pirogov street, Novosibirsk 630090, Russia
e-mail: vvg@igm.nsc.ru, vladimirov58@gmail.com

Владимиров Владимир Геннадьевич, канд. геол.-мин. наук, с.н.с.
Институт геологии и минералогии им. В.С. Соболева СО РАН
630090, Новосибирск, просп. Коптюга, 3, Россия
Новосибирский государственный университет
630090, Новосибирск, ул. Пирогова, 2, Россия
e-mail: vvg@igm.nsc.ru, vladimirov58@gmail.com

Vladimirov, Aleksander G., Doctor of Geology and Mineralogy, Chief Researcher, Professor
V.S. Sobolev Institute of Geology and Mineralogy, Siberian Branch of RAS
3 Ac. Koptyug ave, Novosibirsk 630090, Russia
Novosibirsk State University
2 Pirogov street, Novosibirsk 630090, Russia
Tomsk State University
50 Lenin ave, Tomsk 634050, Russia
e-mail: vladimir@igm.nsc.ru

Владимиров Александр Геннадьевич, докт. геол.-мин. наук, г.н.с., профессор
Институт геологии и минералогии им. В.С. Соболева СО РАН
630090, Новосибирск, просп. Коптюга, 3, Россия
Новосибирский государственный университет
630090, Новосибирск, ул. Пирогова, 2, Россия
Томский государственный университет
634050, Томск, просп. Ленина, 50, Россия
e-mail: vladimir@igm.nsc.ru

Shelepaev, Roman A., Candidate of Geology and Mineralogy, Senior Researcher
V.S. Sobolev Institute of Geology and Mineralogy, Siberian Branch of RAS
3 Ac. Koptyug ave, Novosibirsk 630090, Russia
Novosibirsk State University
2 Pirogov street, Novosibirsk 630090, Russia
e-mail: rshel@igm.nsc.ru

Шелепаев Роман Аркадьевич, канд. геол.-мин. наук, с.н.с.
Институт геологии и минералогии им. В.С. Соболева СО РАН
630090, Новосибирск, просп. Коптюга, 3, Россия
Новосибирский государственный университет
630090, Новосибирск, ул. Пирогова, 2, Россия
e-mail: rshel@igm.nsc.ru

Yakovlev, Vladislav A., Student
Novosibirsk State University
2 Pirogov street, Novosibirsk 630090, Russia
e-mail: yakovlew.official@gmail.com

Яковлев Владислав Александрович, студент
Новосибирский государственный университет
630090, Новосибирск, ул. Пирогова, 2, Россия
e-mail: yakovlew.official@gmail.com

Vasyukova, Elena A., Candidate of Geology and Mineralogy, Junior Researcher
V.S. Sobolev Institute of Geology and Mineralogy, Siberian Branch of RAS
3 Ac. Koptyug ave, Novosibirsk 630090, Russia
Novosibirsk State University
2 Pirogov street, Novosibirsk 630090, Russia
e-mail: helenav@igm.nsc.ru, lenav@inbox.ru

Васюкова Елена Александровна, канд. геол.-мин. наук, м.н.с.
Институт геологии и минералогии им. В.С. Соболева СО РАН
630090, Новосибирск, просп. Коптюга, 3, Россия
Новосибирский государственный университет
630090, Новосибирск, ул. Пирогова, 2, Россия
e-mail: helenav@igm.nsc.ru, lenav@inbox.ru

GEODYNAMICS & TECTONOPHYSICS

PUBLISHED BY THE INSTITUTE OF THE EARTH'S CRUST
SIBERIAN BRANCH OF RUSSIAN ACADEMY OF SCIENCES

2015 VOLUME 6 ISSUE 3 PAGES 311–344 ISSN 2078-502X

http://dx.doi.org/10.5800/GT-2015-6-3-0184

Paleogeodynamics

METASOMATIC AND MAGMATIC PROCESSES IN THE MANTLE LITHOSPHERE OF THE BIREKTE TERRAIN OF THE SIBERIAN CRATON AND THEIR EFFECT ON THE LITHOSPHERE EVOLUTION

L. V. Solov'eva[1], T. V. Kalashnikova[2], S. I. Kostrovitsky[2], A. V. Ivanov[1], S. S. Matsuk[3], L. F. Suvorova[2]

[1] *Institute of the Earth's Crust, Siberian Branch of RAS, Irkutsk, Russia*
[2] *A.P. Vinogradov Institute of Geochemistry, Siberian Branch of RAS, Irkutsk, Russia*
[3] *M.P. Semenenko Institute of Geochemistry, Mineralogy and Ore Formation, National Academy of Sciences of Ukraine, Kiev, Ukraine*

Abstract: The area of studies covers the north-eastern part of the Siberian craton (the Birekte terrain), Russia. The influence of metasomatic and magmatic processes on the mantle lithosphere is studied based on results of analyses of phlogopite- and phlogopite-amphibole-containing deep-seated xenoliths from kimberlites of the Kuoika field. In the kimberlitic pipes, deep-seated xenoliths with mantle phlogopite- and phlogopite-amphibole mineralization are developed in two genetically different rock series: magnesian (Mg) pyroxenite-peridotite series (with magnesian composition of rocks and minerals) and phlogopite-ilmenite (Phl-Ilm) hyperbasite series (with ferrous types of rocks and minerals). This paper is focused on issues of petrography and mineralogy of the xenoliths and describes the evidence of metasomatic / magmatic genesis of phlogopite and amphibole. We report here the first data set of $^{40}Ar/^{39}Ar$ age determinations for phlogopite from the rocks of the magnesian pyroxenite-peridotite series and the ferrous Phl-Ilm hyperbasite series.

The Mg series is represented by a continuous transition of rocks from Sp, Sp-Grt, Grt clinopyroxenite and ortopyroxenite to websterite and lherzolite. Many researchers consider it as a layered intrusion in the mantle [*Ukhanov et al., 1988; Solov'eva et al., 1994*]. The mantle metasomatic phlogopite and amphibole are revealed in all petrographic types of the rocks in this series and compose transverse veins and irregular patchs at grain boundaries of primary minerals. At contacts of xenolith and its host kimberlite, grains of phlogopite and amphibole are often cut off, which gives an evidence of the development of metasomatic phlogopite-amphibole mineralization in the rocks before its' entraiment into the kimberlite. In the xenoliths with exsolution pyroxene megacrystalls, comprising parallel plates of clino- and orthopyroxene ± garnet ± spinel (former high-temperature pigeonite [*Solov'eva et al., 1994*]), the metasomatic phlogopite-amphibole aggregate mainly replace laminar intergrowths of one of pyroxenes and garnet and also develops in the re-crystallized fine-grained rock matrix. This suggests a considerable period of time between the crystallization of rocks of the pyroxenite-peridotite series and the development of phlogopite-amphibole metasomatism.

The Phl-Ilm hyperbasites comprise a complex association of parageneses represented by garnet- and garnetless pyroxenites, websterites, olivine websterites, orthopyroxenites, lherzolites and olivinites. A specific feature of this series is high contents of K, Ti and Fe in the rocks and minerals. The content of phlogopite is widely variable, from a few percent to 40–80 %. The content of ilmenite ranges from a few percent to 15 %, rarely to 30–40 %. Mica and ilmenite contents sharply decrease in garnetized xenolithes, where these two minerals, as soon as olivine and pyroxenes are replaced by garnet.

Euhedral, subhedral, sideronitic and porphyraceous structures in garnetless xenoliths suggest the primary magmatic genesis of the rocks. In the series of Phl-Ilm hyperbasites, a special type of parageneses is represented by strongly deformed phlogopite-amphibole rocks with newly-formed chromite and relict resorbed ilmenite and clinopyroxene. Phl-Ilm rock series is also characterized by a variety of autometasomatic and metasomatic reaction structures. Garnet and phlogopite develop nearly simultaneously at the sub-solidus stage: garnet develops due to cooling of the primary magmatic rocks, and phlogopite develops under the influence of residual rich in potassium and volatiles fluids – melts. Phlogopite in the rocks of the Phl-Ilm series form porphyraceous plates, late intergranular xenomorphic grains, porphyroblasts of the solidus stage and strongly deformed irregular plates in the phlogopite-amphibole rocks. Amphibole occurs in garnetless parageneses and deformed phlogopite-amphibole rocks in amounts of a few percent and up to 40–50%, respectively. Petrographically, the differentiated series of phlogopite-ilmenite hyperbasites belongs to mantle magmatites, except for younger deformed phlogopite-amphibole rocks from zones of deep faults.

Unlike corresponding minerals in the Mg pyroxenite-peridotite series, minerals from the Phl-Ilm hyperbasites are characterized by lower magnesium index (Mg#), considerably higher contents of TiO_2 and FeO, and lower contents of Cr_2O_3 (Table). In diagrams Mg# – TiO_2 and Mg# – Cr_2O_3, metasomatic phlogopite points from Mg series rocks are significantly distant from points of mica from the phlogopite-ilmenite parageneses (Fig. 24). In the parageneses of the Mg pyroxenite-peridotite series, phlogopite plates have homogenous compositions in contrast to zonal phlogopite in the Phl-Ilm hyperbasites. In Phl-Amph metasomatites of the Mg series, amphibole is represented by typical pargasite, and its chemical composition is sharply different from that of K-richterite from the deformed phlogopite-amphibole rocks of the series of the Phl-Ilm hyperbasites (Table).

The $^{40}Ar/^{39}Ar$ age in the range from 1640 to 1800 Ma (Fig. 25) is determined for phlogopite from the metasomatic phlogopite-amphibole veinlets and intergranular reaction patches in the garnet olivine websterite of the Mg series. For mica from the garnetless Phl-Ilm websterites, ages are 869 and 851 Ma (Fig. 25). Mica from the garnet-containing Phl-Ilm lherzolites is much younger (608 and 495 Ma). The age of mica from the deformed phlogopite-amphibole rock is 167 Ma, which is close to the age of kimberlites of the Kuoika field.

Metasomatic phlogopite (1640–1800 Ma) originated somewhat later than the Birekte terrain accretion to the Siberian craton (1.8–1.9 Ga) [*Rosen*, *2003*], and its age determination may be explained by a partial loss of ^{40}Ar in the analysed medium. This age is also close to the late episode when the crust was formed in the Birekte block 1.8–2.1 Ga ago [*Nasdala et al.*, *2014*], and corresponds to the time when radiogenic osmium was supplied into the mantle lithosphere from the subduction zone (1.7–2.2 Ga, according to [*Pernet et al.*, *2015*]). In analyses of minerals in the pyroxenite-peridotite series from the Obnazhennaya pipe, data on the oxygen isotope geochemistry give evidence of an ancient subduction component (Fig. 26). It can be thus assumed that in the mantle lithosphere of the Birekte terrain, phlogopite-amphibole metasomatism took place due to fluids-melts ascending from the subduction zone about 1.8 Ga ago and correlates to the accretion of this block to the Siberian craton. The complex magmatic series of Phl-Ilm rocks formed later than the Mg pyroxenite-peridotite series. The more ancient ages of phlogopite (869–851 Ma) from Phl-Ilm hyperbasites are somewhat higher than the most ancient dating of alkaline ultrabasic-carbonatite Tomtor massif (800 Ga, according to [*Entin et al.*, *1990*]) and the time when the breakup of Rodinia began (825 Ga, according to [*Li et al.*, *2008*]). The difference may be explained by an advance occurrence of high-potassium, titanian, ferrous magmatites in the mantle lithosphere of the Birekte block as compared to their appearance on the surface. Phlogopite from xenoliths with subsolidus garnetization is significantly younger in age (500–600 Ma), may be, due to a loss of radiogenic argon caused by mica replacement. H_2O, K, Ba, F and Cl were abundantly released during the replacement and supplied into the upper layers of the crust and mantle. The mantle high-potassium and high titanian Phl-Ilm series seems comagmatic with the surficial potassium ultramafites and mafites of the Siberian Platform and associated with the earlier episode of the Rodinia breakup.

Key words: Siberian craton, Birekte terrain, lithosphere mantle, mantle xenolith, magmatism, mantle metasomatism, magnesian pyroxenite-peridotite series, ferrous Phl-Ilm hyperbasite series.

Recommended by E.V. Sklyarov

For citation: *Solov'eva L.V., Kalashnikova T.V., Kostrovitsky S.I., Ivanov A.V., Matsuk S.S., Suvorova L.F.* 2015. Metasomatic and magmatic processes in the mantle lithosphere of the Birekte terrain of the Siberian craton and their effect on the lithosphere evolution. *Geodynamics & Tectonophysics* 6 (3), 311–344. doi: 10.5800/GT-2015-6-3-0184.

Метасоматические и магматические процессы в мантийной литосфере Биректинского террейна Сибирского кратона и их влияние на эволюцию литосферы

Л. В. Соловьева[1], Т. В. Калашникова[2], С. И. Костровицкий[2], А. В. Иванов[1], С. С. Мацюк[3], Л. Ф. Суворова[2]

[1] *Институт земной коры СО РАН, Иркутск, Россия*
[2] *Институт геохимии им. А.П. Виноградова СО РАН, Иркутск, Россия*
[3] *Институт геохимии, минералогии и рудообразования им. М.П. Семененко НАН Украины, Киев, Украина*

Аннотация: Введение. Влияние процессов мантийного метасоматизма и магматизма на эволюцию литосферной мантии в северо-восточном Биректинском террейне Сибирского кратона рассмотрено на примере флогопит- и флогопит-амфиболсодержащих глубинных ксенолитов из кимберлитов Куойкского поля (рис. 1).

Глубинные ксенолиты с мантийной флогопитовой и флогопит-амфиболовой минерализацией в кимберлитовых трубках поля развиты в двух генетически разных сериях пород: магнезиальной (Mg) пироксенит-перидотитовой (с магнезиальным составом пород и минералов) и в серии флогопит- ильменитовых (Phl-Ilm) гипербазитов (с железистым типом пород и минералов). В настоящей работе уделяется большое внимание петрографии и минералогии ксенолитов с мантийной флогопитовой и флогопит-амфиболовой минерализацией, и приводятся новые данные по $^{40}Ar/^{39}Ar$ возрасту флогопита.

Методы исследований. Флогопит- и флогопит-амфиболсодержащие парагенезисы ксенолитов были детально изучены в образцах и шлифах. Зерна минералов были проанализированы на содержания главных оксидов на рентгеновском электронно-зондовом микроанализаторе JXA-8200 в Институте геохимии им. А.П. Виноградова СО РАН (г. Иркутск). Анализ изотопного состава кислорода в гранате выполнен в аналитическом центре ДВГИ ДВО РАН (г. Владивосток) на масс-спектрометре Finnigan MAT 252, [*Ignatiev, Velivetskaya, 2004*]. Определение возраста флогопита $^{40}Ar/^{39}Ar$ методом произведено в Институте земной коры СО РАН (г. Иркутск) с использованием мультиколлекторного масс-спектрометра Argus VI.

Петрография и минералогия. Магнезиальная (Mg) серия представлена непрерывным переходом пород от Sp, Sp-Grt, Grt клинопироксенитов, ортопироксенитов к вебстеритам, оливиновым вебстеритам и лерцолитам и рассматривается рядом исследователей как расслоенная интрузия в мантии [*Ukhanov et al., 1988; Solov'eva et al., 1994*]. Мантийная метасоматическая флогопит-амфиболовая минерализация проявлена во всех петрографических типах пород серии и развита в виде секущих прожилков и неправильных участков по границам зерен первичных минералов (рис. 4, 5). В ксенолитах с мегакристаллами пироксенов, состоящих из параллельных пластинок клино- и ортопироксена ± граната ± шпинели (структуры распада высокотемпературного пижонита [*Solov'eva et al., 1994*]), метасоматический флогопит-амфиболовый агрегат развивается преимущественно по пластинчатым вросткам одного из пироксенов и граната и в перекристаллизованной мелкозернистой матрице пород. Это указывает на значительный интервал времени между кристаллизацией пород пироксенит-перидотитовой серии и развитием флогопит-амфиболового метасоматизма.

Phl-Ilm гипербазиты также образуют сложную ассоциацию парагенезисов, представленных Phl-Ilm гранатовыми и безгранатовыми пироксенитами, вебстеритами, оливиновыми вебстеритами, ортопироксенитами, лерцолитами и оливинитами. Характерной особенностью серии являются высокие содержания K, Ti, Fe в породах и минералах. Содержание флогопита в породах широко варьируется – от первых процентов до 40–80 %, ильменита – от первых до 15 %, реже до 30–40 %. Количество слюды и ильменита резко уменьшается в гранатизированных ксенолитах, в которых гранат интенсивно замещает эти минералы, а также первичные силикаты. Панидиоморфнозернистые, гипидиоморфнозернистые, сидеронитовые и порфировидные структуры в негранатизированных ксенолитах указывают на первичный магматический генезис пород. Для пород серии характерно также разнообразие автометасоматических и метасоматических структур. Гранат и флогопит развиваются на субсолидусном этапе близко одновременно: первый за счет охлаждения первичных магматических пород (рис. 11, 12, 14), а второй при воздействии на них остаточных флюидов-расплавов, обогащенных калием и летучими (рис. 8). Особый тип парагенезисов в серии Phl-Ilm гипербазитов представляют сильно деформированные флогопит-амфиболовые породы с новообразованным хромитом и с реликтовыми резорбированными ильменитом и клинопироксеном (рис. 21–23). Дифференцированная серия флогопит-ильменитовых гипербазитов по петрографическим признакам относится к мантийным магматитам, за исключением более поздних деформированных флогопит-амфиболовых пород из зон глубинных разломов.

В отличие от соответствующих минералов Mg пироксенит-перидотитовой серии, минералы из Phl-Ilm гипербазитов имеют значительно меньшую магнезиальность (Mg#) и содержат существенно больше TiO_2, FeO и меньше Cr_2O_3 (таблица). Точки метасоматических флогопитов из пород Mg серии на диаграммах Mg# – TiO_2 и Mg# – Cr_2O_3 существенно отделены от поля точек слюд из флогопит-ильменитовых парагенезисов (рис. 24). Амфибол, представленный в Phl-Amph метасоматитах Mg серии типичным паргаситом по химическому составу резко отличается от K-рихтерита из деформированных флогопит-амфиболовых пород серии Phl-Ilm гипербазитов (таблица).

^{40}Ar/^{39}Ar датирование слюды. $^{40}Ar/^{39}Ar$ возраст флогопита из метасоматических флогопит-амфиболовых прожилков и межзерновых реакционных обособлений в гранатовом оливиновом вебстерите Mg серии варьируется в пределах 1640–1800 млн лет (рис. 25). Слюды из негранатизированных Phl-Ilm вебстеритов показали возраст 869 и 851 млн лет (рис. 25). В гранатизированных Phl-Ilm лерцолитах возраст слюд значительно меньше (608 и 495 млн лет). Слюда из деформированной флогопит-амфиболовой породы показала возраст 167 млн лет, близкий возрасту кимберлитов Куойкского поля.

Дискуссия и результаты. Возраст метасоматического флогопита (1640–1800 млн лет) несколько ниже возраста присоединения Биректинского террейна к Сибирскому кратону (1.8–1.9 млн лет [*Rosen, 2003*]), что, возможно, объясняется частичной потерей ^{40}Ar в анализируемой слюде. С другой стороны, это значение близко интервалу позднего эпизода формирования коры в Биректинском блоке 1.8–2.1 млрд лет [*Nasdala et al., 2014*] и соответствует времени привноса радиогенного осмия в мантийную литосферу из зоны субдукции (1.7–2.2 лет [*Pernet-Fisher et al., 2015*]). Геохимия изотопов кислорода в породах перидотит-пироксенитовой серии из трубки Обнаженная также свидетельствует о присутствии в них древней субдукционной компоненты (рис. 26). Это позволяет предположить, что мантийный флогопит-амфиболовый метасоматизм в литосферной мантии Биректинского террейна осуществлялся флюидами – расплавами, поступавшими из зоны субдукции примерно 1.8 млрд лет назад, и соответствует эпизоду присоединения этого блока к Сибирскому кратону.

Сложная магматическая серия Phl-Ilm пород является более поздней по сравнению с Mg пироксенит-перидотитовой серией. Древний возраст флогопита (869–851 млн лет) из Phl-Ilm гипербазитов несколько превышает наиболее древние датировки щелочного ультраосновного – карбонатитового Томторского массива (800 млн лет [*Entin et al., 1990*]) и время начала распада суперконтинента Родиния (825 млн лет [*Li et al., 2008*]). Эта разница может быть объяснена опережающим проявлением высококалиевых, титанистых, железистых

зистых магматитов в мантийной литосфере Биректинского блока по сравнению с их проявлением на поверхности. Флогопит из ксенолитов с субсолидусной гранатизацией показывает существенно меньшие значения возраста (500–600 млн лет), вероятно, из-за потери радиогенного аргона при замещении слюды. Этот процесс высвобождал большое количество H_2O, K, Ba, F и Cl, поступавших в верхние горизонты коры и мантии. Мантийная высококалиевая и высокотитанистая Phl-Ilm серия, по-видимому, комагматична поверхностным калиевым ультрамафитам и мафитам на Сибирской платформе и связана с ранним эпизодом раскола суперконтинента Родиния.

Главные выводы. 1. Рассмотренные флогопитсодержащие серии ксенолитов из кимберлитовых трубок Куойкского поля принадлежат к разным генетическим образованиям и к разным этапам эволюции литосферной мантии Биректинского террейна. 2. Phl-Amph метасоматизм развивается по породам сложной магнезиальной пироксенит-перидотитовой серии ксенолитов, имеет геохимические черты зоны субдукции и маркирует этап, связанный с присоединением Биректинского континентального блока к Сибирскому кратону ~1.8–1.9 млрд лет. 3. Сложная железистая серия Phl-Ilm гипербазитов относится к типичным мантийным калиевым ультраосновным – основным магматитам. Начало формирования магматической серии Phl-Ilm гипербазитов в мантийной литосфере Биректинского террейна (~869–851 млн лет), возможно, соответствует самому раннему этапу распада суперконтинента Родиния.

Ключевые слова: Сибирский кратон, Биректинский террейн, литосферная мантия, мантийные ксенолиты, магматизм, мантийный метасоматизм, магнезиальная пироксенит-перидотитовая серия, серия железистых флогопит-ильменитовых гипербазитов.

1. Introduction

The Birekte terrain is located in the north-eastern part of the Siberian craton. The geotectonic regional partition suggest that it was formed not later than 2.4 Ga ago (Fig. 1) [*Rosen*, *2003*]. The composition and structure of the mantle lithosphere of this block were mainly discovered by studies of deep-seated xenoliths from the Upper Jurassic–Lower Cretaceous Kuoika kimberlite field [*Ukhanov et al*., *1988; Solov'eva et al., 1994; Howarth et al., 2014*]. It has been noted in many publications that the mantle lithosphere in the north-eastern part of the Siberian craton is significantly different from that of its central part in terms of both thickness and composition [*Pokhilenko et al*., *1999*].

Our study is focused on deep-seated xenoliths with mantle phlogopite- and phlogopite-amphibole mineralization which are found in kimberlite pipes of the Kuoika field (Obnazhennaya, Slyudyanka, Pyatnitsa pipes). The occurrence of primary phlogopite and amphibole in deep-seated xenoliths is generally viewed as a result of different-aged processes of mantle metasomatism [*Menzies, Hawkesworth*, *1987*]. It is remarkable that primary phlogopite in deep-seated xenoliths may be of magmatic genesis [*Solovieva et al*., *1997*].

According to [*Garanin et al., 1985; Ukhanov et al., 1988*], phlogopite- and phlogopite-amphibole mineralization was discovered in two series of deep-seated xenoliths from the Obnazhennaya pipe (Kuoika field), specifically the Mg pyroxenite-peridotite series and the series of Phl-Ilm hyperbasites with a higher Fe content. Nevertheless, phlogopite- and phlogopite-amphibole mantle parageneses remain poorly studied in terms of both composition and time of their occurrence in the mantle lithosphere in the north-eastern block of the Siberian craton. This paper is focused on issues of petrography and mineralogy of the xenoliths and the evidences of metasomatic/magmatic genesis of mantle phlogopite and amphibole. We report here the first data of $^{40}Ar/^{39}Ar$ age determinations for phlogopite from the rocks of the magnesian pyroxenite-peridotite series and the ferrous Phl-Ilm hyperbasite series. Results of our studies reveal the genesis of phlogopite- and phlogopite-amphibole mantle mineralization and its relationships with evolution stages of the mantle lithosphere in the north-eastern block of the Siberian craton.

2. Research methods

Detailed studies of phlogopite and phlogopite- amphibole xenoliths are conducted using rock samples and thin sections. The mantle genesis of mica and amphibole is determined by a number of signs, such as the development of these minerals in a xenolith regardless of a distance to kimberlite, cut-off of phlogopite plates and amphibole grains by the xenolith contact, the composition of phlogopite etc. The fine-grained mica filling the cracks coming from the kimberlite into the xenolith is not considered as pre-kimberlite/mantle one. Grains of minerals are analysed for the main oxides. The analyses were taken using Electron Probe Microanalyzer JXA-8200 at the Vinogradov Institute of Geochemistry, Irkutsk. The isotopes of oxigen were analysed for garnet. We use results of analyses conducted at the Analytical Centre of the Far East Geological Institute, Far East Branch of RAS, using the fluorination BrF_5 method

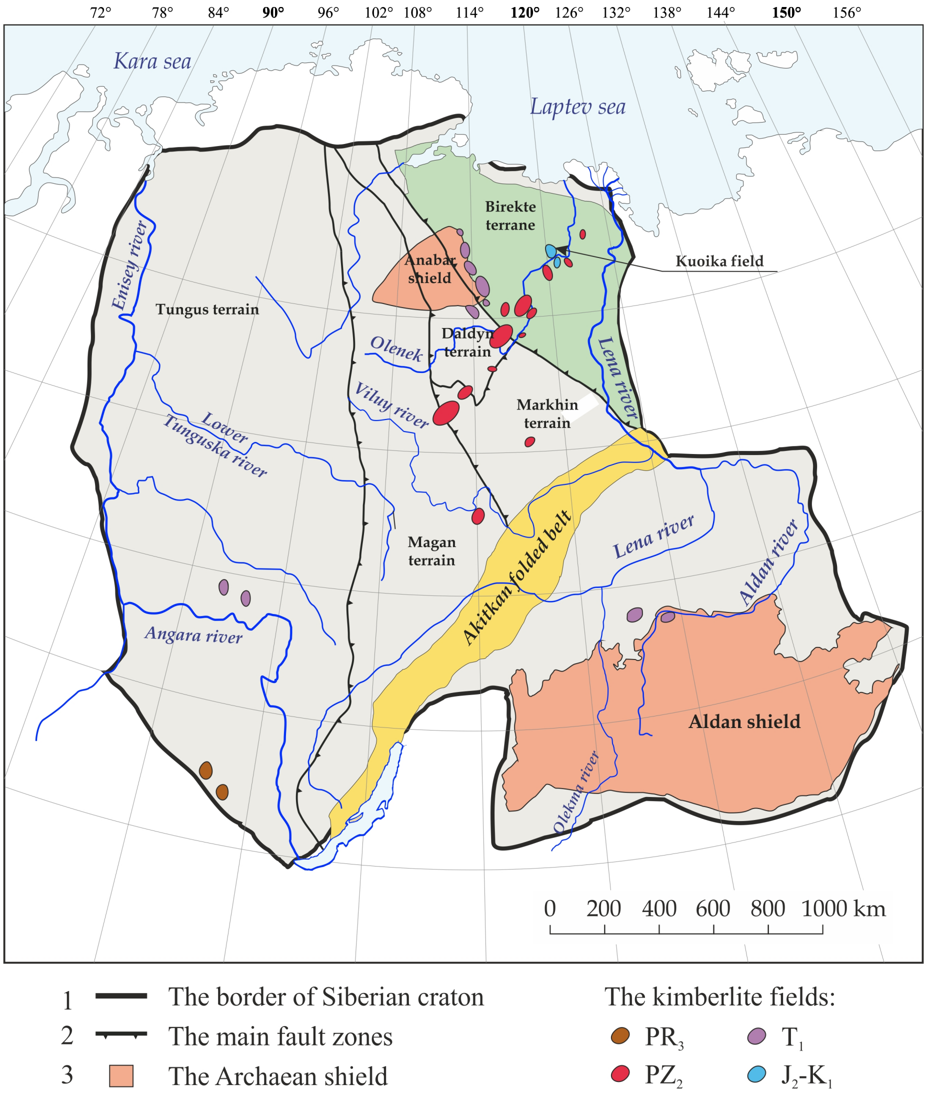

Fig. 1. Schematic map of ancient terrains and kimberlitic fields in the Siberian craton with the authors' modification.

The legend is given in the figure. The craton and the kimberlitic fields are contoured according to [*Khar'kiv et al., 1998*], terrains of the Siberian craton according to [*Rosen, 2003*], and the Anabar crystalline shield according to [*Parfenov, Kuzmin, 2001*].

Рис. 1. Схема расположения древних террейнов и кимберлитовых полей на Сибирском кратоне с некоторыми изменениями авторов статьи.

Условные обозначения приведены на рисунке. Контуры кратона и кимберлитовые поля нанесены по [*Khar'kiv et al., 1998*]; террейны Сибирского кратона – по [*Rosen, 2003*]; Анабарский кристаллический щит – по [*Parfenov, Kuzmin, 2001*].

[*Ignatiev, Velivetskaya, 2004*]. The weight of mineral fractions for analysis ranges from 1 to 2 mg, precision of the method (1σ) amounts to 0.1 ‰ (n=5). Measurements ($\delta^{18}O$) were conducted with a Finnigan MAT 252 isotope mass spectrometer (IRMS). The repeatability of measurements $\delta^{18}O$ for samples amounts to 0.1 ‰. Dating of phlogopites by $^{40}Ar/^{39}Ar$ method was performed at the Institute of the Earth's Crust, SB RAS; an Argus VI multi-collector mass spectrometer and a high-vacuum oven (dual vacuum, heating above 1700 °C) were used. Mica samples (15–30 mg) were wrapped in an aluminium foil and put into a glass ampoule together with BERN4M standards (assumed age of 18.885±0.097 Ma). The glass ampoule was irradiated in a VVR-K nuclear reactor in Tomsk. Radiation parameters were similar to those reported in [*Travin et al., 2009*].

3. Petrography and mineralogy

3.1. Phlogopite-amphibole parageneses in the magnesian pyroxenite-peridotite series of the xenoliths

The Mg pyroxenite-peridotite series of the xenoliths is represented by a continuous transition of rocks from

Sp, Sp-Grt, Grt clinopyroxenites and ortopyroxenites to Sp, Sp-Grt, Grt websterites, olivine websterites and lherzolites [*Ukhanov et al*., *1988*; *Solov'eva et al*., *1994*]. The mantle metasomatic phlogopite and amphibole are revealed in all the petrographic types of the rocks in nearly every twentieth xenoliths and typically are composed of transverse veins and veinlet aggregates at grain boundaries of primary minerals. In metasomatic area amphibole predominates. At contacts of xenolith and host kimberlite, grains of phlogopite and amphibole are often cut off, which gives an evidence of the development of metasomatic phlogopite-amphibole mineralization before xenolith entrainment by the kimberlite. In the exsolution pyroxene megacrystalls (former high-temperature pigeonite [*Solov'eva et al*., *1994*]), comprising parallel plates of clino- and orthopyroxene ± garnet ± spinel, the metasomatic phlogopite-amphibole aggregate mainly replace laminar intergrowths of one of pyroxenes and garnet (Fig. 2). The abundant development of metasomatic amphibole is observed from the contact with cutting phlogopite-amphibole veinlets (Fig. 3–5). Grains of olivine, garnet and clinopyroxene are intensively resorbed at the boundaries with the veinlets. Small amphibole grains are developed from the veinlet into the grains of clinopyroxene (Fig. 3, *B*). In veinlet selvages, clinopyroxene remains as small irregular relics (Fig. 3, *C*). Garnet is replaced by phlogopite at the contact with the phlogopite infill of the veinlets (Fig. 4, *A*, *B*). In the phlogopite-amphibole parts of the veinlets, the texture is close to magmatic euhedral one (Fig. 4, *C*). The grains of pyroxene are filled by small crystals of metasomatic amphibole (Fig. 5, *A*–*D*) which commonly have one or two crystallographic direction.

The undoubted metasomatic character of the phlogopite-amphibole mineralization in the xenoliths of the magnesian pyroxenite-peridotite series and its development before xenoliths entrainment into the kimberlite melt suggest that this process is related to intensive metasomatism of the mantle lithosphere in the north-eastern part of the Siberian craton.

3.2. Phlogopite and phlogopite-amphibole parageneses in xenoliths of the ferrous Phl-Ilm series of hyperbasites

The Phl-Ilm hyperbasites comprise a complex association of parageneses represented by garnet- and garnetless pyroxenites, websterites, olivine websterites, orthopyroxenites, lherzolites and olivinites. High contents of K, Ti and Fe in the rocks and minerals are typical of this series [*Garanin et al., 1985; Ukhanov et al., 1988*]. The content of phlogopite is widely variable, from a few percent to 40–80 %. The content of ilmenite ranges from a few percent to 15 %, rarely to 30–40 %. Mica and ilmenite contents sharply decrease in garnetized xenolithes, where these two minerals, as soon as olivine and pyroxenes are replaced by garnet. Euhedral, subhedral, sideronitic and porphyraceous textures in garnetless xenoliths are suggested the primary magmatic genesis of the rocks. In the series of Phl-Ilm hyperbasites, a special type of parageneses is represented by strongly deformed phlogopite-amphibole rocks with newly-formed chromite and relict resorbed ilmenite and clinopyroxene. The rocks of this series are also characterized by numerous autometasomatic and metasomatic reaction textures and wide ranges of modal mineral compositions: 0–80 % Grt, 1–40 % Ilm, 5–80 % Phl, 0–30 % Cpx, 10–70 % Opx, 0–40 % Ol, and 0.5–2.0 % Sulph. Amphibole occurs in garnetless parageneses and deformed phlogopite-amphibole rocks (with the newly formed chromite) in amounts of a few percent and up to 40–50 %, respectively.

The euhedral texture is essentially preserved in orthopyroxenites and partially websterites (Fig. 6, *A*). These rocks are composed of regular prismatic crystals of orthopyroxene which often have directive orientations. In olivine-containing xenoliths, large elongated crystals of olivine also formed partly idiomorphic crystals. Oval and round-shaped grains of olivine are often included into the grains of orthopyroxene less than into clinopyroxene without any traces of resorption (Fig. 6, *B*). The exsolution lamellae of clinopyroxene are commonly found in orthopyroxene from 10 to 15 % (Fig. 6, *B*). Besides, orthopyroxene contains numerous brownish micro-inclusions (5–20 μm) of ilmenite (≤1 %) which are regularly oriented and translucent (Fig. 6, *C*, *D*). Clinopyroxene- and ilmenite exsolution plates occupy central parts of orthopyroxene grains (almost ¾ of the area) and are absent in the marginal zones. The presence of the exsolution textures indicate an early high-temperature stage in the evolution of the rocks. Ilmenite and phlogopite form xenomorphic grains between earlier silicates without any evident reaction interrelations (Fig. 7, *A*, *B*) and belong to the late stage of magmatic crystallization. Inclusions of ilmenite in phlogopite occur as thin cleavage-oriented plates (≤1–5 μm) in the central parts of the grains or as oval-shaped blebs in the marginal parts (Fig. 7, *A*, *B*). Rare regular phlogopite flakes in orthopyroxene (Fig. 7, *C*, *D*) suggest that small amounts of mica were crystallized in some portions of the melt at the early magmatic stage.

In addition to evidence of typical magmatic genesis, phlogopite shows metasomatic relationships with primary silicates. In both the garnet-containing and garnetless parageneses, phlogopite forms 'windows' with abundant inclusions of small round-shaped grains of ilmenite and pyroxenes being relics of substitution (Fig. 8, *A*). Orthopyroxene crystals are grown through small irregular phlogopite flakes of the common optical orientation (Fig. 8, *B*, *C*). As shown in Fig. 9, *A*, *B*, orphopyroxene and clinopyroxene are intensively

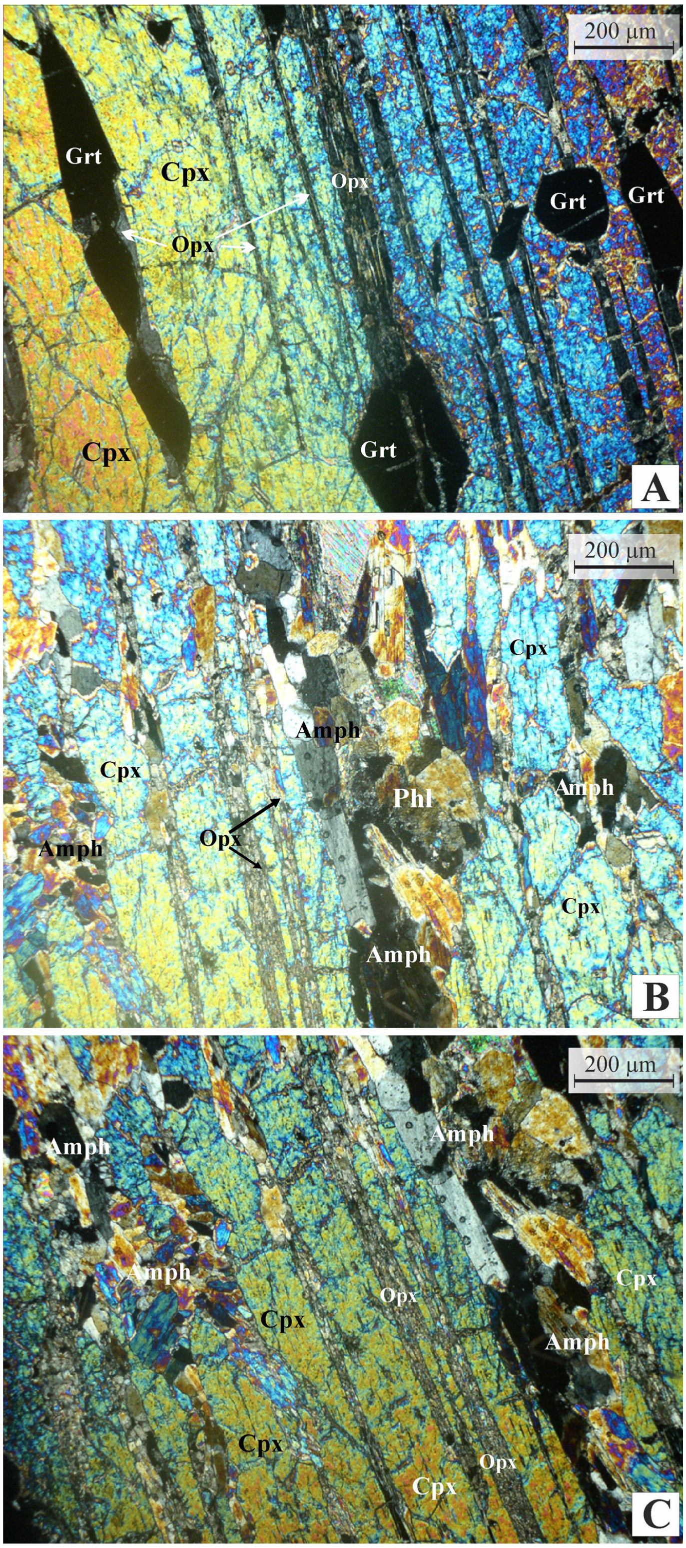

Fig. 2. The photomicrographs of thin section. Development of metasomatic Phl-Amph mineralization on orthopyroxene exsolution plates inside the clinopyroxene megacrystal in megacrystalline garnet websterite.

A – garnet and orphopyroxene exsolution plates inside the clinopyroxene megacrystal. Garnet is also developed in the form of isometric grains; *B, C* – fine-grained aggregate of Amph with rare plates of Phl, replacing mainly orphopyroxene exsolution plates. Images in crossed nicols.

Рис. 2. Развитие метасоматической Phl-Amph минерализации по пластинкам распада ортопироксена внутри мегакристалла клинопироксена в мегакристаллическом гранатовом вебстерите.

А – пластинки распада граната и ортопироксена в мегакристалле клинопироксена, гранат развит также в виде изометричных зерен; *В, С* – мелкозернистый агрегат Amph с редкими пластинками Phl, развивающийся преимущественно по пластинкам распада ортопироксена. Фото шл. в × николях.

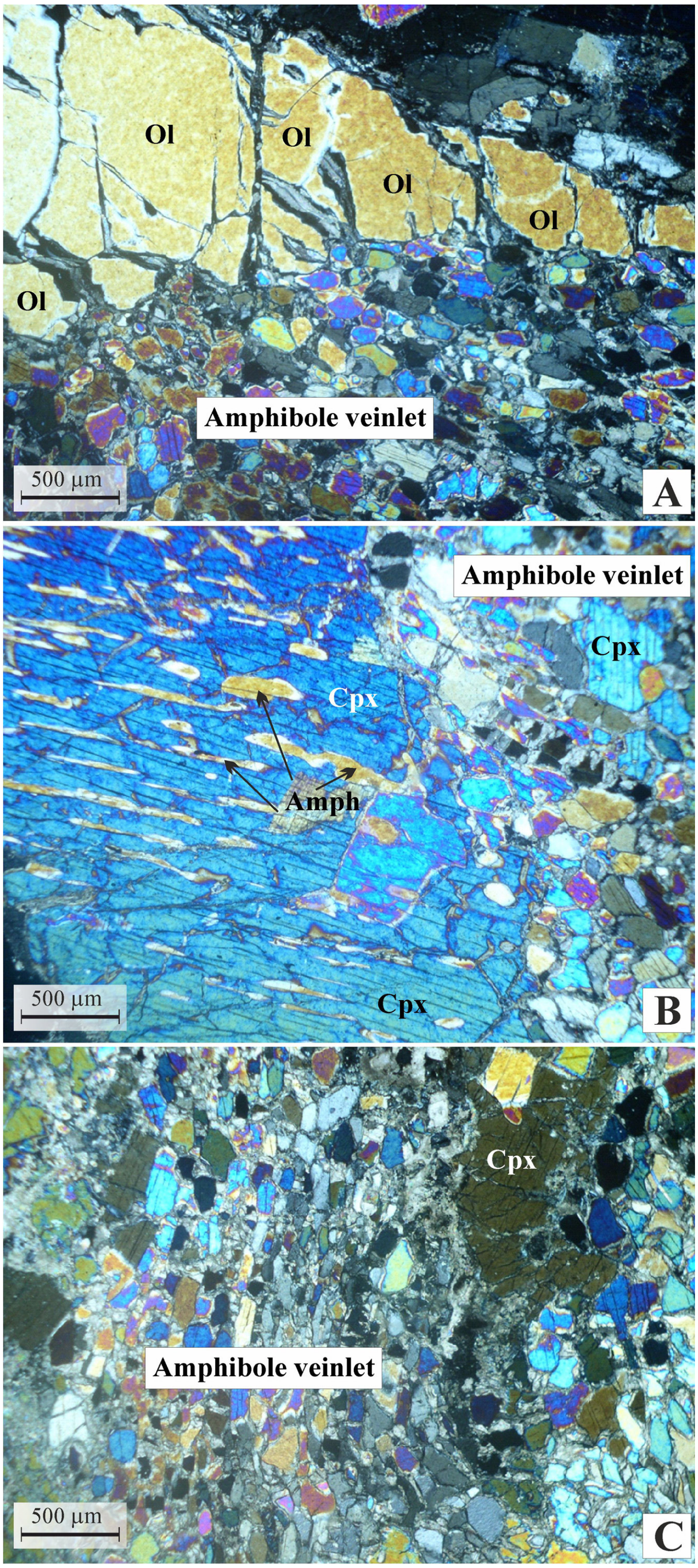

Fig. 3. The photomicrographs of thin section. Amphibole veinlets with rare phlogopite plates in Grt olivine websterite (sample 74-817).

A – resorption of the olivine grain at the contact with the amphibole veinlet; *B* – oriented elongated crystals of amphibole developing in the clinopyroxene grain from the boundary of the amphibole veinlet; *C* – relics of the clinopyroxene grain in selvage of the amphibole veinlet. Images in crossed nicols.

Рис. 3. Амфиболовые прожилки с редкими пластинками флогопита в Grt оливиновом вебстерите (обр. 74-817).

A – резорбция зерна оливина на контакте с амфиболовым прожилком; *B* – ориентированные удлиненные кристаллы амфибола, развивающиеся в зерне клинопироксена от границы амфиболового прожилка; *C* – реликты зерен клинопироксена в зольбандах амфиболового прожилка. Фото шл. в × николях.

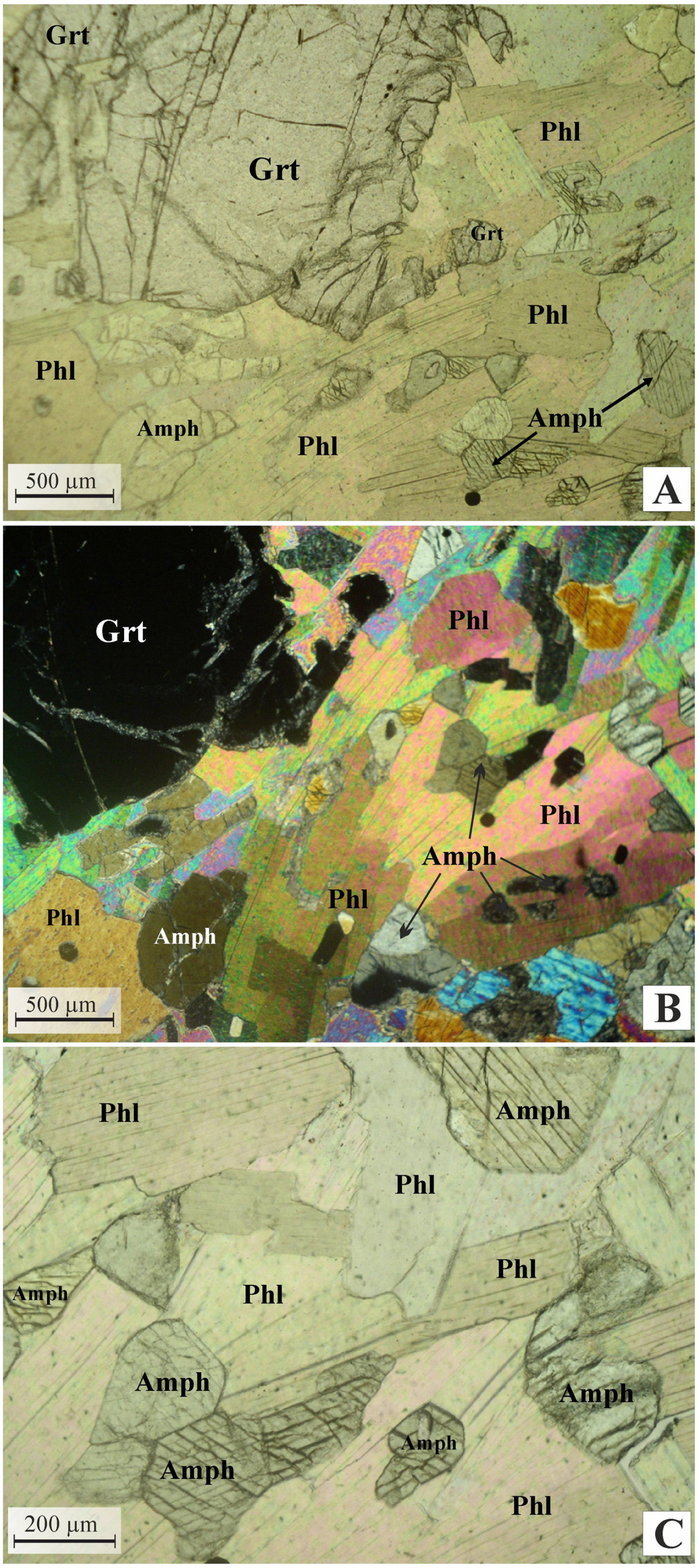

Fig. 4. *A, B* – the photomicrographs of thin section. Resorption of the garnet grain by phlogopite at the boundary with the phlogopite-amphibole veinlet; *C* – the area of the phlogopite-amphibole veinlet with dominating phlogopite.

Cross-sections of regular amphibole crystals are visible. Sample 74-817. Images: *A, C* – without an analyzer; *B* – in crossed nicols.

Рис. 4. *А, В* – резорбция зерна граната флогопитом на границе с флогопит-амфиболовым прожилком; *С* – участок флогопит-амфиболового прожилка с преобладанием флогопита.

Видны сечения правильных кристаллов амфибола. Обр. 74-817. Фото шл.: *А, С* – без анализатора; *В* – в × николях.

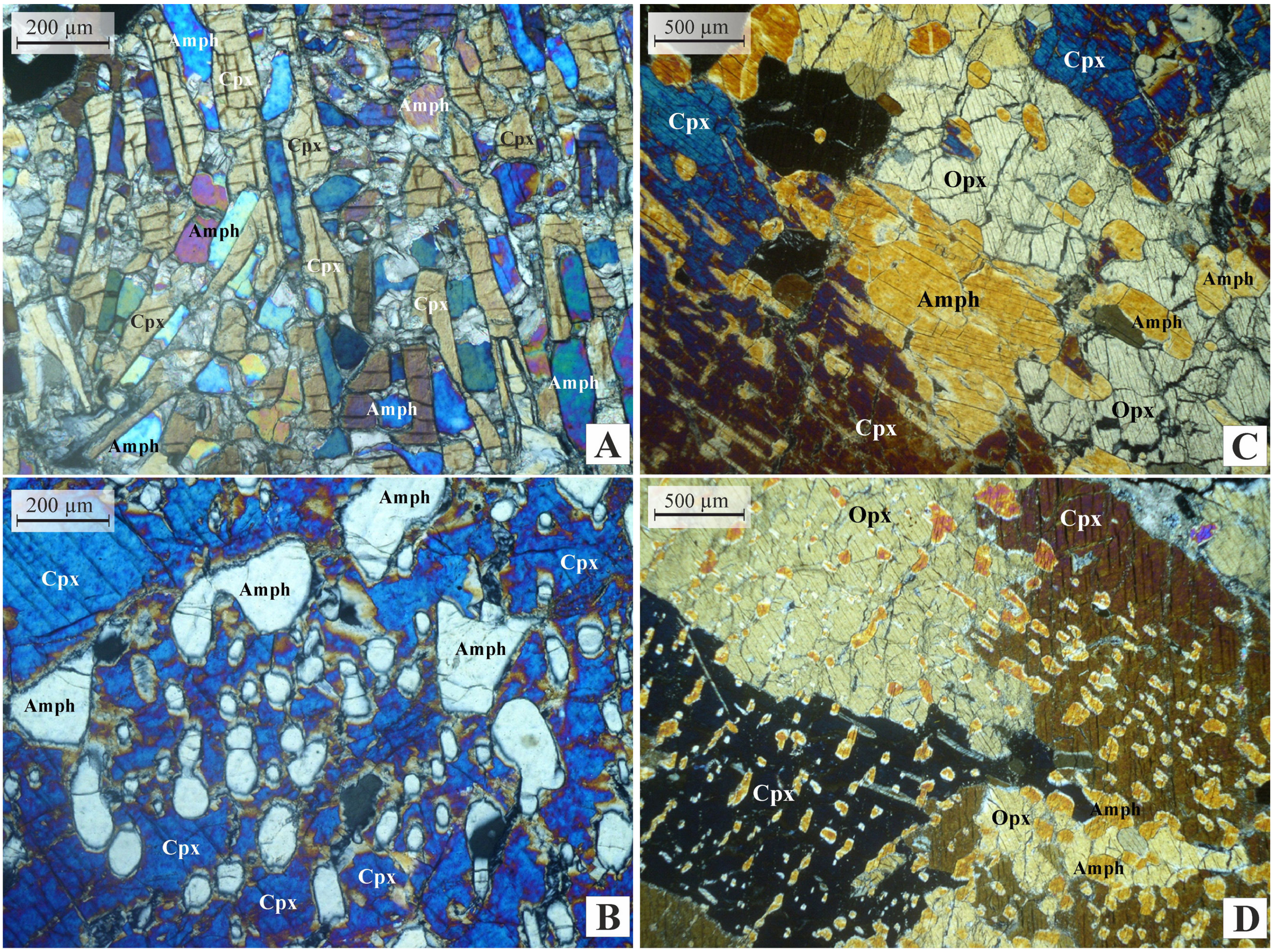

Fig. 5. The photomicrographs of thin section. The abundant development of metasomatic amphibole in clinopyroxene grains.

A – small elongated crystals of amphibole in the clinopyroxene grain (Cpx – cross-section with transversal cleavage and yellow interference colour); *B* – drop-like grains of amphibole (white interference colour) which have single crystallographic orientation in the clinopyroxene grain (blue interference colour). *C* – elongated crystals of amphibole with similar spatial and crystallographic orientation in different grains of clinopyroxene. *D* – small grains of amphibole crossing different grains of clinopyroxene in two mutually perpendicular directions. Sample 74-817. Images in crossed nicols.

Рис. 5. Массовое развитие метасоматического амфибола в зернах клинопироксена.

А – мелкие удлиненные кристаллы амфибола в зерне клинопироксена (Срх – разрез с пересекающейся спайностью и с желтой интерференционной окраской); *В* – каплевидные зерна амфибола (белая интерференционная окраска), имеющие единую оптическую ориентировку в зерне клинопироксена – синяя интерференционная окраска; *С* – удлиненные кристаллы амфибола с одинаковой пространственной и оптической ориентировкой в разных зернах клинопироксена. *D* – мелкие зерна амфибола, пересекающие разные зерна клинопироксена по двум взаимно перпендикулярным направлениям. Обр. 74-817. Фото шл. в × николях.

replaced by phlogopite, and clinopyroxene is reactionnary developing at the earlier grain of orphopyroxene. In many cases, reaction phlogopite develops in the form of palmate porphyroblasts with inclusion of pyroxene and olivine relics (Fig. 9, *C*, *D*). Small zonal plates occuring in fractures of the rocks in the paragenesis with carbonate belong to the later stage and are associated with the influence of the kimberlitic melt on the xenolith (Fig. 10, *A*, *B*).

The most complex relationships are revealed between phlogopite and garnet. The development of garnet at the subsolidus stage is evidenced by the fact that garnet inventively replaced minerals of the primary paragenesis, including phlogopite. In some xenoliths, garnet is dominant, and its content may exceed 80 %. Garnet grains are filled by relics of substituted minerals of the earlier paragenesis, such as Ol, Opx, Cpx, Ilm and Phl (Fig. 11, *A*, *B*), and have a typical sieve-like

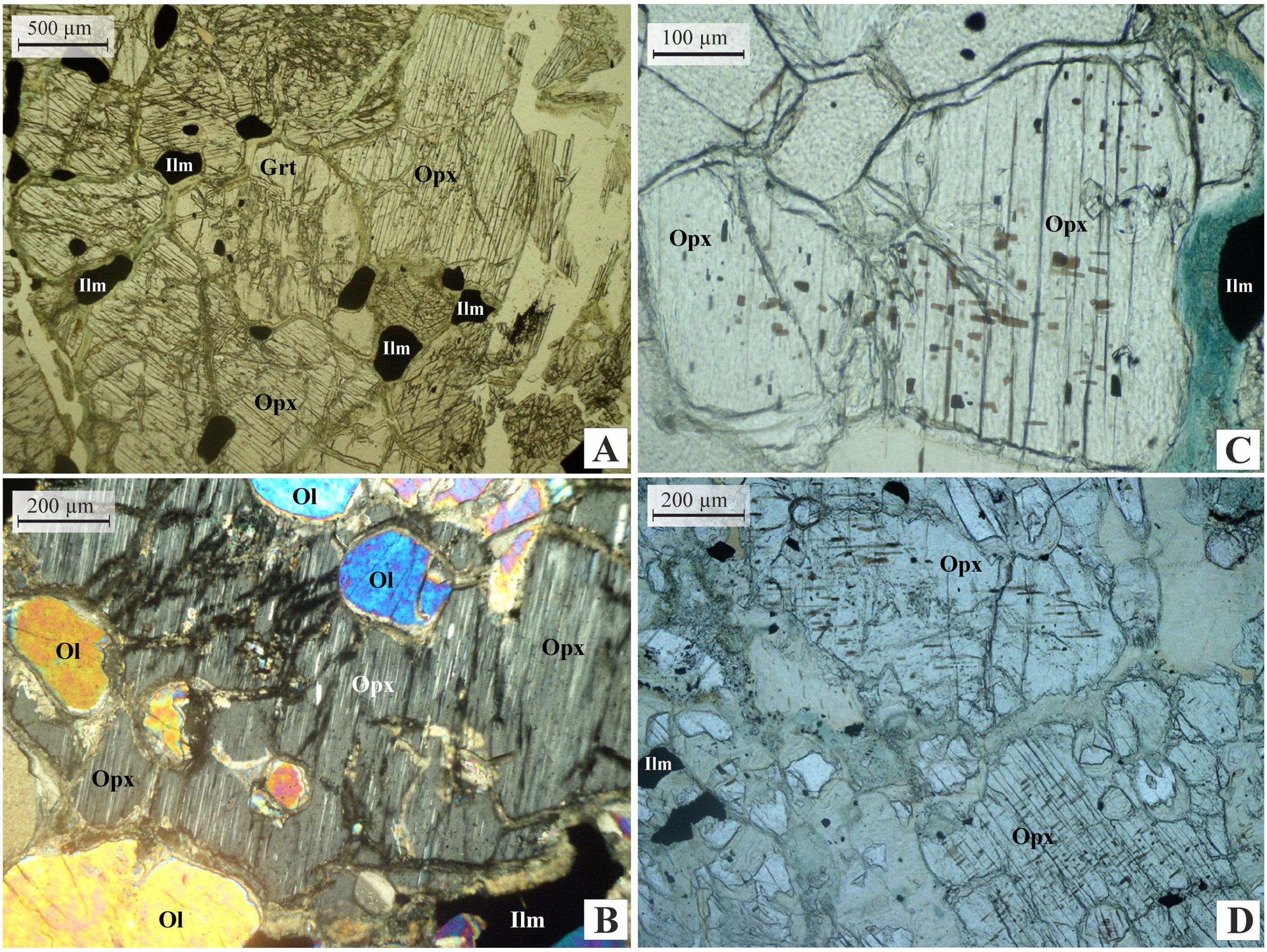

Fig. 6. The photomicrographs of thin section. Relationships between minerals in Phl-Ilm hyperbasites.

A – euhedral texture formed by prismatic crystals of orthopyroxene which are separated by irregular-shaped oval grains of ilmenite; *B* – roundish olivine inclusions in the orthopyroxene grain (homoaxial pseudomorphs). Clinopyroxene exsolution textures are visible in orthopyroxene (parallel light-coloured strips); *C, D* – submicroscopic structures of ilmenite exsolution textures in orthopyroxene. Images: *A, C, D* – without an analyzer; *B* – in crossed nicols.

Рис. 6. Взаимоотношения минералов в Phl-Ilm гипербазитах.

A – панидиоморфнозернистая структура, образованная призматическими кристаллами ортопироксена, между которыми расположены неправильные овальные зерна ильменита; *B* – округлые включения оливина в зерне ортопироксена (гомоосевые псевдоморфозы). В ортопироксене видны структуры распада клинопироксена (параллельные светлые полоски); *C, D* – субмикроскопические структуры распада ильменита в ортопироксене. Фото шл.: *A, C, D* – без анализатора; *B* – в × николях.

fabric in the crossed nicols (Fig. 11, *B*). In the rocks, garnet forms gatherings of round-shaped grains with partial faceting, which are mainly associated with clusters of phlogopite grains. Phlogopite relics are contained in the garnet grains as irregular-shaped or ribbon-shaped inclusions connected with the phlogopite rim at the margins of the garnet grains (Fig. 12, *A*, *B*). Figure 13 shows the replacement of the orphopyroxene grain by the phlogopite plate; the orphopyroxene grain is surrounded by garnet that is reactionary replacing orphopyroxene. Amounts of ilmenite and phlogopite are significantly decreased in the garnetization areas, to suggest the preferred development of garnet on these minerals. Numerous small-sized roundish and semi-faceted hexagonal crystals of pyroxenes, ilmenite and rare phlogopite (Fig. 14, *A*, *B*, *C*) fill the central parts of garnet grains, while the rim of the grains remains free of inclusions. Relict grains of clinopyroxene and orthopyroxene in garnet are often characterized by single extinction to evidence their primary belonging to the same grain. The pseudo-hexagonal faceting of the inclusions is due to the effect of garnet

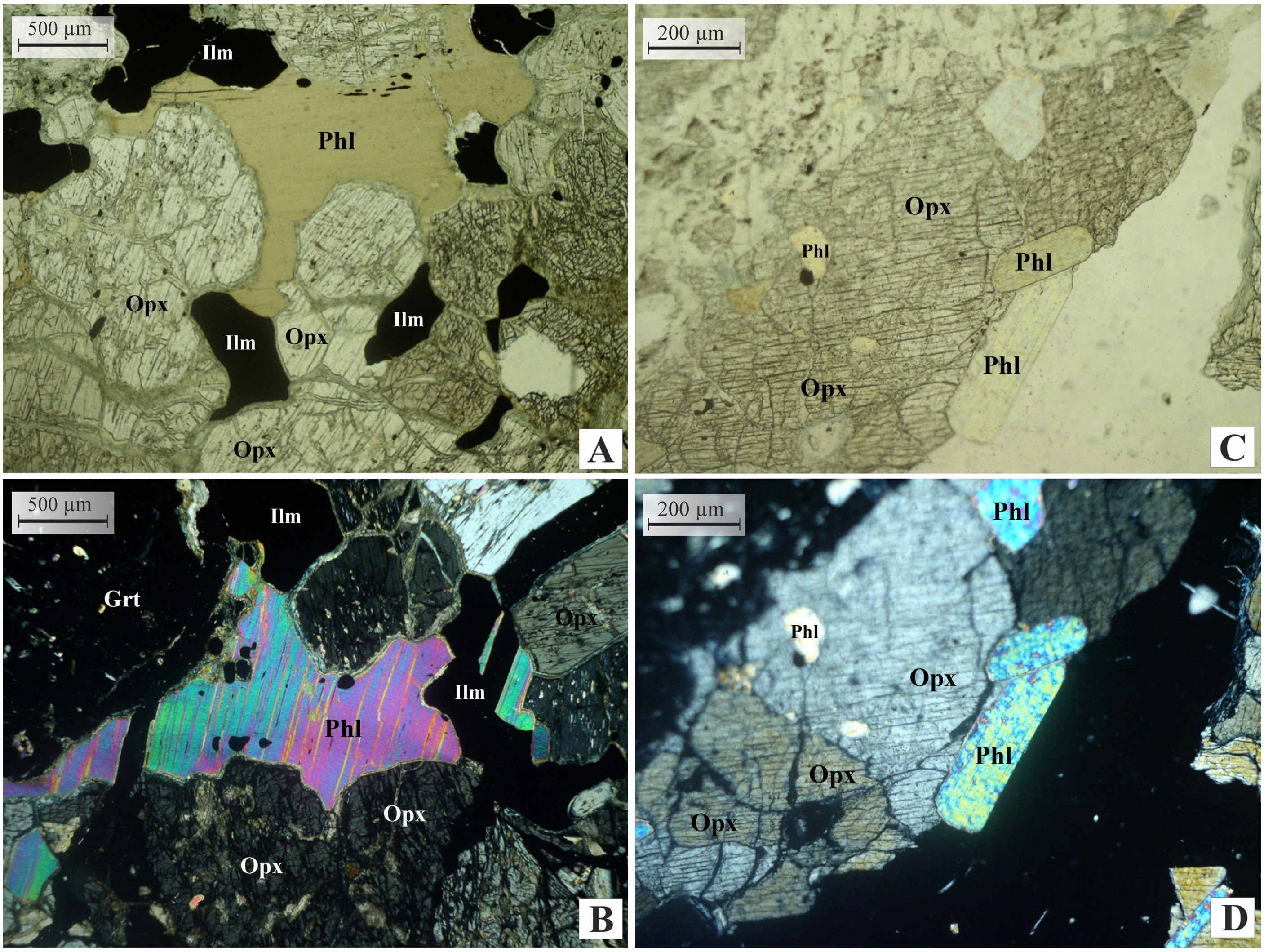

Fig. 7. The photomicrographs of thin section. Relationships between minerals in Phl-Ilm hyperbasites.

A, B – irregular palmate plates of phlogopite and smaller irregular grains of ilmenite between grains of idiomorphic orthopyroxene. Thin (≤5 μm) elongated ilmenite lamellae are present in the phlogopite plates. Larger oval ilmenite grains are associated with margins of the plates; *C, D* – small regular Phl platelets in the orthopyroxene grain. Images: *A, C* – without analyzer; *B, D* – in crossed nicols.

Рис. 7. Взаимоотношения минералов в Phl-Ilm гипербазитах.

A, B – неправильные лапчатые пластинки флогопита и более мелкие неправильные зерна ильменита между зернами идиоморфного ортопироксена. В пластинках флогопита отмечаются тонкие (≤5 мкм) длинные пластинки ильменита. К краям пластинок приурочены более крупные овальные зерна ильменита; *C, D* – правильные мелкие пластинки Phl в зерне Opx. Фото шл.: *A, C* – без анализатора; *B, D* – в × николях.

crystallographic structure.

It should be noted also that evidences of the development of phogopite on garnet are revealed in the garnetized rocks. The boundary between large irregular mica plates and garnet grains has often resorption character (Fig. 15, *A*, *B*). The two minerals often form mutual gulf-shaped boundaries. Roundish inclusions of ilmenite and silicates are visible in garnet. In the centre of the mica flakes there are thin ilmenite platelets, in the margins the ilmenite form roundish inclusions (Fig. 15, *B*). Resorbed garnet relics, that may have been separated from a larger grain, occur in phlogopite (Fig. 16, *A*, *B*). Inclusions of garnet grains in the phlogopite plate (Fig. 16, *C*, *D*) can also be explained by replacing of garnet by phlogopite, though such a conclusion is ambiguous. As evidenced by the above-described observations, relationships between phlogopitization and garnetization are complicated. Obviously, both processes took place at the late stage of rock crystallization and, most probably, at the subsolidus stage when the major part of the minerals was crystallized. The leading role of temperature drop in the development of phlogopite and garnet is suggested by relatively weak signs of deformation, such as insignificantly bending of

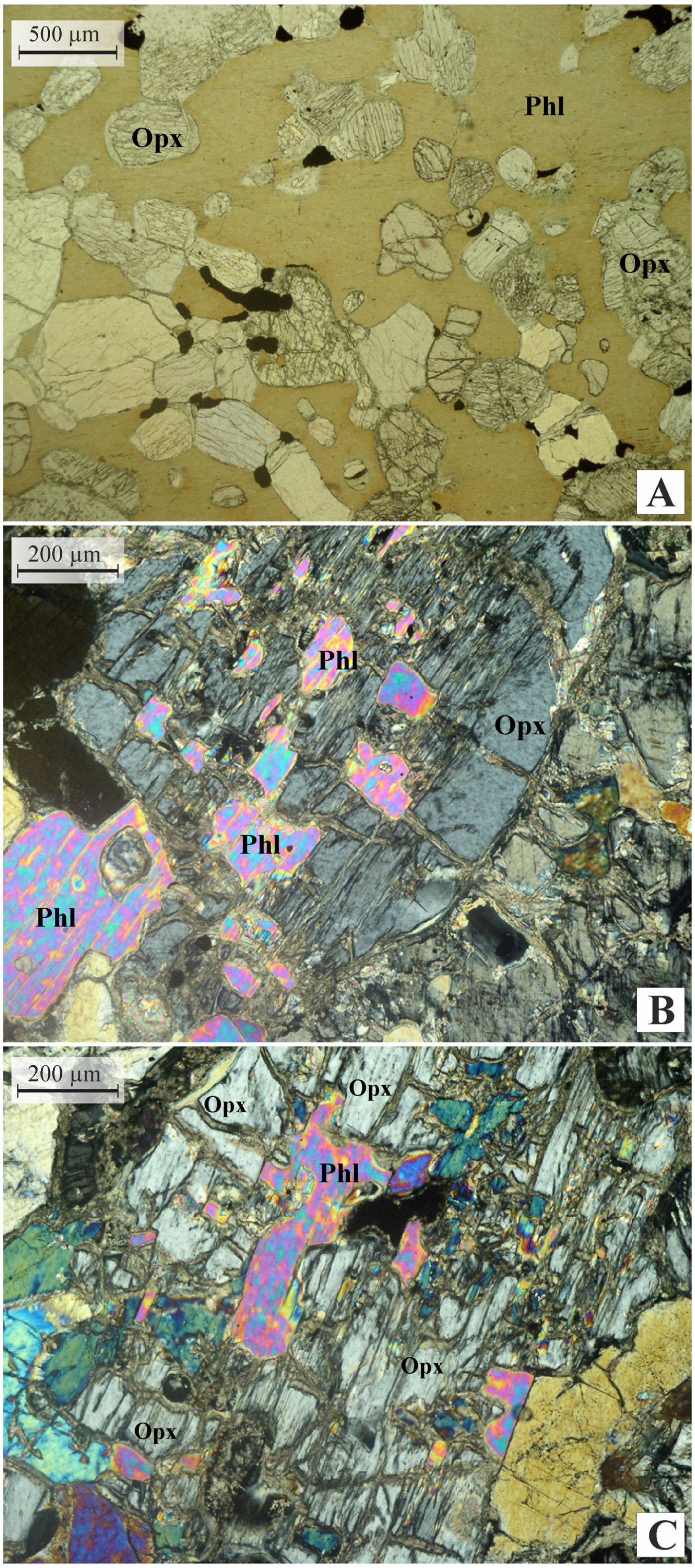

Fig. 8. The photomicrographs of thin section. The character of the metasomatic phlogopite development.

A – metasomatic phlogopite forms 'windows' in the rocks. The large mica plate contains abundant relics of olivine and pyroxenes and resorbed grains of ilmenite (black); *B, C* – intensive phlogopitization of orthopyroxene grains: phlogopite develops in the form of irregular plates with the single crystallographic orientation. Images: *A* – without an analyzer; *B, C* – in crossed nicols.

Рис. 8. Характер развития метасоматического флогопита.

А – заполнение метасоматическим флогопитом участков, своеобразных «окон» в породе. Крупная пластинка слюды содержит обильные реликты оливина, пироксенов и резорбированных зерен ильменита (черное); *B, C* – интенсивная флогопитизация зерен ортопироксена: флогопит развивается в виде неправильных пластинок с единой оптической ориентировкой. Фото шл.: *А* – без анализатора; *B, C* – в × николях.

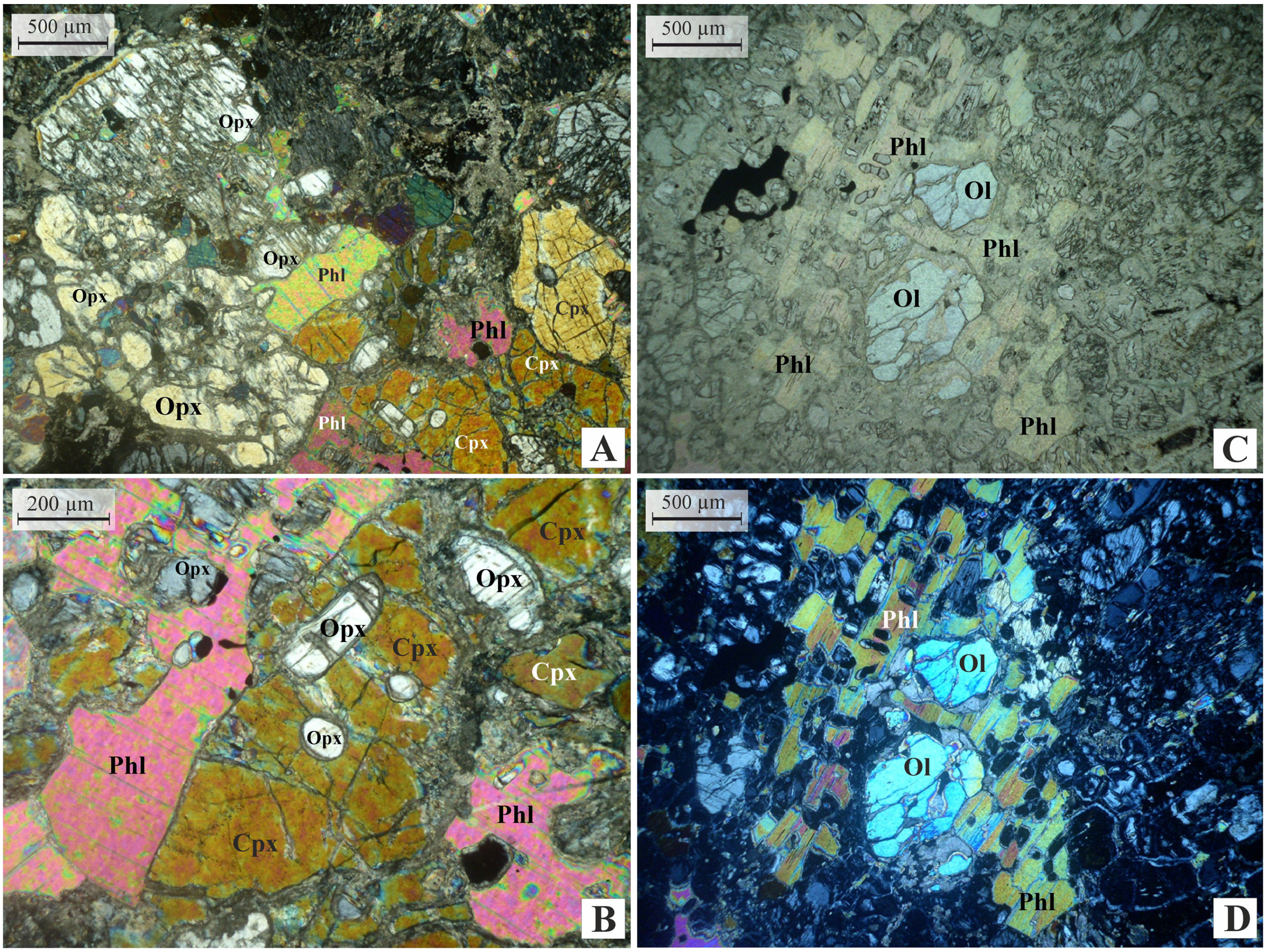

Fig. 9. The photomicrographs of thin section. Reaction development of phlogopite on primary minerals.

A, B – the irregular plate of phlogopite, corroding the grains of orthopyroxene and clinopyroxene; *B* – clinopyroxene develops on orthopyroxene and is replaced by Phl; *C, D* – unregular porphyroblastic plate of phlogopite contains relics of replaced grains of orthopyroxene and olivine. Images: *A, B, D* – in crossed nicols; *C* – without an analyzer.

Рис. 9. Реакционное развитие флогопита по первичным минералам.

A, B – неправильная пластинка флогопита, разъедающая зерна ортопироксена и клинопироксена; *B* – клинопироксен, развивающийся по ортопироксену и замещающийся Phl. В зерне Cpx и в пластинке Phl сохранились одинаково гаснущие реликты зерен Opx; *C, D* – неправильная порфиробластическая пластинка флогопита, содержащая реликты замещенных зерен ортопироксена и оливина, два разобщенных реликта которого имеют одинаковую оптическую ориентировку. Фото шл.: *A, B, D* – в × николях; *C* – без анализатора.

phlogopite plates and slightly undulate extinction of olivine. Phlogopite seems to be formed in the latest magmatic stage from rich in potassium and volatiles residual melts, and later from fluids during autometasomatism. Relationships between garnet and phlogopite are complicated as phlogopitization and garnetization developed almost simultaneously with some advance occurrences of one process in local areas. Residual melt-fluids rich in potassium and volatile components are evidenced by the Phl-Ilm garnetless parageneses with high contents of phlogopite and ilmenite (30–80 % and 15–40 %, respectively). Phlogopite occurs in large porphyraceous plates and fine platelets of the second generation in the fine-grained matrix (Fig. 17, 18). Sometimes ilmenite grains have ideal facets and belong to the matrix paragenesis (Fig. 18, *A*). The specific features of porphyraceous phlogopite I are ilmenite thin regularly-oriented lamellae in the centre and larger roundish ilmenite grains in the marginal zones (Fig. 19, *A*, *B*). The outside rims of phlogopite I and the platelets in the matrix are more intensely brown-coloured (Fig. 20, *A*–*E*). In rare cases, garnet occurs in the

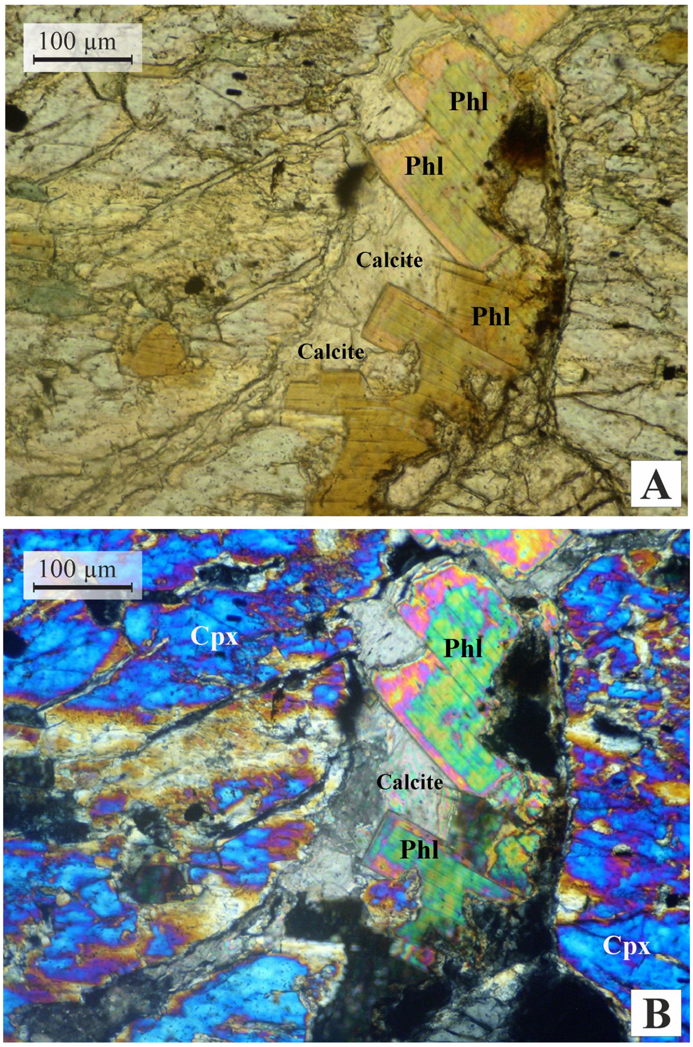

Fig. 10. The photomicrographs of thin section. Late paragenesis of phlogopite with carbonate, which develops along the fractures in the rock.

Regular phlogopite platelets grow on the fracture wall. Phlogopite is almost colourless in narrow rims of the plates. Images: *A* – without an analyzer; *B* – in crossed nicols.

Рис. 10. Поздний парагенезис флогопита с карбонатом, развивающийся по трещинкам в породе.

Правильные пластинки флогопита нарастают на стенку трещинки. В узких краях пластинок флогопит почти бесцветен. Фото шл.: *А* – без анализатора; *В* – в × николях.

form of accessory strongly resorbed grains. The garnet grain is filled in with abundant inclusions of roundish ilmenite grains that are relics of substitution (Fig. 20). The garnet grain seem to be trapped by the melts from the earlier crystallized intrusive phase. The sieve-like structure of the garnet grains with abundant pseudo-hexagonal and isometric relics of pyroxenes, ilmenite and, in some cases, phlogopite suggests that garnet developed mainly in the solid rock after crystallization of all the magmatic minerals. Quite possibly, a part of garnets might have formed at the late stages of crystallization of the melt portions located in the zone of garnet facies. This can be suggested from rare xenoliths of

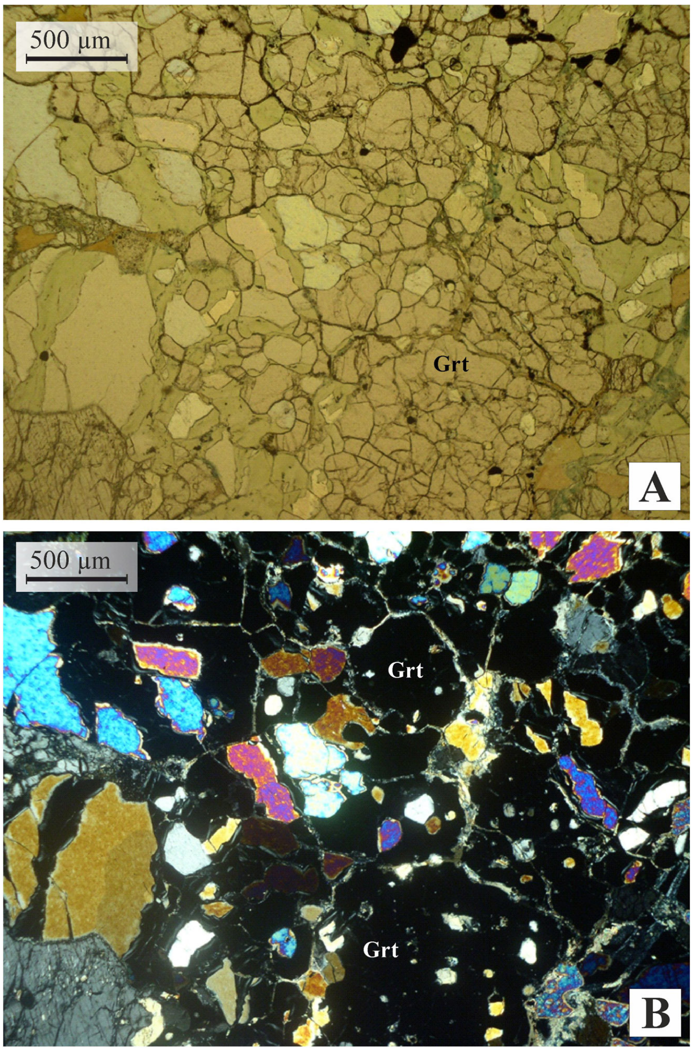

Fig. 11. The photomicrographs of thin section. The abundant development of garnet in the xenolith of the Phl-Ilm garnetized lherzolite.

Numerous relics of minerals of the early paragenesis, such as olivine, pyroxenes, ilmenite and phlogopite, are present inside the garnet grains. Images: *A* – without analyzer; *B* – in crossed nicols. The separate grains of garnet (black) with thin light-coloured margins are visible. Irregular silicates relics are coloured in different interference colours and included in garnet or located at the boundaries of the garnet grains.

Рис. 11. Массовое развитие граната в ксенолите Phl-Ilm гранатизированного лерцолита.

Внутри зерен граната сохранились многочисленные реликты минералов раннего парагенезиса – оливина, пироксенов, ильменита и флогопита. Фото шл.: *А* – без анализатора; *В* – в × николях. Видны отдельные зерна граната (черное), окаймленные тонкими светлыми каймами. Неправильные реликты силикатов окрашены в разные интерференционные цвета и включены в гранат или расположены на границах его зерен.

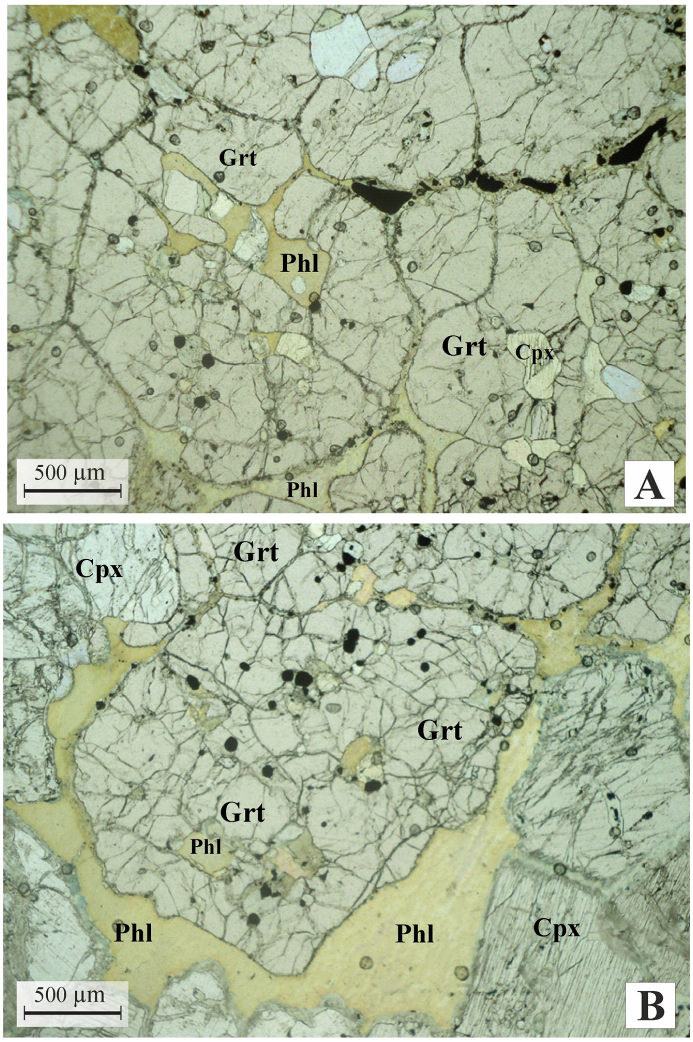

Fig. 12. The photomicrographs of thin section. Polycrystalline aggregate composed of garnet regular grains in the Phl-Ilm garnetized lherzolite (*A*, *B*).

Garnet mainly developed on phlogopite which ribbon-shaped relics are connected with the external rim. Phlogopite in garnet and the rim have single crystallographic orientations. Besides phlogopite, roundish relics of ilmenite (black) and silicates are visible in the garnet grains. Image (*A*) shows larger elongated ilmenite grains which were 'forced out' to the margins of the garnet grains. Images without an analyzer.

Рис. 12. Поликристаллический агрегат из правильных зерен граната в Phl-Ilm гранатизированном лерцолите (*А*, *Б*).

Гранат развит преимущественно по флогопиту, от которого остались лентовидные реликты, соединяющиеся с внешней каймой. Флогопит в гранате и кайма имеют одинаковую оптическую ориентировку и до гранатизации составляли единое зерно. Кроме флогопита в зернах граната видны округлые реликты ильменита (черное) и силикатов. На (*А*) видны более крупные удлиненные зерна ильменита, «вытесненные» на края зерен граната. Фото шл. без анализатора.

orthopyroxenites with very insignificant quantities of phlogopite, wherein garnet forms small regular-shaped grains between the grains of orthopyroxene and does not contain any substitution relics of other minerals.

The deformed phlogopite-amphibole rocks contain regular-shaped microcrystals (5–50 µm) of titanian chromite and resorbed relict grains of ilmenite (3–7 %) and clinopyroxene (≤5 %) (Fig. 21, *A*, *B*). Particular texture features evidence that the rocks were formed under conditions of strong deformation. Elongated prismatic amphibole crystals form narrow rosettes intergrown with strongly deformed irregular-shaped plates of phlogopite (Fig. 22, *A*–*E*). The amphibole crystals are often bended. Inside the phlogopite grains, they look like torn-off relics. Cross-sections of phlogopite resemble a torchs or a quadrangular stars with sharp torn-off edges (Fig. 22, *C*, *D*; Fig. 23, *A*). The phlogopite plates are strongly deformed and dissected into blocks of various orientations that are healed by a fine-grained aggregate of more intensively coloured mica (Fig. 23, *A*–*D*). The ilmenite inclusions are lacking in the phlogopite. In the rocks, ilmenite occurs as elongated irregular-shaped grains with serrated edges indicating its dissolution (Fig. 21, *A*, *B*). Aggregates of prismatic amphibole are associated with micrograins of titanian chromite. Specific textures and mineral compositions of the deformed phlogopite-amphibole rocks suggest

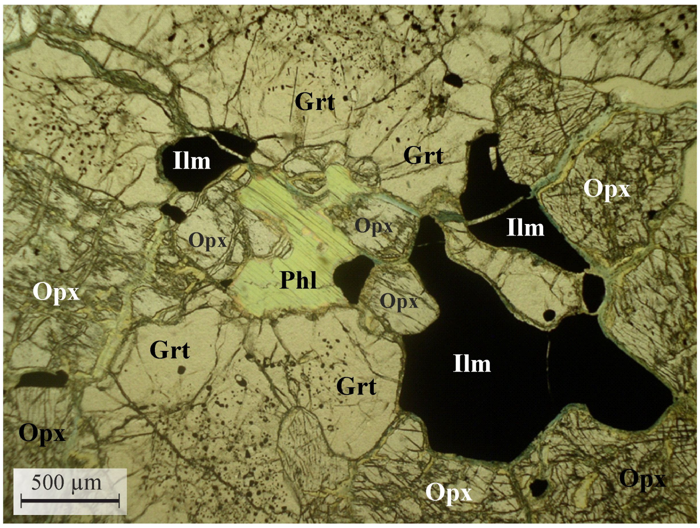

Fig. 13. The photomicrographs of thin section. The irregular Phl plate developing on the Opx grain that is surrounded by growing garnet grain.

Central parts of the Grt grain contain relics of ilmenite (black points). At the right of the image, a gulf-like extension of the garnet cuts the large grain of ilmenite. Image without an analyzer.

Рис. 13. Неправильная пластинка Phl, развивающаяся по зерну Opx, окруженному зернами разрастающегося граната.

Центральные части зерен Grt испещрены черными точками (реликты Ilm). В правой части фото видно, как заливообразное продолжение зерна граната расчленяет крупное зерно ильменита. Фото шл. без анализатора.

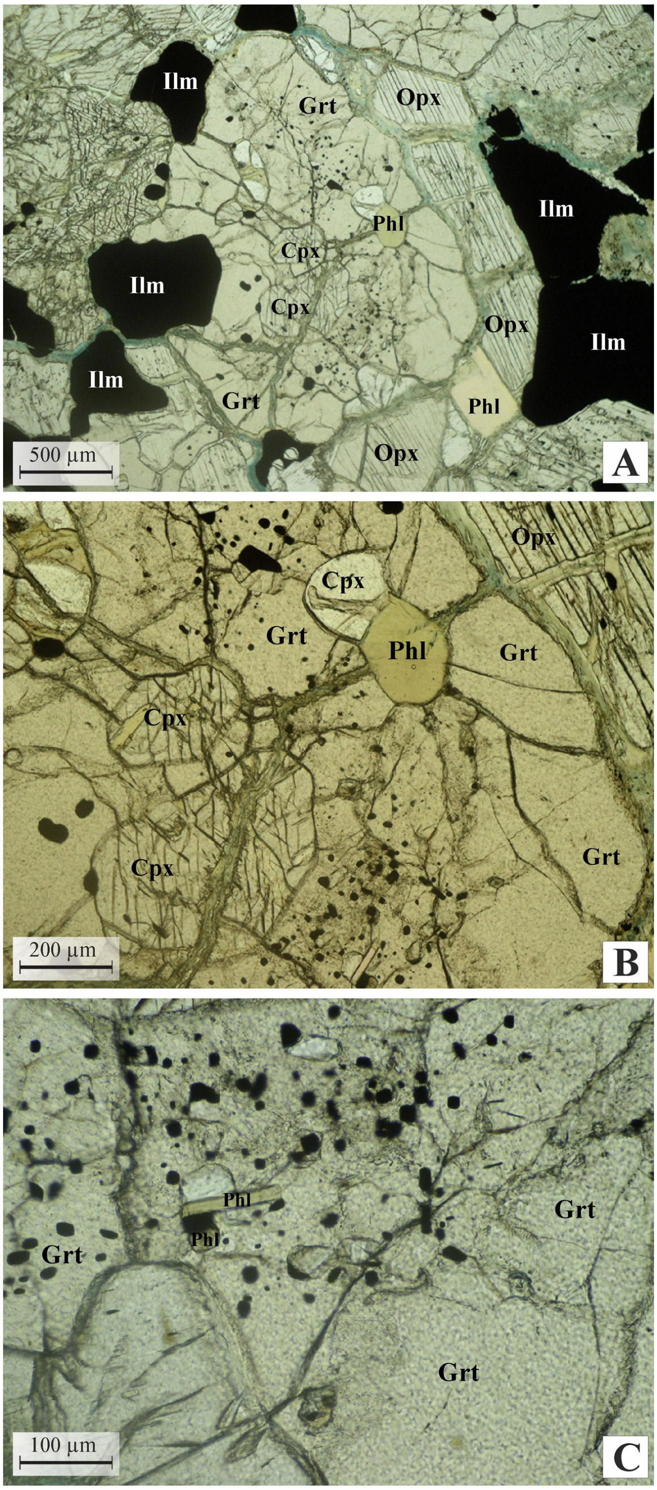

Fig. 14. The photomicrographs of thin section. The garnet porphyroblast has regular crystallographic facets and develops on the orthopyroxene grain in the Phl-Ilm garnetized websterite.

A, B – inside garnet, visible are numerous semi-faceted pyroxene grains, small roundish grains of ilmenite and a hexagonal platelets of phlogopite. In external zone of the garnet porphyroblast, inclusions of relics of other minerals are lacking. In the rock large grains of ilmenite are irregularly shaped. *B* – small regular platelets of phlogopite in the garnet porphyroblast. Images (*B*) and (*C*) show zoomed-up areas given in image (*A*). Images without an analyzer.

Рис. 14. Порфиробласт граната, имеющий правильную кристаллографическую огранку и развивающийся по зерну ортопироксена в Phl-Ilm гранатизированном вебстерите.

A, B – внутри граната видны многочисленные полуограненные зерна пироксенов, округлые мелкие зерна ильменита и гексагональная пластинка флогопита. Во внешней зоне порфиробласта граната включения реликтов других минералов отсутствуют. Крупные зерна ильменита в породе имеют обычно неправильную форму и размеры. *C* – мелкие правильные пластинки флогопита в порфиробласте граната. *B* и *C* – увеличенные участки (*A*). Фото шл. без анализатора.

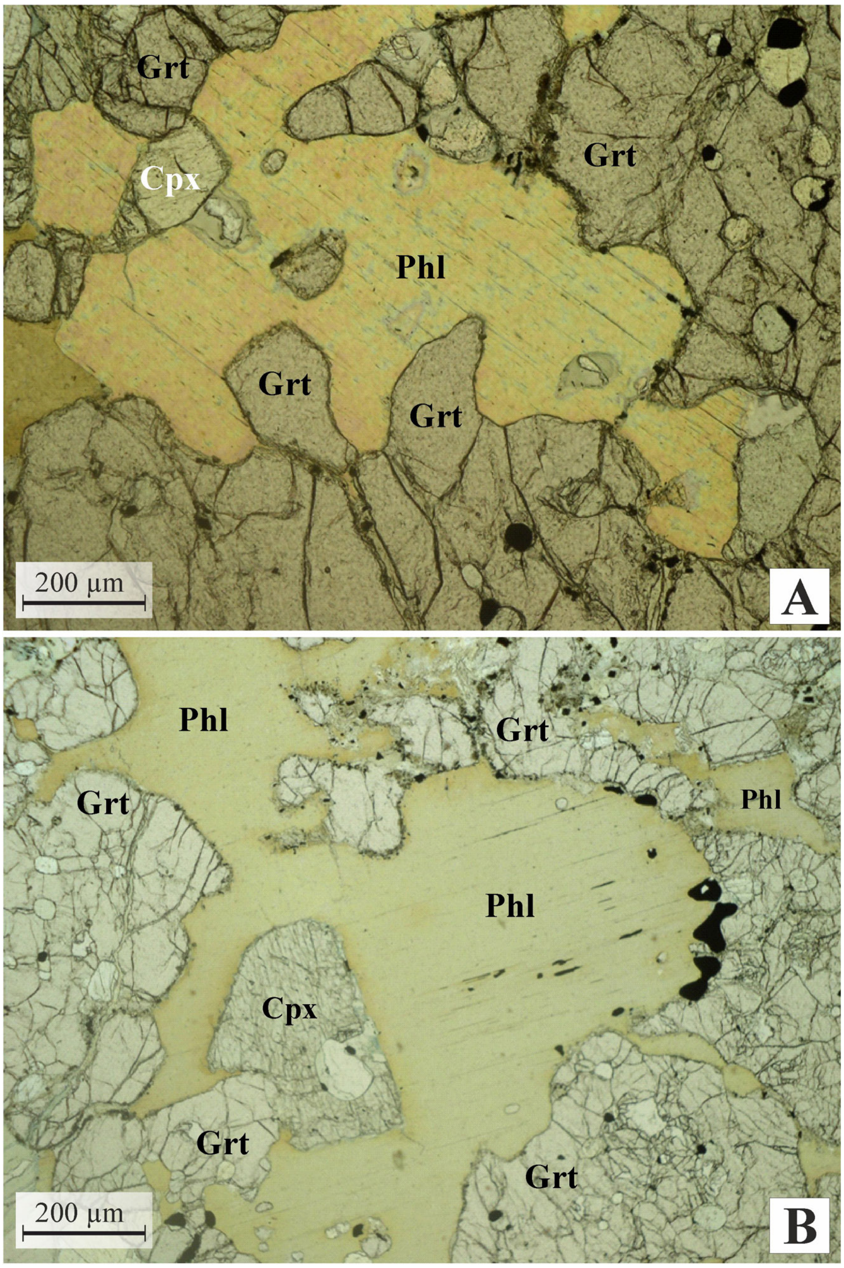

Fig. 15. The photomicrographs of thin section. Reaction boundaries between garnet and phlogopite in the Phl-Ilm garnetized lherzolite.

Grains of both minerals are irregularly shaped and have gulf-like mutual boundaries. Relics of ilmenite and silicates are visible in garnet in images (*A*) and (*B*). In central parts of the phlogopite plate, long thin ilmenite lamellae are oriented along cleavage; at the boundary of the plate, they change to larger oval grains (*B*). Images without an analyzer.

Рис. 15. Реакционные границы между гранатом и пластинками флогопита в Phl-Ilm гранатизированном лерцолите.

Формы зерен того и другого минерала неправильные, с заливообразными взаимными вхождениями. В гранате видны округлые реликты ильменита и силикатов (*A, B*). В центральных частях пластинок флогопита по спайности ориентированы тонкие длинные пластинки ильменита, которые сменяются на границе зерна более крупными овальными зернами (*B*). Фото шл. без анализатора.

their formation under conditions of intensive stress, possibly, in the root parts of deep faults.

The described petrographic features of the ilmenite-phlogopite parageneses in the deep-seated xenoliths from the kimberlites of the Kuoika field are the basis for the following conclusions:

1. The xenoliths of the Phl- Ilm hyperbasites are pieces of the complex mantle magmatic complex characterised by ubiquitous subsolidus metasomatic processes. The primary magmatic origin of the series is

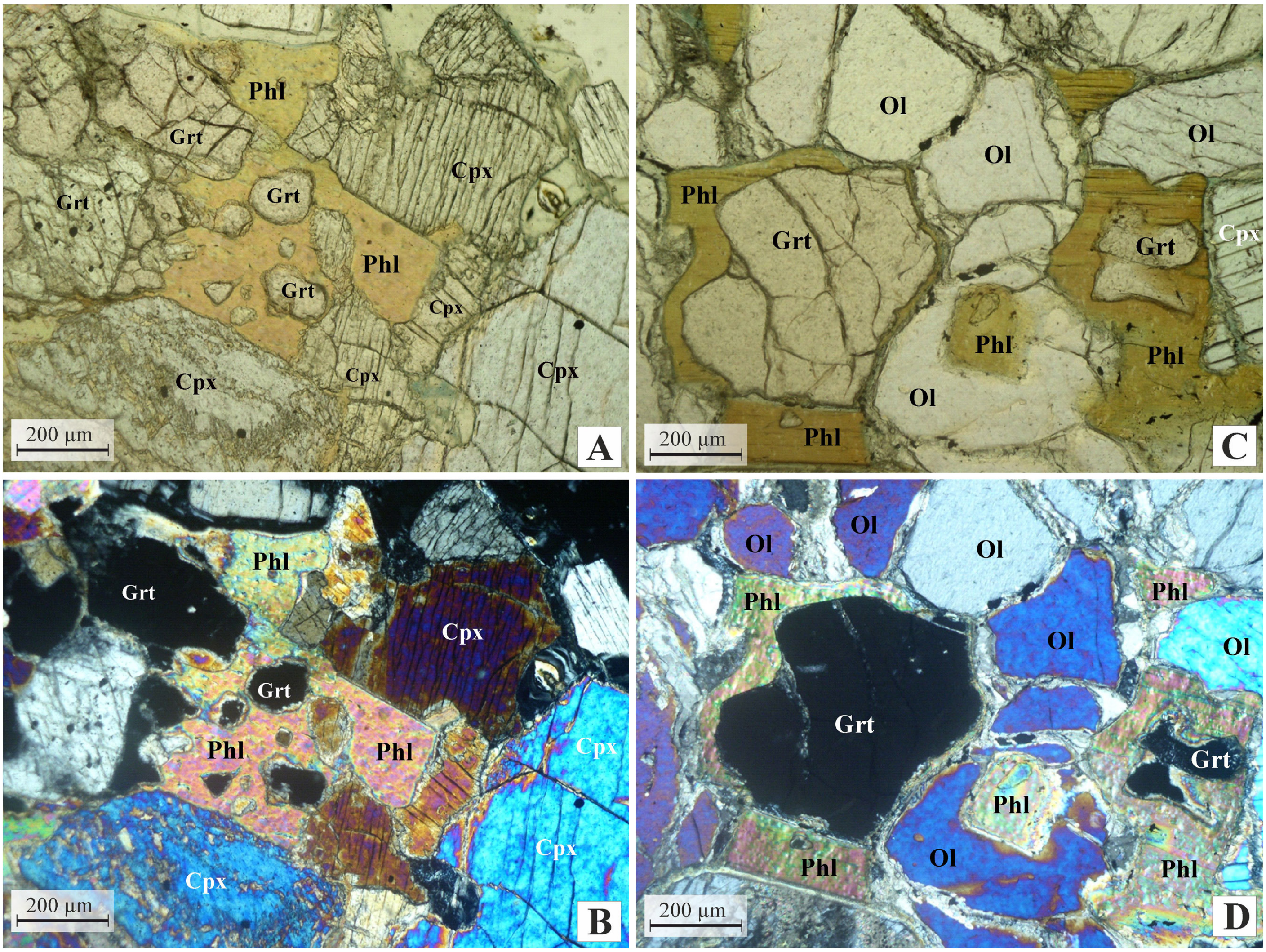

Fig. 16. The photomicrographs of thin section. Reaction relationships between garnet and phlogopite in the Phl-Ilm garnetized clinopyroxenite.

Images (*A*) and (*B*) show that the resorbed part of the clinopyroxene crystal and small grains of garnet (possibly, separated from a larger grain) are present in the phlogopite plate. Boundaries between mica and clinopyroxene and garnet have reaction character. Images (*C*) and (*D*) show isometric grains of garnet in phlogopite plate. In this case, it is impossible to unambiguously determine either phlogopite developed later than garnet or vice versa. Images: *A*, *C* – without an analyzer; *B*, *D* – in crossed nicols.

Рис. 16. Реакционные взаимоотношения между гранатом и флогопитом в Phl-Ilm гранатизированном клинопироксените.

(*A, B*) в пластинке флогопита находятся резорбированная часть кристалла клинопироксена и мелкие зерна граната, возможно, отделенные от более крупного зерна. Границы слюды с клинопироксеном и гранатом имеют реакционный характер. (*C, D*) изометричные зерна граната в пластинках флогопита. Разобщенные пластинки флогопита принадлежат единому зерну, о чем свидетельствует их одинаковое погасание. В данном случае нельзя однозначно судить о более позднем развитии флогопита по отношению к гранату или наоборот. Фото шл.: *A, C* – без анализатора; *B, D* – в × николях.

confirmed by the magmatic sequence of crystallization of the minerals (olivine – orthopyroxene – clinopyroxene with late phlogopite and ilmenite) and the presence of typical magmatic (euhedral, subhedral, sideronitic and porphyraceous) structures.

2. The intensive substitution of the minerals by phlogopite took place, most probably, at the subsolidus stage during the process of autometasomatism when the early intrusive phases were affected by late melts rich in potassium and volatiles. The complex morphological relationships between phlogopite and garnet developing at the given stage suggest their simultaneous occurrence with the advance development of either phlogopitization or garnetization in the local areas of the rocks.

3. The next evolution stage of the Phl-Ilm series

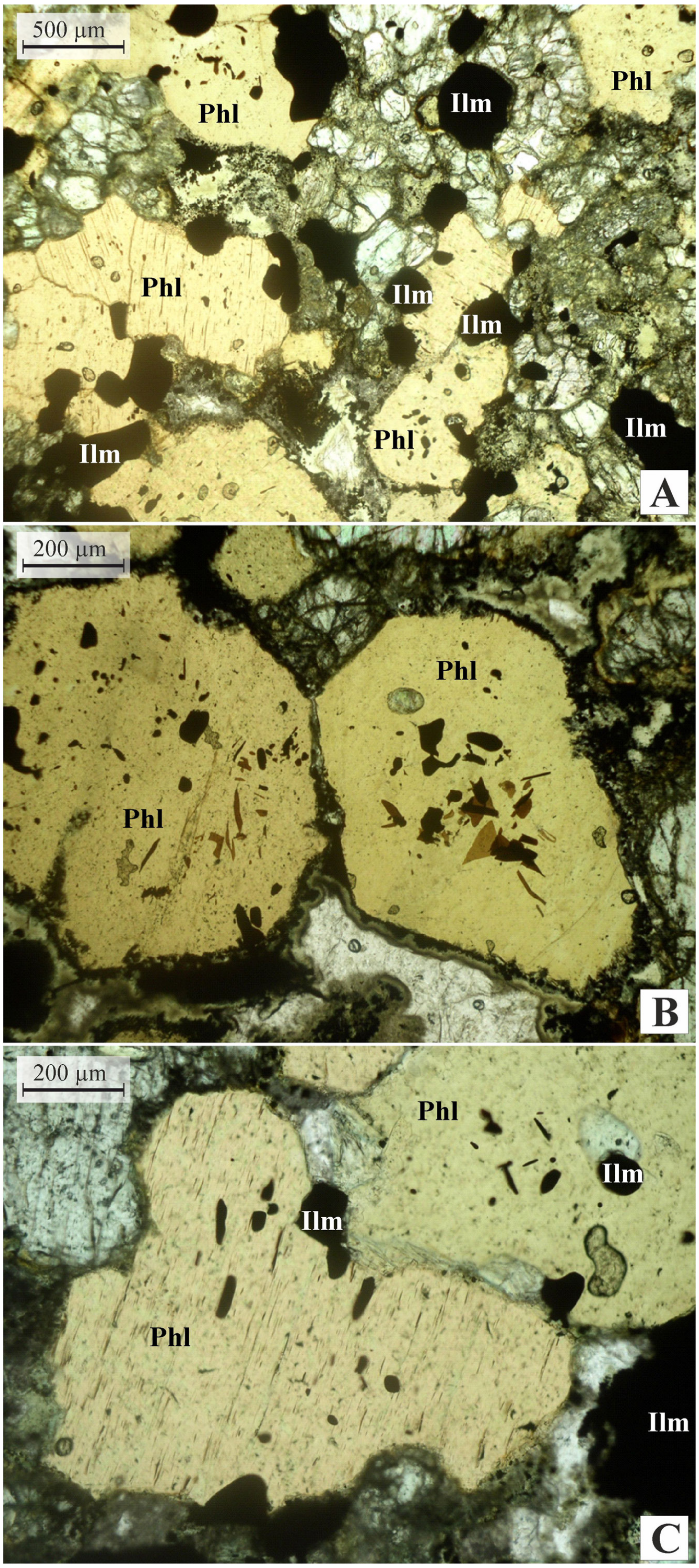

Fig. 17. The photomicrographs of thin section. Porphyrous phlogopite plates in the garnetless Phl-Ilm websterite.

A – the matrix contains small prismatic grains of pyroxenes (mainly orthopyroxene) and oval grains of ilmenite. *B* and *C* –regular plates of phlogopite. Thin transparent lamellae of ilmenite are located along cleavage in mice (*B*). Larger elongated and isometric grains of ilmenite with oval-shaped boundaries tend to be located at the marginal zones of the mica plates (*A, B*). Images without an analyzer.

Рис. 17. Порфировидная структура в безгранатовом Phl-Ilm вебстерите.

A – в породе присутствуют мелкие призматические зерна пироксенов (преимущественно ортопироксен) и овальные, изометричные зерна ильменита. *B* и *C* – правильные вкрапленники флогопита. По спайности в слюде располагаются тонкие просвечивающие пластинки ильменита (*B*). Более крупные удлиненные и изометричные зерна ильменита с овальными ограничениями тяготеют к краевым зонам пластинок слюды (*A, B*). Фото шл. без анализатора.

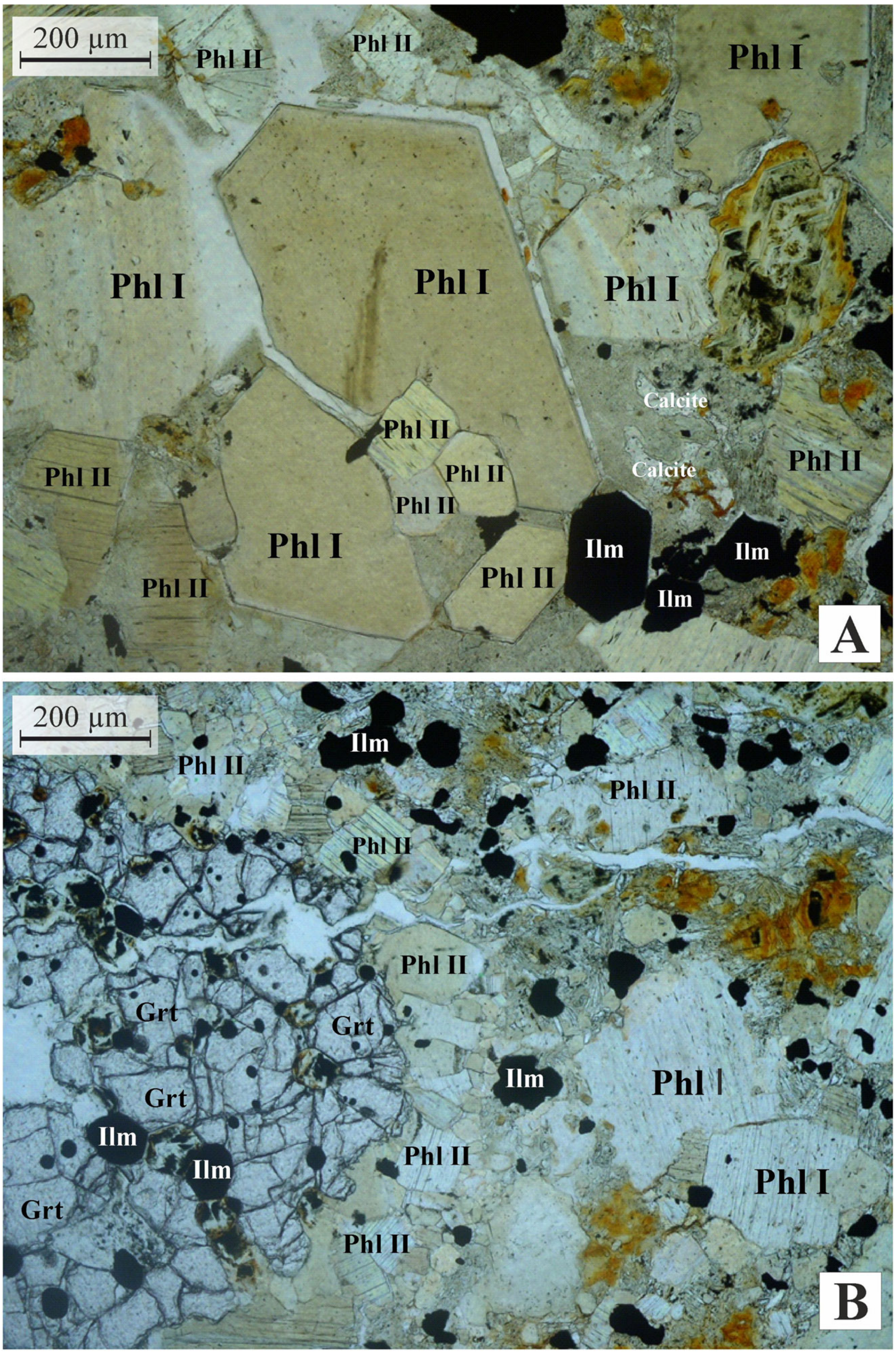

Fig. 18. The photomicrographs of thin section. Porphyrous texture in the Phl-Ilm olivine websterite.

A – regularly-faceted plates of Phl I, flakes of Phl II and an ideally faceted grain of ilmenite are visible. Late serpentine and carbonate are developed in the rock matrix. (*B*) The grain of strongly resorbed garnet that is surrounded by the Phl II reaction rim. In garnet numerous roundish grains of ilmenite are relics of replacing during garnetization. Garnet possibly was caught of the residual high-potassium melt from the earlier intrusive phase. In the rock matrix, irregular grains of ilmenite are resorbed with later processes, including serpentization and carbonitization. Images without an analyzer.

Рис. 18. Порфировидная структура в Phl-Ilm оливиновом вебстерите.

А – видны правильно ограненные вкрапленники Phl I, пластинки флогопита II (Phl II) и идеально ограненный вкрапленник ильменита. В матрице породы развиты поздние серпентин и карбонат. *В* – «вкрапленник» сильно резорбированного граната, окруженного реакционной каймой из Phl II. В гранате видны многочисленные округлые зерна ильменита, являющиеся реликтами замещения при гранатизации. По-видимому, гранат попал в остаточный высоко-калиевый расплав из более ранней интрузивной фазы. Неправильные зерна ильменита в матрице резорбированы более поздними процессами (серпентинизация, карбонатизация). Фото шл. без анализатора.

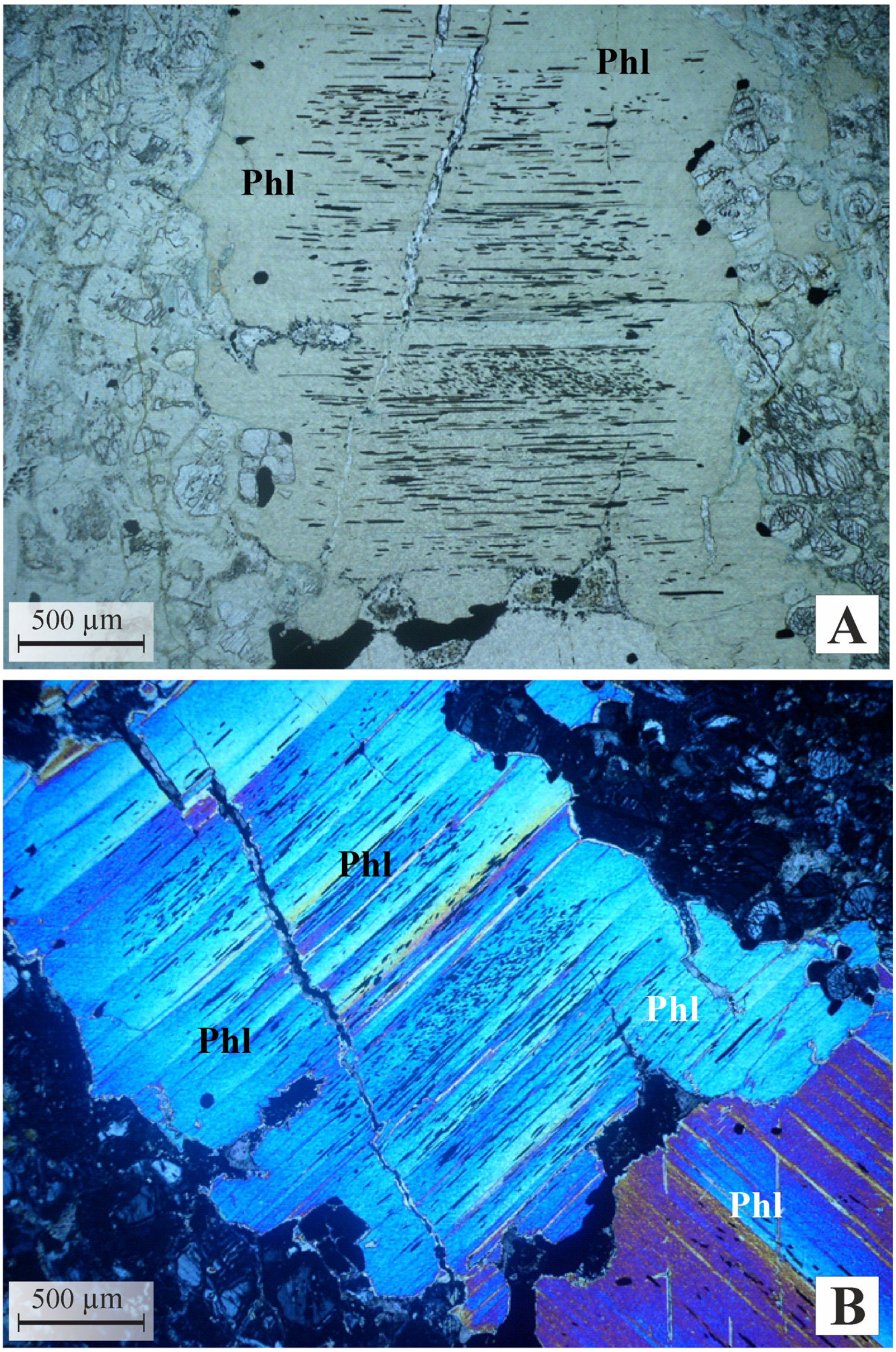

Fig. 19. The photomicrographs of thin section. Oriented thin lamllae of ilmenite in porphyrous phlogopite.

Larger oval-shaped ilmenite grains tend to be located at the margins of the phlogopite plates. Images: *A* – without an analyzer; *B* – in crossed nicols.

Рис. 19. Ориентированное положение тонких пластинок ильменита в порфировидных вкрапленниках флогопита.

К краям вкрапленников тяготеют более крупные овальные зерна ильмената. Фото шл.: *A* – без анализатора, *B* – в × николях.

corresponds to the development of the deformation zones which led to the formation of specific deformed phlogopite-amphibole parageneses with titanian chromite and resorbed relics of clinopyroxene and ilmenite. It is most probable than these rocks developed on the rocks of the Phl-Ilm series in the root parts of the deep fault zones.

Representative compositions of minerals from two

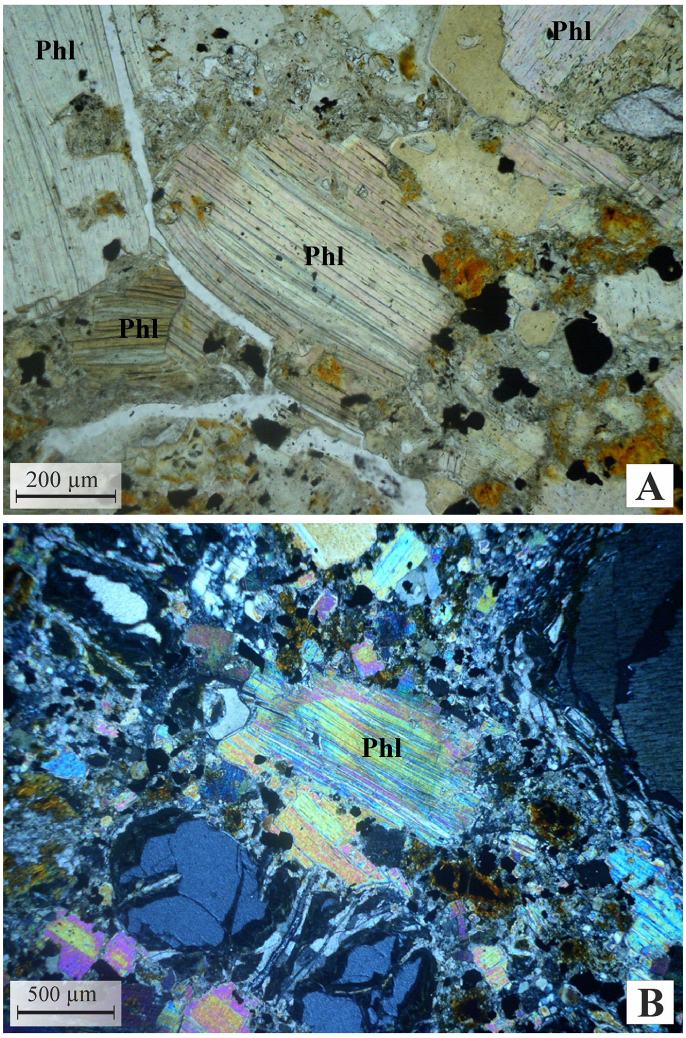

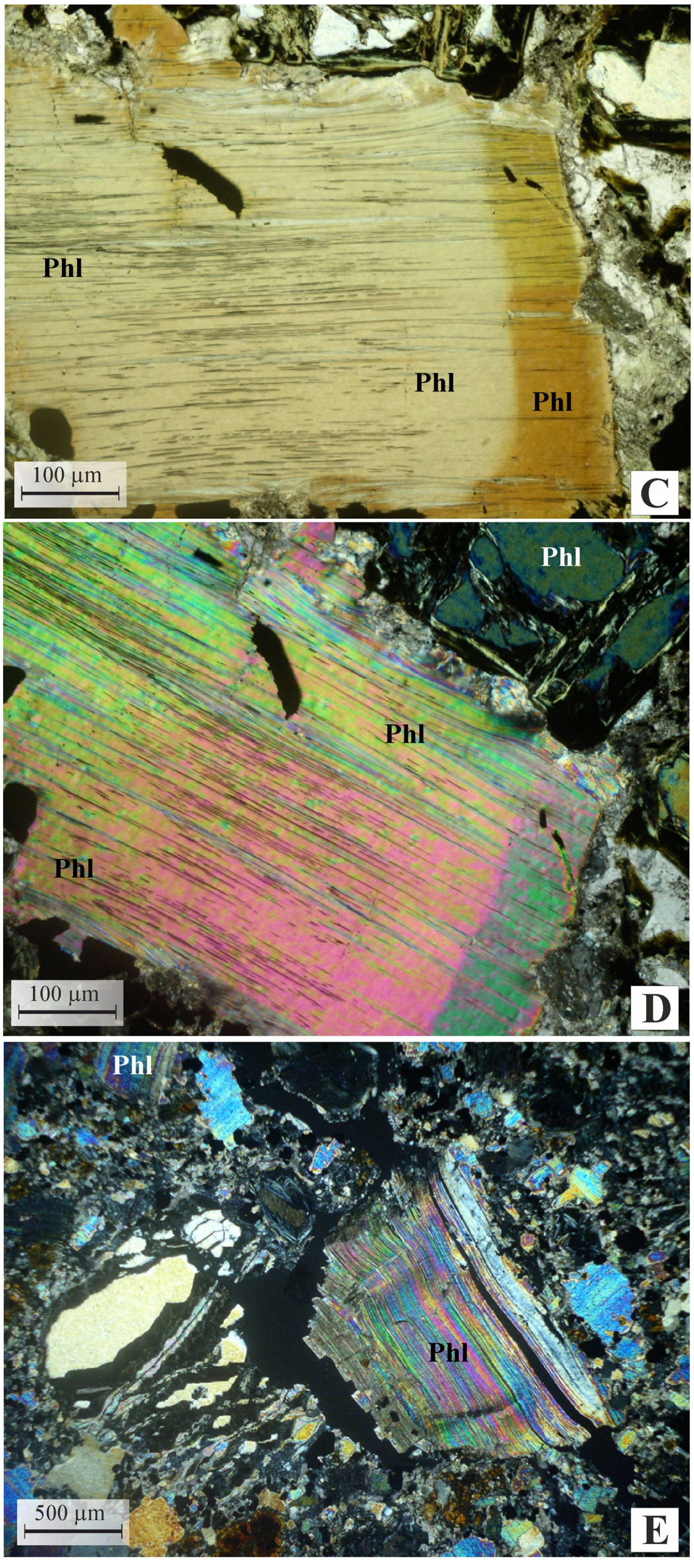

Fig. 20. The photomicrographs of thin section. Zonal porphyrous plates of phlogopite (Phl I).

In images (*A*) and (*C*) the marginal zones are more intensely red and differs by a change in the interference colour (*B, D, E*). In image (*E*), it is clearly visible that porphyrous phlogopite plate was deformed after crystallization of the rocks. Image: *A, C* – without an analyzer; *B, D, E* – in crossed nicols.

Рис. 20. Зональные вкрапленники флогопита (Phl I).

На снимках (*A*) и (*C*), сделанных без анализатора, видна более интенсивно-рыжая окраска внешних зон. Внешняя кайма отличается и по изменению интерференционной окраски (*B*, *D*, *E*). На фото (*E*) четко видна деформация вкрапленника, происходившая уже после кристаллизации пород. Фото шл.: *A*, *C* – без анализатора; *B*, *D*, *E* – в × николях.

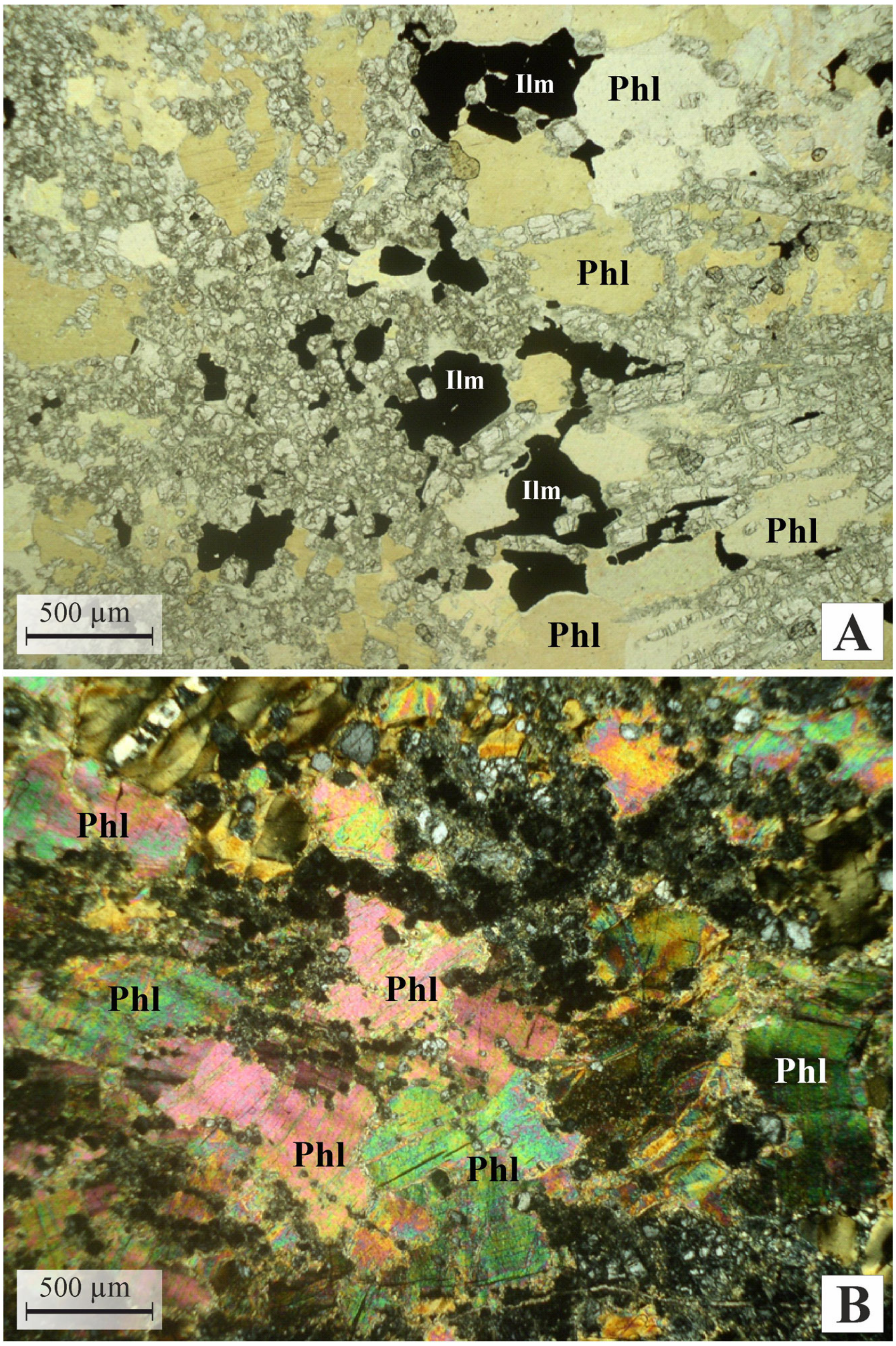

Fig. 21. The photomicrographs of thin section. General texture of the deformed phlogopite-amphibole rocks.

The ragged edges of the phlogopite plates and ilmenite grains are visible. The rocks also contain elongated partially bended crystals of monoclinal amphibole. Images: *A* without an analyzer; *B* – in crossed nicols.

Рис. 21. Общий вид структуры в деформированных флогопит-амфиболовых породах.

Видны совершенно неправильные, с «оборванными» краями пластинки флогопита и зерна ильменита с изъеденными, зазубренными контурами. Остальное выполнение породы состоит из удлиненных частично изогнутых кристаллов моноклинного амфибола. Фото шл.: *A* – без анализатора; *B* – в × николях.

xenoliths of the Mg series with metasomatic phlogopite and amphibole and five xenoliths of the Phl-Ilm series of hyperbasites are given in Table. The main rock-forming minerals in the metasomatically altered xenoliths of the Mg series are not significantly different from the corresponding minerals from xenoliths that do not contain any metasomatic minerals [*Solov'eva et al., 1994*]. This observation may indirectly suggest that

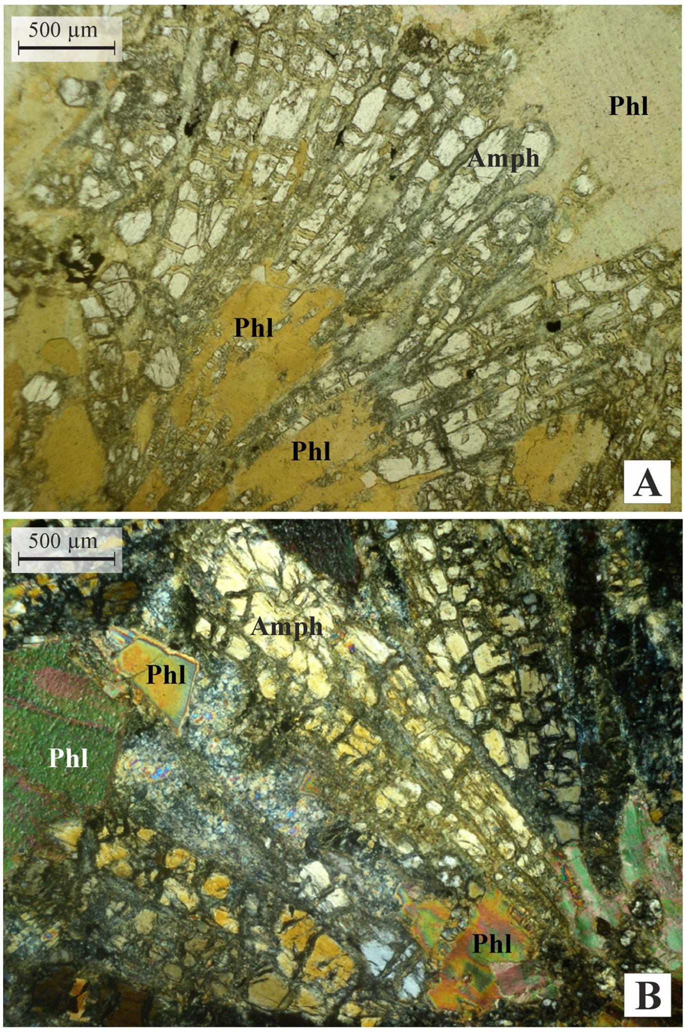

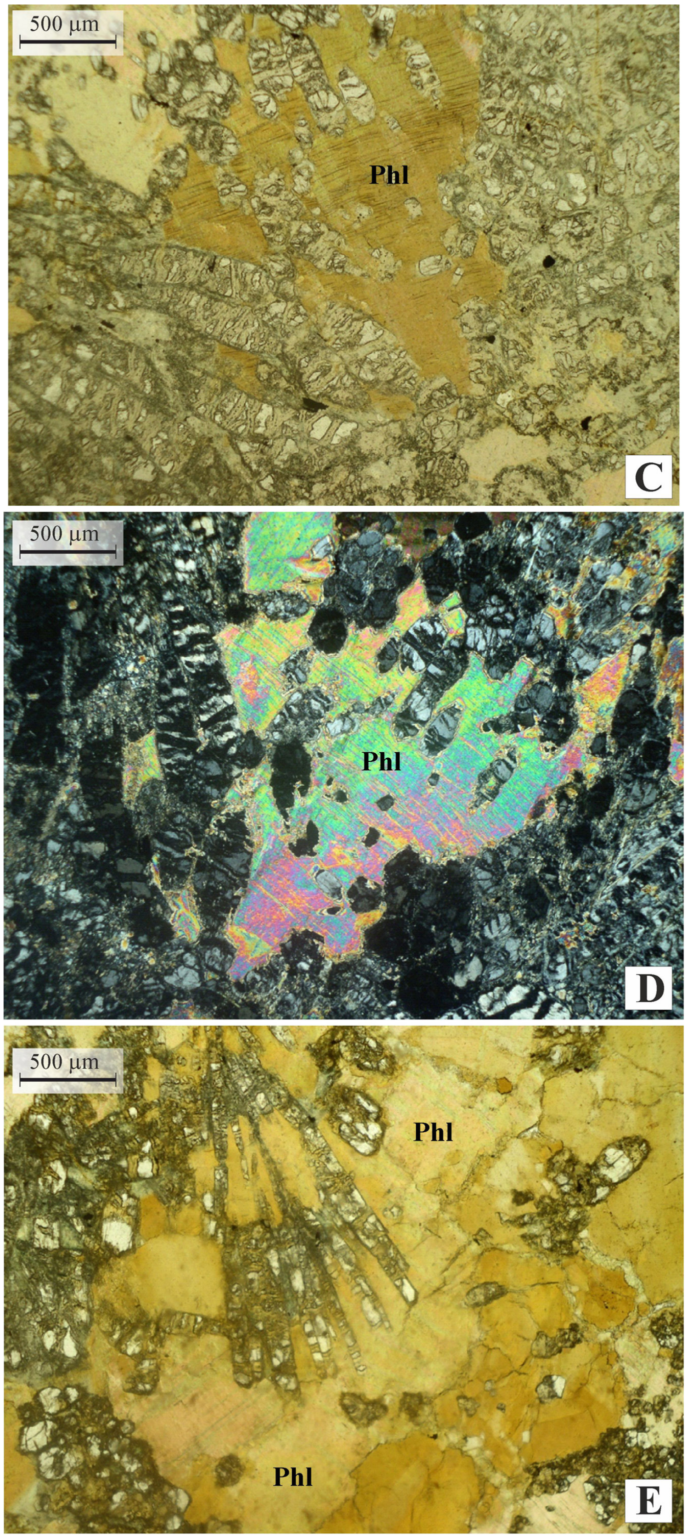

Fig. 22. The photomicrographs of thin section. Monoclinal amphibole rosettes in intergrowths with irregular-shaped grains of phlogopite (*A*–*E*).

Images (*C*) and (*D*) show a typical torch-like form of phlogopite, bended cleavage of mica and elongated crystals of amphibole. (*E*) The initially single phlogopite plate was granulated into several small platelets. Images: *A, C, E* – without an analyzer; *B, D* – in crossed nicols.

Рис. 22. Розетки моноклинного амфибола в сростках с неправильными зернами флогопита (*А*–*Е*).

На снимках (*C*) и (*D*) видна характерная факелообразная форма флогопита, а также изгиб спайности слюды и удлиненных кристаллов амфибола. *E* – изначально единая пластинка флогопита гранулирована на несколько более мелких. Фото шл.: *A, C, E* – без анализатора; *B, D* – в × николях.

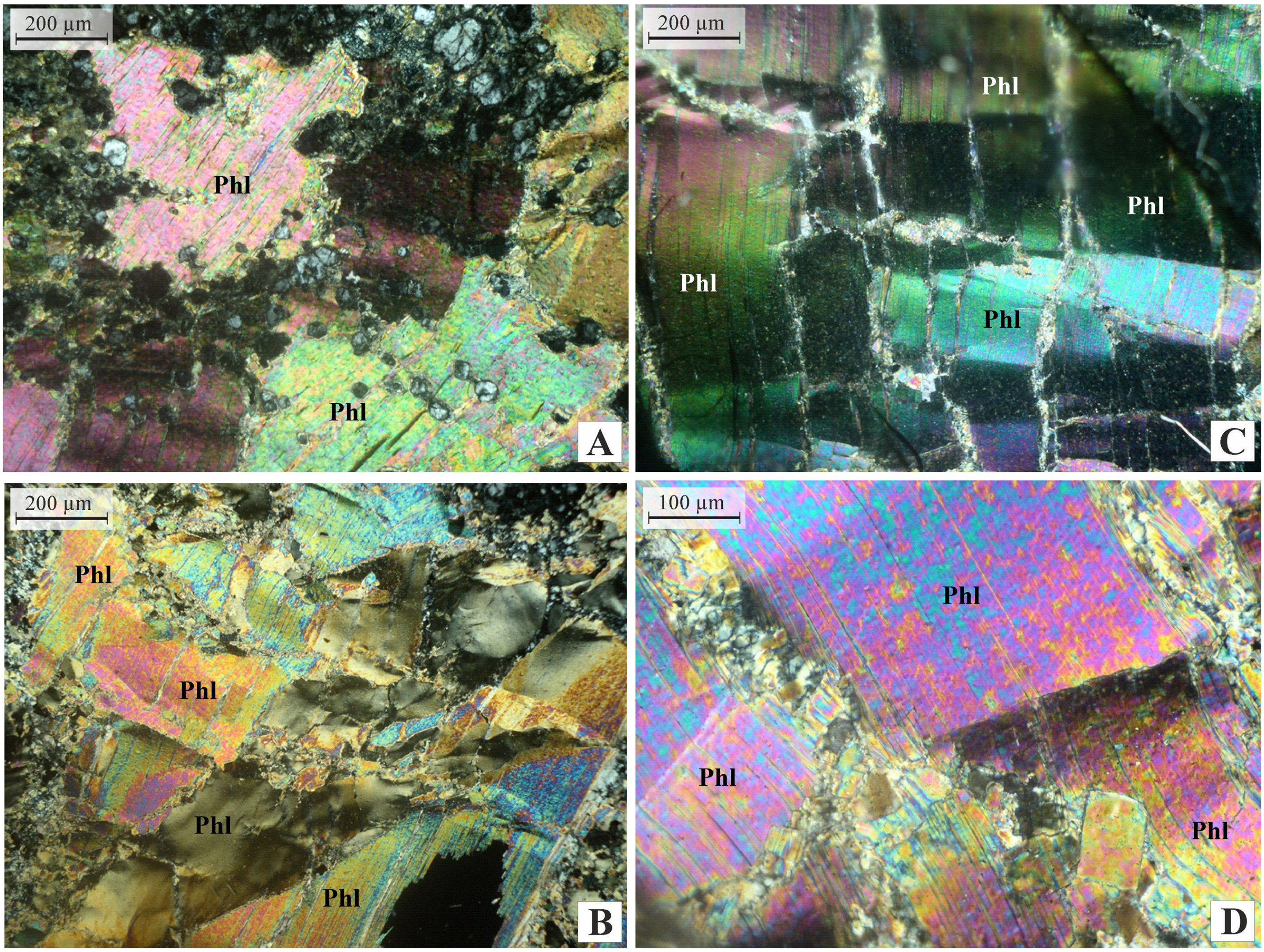

Fig. 23. The photomicrographs of thin section. Deformation of phlogopite plates.

A – general view of the plates in the rock. Images (*B, C, D*) show that the phlogopite plates were granulated into blocks of various orientations, which are separated by the fine-grained mica aggregate. The latter contains a few larger regular-shaped recrystallized platelets. Images in crossed nicols.

Рис. 23. Характер деформации пластинок флогопита.

A – общий вид пластинок в породе. При более сильном увеличении видно (*B, C, D*), как пластинки слюды гранулируются на разноориентированные блоки, разделенные мелкочешуйчатым слюдяным агрегатом. В последнем появляются более крупные правильные перекристаллизованные пластинки Фото шл. в × николях.

the entire magnesian pyroxenite-peridotite series was subject to metasomatic modification, and the process took place with chemical reequilibration of primary and newly-formed minerals. This assumption is supported by the lack of zonation in the crystals of phlogopite and amphibole. Unlike the corresponding minerals in the Phl-Ilm series of hyperbasites, the main minerals in the Mg series are characterized by the higher magnesium index (Mg#), considerably lower contents of TiO_2, FeO and higher contents of Cr_2O_3 (Table).

In diagrams Mg# – TiO_2 and Mg# – Cr_2O_3, metasomatic phlogopite points from rocks of the Mg series are significantly distant from the field of points of mica from the phlogopite-ilmenite parageneses (Fig. 24, *A*, *B*). The metasomatic phlogopite from rocks of the Mg series contains more chrome oxide, less titanium oxide and have significantly higher contents of magnesium. Within the parageneses of the Phl-Ilm series, the lowest magnesium contents and the highest titanium contents are typical of mica from the deformed phlogopite-amphibole rocks. The phlogopite flakes from these rocks have either high or low contents of chrome. In the more intensively coloured marginal rims of the phlogopite plates, especially in the large porphyrious ones, the Mg content is lower, while the content of

Chemical compositions of minerals in deep-seated xenoliths with phlogopite and phlogopite-amphibole mineralization in the Obnazhennaya kimberlitic pipe

Химический состав минералов в глубинных ксенолитах с флогопитовой и флогопит-амфиболовой минерализацией в кимберлитовой трубке Обнаженная

Sample	**74-817**						**74-296a**			**7-365**		
Mineral	**Ol**	**Opx**	**Cpx**	**Grt**	**Phl**	**Amph**	**Opx**	**Phl**	**Amph**	**Ol**	**Opx**	**Cpx**
SiO_2	40.39	57.06	54.16	41.97	39.31	47.28	57.24	39.06	46.97	39.83	56.02	54.72
TiO_2		0.04	0.19	0.08	0.46	0.59	0.04	0.50	0.42		0.19	0.35
Al_2O_3		0.93	3.57	22.72	14.89	9.79	1.34	15.05	10.83	0.04	1.24	2.67
Cr_2O_3		0.14	0.89	1.21	0.69	0.59	0.34	0.90	1.81	0.02	0.22	0.78
FeO	7.38	4.54	2.71	8.23	3.14	3.32	5.25	3.00	3.56	14.58	8.88	5.16
MnO	0.06	0.05	0.08	0.31	0.04	0.04	0.11	0.02	0.08	0.14	0.14	0.12
MgO	51.32	36.75	15.41	21.59	25.31	20.44	36.08	25.20	20.23	45.90	32.32	16.22
CaO		0.22	19.97	4.21		8.91			8.71	0.04	0.82	18.32
Na_2O		0.05	3.06	0.02	1.09	5.34		2.00	5.10		0.227	2.42
K_2O					9.52	1.21		6.63	0.37		0.020	0.01
NiO	0.45	0.14			0.12	0.05	0.02	0.18	0.08	0.26		
SrO								0.16				
BaO				0.06	0.76	0.04		2.78				
F		0.11	0.05	0.10	0.06	0.07						
Cl					0.03	0.03						
Total	**99.73**	**100.02**	**100.07**	**100.47**	**95.38**	**97.65**	**100.42**	**92.70**	**98.16**	**100.80**	**100.08**	**100.78**
Mg#	92.52	93.50	91.02	82.37	93.48	91.65	92.4	93.7	91.0	84.9	86.6	84.9

Sample	**7-365**					**O-42-87**			**O-22-87**			
Mineral	**Grt**	**Phl I**	**Phl II**	**Ilm I**	**Ilm II**	**Cpx**	**Phl**	**Ilm**	**Opx**	**Cpx**	**Phl**	**Ilm**
SiO_2	41.57	39.93	39.70	0.00	0.04	54.26	40.94	0.03	55.602	54.60	42.06	0.00
TiO_2	0.64	1.88	2.82	51.06	42.16	0.16	0.90	50.48	0.05	0.31	1.24	50.09
Al_2O_3	20.79	12.83	12.77	0.88	0.66	0.96	11.53	0.08	0.095	0.94	11.29	0.11
Cr_2O_3	1.35	0.47	0.51	2.30	2.06	0.67	0.09	0.87	0.063	0.56	0.13	0.83
FeO	12.12	6.14	6.29	33.37	44.15	5.32	6.07	38.20	9.671	5.45	6.04	39.02
MnO	0.41	0.03	0.02	0.18	0.65	0.11	0.02	0.35	0.237	0.13	0.01	0.35
MgO	17.88	22.53	21.34	11.80	5.96	15.82	24.96	10.05	34.053	16.11	24.83	9.74
CaO	5.03			0.04	0.25	20.10		0.01	0.36	20.15		0.02
Na_2O	0.09	0.21	0.31			2.496	0.23		0.105	2.17	0.27	
K_2O	0.01	10.47	10.46			0.01	10.58				10.55	
NiO												
SrO			0.032								0.002	
BaO			0.352				0.131				0.134	
F		0.162	0.268				0.332				0.418	
Cl		0.048					0.011					
Total	**99.89**	**94.68**	**94.86**	**99.58**	**95.93**	**99.90**	**95.78**	**100.08**	**100.24**	**100.40**	**96.98**	**100.16**
Mg#	72.4	86.7	85.8	38.6	19.4	84.1	88.0	31.9	86.2	84.1	88.0	30.8

Sample	**7-371**					
Mineral	**Ol**	**Phlc**	**Phlr**	**Phlr1**	**Ilm**	**Amph**
SiO_2	38.37	39.99	39.46	38.79	0.07	55.93
TiO_2	0.00	1.01	3.02	4.02	52.77	0.16
Al_2O_3	0.00	13.07	13.17	13.26	0.68	1.06
Cr_2O_3	0.00	0.49	1.12	0.58	1.83	0.37
FeO	20.42	5.86	6.04	5.91	32.24	2.41
MnO	0.18	0.01	0.02	0.04	0.25	0.05
MgO	41.78	22.67	22.05	21.46	11.97	22.60
CaO	0.05				0.03	6.73
Na_2O		0.80	0.37	0.32		5.56
K_2O		9.65	9.40	10.47		3.14
NiO	0.072					
SrO		0.015	0.023			0.03
BaO		0.129	0.064	0.065		0.05

E n d   o f   T a b l e

О к о н ч а н и е   т а б л и ц ы

Sample	**7-371**					
Mineral	**Ol**	**Phlc**	**Phlr**	**Phlr1**	**Ilm**	**Amph**
F		0.321	0.173	0.236		0.33
Cl		0.015	0.013	0.016		
Total	**100.87**	**94.02**	**94.93**	**95.14**	**99.84**	**98.41**
Mg#	78.5	87.3	86.7	86.6	39.8	94.3

N o t e. Mg series: sample **74-817** – Grt olivine websterite with Phl-Amph metasomatic veinlets; sample **74-296a** – megacrystalline Grt orthopyroxenite with metasomatic Phl–Amph mineralization. Series of Phl-Ilm hyperbasites: sample **7-365** – Phl-Ilm garnetized lherzolite; sample **O-42/87** – porphirous Phl-Ilm websterite; sample **O-22/87** – porphirous Phl-Ilm olivine websterite; sample **7-371** – deformed Phl-Amph rocks with accessory Ti-chromite and relict Ilm.

П р и м е ч а н и е. Mg серия: обр. **74-817** – Grt оливиновый вебстерит с метасоматическими прожилками Phl и Amph; обр. **74-296a** – мегакристаллический Grt ортопироксенит с метасоматической Phl – Amph минерализацией. Серия Phl-Ilm гипербазитов: обр. **7-365** – Phl-Ilm гранатизированный лерцолит; обр. **O-42/87** – порфировидный Phl-Ilm вебстерит; обр. **O-22/87** – порфировидный Phl-Ilm оливиновый вебстерит; обр. **7-371** – деформированная Phl-Amph порода с акцессорным Ti-хромитом и с реликтовым Ilm.

titanium is higher as compared to those in the central parts (Fig. 24). A possible cause might be that exsolution textures of ilmenite precipitated in the centre of phlogopite grains, and this process was accompanied by depletion by titanium oxide and ferrum oxide. At the margins of the large phlogopite plates, ilmenite exsolution lamellae are lacking and changed by larger isometric grains. This suggests that the main portion of ilmenite precipitated from the melt at the latest stages of crystallization simultaneously with the growth of the late rims on phlogopite and of small mica flakes of the second generation.

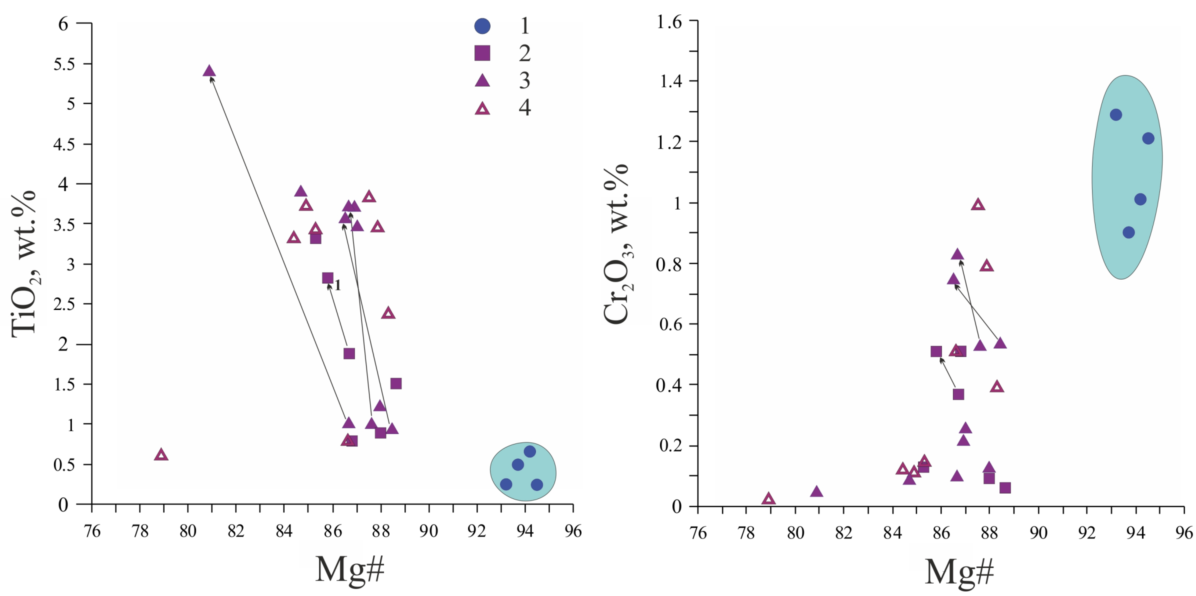

Fig. 24. Mg# vs. TiO_2 and Mg# vs. Cr_2O_3 in phlogopites from rocks of the Mg pyroxenite-peridotite and Phl-Ilm series.

1 – metasomatic phlogopite from the rocks of the Mg series; *2* – phlogopite from garnetless and garnetized Phl-Ilm hyperbasites; *3* – phlogopite from porphyrous garnetless Phl-Ilm hyperbasites; *4* – phlogopite from deformed phlogopite-amphibole rocks with newly-formed chromite. Arrow tips refer to compositions of phlogopite from the marginal zones of porphyrous plates or from smaller platelets in the matrix (solid symbols).

Рис. 24. Соотношение Mg# - TiO_2 и Mg# - Cr_2O_3 во флогопите из пород Mg пироксенит-перидотитовой и Phl-Ilm серий.

1 – метасоматический флогопит из пород Mg серии; *2* – флогопит из безгранатовых и гранатовых Phl-Ilm гипербазитов; *3* – флогопит из порфировидных безгранатовых Phl-Ilm гипербазитов; *4* – флогопит из деформированных флогопит-амфиболовых пород с новообразованным хромитом и реликтовыми ильменитом, клинопироксеном. Окончание стрелок означает состав флогопита из краевых зон порфировидных выделений флогопита или из мелких пластинок в матрице (залитые значки).

By its chemical composition, amphibole represented by typical pargasite in the Phl-Amph metasomatites of the Mg series (Table) [*Ukhanov et al.*, *1988*]) is obviously different from K-richterite from the deformed phlogopite-amphibole rocks. The latter has significantly larger contents of SiO_2 and K_2O and several-fold lower contents of Cr_2O_3 and Al_2O_3.

Ilmenites from the Phl-Ilm parageneses of all the three groups have high contents of MgO (9.7–12 %), except the late micrograin in the cavern in the garnet grain (6 %). All the ilmenites listed in Table 1 differ from ilmenites of the ultrabasic diamond paragenesis with the lower content of TiO_2 [*Patrin et al.*, *2004*]. The micrograin from the cavern in the garnet grain contains more MnO and less TiO_2 as compared to other analysed ilmenites. Considering the content of the main oxides, the relict resorbed ilmenite from the deformed phlogopite-amphibole rocks (7-371) is similar to Ilm I from the garnetized Phl-Ilm lherzolite (7-365). Ilmenite from garnetless Phl-Ilm websterites (O-42/87 and O-22/87) contains significantly less Cr_2O_3 and more FeO as compared to ilmenite from the garnetized Phl-Ilm lherzolite (7-365). Due to high contents of phlogopite and ilmenite and higher contents of Fe in silicates, the Phl-Ilm hyperbasites from the pipes of the Kuoika field belong to high-potassium, titanian and ferrous basites-ultrabasites.

4. ^{40}AR/^{39}AR DATING OF MICA

Results of $^{40}Ar/^{39}Ar$ dating for mica from the phlogopite-containing xenoliths of the Mg pyroxenite-peridotite and Phl-Ilm series are given in Fig. 25. According to the $^{40}Ar/^{39}Ar$ method, ages of phlogopites from the metasomatic inclusions and veins in the garnet olivine websterite (74-817) range from ~1640 to 1800 Ma. Mica from the garnetless Phl-Ilm parageneses (O-22/87 and O-42/87) has similar ages for high-temperature stages (~869 and 851 Ma, respectively) (Fig. 25). Phlogopite from the garnetized Phl-Ilm lherzolites (12/7 and 7-365) has significantly younger ages, ~608 and 495 Ma, respectively. Mica from the deformed phlogopite-amphibole rocks Sl-3 has an approximate age of 167 Ma, which is close to the age of kimberlites of the Kuoika field [*Howarth et al.*, *2014*].

5. DISCUSSION AND RESULTS

The age determinations for mica confirm the conclusion based on the data on petrography, mineralogy and chemistry of the minerals: the phlogopite and phlogopite-amphibole parageneses of the Mg pyroxenite-peridotite and the Phl-Ilm basite-ultrabasite series are represented by two discrete mantle rock associations in the mantle lithosphere of the Birekte terrain. Xenoliths with the combined presence of minerals of both series are lacking.

The specific features, such as the cumulative type of banding, high temperatures (1250–1500 °C) of the start of crystallization of exsolution megacrystals of pyroxenes, the presence of deformed globules of sulphides and others, give grounds to consider the Mg pyroxenite-peridotite series as the layered intrusion in the mantle [*Ukhanov et al., 1988; Solov'eva et al., 1994*]. The average chemical composition of the rocks in this series is close to that of the Al-undepleted komatiites [*Solov'eva et al., 1994*]. For four crystals of zircon from kimberlites of the Rubin pipe (Kuoika filed), ages determined by the SHRIMP method fall into two groups, 1.8–2.1 (~1.95 Ga in average) and 2.3–2.6 Ga (~2.4 Ga in average) [*Nasdala et al.*, *2014*]. In the opinion of the authors, the above-mentioned ranges reflect the main evolution stages of the crust in the Birekte block. The average most ancient age (~2.4 Ga) is actually similar to the formation time of the Birekte terrain (~2.4 Ga), according to [*Rosen*, *2003*]. In the first approximation, this age can be viewed as the formation time of the layered magmatic Mg series in the mantle. The average age of 1.9 Ga corresponds, according to [*Rosen*, *2003*], to the accretion time of the Birekte terrain to the Siberian craton (~1.8–1.9 Ga). The estimated $^{40}Ar/^{39}Ar$ age of metasomatic phlogopite from the xenolith in the Mg series (~1.64–1.8 Ga) is close to the latest event. The lower age of mica may be due to a partial loss of ^{40}Ar. The rocks of the Mg series from the Obnazhennaya pipe have another particular feature: values of $\delta^{18}O$ in garnets and clinopyroxenes from peridotites, websterites and garnet clinopyroxenites have a considerable admixture of subduction oxygen (Fig. 26 [*Taylor et al.*, *2003, 2005*]). It can thus be assumed that at some stage, the mantle lithosphere substance under the Birekte block was subject to fluid-melt metasomatism in the subduction zone. According to [*Pernet-Fisher et al.*, *2015*], radiogenic osmium was supplied into the mantle lithosphere of the Birekte block by sulphur-rich fluids from the subduction zone between 1.7 and 2.2 Ga, and this period correlates with the age of phlogopite from the phlogopite-amphibole metasomatites (1.64–1.8 Ga). As noted in the petrographic description, the phlogopite-amphibole veinlets have a typical magmatic euhedral texture, i.e. they might have crystallised from the melts. Based on the reviewed data, it can be suggested that in the mantle lithosphere of the Birekte terrain, phlogopite-amphibole metasomatism of the rocks of the magnesian pyroxenite-peridotite series was resulted by fluids-melts ascending from the subduction zone.

This assumption does not contradict to the data on the mantle pyroxenites containing graphite and the lower-crust metabasite granulites from the kimberlitic

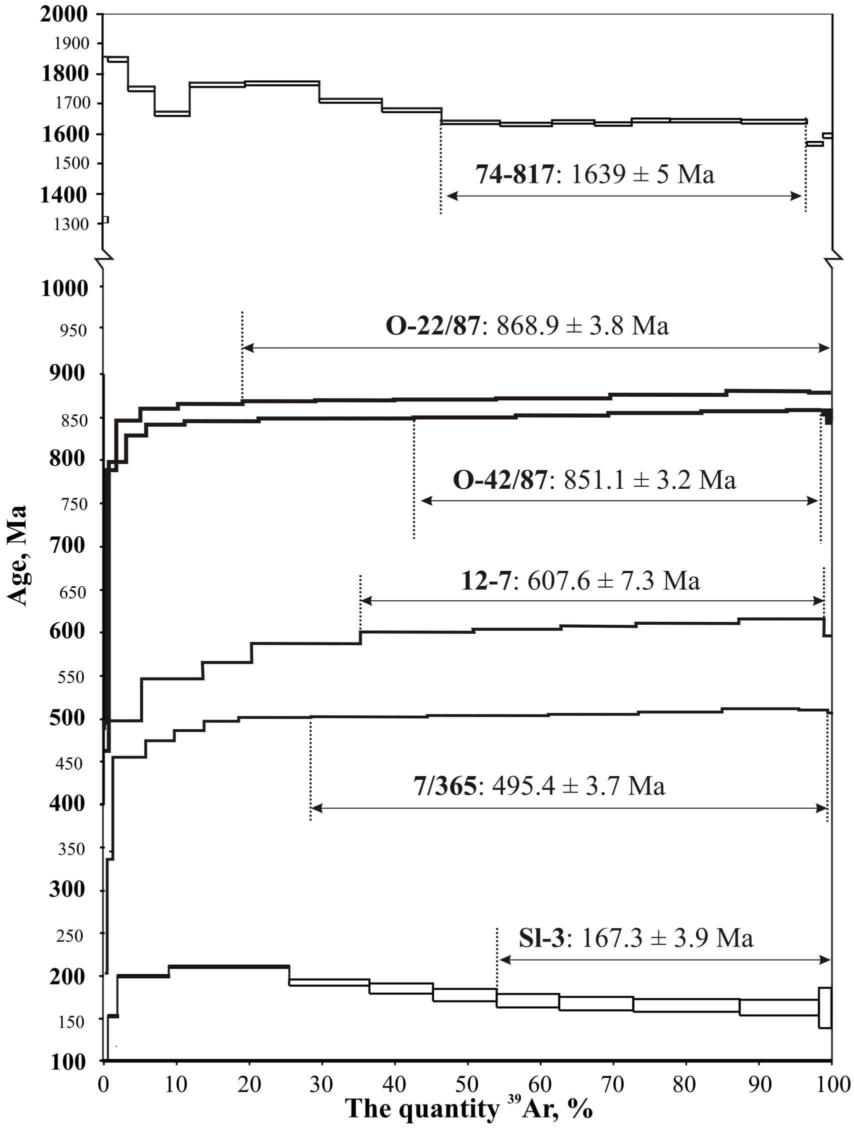

Fig. 25. Ages of phlogopite (according to the $^{40}Ar/^{39}Ar$ method) in xenoliths of the Mg pyroxenite-peridotite series (sample 74-817) and the Phl- Ilm series (sample O-22/87 and O-42/87 – garnetless Phl-Ilm hyperbasites; 12-7 and 7-365 – intensive garnetized Phl-Ilm lherzolites; sample Sl-3 – deformed Phl-Amph rock). Mineral compositions of samples 74-817, O-22/87, O-42/87 and 7-365 are given in Table.

Рис. 25. Возраст флогопитов, полученный методом $^{40}Ar/^{39}Ar$ датирования в ксенолитах Mg пироксенит-перидотитовой серии (обр. 74-817) и Phl- Ilm серии (обр. O-22/87, O-42/87 – безгранатовые Phl-Ilm гипербазиты; 12-7 и 7-365 – интенсивно гранатизированные Phl-Ilm лерцолиты; обр. Сл-3 – деформированная Phl-Amph порода). Состав минералов из образцов 74-817, O-22/87, O-42/87, 7-365 приведен в таблице.

pipes of the Kuoika field. In the deep-seated xenoliths from the Obnazhennaya and Slyudyanka kimberlitic pipes, graphite-bearing orthopyroxenites and websterites are found, which are viewed as crystal cumulative rocks in boninite dykes with the biogenic matter added under island-arc conditions, as suggested by studies of oxygen and sulphur isotopes and bulk rock geochemistry [*Solov'eva et al., 2010*]. By their geochemical characteristics, the xenoliths of basite granulites from the pipes of the Kuoika field (which are representing the lower crust in the Birekte terrain) are determined as result of fractional crystallization of the island-arc low-potassium tholeiites [*Solov'eva et al., 2004*]. Therefore, it can be assumed that the accretion of the Birekte microcontinent/terrain to the Siberian craton, being a larger continental block, took place about 1.8 Ga ago in the subduction zone.

The Phl–Ilm parageneses of the xenoliths represent the differentiated magmatic series with ubiquitous processes of subsolidus garnetization and autometasomatic phlogopitization. According to results of the whole-rock chemical analyses, the rocks of this series

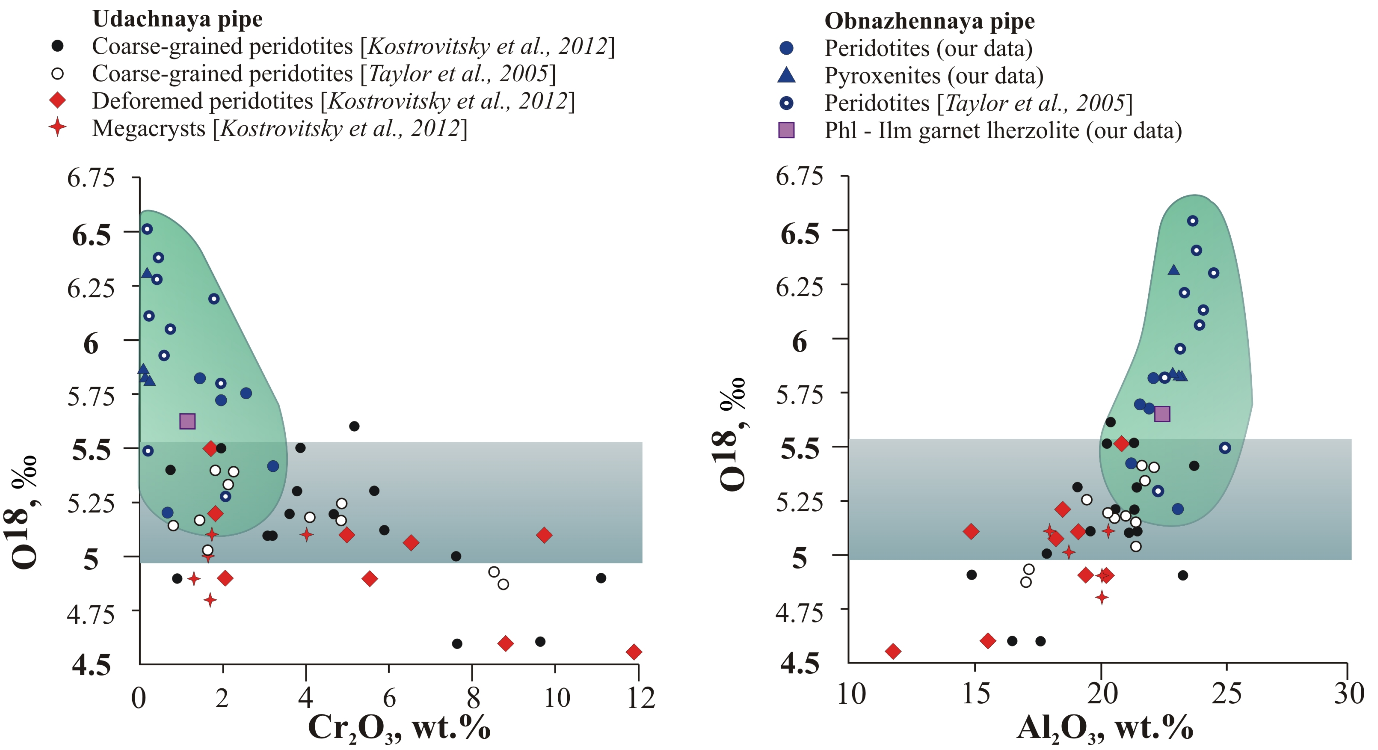

Fig. 26. Cr_2O_3 vs. ^{18}O and Al_2O_3 vs. ^{18}O in garnet from peridotites and pyroxenites of the Mg series, from Phl-Ilm lherzolite (Obnazhennaya pipe) and coarse-grained and deformed peridotites and megacrysts (Udachnaya pipe). The range of mantle values for garnet is shown by the blue strip.

Рис. 26. Соотношение Cr_2O_3 – ^{18}O и Al_2O_3 – ^{18}O в гранате из перидотитов и пироксенитов Mg серии, из Phl-Ilm лерцолита (трубка Обнаженная) и из зернистых, деформированных перидотитов и мегакристов трубки Удачная. Голубая полоса – диапазон мантийных значений для граната.

can be classified as high-potassium basites and ultrabasites. The most ancient ages of phlogopites in this series (869 and 851 Ma) belong to the Upper Proterozoic and are close to the early age of the alkali-ultrabasic carbonatite Tomtor pluton-volcano (800 Ma, [*Entin et al., 1990*]). The younger ages of phlogopite in the garnetized parageneses (608 and 495 Ma, samples 12-7 and 7/365) may be related to the loss of radiogenic ^{40}Ar due to its substitution by garnet. During this process, H_2O, K, Ba, F and Cl were supplied into the upper layers of the crust and mantle. The age of phlogopite in xenolith Sl-307 (167 Ma), which is close to the age of the kimberlites of the Kuoika field, may reflect the influence of the kimberlitic melt.

In this context, the entire complex series of the Phl-Ilm parageneses from the xenoliths in kimberlites of the Kuoika field can be considered as the high-potassium mantle rocks being deep sources of high-potassium magmatites on the surface. The latter may include the complex long-term alkali ultrabasic-carbonatite Tomtor pluton-volcano as well as the series of dykes and sub-effusive K-basites and lamproites [*Shpunt, Shamshina, 1989*; *Kiselev et al., 2012*]. Besides, it is not improbable that the intensively deformed phlogopite-amphibole rocks, that mark the deep weakened zones in the mantle lithosphere, guided the alkali potassium magma to the surface. According to [*Li et al., 2008*], the formation of Rodinia to its maximum size took place between 1000 and 900 Ma, and the first major episode of its breakup due to the plume impact occurred 825 Ma ago. Although the ages of phlogopite from the Phl-Ilm websterites (869 and 851 Ma) are by 45, 25 Ma larger than the initial stage of Rodinia breakup according to [*Li et al., 2008*], it can be assumed that the formation of the high-potassium, titanian and ferrous magmatites in the mantle took place in advance of their occurrence on the surface. In the Siberian craton, the Rodinia breakup was accompanied by magmatism due to the impact of the Upper Proterozoic plume [*Li et al., 2008*].

Thus, the Phl-Amph metasomatites developed in the mantle lithosphere of the Birekte block on the rocks of the early magmatic Mg pyroxenite-peridotite series are markers of the stage related to the accretion of this block to the Siberian craton (~1.8–1.9 Ga). In the mantle lithosphere of the Birekte terrain, the magmatic series of the Phl-Ilm hyperbasites occurred much later (~869–851 Ma) corresponding to the start of Rodinia breakup [*Li et al.*, *2008*]. The deformed phlogopite-amphibole rocks were formed as metasomatites of the deep fault zones drained the upper mantle.

6. Main conclusions

1. The petrographic, chemical and geochemical features of discussed phlogopite and phlogopite-amphibole xenoliths from the kimberlitic pipes of the Kuoika field (i.e. the north-eastern part of the Siberian craton) are evidence of different stages in the evolution of the mantle lithosphere of the Birekte terrain.

2. The Phl-Amph metasomatites develop on the rocks of the complex Mg pyroxenite-peridotite series of the xenoliths, belonging to the ancient layered mantle intrusion. In the rocks of this series, the Phl-Amph metasomatism gave geochemical features of the subduction zone and marked the stage related to the accretion of the Birekte continental block to the Siberian craton (~1.8–1.9 Ga).

3. The complex series of the Phl-Ilm rocks taken out by kimberlites of the Kuoika field in the form of xenoliths is the later series as compared to the Mg pyroxenite-peridotite series and the Phl-Amph metasomatites. The Phl-Ilm hyperbasites can be classified as typical mantle potassium ultrabasic-basic magmatites. The deformed phlogopite-amphibole rocks are typical metasomatic rocks of the deep faults; they formed at the expense of the earlier Phl-Ilm rocks. The outset of the formation of the magmatic series of the Phl-Ilm hyperbasites in the mantle lithosphere of the Birekte terrain (~869–851 Ma) corresponds to the start of Rodinia breakup [*Li et al.*, *2008*]. The high-potassium, titanian and ferrous rocks of this series were the feeding mantle sources for potassium ultrabasic and basic magmatism in the Upper Proterozoic and the Lower Cambrian in the northern part of the Siberian platform.

7. References

Entin A.R., Zaitsev A.I., Nenashev N.I., Vasilenko V.B., Orlov A.I., Tyan O.A., Olkhovik Yu.A., Olshtynsky S.I., Tolstov A.V., 1990. About the sequence of geological events related to the intrusion of the Tomtor alkaline ultramafic and carbonatite massif, North-Western Yakutia. *Geologiya i Geofizika* (*Russian Geology and Geophysics*) 31 (12), 42–50 (in Russian) [*Энтин А.Р., Зайцев А.И., Ненашев Н.И., Василенко В.Б., Орлов А.И., Тян О.А., Ольховик Ю.А., Ольштынский С.И., Толстов А.В*. О последовательности геологических событий, связанных с внедрением Томторского массива ультраосновных щелочных пород и карбонатитов (Северо-Западная Якутия) // *Геология и геофизика*. 1990. Т. 31. № 12. С. 42–50].

Garanin V.K., Kudryavtseva G.P., Khar'kiv A.D., Chistyakova V.F., 1985. The mineralogy of ilmenite hyperbasites from the Obnazhennaya kimberlitic pipe. *Izvestiya AN SSSR*, *Seriya geologicheskaya* (5), 85–101 (in Russian) [*Гаранин В.К., Кудрявцева Г.П., Харькив А.Д., Чистякова В.Ф.* Минералогия ильменитовых гипербазитов из кимберлитовой трубки Обнаженная // *Известия АН СССР, серия геологическая*. 1985. № 5. С. 85–101].

Howarth G.H., Barry P.H., Pernet–Fisher J.F., Baziotis I.P., Pokhilenko N.P., Pokhilenko L.N., Bodnar R.J., Taylor L.A., Agashev A.M., 2014. Superplume metasomatism: Evidence from Siberian mantle xenoliths. *Lithos* 184–187, 209–224. http://dx.doi.org/10.1016/j.lithos.2013.09.006.

Ignatiev A.V., Velivetskaya T.A., 2004. The laser method of sample-preparation for analyses of stable isotopes of oxygen in silicates and oxides. In: Abstracts of the XVII Stable Isotopes Symposium. Institute of Geochemistry and Analytical Chemistry, Moscow, p. 96–97 (in Russian) [*Игнатьев А.В., Веливецкая Т.А.* Лазерная методика подготовки проб для анализа стабильных изотопов кислорода силикатов и окислов // XVII симпозиум по стабильным изотопам: Тезисы докладов. М.: ГЕОХИ, 2004. С. 96–97].

Khar'kiv A.D., Zinchuk N.N., Kryuchkov A.I., 1998. Primary Diamond Deposits of the World. Nedra Publishing House, Moscow, 555 p. (in Russian) [*Харькив А.А., Зинчук Н.Н., Крючков А.И.* Коренные месторождения алмазов мира. М.: Недра, 1998. 555 с.].

Kiselev A.I., Yarmolyuk V.V., Kolodeznikov I.I., Struchkov K.K., Egorov K.N., 2012. The northeastern boundary of the Siberian craton and its formation peculiarities (derived from occurrences of Early Cambrian and Devonian intraplate magmatism). *Doklady Earth Sciences* 447 (1), 1252–1258. http://dx.doi.org/10.1134/S1028334X12110098.

Kostrovitsky S.I., Solov'eva L.V., Gornova M.A., Alymova N.V., Yakovlev D.A., Ignat'ev A.V., Velivetskaya T.A., Suvorova L.F., 2012. Oxygen isotope composition in minerals of mantle parageneses from Yakutian kimberlites. *Doklady Earth Sciences* 444 (1), 579–584. http://dx.doi.org/10.1134/S1028334X12050030.

Li Z.X., Bogdanova S.V., Collins A.S., Davidson A., De Waele D., Ernst R.E., Fitzsimons I.C.W., Fuck R.A., Gladkochub D.P., Jacobs J., Karlstrom K.E., Lu S., Natapov L.M., Pease V., Pisarevsky S.A., Thrane K., Vernikovsky V., 2008. Assembly, configuration, and break-up history of Rodinia: a synthesis. *Precambrian Research* 160 (1–2), 179–210. http://dx.doi.org/10.1016/j.precamres.2007.04.021.

Menzies M.A., Hawkesworth C.J. (Eds.), 1987. Mantle Metasomatism. Academic Press, New York, 472 p.

Nasdala L., Kostrovitsky S.I., Kennedy A.K., Zeug M., Esenkulova S.A., 2014. Retention of radiation damage in zircon xenocrysts from kimberlites, Northern Yakutia. *Lithos* 206–207, 252–261. http://dx.doi.org/10.1016/j.lithos.2014.08.005.

Parfenov L.M., Kuzmin M.I. (Eds.), 2001. Tectonics, Geodynamics and Metallogeny of the Sakha Republic (Yakutia). MAIK Nauka/Interperiodika, Moscow, 571 p. (in Russian) [*Тектоника, геодинамика и металлогения территории Республики Саха (Якутия)* / Отв. ред. Л.М. Парфенов, М.И. Кузьмин. М.: МАИК «Наука/Интерпериодика», 2001. 571 с.].

Patrin G.S., Matsuk S.S., Kostrovitsky S.I., Alymova N.V., 2004. The mineralogical features and chemistry of ilmenite from lower mantle xenoliths. *Mineralogical Journal* (Ukraine) 26 (4), 60–77 (in Russian) [*Патрин Г.С., Мацюк С.С., Костровицкий С.И., Алымова Н.В.* Минералогия ильменита из глубинных ксенолитов в кимберлитах (типохимизм, генетическое и поисковое значение) // *Мінералогічний журнал* (Украина). 2004. Т. 26. № 4. С. 60–77].

Pernet-Fisher J.F., Howarth G.H., Pearson D.G., Woodland S., Barry P.H., Pokhilenko N.P., Pokhilenko L.N., Agashev A.M., Taylor L.A., 2015. Plume impingement on the Siberian SCLM: Evidence from Re-Os isotope systematics. *Lithos* 218–219, 141–154. http://dx.doi.org/10.1016/j.lithos.2015.01.010.

Pokhilenko N.P., Sobolev N.V., Kuligin S.S., Shimizu N., 1999. Peculiarities of distribution of pyroxenite paragenesis garnets in Yakutian kimberlites and some aspects of the evolution of the Siberian craton lithospheric mantle. In: Proceedings of the 7th International Kimberlite Conference. RedRoof Design, Cape Town, p. 689–698.

Rosen O.M., 2003. The Siberian craton: tectonic zonation and stages of evolution. *Geotectonics* 37 (3), 175–192.

Shpunt B.R., Shamshina E.A., 1989. The Late Vendian potassium alkaline volcanites of the Olenek uplift (North-Eastern Siberian platform). *Doklady AN SSSR* 307 (2), 678–682 (in Russian) [*Шпунт Б.Р., Шамшина Э.А.* Поздневендские калиевые щелочные вулканиты Оленекского поднятия (северо-восток Сибирской платформы) // *Доклады АН СССР*. 1989. Т. 307. № 2. С. 678–682].

Solovieva L.V., Egorov K.N., Markova M.E., Kharkiv A.D., Popolitov K.E., Barankevich V.G., 1997. Mantle metasomatism and melting in deep-seated xenoliths from the Udachnaya pipe, their possible relationship with diamond and kimberlite formation. *Geologiya i Geofizika* (*Russian Geology and Geophysics*) 38 (1), 172–193.

Solov'eva L.V., Gornova M.A., Markova M.E., Lozhkin V.I., 2004. Geochemical identification of granulites in xenoliths from Yakutian kimberlites. *Geochemistry International* 42 (3), 220–235.

Solov'eva L.V., Vladimirov B.M., Dneprovskaya L.V., Maslovskaya M.N., Brandt S.B., 1994. Kimberlite and Kimberlite-Similar Rocks: Material of the Upper Mantle beneath Ancient Platforms. Nauka, Novosibirsk, 256 p. (in Russian) [*Соловьева Л.В., Владимиров Б.М., Днепровская Л.В., Масловская М.Н., Брандт С.Б.* Кимберлиты и кимберлитоподобные породы: вещество верхней мантии под древними платформами. Новосибирск: Наука, 1994. 256 с.].

Solov'eva L.V., Yasnygina T.A., Kostrovitsky S.I., 2010. Isotopic and geochemical evidence for a subduction setting during formation of the mantle lithosphere in the northeastern part of the Siberian craton. *Doklady Earth Sciences* 432 (2), 799–803. http://dx.doi.org/10.1134/S1028334X1006019X.

Taylor L.A., Snyder G.A., Keller R., Remley D.A., Anand M., Wiesli R., Valley J., Sobolev N.V., 2003. Petrogenesis of group A eclogites and websterites: Evidence from the Obnazhennaya kimberlite, Yakutia. *Contributions to Mineralogy and Petrology* 145 (4), 424–443. http://dx.doi.org/10.1007/s00410-003-0465-y.

Taylor L.A., Spetsius Z.V., Wiesli R., Spicuzza M., Valley J.W., 2005. Diamondiferous peridotites from oceanic protoliths: Crustal signatures from Yakutian kimberlites. *Russian Geology and Geophysics* (*Geologiya i Geofizika*) 46 (12), 1176–1184.

Travin A.V., Yudin D.S., Vladimirov A.G., Khromykh S.V., Volkova N.I., Mekhonoshin A.S., Kolotilina T.B., 2009. Thermochronology of the Chernorud granulite zone, Ol'khon region, Western Baikal area. *Geochemistry International* 47 (11), 1107–1124. http://dx.doi.org/10.1134/S0016702909110068.

Ukhanov A.V., Ryabchikov I.D., Khar'kiv A.D., 1988. Lithospheric Mantle of Yakutian Kimberlite Province. Nauka, Moscow, 286 p. (in Russian) [*Уханов А.В., Рябчиков И.Д., Харькив А.Д.* Литосферная мантия Якутской кимберлитовой провинции. М.: Наука, 1988. 286 с.]

Solov'eva, Lidia V., Doctor of Geology and Mineralogy, Lead Researcher
Institute of the Earth's Crust, Siberian Branch of RAS
128 Lermontov street, Irkutsk 664033, Russia
Tel.: (3952)425434; ✉ e-mail: Solv777@crust.irk.ru

Соловьева Лидия Васильевна, докт. геол.-мин. наук, в.н.с.
Институт земной коры СО РАН
664033, Иркутск, ул. Лермонтова, 128, Россия
Тел.: (3952)425434; ✉ e-mail: Solv777@crust.irk.ru

Kalashnikova, Tatiana V., Junior Researcher
A.P. Vinogradov Institute of Geochemistry, Siberian Branch of RAS
1A Favorsky street, Irkutsk 664033, Russia
e-mail: Kalashnikova@igc.irk.ru

Калашникова Татьяна Владимировна, м.н.с.
Институт геохимии им. А.П. Виноградова СО РАН
664033, Иркутск, ул. Фаворского, 1А, Россия
e-mail: Kalashnikova@igc.irk.ru

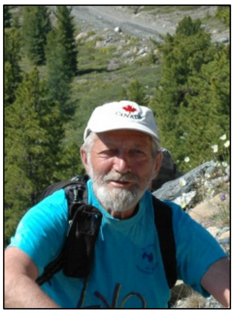

Kostrovitsky, Sergei I., Doctor of Geology and Mineralogy, Lead Researcher
A.P. Vinogradov Institute of Geochemistry, Siberian Branch of RAS
1A Favorsky street, Irkutsk 664033, Russia
e-mail: Serkost@igc.irk.ru

Костровицкий Сергей Иванович, докт. геол.-мин. наук, в.н.с.
Институт геохимии им. А.П. Виноградова СО РАН
664033, Иркутск, ул. Фаворского, 1А, Россия
e-mail: Serkost@igc.irk.ru

Ivanov, Alexei V., Doctor of Geology and Mineralogy, Lead Researcher
Institute of the Earth's Crust, Siberian Branch of RAS
128 Lermontov street, Irkutsk 664033, Russia
Tel.: 8(3952)427117; e-mail: aivanov@crust.irk.ru

Иванов Алексей Викторович, докт. геол.-мин. наук, в.н.с.
Институт земной коры СО РАН
664033, Иркутск, ул. Лермонтова, 128, Россия
Тел.: 8(3952)427117; e-mail: aivanov@crust.irk.ru

Matsuk, Stanislav S., Doctor of Geology and Mineralogy, Lead Researcher
M.P. Semenenko Institute of Geochemistry, Mineralogy and Ore Formation
of the National Academy of Sciences of Ukraine
34 Acad. Palladin Ave., Kyiv 03680, Ukraine
e-mail: Smatsyuk@hotmail.com

Мацюк Станислав Степанович, докт. геол.-мин. наук, в.н.с.
Институт геохимии, минералогии и рудообразования им. Н.П. Семененко НАН Украины
03680, Киев, проспект Акад. Палладина, 34, Украина
e-mail: Smatsyuk@hotmail.com

Suvorova, Ludmila F., Candidate of Chemistry, Chief Specialist
A.P. Vinogradov Institute of Geochemistry, Siberian Branch of RAS
1A Favorsky street, Irkutsk 664033, Russia
e-mail: Suvorova@igc.irk.ru

Суворова Людмила Филипповна, канд. хим. наук, главный специалист
Институт геохимии им. А.П. Виноградова СО РАН
664033, Иркутск, ул. Фаворского, 1А, Россия
e-mail: Suvorova@igc.irk.ru

GEODYNAMICS & TECTONOPHYSICS

PUBLISHED BY THE INSTITUTE OF THE EARTH'S CRUST
SIBERIAN BRANCH OF RUSSIAN ACADEMY OF SCIENCES

2015 VOLUME 6 ISSUE 3 PAGES 345–364

ISSN 2078-502X

http://dx.doi.org/10.5800/GT-2015-6-3-0185

Recent Geodynamics

GEODYNAMICS AS WAVE DYNAMICS OF THE MEDIUM COMPOSED OF ROTATING BLOCKS

A. V. Vikulin

Institute of Volcanology and Seismology, Far East Branch of RAS, Petropavlovsk-Kamchatsky, Russia

Abstract: The geomedium block concept envisages that stresses in the medium composed of rotating blocks have torque and thus predetermine the medium's energy capacity (in terms of [*Ponomarev*, *2008*]). The present paper describes the wave nature of the global geodynamic process taking place in the medium characterized by the existence of slow and fast rotation strain waves that are classified as a new type of waves. Movements may also occur as rheid, superplastic and/or superfluid motions and facilitate the formation of vortex geological structures in the geomedium.

Our analysis of data on almost 800 strong volcanic eruptions shows that the magma chamber's thickness is generally small, about 0.5 km, and this value is constant, independent of the volcanic process and predetermined by properties of the crust. A new magma chamber model is based on the idea of 'thermal explosion'/'self-acceleration' manifested by intensive plastic movements along boundaries between the blocks in conditions of the low thermal conductivity of the geomedium. It is shown that if the solid rock in the magma chamber is overheated above its melting point, high stresses may occur in the surrounding area, and their elastic energy may amount to 10^{15} joules per 1 km^3 of the overheated solid rock. In view of such stresses, it is possible to consider the interaction between volcano's magma chambers as the migration of volcanic activity along the volcanic arc and provide an explanation of the interaction between volcanic activity and seismicity within the adjacent parallel arcs.

The thin overheated interlayer/magma chamber concept may be valid for the entire Earth's crust. In our hypothesis, properties of the Moho are determined by the phase transition from the block structure of the crust to the non-block structure of the upper mantle.

Key words: geodynamics, force moment, rotational waves, rheid flow, gravitational waves.

Recommended by S.I. Sherman

For citation: *Vikulin A.V.* 2015. Geodynamics as wave dynamics of the medium composed of rotating blocks. *Geodynamics & Tectonophysics* 6 (3), 345–364. doi:10.5800/GT-2015-6-3-0185.

ГЕОДИНАМИКА КАК ВОЛНОВАЯ ДИНАМИКА БЛОКОВОЙ ВРАЩАЮЩЕЙСЯ СРЕДЫ

А. В. Викулин

Институт вулканологии и сейсмологии ДВО РАН, Петропавловск-Камчатский, Россия

Аннотация: В работе развивается концепция блоковой геосреды применительно к геодинамическому (сейсмическому и вулканическому) процессу. Работу, в целом, можно представить в виде четырех частей: *введения*, *шести разделов*, кратко описывающих разработанную ранее автором ротационную модель сейсмотектонического процесса, *трех разделов*, посвященных развитию блоковой концепции применительно к вулканическому процессу, и *обсуждения результатов*.

Во *введении* на примере анализа исследований, проводимых в течение последних десятилетий сотрудниками Института земной коры СО РАН, показывается, что концепция тектонофизического процесса Байкальской рифтовой зоны, разрабатываемая в рамках разломной тектоники на региональном уровне, не позволяет видеть всю картину в целом. Региональные концепции существенным образом опираются на представления

о разломах, представления о блоковой среде используются чисто формально. И, несмотря на большие успехи [*Sherman, 2014*], уже на первых этапах построения региональной модели ученые вынуждены вводить взаимосвязи между ее параметрами, тем самым резко ограничивая возможности интерпретации модели на заключительных этапах исследования. Отмечается, что принцип Сен-Венана в применении к задачам сейсмологии и геодинамики не может рассматриваться как фундаментальный.

В разделе «*Напряжения с моментом силы*» проводится построение механически очевидной модели движения блока, являющегося частью вращающейся среды – геосреды. Показывается (рис. 1), что в блоковой вращающейся и передвигающейся вдоль поверхности Земли геосреде генерируется упругое поле с моментом силы, которое действует на блоки через их поверхности. Такие свойства упругого поля являются следствием закона сохранения момента количества движения. Движение блока во вращающейся системе координат механически эквивалентно движению блока в невращающейся (инерциальной) системе координат под действием собственного момента силы (спина), который в окружающем блок пространстве создает упругое поле с моментом силы. Такие напряжения в геосреде накапливаются, что и может объяснить ее известное свойство – энергонасыщенность [*Ponomarev, 2008*].

В разделе «*Близкодействие и дальнодействие ротационного упругого поля*» показывается, что поле упругих напряжений с моментом в геосреде описывается симметричным тензором напряжений. Оно характеризуется близкодействием – «моментным» взаимодействием рядом расположенных блоков, и дальнодействием – «энергетическим» взаимодействием всех блоков сейсмического пояса, протягивающегося на десятки тысяч километров, что может являться отражением общего физического принципа – корпускулярно–волнового дуализма. В ротационной концепции не требуется привлекать модель Коссера, которая является математической, не физической.

В разделах «*О ротационных волнах в блоковых вращающихся геосредах*» и «*Новый тип геодинамических колебаний*» описывается разработанная ранее автором в рамках блоковой концепции геосреды модель ротационного сейсмотектонического процесса [*Vikulin, 2011*]. Характерными скоростями волновой модели являются $c_0 = \gamma\sqrt{V_R V_S}$, $c_0 \approx 1 - 10$ см/с (8) и (9) и V_S≈1–10 км/с (10). Значение первой c_0 – «солитонной» предельной скорости – определяется только угловой скоростью вращения Земли вокруг своей оси, откуда и название модели – ротационная. Вторая V_{ex} – «экситонная» предельная скорость – является скоростью упругих сейсмических волн. Отмечается, что такие же, по сути, деформационные волны [*Khachai O.A., Khachai O.Yu., 2012; Khachai et al., 2013*] инструментально зарегистрированы в шахтах. Проводится сопоставление теоретических модельных решений с данными о скоростях миграции очагов землетрясений. Отмечается и качественное и количественное совпадение с такими же и решениями и значениями характерных скоростей, соответственно. Формулируется вывод о том, что ротационные волны – это новый тип волн, являющихся для блоковых вращающихся сред такими же характерными, как и продольные и поперечные сейсмические волны.

В разделе «*Реидные свойства геосреды*» отмечено, что медленные ротационные волновые движения могут быть ответственными за сверхпластичные течения [*Leonov, 2008*] геосреды – ее реидные [*Carey, 1954*] свойства [*Vikulin, Ivanchin, 2013a*]. Отмечается, что физическим аналогом такого движения может являться сверхтекучесть.

В разделе «*Ротационные и маятниковые волны*» показывается, что описание волнового геодинамического процесса в рамках ротационной модели близко такому же, по сути, блоковому описанию с позиции концепции «композиции и декомпозиции вещества Земли» [*Oparin et al., 2010*]. Это позволяет ротационные и маятниковые, а также и деформационные [*Khachai O.A., Khachai O.Yu., 2012; Khachai et al., 2013*] волны отнести к одному классу явлений – взаимодействию блоков геосреды между собой посредством упругого поля с моментом силы.

В разделе «*Блоковая геосреда и вулканизм*» отмечается, что отражением блокового строения среды может являться магматический очаг, питающий извержения действующего вулкана.

В разделе «*О параметрах магматических очагов*» с использованием большого объема данных об извержениях вулканов планеты показывается, что толщина магматического очага является инвариантом наиболее общих статистических распределений, характеризующих вулканический процесс (рис. 3 и 4), и, как следствие, мало изменяющейся величиной Δh=0.5±0.1 км (19). Это позволяет толщину магматического очага рассматривать как постоянную величину, не зависящую от вулканического процесса, которая определяется геодинамическими параметрами земной коры, ее блоковым строением. При размерах кальдер до D=10–15 км и более форма очага близка блинообразной: $D \gg \Delta h$.

В разделе «*Магматический очаг как состояние земной коры*» для блоковой геосреды, вдоль границ которой возможны интенсивные пластические деформации [*Magnitskii et al., 1998; Turcotte, Schubert, 1985*], с использованием разработанной в материаловедении концепции «теплового самоускорения» [*Ivanchin, 1982*] проводится построение модели «тонкого» (блинообразного) магматического очага. В пределах земной коры в результате малой теплопроводности горных пород и интенсивной пластической деформации вдоль границы залегания кристаллического фундамента на глубине 6 км (Камчатка) может реализоваться состояние перегретого выше точки плавления вещества, находящегося в твердой фазе. При локальных плавлениях в очаге и увеличении его объема в окружающей очаг земной коре создаются упругие напряжения, величина которых может достигать 10^{15} Дж на 1 км^3 перегретой породы. Такие напряжения сопоставимы с напряжениями в очагах сильнейших тектонических землетрясений с магнитудами около 8 и более. «Энергетическая» близость магматических и сейсмических рядом расположенных очагов в рамках модели блоковой гесореды позволяет объяснить и взаимодействие вулканов между собой (миграцию вулканической активности [*Vikulin et al., 2010, 2012, 2013*]), и взаимодействие вулканизма, сейсмичности и тектоники [*Vikulin, 2011; Vikulin et al., 2013*]. Развитые представления распространяются на границу Мохо. Формулируется гипотеза, согласно которой подошва земной коры может представлять собой фазовую поверхность, ниже которой геосреда не является блоковой, способной к сдвиговому течению.

В разделе «*Обсуждение результатов*» рассматривается ряд возможностей ротационной модели. Проблема взаимосвязи энергонасыщенности, реидности и способности двигаться вихревым способом, с одной стороны, и сильной нелинейности геосреды – с другой, сформулирована как фундаментальная задача геодинамики и тектонофизики. Свойство энергонасыщенности геосреды, ее нахождение в напряженном состоянии [*Rykunov et al., 1979*], способном ее разрушить [*Bogdanovich, 1909; Ponomarev, 2008*], показывают, что землетрясение, скорее всего, происходит не в соответствии с теорией Ф. Рейда, т.е. не в результате создания локальных напряжений в очаге будущего землетрясения и преодоления предела прочности горных пород. Землетрясение в рамках развиваемой автором ротационной концепции является результатом дальнодействующего взаимодействия всех блоков земной коры и создания в области очага будущего землетрясения и прилегающих к ней блоков условий для их близкодействующего взаимодействия, которое может сопровождаться образованием свободной поверхности разрыва и излучением сейсмических волн. В рамках ротационной концепции механизм «зацепления» блоков и плит друг за друга и «выделения» тепла за счет трения их границ становится маловероятным.

Ключевые слова: геодинамика, момент силы, ротационные волны, реидное течение, гравитационные волны.

> There is no "relativity of rotation." A rotating system is *not* an inertial frame, and the laws of physics are different.
>
> *R. Feynman* [*Feynman et al., 1964*]

> Относительности вращения не существует. Вращательная система – *не инерциальная* система, и законы физики в ней другие.
>
> *Р. Фейнман* [*Feynman et al., 1964*]

> Geological time scale is close to the scale of the Universe. Geologists own chronicle, which recorded the events of history of the Earth, as well as the Universe.
>
> *D.V. Nalivkin* [*Nalivkin, 1969*]

> Масштаб геологического времени близок к масштабу Вселенной. Геологи владеют летописью, в которой записаны события истории Земли, а также и Вселенной.
>
> *Д.В. Наливкин* [*Nalivkin, 1969*]

1. INTRODUCTION

The Baikal region and its neighbouring territories are the best studied among many areas subject to traditional geodynamic studies, including comprehensive geological and geophysical observations with regards to tectonophysical concepts. The research team under the leadership by Prof. S.I. Sherman from the Institute of the Earth's Crust, SB RAS has conducted detailed studies in this region for several decades. They have proposed and developed a tectonophysical model of the deep structure of faults in Central Asia [*Sherman et al., 1992, 1994*]. Results of their pioneering studies include the following:

– Large faults in lithosphere extension zones are physically modelled, and quantitative parameters of deformation in zones of large faults are established [*Sherman et al., 2001*];

– An original geodynamic model is developed to show how rift basins in Pribaikalie and Transbaikalie develop in space and time [*Lunina et al., 2009*];

– A seismic zone is modelled in terms of tectonophysics [*Sherman, 2009*]; the model shows that sources of rare strong earthquakes are clustered in linear or arc-shaped systems [*Sherman, 2013*] and migration velocities of earthquakes K≥12 (M≥4–5) range from 1 to 100 km per year [*Sherman, 2013; Sherman, Gorbunova, 2008*]; according to [*Vikulin et al., 2012a, 2012b*], these values do not contradict with the relevant global data;

– According to above-mentioned model, faults are activated by *slow strain waves of excitation* which are generated by interplate and interblock movements of the lithosphere [*Sherman, Gorbunova*, *2008*] and can also occur in zones wherein seismicity is slowly migrating [*Sherman*, *2009, 2013; Sherman et al., 2011*]; a general assumption is that $L \geq l$, wherein L is strain wave length and l is length of a fault activated by strain waves [*Sherman et al*., *2008*];

– It is revealed that two major fault zones in the Baikal rift zone and the Amur River region are related; active faults are identified in both regions; it is established that the fault activation is manifested by seismicity and caused by trigger mechanisms with the leading role of slow strain waves [*Sherman, 2013; Sherman et al., 2011*].

The above-mentioned tectonophysical model of the wide geodynamic zone, including Central Asia and the Amur River region, is based on the concept of the fault-block geomedium and the assumption that faults are activated in real time by slow strain waves, and the fault activation is accompanied by seismic events that sequentially take place along the faults. It is believed that developing the tectonophysical model of the seismic process can "give an insight to regularities of earthquake location in space and time and facilitate seismic forecasting" [*Sherman*, *2009*]. The current model is based on commonly accepted geological, geophysical and tectonophysical concepts of the geodynamic process. In general, it seems promising and compliant with the major concepts that are internationally accepted in modern geoscience. Undoubtedly, this model is an important contribution to the Earth sciences.

The above-mentioned research results are consolidated in [*Sherman*, *2014*]. S.I. Sherman and his colleagues have proposed and develop the tectonophysical concept of the Baikal rift zone development. In his book, S.I. Sherman states that their concept does not depend on *physical* concepts of seismicity (p. 6) and is thus universally applicable.

However, a review of the tectonophysical model of Central Asia with respect to the planetary scale [*Vikulin et al*., *2012b*] reveals a seemingly insignificant inconsistency and raises a number of important questions.

As mentioned above, the model estimates of velocities of earthquake sources migration along the faults are generally consistent with the global data. Nonetheless, the detailed analysis of migration velocities in geodynamic settings of all active zones of the Earth [*Vikulin et al., 2012a*] shows that this is not exactly the case. The model estimates of velocities of earthquake sources migration along the faults in Central Asia do not contradict with similar plots constructed for the Pacific margin and the Alpine-Hymalayan belt (i.e. compression zones), but are in conflict with the plots constructed for the Middle Atlantic ridge (i.e. extension zone). Thus, the earthquake migration estimates for Central Asia at the regional level are contradicting with the estimates at the planetary level. Otherwise, it has to be accepted that the studied region of Central Asia is not a rift, or it should be clarified that the earthquake migration estimates for the Baikal region refer to one of its flanges rather than to the entire rift zone. This poses the questions: – Which flange in particular? – What is the difference between the flanges? The regional model fails to provide answers to these questions.

In the regional tectonophysical models, including the model of Central Asia, the concept envisaging the block structure of the geomedium is applied formally or 'rhetorically' – such models are typically constructed with reference to boundaries between the blocks and block length values rather than blocks themselves and their volumes, and the models thus consider waves propagating along the boundaries between the blocks (i.e. along the faults), but not the waves propagating inside the block medium. This terminological 'swapping' – 'speaking about blocks, while thinking about faults'– is not just a habitual use of '*fault*' as a commonly accepted term with a 'standard' reference to the local stress accumulation mechanism (according to H. Rheid) and its modifications. In the regional tectonic models, the accumulated energy is not released – it is redistributed in the form of slow strain waves, while in seismic models, the energy is released by slow strain waves. The notions are substituted 'automatically' or 'by analogy' as a result of ignoring the major consequence of the geomedium block concept which states that stresses are redistributed in the geomedium's *volume* (p. 193–197, 332–334 in [*Sadovsky*, *2004*]). The idea of stress redistribution is supported by detailed seismic monitoring data obtained recently in mining projects in Russia [*Mulev et al*., *2013*]: "While a combined machine is moving inside the mine, the seismic energy release plot is changing; once the machine is stopped, the corresponding isolines in the plot are immediately 'frozen' in real time". In other words, even when an insignificant rock volume is 'extracted' from the massif, stresses are significantly redistributed[1]. The 'volume' mechanism of stress redistribution in the geomedium is in conflict with the tectonophysical (actually, 'fault-based') interpretation of the data obtained for Central Asia. In fact, an obscure issue is how a non-radiating fault, being only activated [*Sherman, Gor-*

[1] It follows from the instrumental seismological data published in [*Mulev et al., 2013*] that the Saint-Venant's principle (being local, according to [*Sedov, 1973*], p. 364–365) is not applicable to solving the geophysical problems. Seismologists and geophysicists consider the Saint-Venant's principle as fundamental (page 11 in [*Riznichenko, 1985*], though a sufficient justification of this approach is lacking. This problem is discussed in detail in [*Vikulin, 2014a*]. Below in the present paper, a geodynamic justification of the Saint-Venant's principle is provided under the rotation concept, and it is suggested that long-range interaction takes place between the geomedium blocks.

bunova, *2008*], can 'be aware' of the length of the wave passing through this fault.

The geomedium block structure is a challenging subject for both the Earth sciences and practical applications, and the key problem is to specify what part of the geomedium should be regarded as a block and what part is a boundary of this block. At the conference held in Irkutsk in August 2014, the report on this problem [*Tveritinova, Vikulin*, *2014*] sparked off a dispute that was lively, although not completed by any specific conclusion, and the participants agreed that the definitions need to be sorted out.

The seismic and geodynamic setting of the entire Baikal-Amur River zone as a global interplate boundary [*Sherman et al*., *2011*] has not been fully clarified yet, and the knowledge is mainly based on the regional and hypothetical conclusions that are 'cross-linked' only with regard to some separate ideas. With account of the current uncertainties, 'paving a pathway to regional earthquake forecasting' [*Sherman, 2009, 2014; Sherman, Gorbunova, 2008; Sherman et al., 1992, 1994, 2001, 2011*] may appear not that straight forward.

The 'regional' approach fails to provide a comprehensive view, and relationships between model parameters have to be introduced to design a model, which means setting up strong limitations on potential interpretations of consequences following the model at the final stage of modelling which is most important for geodynamics. A more general approach can facilitate finding original pathways to reviewing and solving *geodynamic* problems in the Earth sciences [*Vikulin et al., 2012a, 2012b*].

2. Stresses with force momentum in the geomedium composed of blocks

An important scientific achievement of the past decades is the justification of the hypothesis of the block structure of the geological medium [*Peive*, *1961*] / geomedium (p. 5–20 in [*Nikolaev*, *1987*]) / geophysical medium (p. 332–334 in [*Sadovsky*, *2004*]).

The Earth crust is subject to motions and changes as the crustal blocks and plates migrate on the Earth surface (Fig. 1). Properties of the crust are predetermined by the Earth *rotation* and its structure composed of the blocks that are subject to translational motions at the Earth surface [*Vikulin, 2010, 2011; Vikulin, Ivanchin, 2013a*].

The coordinate system, that is fixed for the body (i.e. the Earth), rotates with angular velocity $\mathbf{\Omega}$ that does not depend on the coordinate system as it is – in the given moment of time, all systems of the kind are rotating around axes (that are parallel to each other) with absolute velocity $\mathbf{\Omega}$ [*Landau, Lifshitz, 1973*]. Thus, regardless of its size, *any* block/plate is characterized by impulse momentum $\mathbf{M}$ that is independent of the block/plate size and origin and directed parallel to the body's (i.e. Earth's) rotation axis: $\mathbf{M} = \mathrm{I}\mathbf{\Omega}$, where I is inertia momentum of the block/plate. As shown in Fig. 1, *a*, crustal movements from position $\mathbf{M_1}$ to position $\mathbf{M_2}$ lead to changes in the direction of momentum, $\mathbf{M_1}\rightarrow\mathbf{M_2}$ because of the rigid relationship between the block and the Earth that rotates with angular velocity $\mathbf{\Omega}$. Under the impulse momentum preservation law, when the direction and, consequently, value of $\mathbf{M}$ is changed, the block is subject to force momentum $\mathbf{K}$.

The value and direction of force momentum $\mathbf{K}$ can be estimated theoretically as follows. It is assumed that the block is a uniform ball-shaped body that is stopped in position $\mathbf{M_2}$ and subject to elastic stresses with force momentum $\mathbf{P_2}$ (see Fig. 1, *b*). Then elastic stresses with force momentum $\mathbf{P_1}$ are applied to rotate the block to its initial state with momentum $\mathbf{M_1}$. With the assumption that kinetic energy of the block's rotation is converted to elastic stresses and vice versa without any loss of energy ($|\mathbf{P_1}| = |\mathbf{P_2}| = |\mathbf{P}|$), the cosine law is applied to force momentum $\mathbf{K}$:

$$|K| = 2|P|\sin\beta/2. \qquad (1)$$

It should be noted that elastic stresses with force momentum $\mathbf{K}$ are applied to the block across its surface from the side of its *surrounding* crust and lithosphere [*Vikulin, Ivanchin*, *2013a*].

Therefore, in the rotation model [*Vikulin, 2009, 2010, 2011; Vikulin, Ivanchin, 2013a; Vikulin et al., 2010, 2013*], the block's movement with angular velocity $\mathbf{\Omega}$ is mechanically equivalent to its movement in the non-rotating/inert system of coordinates under the impact of its own force momentum $\mathbf{K}$ that generates an elastic field with force momentum (equation 1) in the medium surrounding the block (as a consequence of the impulse momentum conservation law).

The 'internal' and/or own [*Peive*, *1961*] momentum $\mathbf{M}$, that is actually a macrospin (p. 146–148 in [*Sedov*, *1973*]), has a specific feature – under the impulse momentum conservation law, the geomedium cannot be 'deprived' of it by any means, including plastic deformation. Thus, as a result of the translational motion of the block along the Earth surface (due to increasing block rotation angle β and constancy of the angle α, Fig. 1), rotation stresses with force momentum (equation 1) occur in the crust. The accumulation of such stresses provides an explanation [*Vikulin, Ivanchin*, *2013a*] of such a property of the crust as energy capacity (in terms of [*Ponomarev*, *2008*]). In fact, a similar conclusion was drawn by geologists at the end of the 19th century and in the early 20th century on the basis of observations of auto-destruction of rock samples

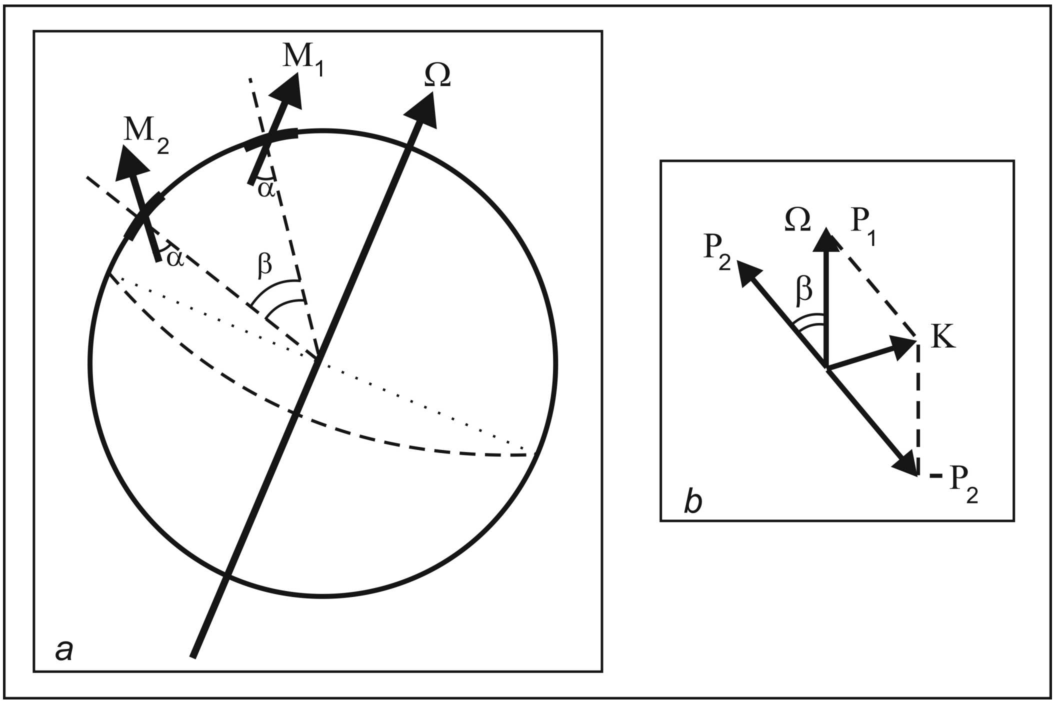

Fig. 1. While the crustal block moves from position $\mathbf{M_1}$ to position $\mathbf{M_2}$ (i.e. rotates by angle β) (*a*), stresses with force momentum **K** are 'generated' in the crust and the lithosphere, force momentum **K** is applied to the block from its surrounding medium (*b*). α – the angle between the momentum **M** and the vertical to the Earth surface, which remains constant during the block movement. See explanations in the text.

Рис. 1. Движение блока земной коры из положения с моментом импульса $\mathbf{M_1}$ в положение $\mathbf{M_2}$ (поворот блока на угол β) (*a*), сопровождающееся «генерацией» в земной коре и литосфере напряжений с моментом силы **К**, прикладываемым к блоку со стороны окружающей его среды (*b*). Пояснения в тексте.

extracted to the ground surface [*Bogdanovich*, *1909*]. Besides, the fact that the Earth's crust is permanently subject to stresses is confirmed by the available geophysical data obtained by instrumental measurements [*Rykunov et al.*, *1979*; *Nikolaev*, *2003*; *Chebotareva*, *2011*; *Khachai O.A., Khachai O.Yu.*, *2012*].

3. Short- and long-range impacts of the rotational elastic field

The rotation concept (p. 124–136 in [*Vikulin*, *2011*]) is applied to solve the following two-point boundary-value problem: a ball-shaped block has radius R_0; its own momentum is given by equation 1 for the inert non-rotating spherical system of coordinates (r, φ, θ) with the starting point (r=0) in the block's centre; angle φ is calculated in the plane located perpendicular to the block's rotation axis (θ=π/2); displacements at the infinite are zero; the non-zero-value force momentum does not depend on the block's size. According to theoretical estimations for the geomedium surrounding the block (i.e. $r > R_0$) [*Vikulin*, *2010*], the stress field is estimated as follows:

$$\sigma_{r\varphi} = \sigma_{\varphi r} = 4\Omega R_0^4 r^{-3}\sqrt{\frac{\rho G}{5\pi}}\sin\theta\sin\beta/2 \qquad (2)$$

(values of other components are zero). The stress field is symmetrical[2]. Its energy is $W_0 = \frac{16}{15}\pi\rho\Omega^2 R_0^5\sin^2\beta/2$, and the force momentum/ seismic momentum is $K_0 = -8\pi^{3/2}\Omega R_0^4\sqrt{\frac{\rho G}{5}}\sin\beta/2$, where ρ=3 g/cm³ and G=10¹¹ n/m² are density and shear modulus of the crust, respectively, Ω=7.3·10⁵ rad/sec is angular velocity of the Earth rotation around its axis, R_0 is typical size of the block/earthquake source with $M \approx 8$, and suffix number (*0*) refers to the block's 'own' energy and torque.

In [*Vikulin*, *2010*, *2011*], the model is applied to study the interaction between *any* two blocks with sizes R_{01} and R_{02}, which are located at distance l from each other. The interaction energy and force momentum are

[2] A fundamental role of 'stress tensor symmetry' for mechanics of continua, including the geomedium, is discussed in [*Vikulin, Ivanchin*, *2013a*]. They also draw attention to the fact that the non-physical character of the model proposed by Cosserat E. and F. [*Cosserat E. et F.*, *1909*] was noted immediately after its publication (p. 26 in [*Hirth*, *Lothe*, *1968*]).

estimated as follows: $W_{\text{int}} = \frac{3}{2}\pi\rho\Omega^2 R_{01}^4 R_{02}^4 l^{-3}\cos\phi$, and $K_{\text{int}} = -\frac{3}{2}\pi\rho\Omega^2 R_{01}^4 R_{02}^4 l^{-3}\sin\phi$, respectively. In case of equal-size blocks (R_{01}=R_{02}), interaction energy W_{int} and force momentum K_{int} become similar to their own energy W_0 and own force momentum K_0 (W_{int}=W_0, and K_{int}=K_0 [*Vikulin, 2010*]) at distances l_{0W} and l_{0K} estimated in [*Vikulin, Ivanchin, 2013a*] as follows:

$$l_{0W} \approx 10^2 R_0, \tag{3}$$

$$l_{0K} \approx R_0. \tag{4}$$

Equation (3) shows that the interaction between the blocks, which controls their energy exchange, is manifested across large distances exceeding the block sizes and can be thus termed the *long-range*[3] interaction. In seismology, such interaction is well-known and evidenced by the migration of earthquake sources along seismic belts for long distances amounting to dozens of thousand kilometres [*Vikulin et al., 2012a, 2012b*], as well as by remote fore- and aftershocks [*Prozorov, 1978*] and coupled earthquakes (p. 119–123 in [*Vikulin, 2011*]).

The instantaneous interaction between the blocks controls their momentum exchange and, according to equation (4), propagates to small distances not exceeding the block sizes. It can thus be called the *short-range* interaction. Such interaction is also well-known and evidenced by strong earthquakes, including coupled and multiple earthquakes with long-length sources (1000 km and more). Their sub-sources (with lengths ranging from 100 to 300 km) are involved in the instantaneous interaction and generate intensive own oscillations of the planet (p. 244–258 in [*Vikulin, 2011*]).

The above-mentioned theoretical solutions obtained for stress field σ, elastic energies W_0 and W_{int} and momentums K_0 and K_{int} are applicable to *any* block and *any* couple of the geomedium blocks. The summary of the stress fields may show the planet's elastic field that is 'self-congruent' and predetermines a rotation component in motions of each geomedium block. The stress fields may vary by scale and have variable complex shapes in various geodynamic polygons due to the irregular structure of the geomedium and different modes of the geomedium block motions. In view of the above, the block rotation pattern in Central Asia is chaotic and multi-directional (Fig. 2). In other regions studied in other scales with insignificant local inconsistencies, stress field patterns may seem regular and manifested in geophysical fields by vortex, ring-shaped and other non-linear geological structures (see Figures 1, 2, 7 and 8 in [*Vikulin, 2010*]).

In physics, short- and long-range actions are often related to corpuscular and wave interactions taking place across boundaries of particles and across the medium wherein the particles are located, respectively. Under the geomedium block concept, the blocks can be viewed as 'elementary' particles. Therefore, in terms of physics, the geodynamics of block interactions in the rotation model can be viewed as a manifestation of the general physical principle of corpuscular–wave dualism envisaging that movements of geophysical blocks, tectonic plates and geological structures have both corpuscular and wave features, as discussed below.

4. ROTATION WAVES IN THE GEOMEDIUM COMPOSED OF ROTATING BLOCKS

For the block that generates an elastic field with force momentum (1) and interacts with elastic fields generated by other blocks of similar sizes in a mass chain, the movement law is established as the sine–Gordon equation (p. 85–95 in [*Vikulin, 2011*]). In this case, a seismic belt is modelled by a unidimentional chain of the crustal blocks/earthquake sources interacting with each other. Each block is characterized by inertia momentum I and volume $V = 4/3(\pi R_0^3)$.

The block motion can be given by the following equation: $I\frac{\partial^2\beta}{\partial t^2} = K_0 + K_1$, where K_0 is force momentum corresponding to the elastic stress field generated by an individual block; K_1 is force momentum controlling the interaction of the block with other blocks included in the chain. It is generally assumed that K_1 is proportional to both the elastic energy accumulated due to motions of the corresponding block ($V\frac{\partial^2\beta}{\partial z^2}$, where z is distance along the chain of mass/blocks) and the elastic energy of other blocks included in the mechanical chain. The block motion can be thus given by the following dimensionless equation:

$$\frac{\partial^2\theta}{\partial\xi^2} - \frac{\partial^2\theta}{\partial\eta^2} = \sin\theta, \tag{5}$$

where $\theta = \beta/2$, $\xi = k_0 z$ and $\eta = v_0 k_0 t$ are dimensionless coordinates, and t is time. Taking into account that the wave length is close to the block size ($\lambda \approx R_0$), and wave number is $k_0 = 2\pi/R_0$, the following equation is obtained for process development velocity v_0 typical of the motion (equation 5):

$$v_0 = \sqrt{\frac{15}{8\pi^2\sqrt{5\pi}}\Omega R_0\sqrt{\frac{G}{\rho}}} \approx \sqrt{\frac{\sqrt{15}}{8\pi^2}V_R V_S} = 0.2\sqrt{V_R V_S}, \tag{6}$$

[3] As noted above, with account of the long-range interaction between the geomedium blocks, the local Saint-Venant principle becomes inapplicable to solving the problems of geodynamics. Flexural-torsional strain problems cannot be solved on the basis of this principle either (p. 33 in [*Bezukhov, 1953*]).

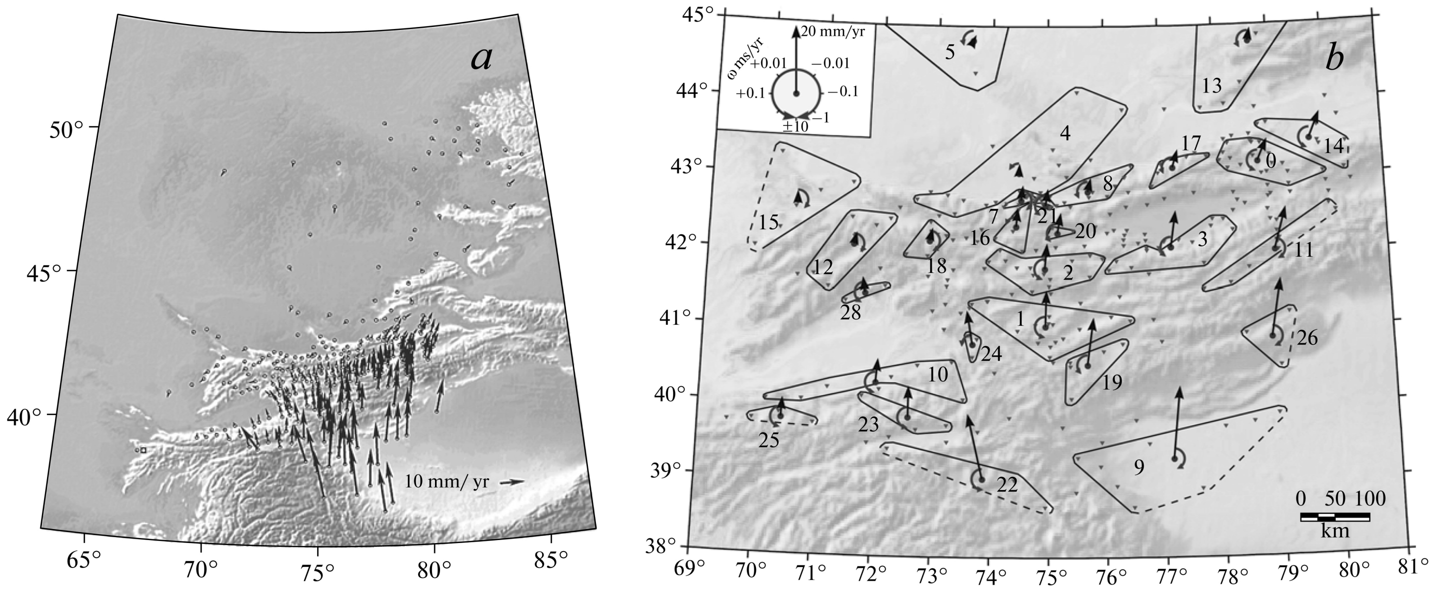

Fig. 2. GPS data obtained at 323 observation points in Central Asian polygon in the period from 1995 to 2005 [*Kuzikov, Mukhamediev, 2010*].

Dots show the observation points. *a* – displacement vectors of the entire polygon; *b* – differentiated rotation of blocks (viewed as rigid bodies), according to data from clusters of observation points characterised by zero horizontal displacements against each other.

Рис. 2. Данные 323 пунктов GPS-наблюдений на Центрально–Азиатском полигоне в 1995–2005 гг., обозначенных точками [*Kuzikov, Mukhamediev, 2010*].

a – вектора смещений всего полигона, в целом; *b* – дифференцированные вращения блоков как жестких образований, в каждом блоке выявленные по таким совокупностям наблюдательных пунктов, имеющих нулевые горизонтальные перемещения друг относительно друга.

where $V_R = \Omega R_0$, and $V_S \approx 4$ km/sec is velocity of a transversal seismic wave.

The form of equation (5) is predetermined by equation (1) used to estimate the force momentum of the elastic field generated by an individual block. It is thus assumed that sine–Gordon equation (5) and its right part ($sin\theta$) can be viewed, in terms of mathematics, as the law of impulse momentum preservation in wave processes. This is a principal assumption – when applied to the rotation problem of interrelated blocks arranged in a chain, it allows us not to consider any interaction between blocks due to friction along their boundaries, while the interaction needs to be considered in the elasticity theory (as shown, for example, in [*Nikolaevsky, 1996*]). Logically, this approach facilitates a physically 'transparent' interpretation of the typical velocity (equation 6) of the geophysical process described by sine–Gordon equation (5), if the rotation problem of stress fields around the block, that is rotating due to its own momentum, is solved under the classical theory of elasticity [*Landau, Lifshitz, 2003*] with a *symmetric stress tensor* (equation 2).

Equation (6) shows that if physical parameters G, ρ and R_0 are fixed, velocity v_0 depends *only* on angular velocity Ω (via inertia momentum I and volume V of the block). This means that the actual cause of such strain is *Earth rotation* (p. 237–243 in [*Vikulin, 2011*]). This is why the model introduced in [*Vikulin, 2011*] is called *"rotation model"*. Given the above-mentioned parameters of the crust, the typical velocity is $v_0 = 10 - 10^2$ m/sec.

In this case, we analyse a chain of irregularly rotating blocks characterised by deviations of force momentums that diverge from those in equilibrium positions (μ). In general, such a chain corresponds to the seismic process in nature. Friction α_f along the block boundaries is taken into account, though it is viewed not as a mechanism of interaction between the blocks due to their 'hitch-up' to each other (as envisaged in the elasticity theory), but as a dissipative factor that hinders the rotation interaction between the blocks. Based on the above, the law of block motions in the chain can be thus shown by a modified sine–Gordon equation (p. 237–243 in [*Vikulin, 2011*]):

$$\frac{\partial^2\theta}{\partial\xi^2} - \frac{\partial^2\theta}{\partial\eta^2} = \sin\theta + \alpha_f\frac{\partial\theta}{\partial\eta} + \mu\delta(\xi)\sin\theta. \qquad (7)$$

A numerical solution of equation (7) is found by the McLaughlin–Scott method. In this case, $\delta(\xi)$ is the Dirac function. In the model, initial conditions are given with regard to an average strain velocity in seismically active regions, and coefficients of friction α_f and inhomogeneity μ correspond to those of real faults. If blocks/earthquake sources are interacting mainly due to creeping (i.e. in case of the slowly developing seismic process), an asymptotic value of rotation strain transfer velocity is $c_0 \approx 1-10$ cm/sec (p. 237–243 in [*Vikulin*, *2011*]).

Under the model envisaging that the non-linear geomedium is composed of blocks, it is acceptable that velocity $\{v_0, c_0\}$, that is typical of the transfer of solitonic rotation strain (i.e. stress with torque), can be estimated as follows [*Vikulin, Ivanchin*, *2013a*]:

$$c_0 = \gamma\sqrt{V_R V_S},\ \ c_0 \approx 1-10 \text{ cm/sec}, \qquad (8)$$

where $\gamma = k^{-1} \approx 10^{-4}$ is non-linear parameter characterising a chain of blocks/cluster of earthquake sources that make up a seismic belt; the block/cluster is variable in size; its rotation is irregular due to friction; $k \approx 10^4(10^3-10^5)$ is geomedium non-linearity coefficient that is equal to the ratio between elastic constants of the third order and elastic constants of the second order, i.e. linear moduli of elasticity [*Nikolaev*, *1987*].

It is noteworthy that instrumental records in mines have also revealed 'slow' and 'fast' strain waves [*Khachai et al.*, *2013*] and oscillation waves (μ-waves) [*Oparin et al.*, *2010*].

5. A NEW TYPE OF GEODYNAMIC OSCILLATIONS

In our study, we compare experimental data on the migration of earthquake sources [*Vikulin et al.*, *2012a, 2012b*] and theoretical solutions of the sine-Gordon equation (p. 124–136 in [*Vikulin*, *2011*]) [*Davydov*, *1982*] and find two solutions that correspond to limiting energies [*Vikulin*, *2010*], i.e. slow solitons (sol) and fast exitons (ex) (in terms of [*Davydov*, *1982*])[4]. The slow solitons control the global migration of earthquake sources within an entire seismic belt (i.e. 'long-range action of energy') with the following limiting velocity:

$$V_{sol} \le c_0 \approx 1-10 \text{ cm/sec}. \qquad (9)$$

The fast exitons control the local migration of fore- and aftershocks in sources of strong earthquakes (i.e. 'instantaneous' *short*-range interaction) with a limiting seismic (s) velocity as follows:

$$c_0 < V_{ex} \le V^s \approx 1-10 \text{ km/sec}. \qquad (10)$$

[4] Definitions of exitons differ in the literature [*Davydov, 1976; Ziman, 1974*, and others]. In this paper, solitons and exitons are viewed as excitations according to [*Davydov*, *1982*].

The slow solitons (9) and fast exitons (10), as a reflection of the general physical principle of wave-particle duality, are, in fact, a new type of geodynamic fluctuations. They are characteristic of the block rotating medium /geomedium in the same way as longitudinal and transverse seismic waves for a 'normal' body.

Based on plate dimensions and movement velocities of plate boundaries, two relationships are established between plate boundary length L and its movement velocity V, $L_{1,2}(V)$ (p. 313–316 and 317–322 in [*Vikulin*, *2011*]). Relationship $LgL_1 \approx (0.7 \pm 0.3)LgV_1$ is close to $LgL \approx LgV$ that characterizes spreading and subduction [*Zharkov*, *1983*; *New Global Tectonics*, *1974*] and actually corresponds to the 'long-range' soliton action (9). The second relationship $LgL_2 \approx (0.4 \pm 0.2)LgV_2$ is close to $LgL \approx 0.3LgV$ that determines fault activation in Central Asia [*Sherman, Gorbunova*, *2008*]. In our opinion [*Vikulin*, *2010*], it corresponds to 'instantaneous action' (10). Tectonic solitons and exitons, as excitations corresponding to relationships $L_{1,2}(V)$, control changes of the tectonic activity at the Earth surface, while seismic disturbances (9) and (10) predetermine the seismic activity migration along the belts.

The conclusion about the existence of "a new type of solitary waves" with "limiting velocity values" is also stated for non-local elastic solids [*Pamyatnykh, Ursulov*, *2012*]. The idea of a 'slow' mode "propagating with a velocity that is much lower than the velocity of sound in liquids, solid granules and gas" is theoretically and experimentally supported by results of theoretical and experimental studies [*Rudenko et al.*, *2012*]. "The slow dynamics" and its impact on "the elastic properties of materials" are specified in [*Korobov et al.*, *2013*]. The idea of the new type of rotation waves [*Vikulin*, *2010, 2011*], as the consequence of the concept envisaging that the geomedium is composed of rotating blocks, is consistent with results of theoretical and instrumental acoustic studies of 'normal' solids [*Korobov et al., 2013; Pamyatnykh, Ursulov, 2012; Rudenko et al., 2012*].

6. RHEID PROPERTIES OF THE GEOMEDIUM

There is much evidence of movements at the Earth's surface from earthquake focal areas which are manifestted by 'humps' and often accompanied by rotation [*Vikulin*, *2008*]. Such a case is described in [*Ionina, Kubeev*, *2013*] – during the catastrophic earthquake in China on 16 December 1920, "a missionary had to put his legs wide apart like a drinker trying to remain steady on his feet as he experienced strong rotational movements underneath" (p. 124). In 1930s, geophysical and geological data on 'slow' movements of the geomedium (typically lasting for 10–10^{13} sec) were consolidated, and terms of 'rheid deformation' [*Geological Dictionary, 1978; Carey, 1953*] and 'superplastic deformation' of the Earth were introduced to denote "a flow of the material in the solid state" [*Leonov*, *2008*]. It is shown below that the above-described state of the geomedium is a direct consequence of its motions due to rotation.

A review of definitions of the rheological properties of the Earth [*Vikulin*, *2009*] shows that the Debye temperature θ_d of the geomedium can be given as follows [*Zharkov*, *1983*]:

$$\theta_d \approx 10^{-3}\bar{V}(H)\sqrt[3]{\rho(H)}, \tag{11}$$

where $\bar{V}$ is average velocity of excitations in the geomedium, cm/sec; ρ is density of the geomedium, g/cm^3; H is depth, km. If an average velocity (determined by longitudinal and transverse seismic velocities) for the lithosphere and upper mantle ranges from 1 to 10 km/sec, the Debye temperature is high enough. If H=100 km, $\theta_d \approx 660\ °C \approx 1000\ °K$, and these values correlate well with the common model of the Earth physics [*Zharkov*, *1983*].

The situation radically changes in case of transition to rotation mode c_0 (equation 8) that is determined by motions of the geomedium blocks, tectonic plates and geological structures in the aggregate[5]. According to equation 8, limiting velocity value c_0 is at least five orders lower than the longitudinal and transverse seismic velocities, and the Debye temperature (equation 11) is thus very low:

$$\theta_d \approx 10^{-2}K.$$

This provides for potential quantum, frictionless superfluid motions of the geomedium [*Vikulin*, *2013*], i.e. its rheidity [*Vikulin, Ivanchin*, *2013a*] and/or superplastic flow in the solid state [*Leonov*, *2008; Carey, 1953*].

The Debye temperature is proportional to the maximum possible frequency of oscillations of the complete set of particles composing the medium [*Ziman*, *1974*] or a set of mesovolumes of a solid body or all the geomedium blocks, tectonic plates and other geological structures of the Earth. According to [*Vikulin*, *2011*] (p. 244–258), in case of the Earth, the frequency is given by Chandler frequency typical of the aggregate oscillation of all the blocks in the seismotectonic belt. Actually, the oscillation of the entire belt is determined by the energy of 'zero' oscillations, i.e. energy E_0 (see. Fig. 6 in [*Vikulin*, *2010*]).

[5] The Earth crust is a solid body. Therefore, applying the Debye theory to geodynamic problems is reasonable in terms of physics, to prove a possibility of transition under the Debye theory to rotation mode c_0, a transition from elastic phonons to tectonic solitons (equation 9). An elastic phonon is a quantum of the interaction between 'point-size' atoms (i.e. atoms of zero size, without elastic own momentum) in the crystal lattice. A tectonic soliton is a carrier of the geodynamic interaction between (rotating) blocks of the geomedium. It has a considerable size and, respectively, its own torque.

7. Rotation waves and oscillation (μ) waves

Under the geomedium block approach, considering fracturing and "composition and decomposition of the Earth material" as the major processes [*Oparin, Vostrikov*, *2010*], oscillation **(**μ**)** waves in the geomedium are viewed as waves that predetermine geodynamic processes [*Oparin et al*., *2010*]. Velocities of both oscillation **(**μ**)** and rotation waves are lower than velocities of longitudinal waves. To experimentally substantiate the existence of μ-waves, oscillation is analysed in chains of rigid massive blocks that are analogous to the chain of blocks in the rotation model. Two types of waves are revealed in both the rotation model and the chains [*Oparin et al., 2007*]. According to estimations based on laboratory experiments [*Oparin, Vostrikov*, *2010*], velocities of oscillation **(**μ**)** waves amount to 10^2–10^3 m/sec and are close to seismic wave velocities. Oscillation **(**μ**)** wave velocities measured on site range from 1 to 10 cm/sec [*Oparin, Vostrikov*, *2010*] and are close to the typical rotation wave velocity, c_0 (equation 8).

As shown above, in the framework of the wave geodynamics, both the approach based on the rotation concept [*Vikulin*, *2009*, *2010*, *2011*; *Vikulin, Ivanchin*, *2013a*] and the approach considering "composition and decomposition of the Earth material" [*Oparin, Vostrikov*, *2010*; *Oparin et al*., *2007*, *2010*] yield similar results, while being developed independently of each other. Therefore, the rotation and oscillation **(**μ**)** waves can be considered as a phenomenon of one and the same class – interaction between the geomedium/rotating medium blocks in the field of elastic stresses with a force momentum. The methods used to study the oscillation **(**μ**)** waves [*Oparin et al*., *2007*] and strain waves [*Khachai et al.*, *2013*] may prove useful for developing a technology to ensure proper recording of the rotation waves, which are currently detected (similar to tectonic waves [*Bykov*, *2005*]) by indirect methods, and instrumental methods for this purpose are still lacking.

8. The block geomedium and volcanism

The above concepts of waves that occur during the seismotectonic process in the block geomedium seem to be applicable to volcanic processes. In fact, volcanic belts of the Earth, as well as seismically active zones are the largest linear structures of the planet. They occurred in the Early Cretaceous and developed in quite a synchronous pattern (p. 460 in [*Krasny, 2004*]). In studies of the three most active volcanic belts of the Earth – Pacific, Alpine-Himalayan and Mid-Atlantic belts, it is revealed that the volcanic activity migration, as well as the migration of seismic/tectonic activity, is a manifestation of the wave geodynamic process [*Vikulin et al.*, *2010*, *2012*].

A reflection of the 'block character' of the volcanic process and a 'quantum' characteristic of a single volcanic eruption is a magma chamber feeding the volcanic eruption which is an analogue of an earthquake in the seismic process. Several definitions of a magma chamber /reservoir/ are given in [*Vlodavets*, *1984*]. According to the most general definition that is not contradicting with the others, a magma chamber is an isolated volume feeding the volcano [*Geological Dictionary*, *1978*]. Processes taking place in the magma chamber have not been fully clarified yet [*Vlodavets*, *1984*; *Luchitsky*, *1971*; *Macdonald*, *1975*]. Nevertheless, in case of a sufficiently intense volcanic eruption when a large volume of volcanic material is conveyed to the ground surface, the size of a magma chamber can be estimated from the size of a caldera, i.e. a large circular-shaped area (with a diameter of 10 to 15 km and more) of the volcanic depression with sloping walls (that can be several hundred metres high) which formed due to eruption (p. 123 in [*Vlodavets*, *1984*]).

Many notions in volcanology have not been clearly defined yet, and a precise definition of 'caldera' is also lacking (p. 123–129 in [*Vlodavets*, *1984*]). The available data on calderas are reviewed in many publications, including [*Luchitsky*, *1971*; *McDonald*, *1975*; *Leonov, Grib*, *2004*; *Laverov*, *2005*; *Vikulin, Akmanova, 2014*; *Vikulin, Ivanchin*, *2015*]. In our study, without going into detail, we refer to the above-mentioned general definition of 'caldera'.

Our attempt to 'incorporate' the volcanic process in the geomedium block concept under the rotational approach is described below.

9. The parameters of magma chambers

Plotting the numbers and sizes of volcanic eruptions of the recent Kuril-Kamchatka volcanoes. In the region under study, the most complete and regionally consistent database, including numbers of recent (past 200 thousand years) eruptions and sizes of volcanic forms, is available for the Kuril-Kamchatka arc [*Vikulin, Akmanova*, *2014*]. Based on the data on 70 volcanoes that erupted 676 times (N) in the past 9.5 thousand years, the eruption repeatability is given in the range of volcanic explosivity indices $2 \leq W \leq 7$ [*Siebert et al.*, *2010*] as follows [*Vikulin et al.*, *2012a*, *2012b*]:

$$LgN=3.60-(0.48\pm0.06)W. \qquad (12)$$

With account of the relationship between the 'energy' characteristics of eruption and the volume of erupted material (W and V, respectively): $W=LgV+5$, $[V]$=km^3 [*Siebert et al.*, *2010*], the eruption repeatability (equation 12) can be given in terms of 'volume':

$$LgN=1.15-(0.48\pm0.06)LgV,\ [V]=\text{km}^3. \qquad (13)$$

By applying the mid-square method to analyse the data from [*Laverov*, *2005*] on recent volcanic forms, including calderas and large craters on cones and flat tops of underwater volcanoes (N=287), the following distribution of volcanic form numbers N by square areas S is yielded:

$$LgN=(2.32\pm0.16)-(0.47\pm0.14)LgS,\ [S]=\text{km}^2. \qquad (14)$$

The above equations show that the 'inclination angle' of the 'energy' and/or 'volume' distribution (W and V in equations 12 and 13, respectively) amounts to 0.48±0.06, which is practically coincident with the 'inclination angle' of the distribution of the volcanic form numbers by their square areas S (equation 14): 0.47±0.14. It should be noted that the volcanic eruptions number (N=676) and the volcanic forms number (N=278) are statistically significant. The energy range and the sizes of calderas in equations (12), (13) and (14) cover the whole spectrum of volcanic eruptions, including those with maximum values, W_{max}=7, V_{max}≈100 km^3, and S_{max}=20×25 km^2.

Essentially, equations (12), (13) and (14) show fairly general statistical distributions that are typical of the volcanic process taking place in a wide region within a large time period. The similar inclination angles of the energy (12) and/or volume (13) and square area (14) distributions suggest the following hypothesis: the ratio of erupted material volume V to area S of the resultant volcanic form (that is large enough) is constant:

$$V/S=\Delta h=const. \qquad (15)$$

Being actually an invariant of more general statistical distributions, hypothetical equation (15) has a fundamental importance for volcanology [*Vikulin, Akmanova*, *2014*].

Eruptions of volcanoes of the planet. The inclination angle of the volcanic eruption recurrence plot [*Vikulin et al.*, *2012a*] is given as follows:

$$LgN\approx-(0.52\pm0.05)W. \qquad (16)$$

It is equal to the inclination angle of a similar plot constructed for the Kuril-Kamchatka volcanoes (equation 12). With reference to the data on volcanoes of the planet [*Vikulin, Ivanchin*, *2015*], the volcanic eruption numbers are plotted against the areas of resultant calderas and volumes of erupted material.

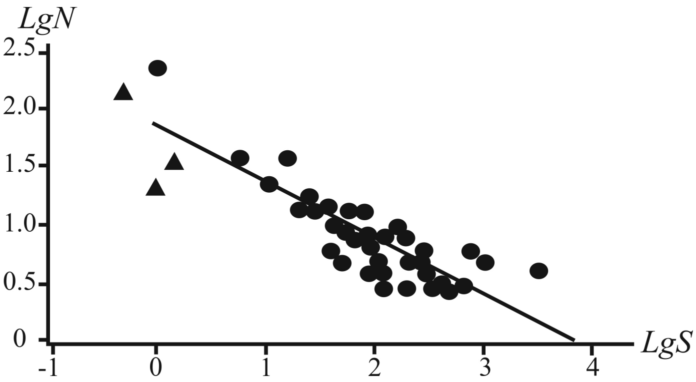

Fig. 3. Numbers of calderas (points) (N=373) and large craters on cones (triangles) (N=175) versus areas S (km^2).

Рис. 3. Распределение чисел N=373 кальдер (точки) и крупных воронок N=175 на конусах (треугольники) по величинам их площадей S (км^2), образованных на вулканах планеты.

Figure 3 shows a plot of numbers of calderas versus their areas: $LgN=f(LgS)$, N=373. In Figure 4, numbers of eruptions are shown versus erupted volumes: $LgN=f(LgV)$, N=125. The mid-square method is applied to analyse relationships shown in Figures 3 and 4 and given by equations (17) and (18), respectively (see below); correlation coefficients are 0.9 and 0.7, respectively. Intervals for averaging the initial values of S and V are increased with increasing values of S and V in order to provide a sufficiently uniform spacing of averaged values in the logarithmic scale.

$$LgN=(1.86\pm0.11)-(0.49\pm0.05)LgS,\ [S]=\text{km}^2, \tag{17}$$

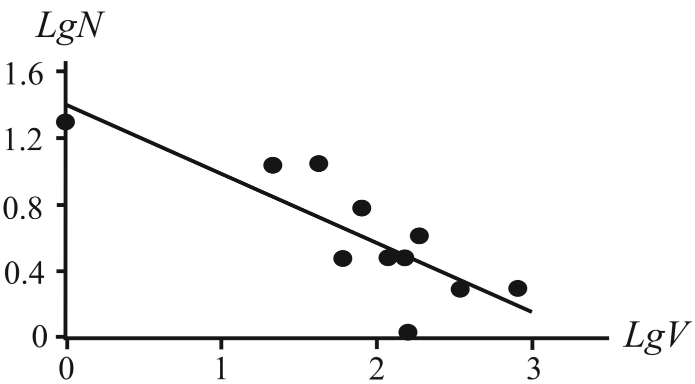

Fig. 4. Numbers of eruptions versus material volumes V (km^3) erupted by volcanoes of the planet (N=125).

Рис. 4. Распределение чисел извержений как функция объемов выброшенного материала V (км^3), N=125, при извержениях вулканов планеты.

$$LgN=(1.41\pm0.19)-(0.42\pm0.09)LgV,\ [V]=\text{km}^3. \tag{18}$$

Parameters of calderas – diameter D, area S, and erupted material volume V – are variable in wide ranges: D=2÷150 km, S=2÷4.648 km^2, V=0.3÷3000 km^3. Nonetheless, it is established that the inclination angles of the plots showing the distribution of areas S (equation 17) and erupted material volumes V (equation 18) are similar, and the statistically significant reliability is high, minimum 0.7. This finding is actually similar to the conclusion that the ratio is constant in a wide range of scales of V and S.

Thus, the available data on the volcanic eruptions in the past 33 Ma support the hypothesis that $\Delta h=const$ (equation 15), i.e. does not depend on parameters of the volcanic process.

Thickness of a magma chamber. Based on the above, it is possible to estimate a magma chamber thickness from parameters of a volcanic eruption. For this purpose, equation (15) is used with data on volcanic eruptions with known values of S and V (N=125). The volumes of volcanic eruptions of the planet are recalculated by the method proposed by I.V. Melekestsev, taking into account the fact that densities of magma at different focal depths and densities of eruption products on the ground surface are different [*Laverov, 2005*]. It is shown that equation (15) is valid [*Vikulin, Akmanova, 2014*]:

$$\Delta h=0.5\pm0.1\ \text{km}. \tag{19}$$

Minimum and maximum values of magma chamber thickness estimated from data on 125 volcanic eruptions (each with known caldera area S and erupted material volume V) range from a few meters to a few kilometres. These values do not contradict with thicknesses of molten granitoid layers formed while the rocks were irreversibly deformed during folding of the crust in the Pamirs [*Magnitskii et al., 1998*].

For a caldera with an average diameter D ranging from 10 to 15 km, a magma chamber which thickness is estimated from (19) is represented by a thin 'pancake-shaped' layer: $D>>\Delta h$.

Noteworthy are the following 'coinciding' features. Firstly, thicknesses of magma chamber Δh are close to heights of caldera sides h, and the minimum and maximum thickness values are generally close ($\Delta h \approx h$), which gives grounds to consider this fact in support of the hypothesis of a thin magmatic chamber with a permanent thickness. Secondly, as shown in Fig. 3, analytical equation (17) cannot be significantly changed by data on large craters on cinder cones (marked by triangles) (N=175, i.e. almost a half of the number of calderas, N=373). As such, distinctions between large craters on cinder cones and calderas are eliminated under the thin magma chamber concept, as shown in equations (15) to (19). In other words, the very concept of a caldera-generating eruption viewed as a 'specific' class of eruptions becomes meaningless.

Equation (19) is based on analyses of different data sets including (1) data on the entire planet and individual regions, specifically the Kuril-Kamchatka arc, Kamchatka, Kuril Islands and individual volcanoes located in the Kuril Islands and Kamchatka; (2) data covering different time periods, specifically data on volcanic eruptions of the Earth during the period of 33 Ma, and recent volcanic eruptions in the Kuril-Kamchatka region; (3) data from regions with different geotectonic settings; and (4) data on different types of volcanoes and different eruptions. Thus, there are grounds to consider that the small thickness of the magma pocket in equation (19) is a constant that *does not depend on the volcanic process* [*Vikulin, Akmanova, 2014*].

10. A MAGMATIC CHAMBER AS THE STATE OF THE CRUST

The model of a 'pancake-shaped' thin magma chamber in the crust. Recent instrumental geophysical studies conducted at volcanoes in the Kuril-Kamchatka region show that their magma chambers are generally located at depths from 5 to 30 km [*Anosov et al., 1990; Balesta, 1981; Fedotov, 1984; Ermakov, Shteinberg, 1999; Fedotov, Masurenkov, 1991*], i.e. within the crust composed of blocks. Therefore, the magma chamber thickness, which is independent of the volcanic process, may depend only on geodynamic movements of the blocks.

The following data can provide prerequisites for a statement of the problem. Heat generation in the crust due to mechanical movements of the crustal blocks was described in general terms by P.N. Kropotkin [*1948*]. Potential melting of the material in fault zones due to dissipative heating during shifting of the crustal blocks was noted in many publications on geodynamic modelling (for instance, p. 308–310 in [*Turcotte, Schubert, 1985*]). The first quantitative model of granitoid melting in the crust as a result of its intensive deformation during folding (a case of the Pamirs) was proposed in [*Magnitskii et al.*, *1998*]. It should be emphasized that under this approach it is not required to refer to the fluid concept in discussion of melting. The potential existence of polingenic magma chambers in the crust was substantiated in [*Ermakov*, *1977*] and confirmed by results of instrumental geophysical observations [*Balesta*, *1981*].

The thin 'pancake-shaped' magma chamber model is based on principles established in the material science of solids with intensive plastic deformation; in case of low heat transfer, the plastic deformation zone can become considerably heated under the impact of such deformations and even destroyed [*Ivanchin*, *1982*].

The main provisions of the model [*Vikulin, Ivanchin*, *2015*] are as follows. Local plastic deformation ε may be high ($\varepsilon \approx 1$) in sliding bands and low outside the bands ($\varepsilon \approx 0$). As the strain rate is exponentially dependent on stress and temperature, the temperature in the area subject to plastic deformation may increase due to heat emission. In case of a small thermal conductivity factor, when heating is not compensated, the temperature in the zone of intensive plastic deformation may continuously grow until transition to the thermal self-acceleration mode, which typically results in partial destruction of the deforming body, and in many cases such destruction results from melting.

A heated band may form under the following physically transparent conditions: on the one hand, deformation should be fast enough not to give time for the generated heat to be removed by thermal conductivity; on the other hand, it should be slow enough to provide a sufficient time for the plastic deformation rate and the specific heat capacity to decrease due to stress relaxation.

With account of the low thermal conductivity of the crust, thermodynamic calculations are obtained for the following conditions: a magma chamber is a solid that is heated to the temperature above its melting point; it is located at the depth of the crystalline basement boundary, H=5–6 km (Kamchatka) and composed of aluminium which thermal properties are similar to those of magma. (All the thermodynamic parameters of aluminium and their dependence on temperature and pressure are known). Based on the thermodynamic calculations, it is shown that when local melting takes place and the magma chamber's volume is increasing, an additional pressure is generated around the magma chamber and the field of elastic stresses occurs; its energy is about 10^{15} joules per 1 km^3 of the overheated rock. Considering the elastic energy accumulated around magma pockets, overheated magma chambers of relatively strong (W>4; V>0.1 km^3) eruptions appear to be similar to sources of the strongest earthquakes (M=8 and above) which lengths range from 100 to 200 km and above. In the block geomedium model, the similarity of the neighbouring magma chambers and seismic sources in terms of energy can be viewed as an explanation of both the interaction between volcanoes (i.e. migration of volcanic activity according to [*Vikulin et al.*, *2010*, *2012a*, *2012b*]) and the interaction between volcanism, seismicity and tectonics [*Vikulin*, *2011*; *Vikulin et al.*, *2013*].

The above general conclusion is supported by data on the three adjacent large cones of the northern eruption of the Tolbachik volcano in Kamchatka, which formed one after another during the eruption in 1975 and 'migrated' along the entire Tolbachik zone of cinder cones [*Fedotov, 1984*]. It is also supported by data on calderas (D=10 km and above) that migrated along the 500-km long Snake River valley in the USA; the calderas were formed during eight strongest eruptions (W≥6–7; V≥10–100 km^3) in the past 16 Ma [*Koronovsky*, *2012*], data on volcanoes that migrated along the central Pacific Ocean for distances from 800 to 1000 km and formed the chain of Hawaii Islands [*Mcdonald*, *1985*], and data on volcanic activity migration at the Earth surface [*Luchitsky*, *1971*].

The Mohorovicic discontinuity (Moho). It is stated in [*Peive*, *1961*] that the "most important conclusion of modern tectonics, which forces us to review our concepts, is that the crust ... is partitioned into blocks not only by a system of steeply dipping and vertical tectonic surfaces but also by gently dipping and horizontal surfaces. ... Deep tangential tectonic zones located in areas of high pressures and temperatures are zones with 'plastic flow' ... and primary magma chambers. ... Mechanical movements of the crustal material are the main source of this energy". According to [*Peive*, *1961*; *Magnitskii et al*., *1998*], mechanisms of plastic flow in thin layers along surfaces of the blocks are quite real and can be applied to other tectonic boundaries in the crust.

Among all the layers within the upper mantle, only the Moho is quite reliably established in all the regions of the Earth. Therefore, the concept of an overheated transition layer, which depth is constant, sounds reasonable with reference to the Moho, in the first instance.

It is not known whether the upper mantle located below the base of the crust is composed of blocks. We can only be certain that the crust has the block structure. Under the p–T conditions at the Moho, it can be expected that the geomedium below the crust may not be composed of blocks. In this case, another reason against the block structure is the assumption that a volume flow [*Leonov*, *2008*] is more typical of the substance below the Moho than a shear flow. Under the concepts of the rotational mechanics of the block geomedium [*Vikulin, 2011; Vikulin et al., 2013*] and the model of 'thermal explosion' and 'thermal self-acceleration' [*Ivanchin, 1982; Vikulin, Akmanova, 2014; Vikulin, Ivanchin, 2015*], it can be assumed that the base of the Earth's crust is represented by a phase surface, below which the geomedium (including the lithosphere and upper mantle) is not composed of blocks, and the shear flow cannot occur in it or may occur but to a lower extent than in the crust [*Vikulin, Ivanc*hin, *2013b*]. Our approach described above is close to the Moho model described in [*Pavlenkova*, *2013*].

Thus, the conclusion, which is fundamental for both volcanology and geodynamics, is that a magma pocket is a thin layer, and its thickness depends on properties of the crust. Our conclusion makes it possible within the framework of the rotation model [*Vikulin*, *2011*; *Vikulin, Ivanchin*, *2013b*; *Vikulin et al*., *2013*] to consistently 'mate' the views on the volcanic process [*Vikulin, Akmanova*, *2014*; *Vikulin, Ivanchin*, *2015*], the block geomedium concept and the idea of the wave geodynamic process.

11. Discussion of results

Our review shows that the regional tectonophysical studies of the Baikal fault zone [*Sherman*, *2014*] have some major shortcomings. In the reviewed regional studies and analyses, the fault structure of the geomedium was mainly referred to, while the block geomedium concept was not actually applied. The migration of earthquake sources was taken into account in the tectonophysical modelling of the regional processes, and an important conclusion was stated: "Deformation/strain waves should be introduced in the scope of the geophysical medium concept and viewed as its dynamic parameter" (p. 283 in [*Sherman*, *2014*]). However, in the cited publication, the strain wave process was considered mainly on the basis of the fault tectonics concept without any reference to the mechanism of stress redistribution in the geomedium's volume.

The present paper describes the rotation concept that can be useful for eliminating the difficulties associated with the need to take into account both the block structure of the geomedium and the wave process taking place in the geomedium. It is shown that the geomedium is a body composed of rotating blocks, and stresses with torque are generated in the geomedium. As a consequence of the momentum conservation law, such stresses predetermine the energy capacity (in terms of [*Ponomarev*, *2008*]) of the geomedium. In our study, the new type of rotation waves is reviewed, and it is shown that slow and fast strain waves (and/or tectonic waves [*Bykov*, *2005*] and/or oscillation **(μ)** waves [*Oparin, Vostrikov*, *2010*] and/or strain waves [*Khachai et al*., *2013*]) can occur in the geomedium composed of rotating blocks as a consequence of the wave-particle duality. The fast and slow strain waves are as typical for the geomedium composed of rotating blocks as longitudinal and transverse seismic waves for the 'normal' solid.

In the geomedium, movements can also take place as rheid and/or super-fluid flow [*Vikulin*, *2013*] and/or super-plastic flow [*Leonov*, *2008*; *Carey*, *1954*] which is most probably associated with the energy capacity of the geomedium and its ability to generate vortex, ring-shaped and other non-linear geological structures [*Vikulin*, *2014b*]. In terms of physics (p. 5–20 in

[*Nikolaev*, *1987*], this state of the geomedium corresponds to its geometric rotational–structural nonlinearity.

In geodynamics and tectonophysics, a fundamental challenge and *experiment crucis*, i.e. crucial/critical experiment [*Vikulin*, *2013, 2014a, 2014b*], is to reveal the relationship between the geomedium's energy capacity, rheidity and vortex motion ability, on the one hand, and it's clear nonlinearity [*Nikolaev*, *1987*], on the other hand.

Considering the geomedium's energy capacity [*Ponomarev*, *2008*] and its state of stresses [*Nikolaev*, *2003*; *Rykunov et al.*, *1979*], which can destroy the geomedium [*Bogdanovich*, *1909*; *Ponomarev*, *2008*], it can be suggested that an earthquake is most likely to occur out of compliance with the Raid theory, i.e. not as a result of local stresses in the future earthquake source in excess of the tensile strength of rocks. Under the rotation concept proposed by the author, an earthquake in the energy-saturated medium (ready for destruction) can result from the long-range interaction between all blocks of the crust through a long/geological time span. Besides, it can occur as a consequence of specific conditions in the future earthquake source and its adjacent blocks which provide for the short-range interaction between the blocks and may be accompanied by the formation of a free surface of a fault and emission of seismic waves.

Magma chambers feeding volcanic eruptions are a reflection of the 'block character' of the volcanic process. Our analysis of the data on almost 800 strong volcanic eruptions, that were followed by the formation of calderas and the transition of large volumes of volcanic material to the ground surface, shows that the magma chamber's thickness is generally small, about 0.5 km, and this value is constant, independent of the volcanic process and predetermined by properties of the crust.

We propose the new magmatic chamber model based on the ideas of 'thermal explosion' and 'thermal self-acceleration'. It can supplement and develop the well-known concepts of potential heat generation in the crust [*Kropotkin*, *1948*; *Ermakov*, *1977*; *Turcotte, Schubert*, *1985*; *Magnitskii et al.*, *1998*]. The model envisages intensive plastic movements along the boundaries of the blocks in conditions of the low thermal conductivity of the geomedium. If the solid material in the magma chamber is heated to the temperature above the melting point, elastic stresses with energy up to 10^{15} joules per 1 km^3 of the overheated rock can be accumulated in the area around the magma chamber. Such stresses are comparable to stresses in the sources of the strongest earthquakes. This can provide an explanation of the interaction between volcanoes (manifested by the migration of volcanic activity along the volcanic arc) and the interaction between the volcanic and seismic processes taking place in the adjacent and parallel belts.

Under the above concepts, the magma chambers are viewed as 'normal' blocks of the crust which have the same rotational properties as the blocks/earthquake sources.

This idea of thin overheated interlayers/volcanic chambers is valid for the entire crust of the Earth. In our hypothesis, it is stated that properties of the Moho are determined by the phase transition from the block structure of the crust to the non-block structure of the upper mantle.

12. Conclusions

Our conclusions [*Vikulin et al.*, *2012b*], that are based on the physical and mathematical models developed by the author and his colleagues, are of fundamental importance for geodynamics. A brief review of the conclusions is given below.

1. In geodynamics, a currently popular idea envisages the mechanism of 'hitching' of blocks and plates with each other and heat 'emission' due to friction at their boundaries. However, it becomes 'useless' under the rotation concept – this mechanism is unlikely to occur. It is suggested by models of 'thermal explosion'/'self-acceleration' and intensive deformation due to geological processes [*Magnitskii et al.*, *1998*] that overheated areas may occur in the crust, and phase transitions (from solids to liquids with free gas separation) may take place in such areas.

2. The concept of the geomedium composed of rotating blocks can facilitate solving the problems of geodynamics without any need to employ the currently popular models of magma ascent from the mantle (possibly, core) depths.

3. The problem of the Earth thermals and 'hot spots' can be considered from other positions. Within such zones, the kinetic energy generated by the rotation of the geomedium blocks and plates is partially converted into elastic stresses with torque (equation 1). It can be released not only by earthquakes, volcanic eruptions and tectonic plate movements, but also by the generation of heat that is redistributed inside the Earth and brought to the ground surface by various mechanism, including rotation waves with specific wave velocity c_0 (equation 8).

13. Acknowledgement

The author is grateful to Sh.A. Mukhamediev who thoroughly analysed the initial paper and thus encouraged the author to review and significantly improve it.

14. References

Anosov G.I., Argentov V.V., Abdurakhmanov A.I. et al., 1990. The deep structure of the Uratman volcano. *Vulkanologiya i Seismologiya* (4), 85–91 (in Russian) [*Аносов Г.И., Аргентов В.В. Абдурахманов А.И. и др*. Глубинное строение вулкана Уратман // *Вулканология и сейсмология*. 1990. № 4. С. 85–91].

Balesta S.T., 1981. The Earth Crust and Magma Pockets in Recent Volcanism Areas. Nauka, Moscow, 135 p. (in Russian) [*Балеста С.Т*. Земная кора и магматические очаги областей современного вулканизма. М.: Наука, 1981. 135 с.].

Bezukhov N.I., 1953. The Theory of Elasticity and Plasticity. State Publishing House of Techn.-Theor. Literature, Moscow, 420 p. (in Russian) [*Безухов Н.И.* Теория упругости и пластичности. М.: Госуд. изд-во техн.-теор. лит-ры, 1953. 420 с.].

Bogdanovich K.I., 1909. Earthquakes in Messina and San Francisco. St. Petersburg, 165 p. (in Russian) [*Богданович К.И.* Землетрясения в Мессине и Сан Франциско. СПб., 1909. 165 с.].

Bykov V.G., 2005. Strain waves in the Earth: Theory field data, and models. *Russian Geology and Geophysics* 46 (11), 1176–1190.

Carey S.W., 1953. The rheid concept in geotectonics. *Journal of the Geological Society of Australia* 1 (1–2), 67–117. http://dx.doi.org/10.1080/14400955308527848.

Chebotareva I.Y., 2011. Methods for passive study of the geological environment using seismic noise. *Acoustical Physics* 57 (6), 857-865. http://dx.doi.org/10.1134/S1063771011060042.

Cosserat E. et F., 1909. Theorie des corps deformables. Hermann, Paris. 226 p.

Davydov A.S., 1976. Physics of Solid Bodies. Nauka, Moscow, 640 p. (in Russian) [*Давыдов А.С.* Физика твердого тела. М.: Наука, 1976. 640 с.].

Davydov A.S., 1982. Solitons in quasi-one-dimensional molecular structures. *Soviet Physics Uspekhi* 25 (12), 898–918. http://dx.doi.org/10.1070/PU1982v025n12ABEH005012.

Ermakov V.A., 1977. Formational Segmentation of Quaternary Igneous Rocks. Nedra, Moscow, 223 p. (in Russian) [*Ермаков В.А*. Формационное расчленение четвертичных вулканических пород. М.: Недра, 1977. 223 с.].

Ermakov V.A., *Shteinberg G.S*., 1999. The Kudryavy volcano and the evolution of the Medvezhaya caldera, Iturup Island, Kuril Islands. *Vulkanologiya i Seismologiya* (3), 19–40 (in Russian) [*Ермаков В.А., Штейнберг Г.С*. Вулкан Кудрявый и эволюция кальдеры Медвежья (о-в Итуруп, Курильские о-ва) // *Вулканология и сейсмология*. 1999. № 3. С. 19–40].

Fedotov S.A. (Ed.), 1984. *The Major Fracture-Type Eruption of Tolbachik Volcano. Kamchatka. 1975–1976*, Nauka, Moscow, 638 p. (in Russian) [Большое трещинное Толбачинское извержение. Камчатка. 1975–1976 / Ред. С.А. Федотов. М.: Наука, 1984. 638 с.].

Fedotov S.A., Masurenkov Yu.P. (Eds.), 1991. Active Volcanoes of Kamchatka. Two volumes. Nauka, Moscow, vol. 1, 320 p.; vol. 2, 415 p. (in Russian) [*Действующие вулканы Камчатки*. В 2-х т. / Ред. С.А. Федотов, Ю.П. Масуренков. М.: Наука, 1991. Т. 1. 320 с. Т. 2. 415 с.].

Feynman R.P., Leighton R.B., Sands M., 1964. The Feynman lectures on physics. Vol. 2. Addison-Wesley Publishing Company, Inc., Massachusetts, Palo Alto, London, 296 p.

Geological Dictionary, 1978. Nedra, Moscow, vol. 2, 456 p. (in Russian) [*Геологический словарь*. М.: Недра, 1978. Т. 2. 456 с.].

Hirth J.P., Lothe J. 1968. Theory of Dislocations. McGraw-Hill, New York, 600 p.

Ionina N.A., Kubeev M.N., 2013. The 100 Major Catastrophes. Veche, Moscow, 432 p. (in Russian) [*Ионина Н.А., Кубеев М.Н*. 100 великих катастроф. М.: Вече, 2013. 432 с.].

Ivanchin A.G., 1982. The Role of Cooperative Effects in the Energy Dissipation During Movements of Dislocations. Candidate of Physics and Mathematics Thesis. Institute of Atmospheric Optics, SB RAS, Tomsk, 131 p. (in Russian) [*Иванчин А.Г.* Роль кооперативных эффектов при движении дислокаций в диссипации энергии: Дис. … канд. физ.-мат. наук. Томск: ИОА СО АН СССР, 1982. 131 с.].

Khachai O.A., Khachai O.Yu., 2012. About the non-linear dynamic modelling of responses of the heterogenic medium to strong explosive impacts. In: Tectonophysics and Top Issues of Earth Sciences. Proceedings of the 3rd Tectonophysical Conference, 8–12 October 2012. IPE RAS, Moscow, vol. 2, p. 415–418 (in Russian) [*Хачай О.А., Хачай О.Ю*. О построении нелинейной динамической модели отклика гетерогенной среды на сильные взрывные воздействия // Тектонофизика и актуальные вопросы наук о Земле: Материалы третьей Тектонофизической конференции. Т. 2. М.: ИФЗ РАН, 2012. С. 415–418].

Khachai O.A., Khachai O.Yu., Klimko V.K. et al., 2013. Kinematic and dynamic characteristics of slow strain waves in the natural massif as a response to blast impacts. In: Geodynamics and the state of stresses of the Earth interior. Proceedings of the 20th All-Russia Scientific Conference. Mining Institute SB RAS, Novosibirsk, p. 38–42 (in Russian) [*Хачай О.А., Хачай О.Ю., Климко В.К. и др*. Кинематические и динамические характеристики медленных деформационных волн в породном массиве как отклик на взрывные воздействия // Геодинамика и напряженное строение недр Земли: Труды XX Всероссийской научной конференции. Новосибирск: ИГД СО РАН, 2013. С. 38–42].

Korobov A.I., Odina N.I., Mekhedov D.M., 2013. Effect of slow dynamics on elastic properties of materials with residual and shear strains. *Acoustical Physics* 59 (4), 387–392. http://dx.doi.org/10.1134/S106377101304009X.

Koronovsky N., 2012. The Yellowstone supervolcano. *Nauka i Zhizn* (*Science and Life*) (5), 110–113 (in Russian) [*Короновский Н.* Йеллоустонский супервулкан // *Наука и жизнь*. 2012. № 5. С. 110–113].

Krasny L.I. (Ed.), 2004. Earth Planet. Encyclopaedia. Tectonic and Geodynamics. VSEGEI, St. Petersburg, 652 p. (in Russian) [*Планета Земля*. Энциклопедический справочник. Том «Тектоника и геодинамика» / Ред. Л.И. Красный. СПб.: ВСЕГЕИ, 2004. 652 с.].

Kropotkin P.N., 1948. Main problems of energy of tectonic processes. *Izvestiya AN SSSR* (5), 89–104 (in Russian) [*Кропоткин П.Н.* Основные проблемы энергетики тектонических процессов // *Известия АН СССР*. 1948. № 5. С. 89–104].

Kuzikov S.I., Mukhamediev S.A., 2010. Structure of the present-day velocity field of the crust in the area of the Central-Asian GPS network. *Izvestiya, Physics of the Solid Earth* 46 (7), 584–601. http://dx.doi.org/10.1134/S1069351310070037.

Landau L.D., Lifshits E.M., 1973. Mechanics. Nauka, Moscow, 208 p. (in Russian) [*Ландау Л.Д., Лифшиц Е.М.* Механика. М.: Наука, 1973. 208 с.].

Landau L.D., Lifshits E.M., 2003. Theory of Elasticity. Nauka, Moscow, 264 p. (in Russian) [*Ландау Л.Д., Лифшиц Е.М.* Теория упругости. М.: Наука, 2003. 264 с.].

Laverov N.P. (Ed.), 2005. Recent Volcanism in the Territory of Russia. Nauka, Moscow, 604 p. (in Russian) [Новейший и современный вулканизм на территории России / Ред. Н.П. Лаверов. М.: Наука, 2005. 604 с.].

Leonov M.G., 2008. Tectonics of Consolidated Crust. Nauka, Moscow, 457 p. (in Russian) [*Леонов М.Г.* Тектоника консолидированной коры. М.: Наука, 2008. 457 с.].

Leonov M.G., Grib E.N., 2004. Structural Positions and Volcanism of Quaternary Calderas of Kamchatka. Dalnauka, Vladivostok, 189 p. (in Russian) [*Леонов В.Л., Гриб Е.Н.* Структурные позиции и вулканизм четвертичных кальдер Камчатки. Владивосток: Дальнаука, 2004. 189 с.].

Luchitsky I.V., 1971. Fundamentals of Paleovolcanology. V. 1. Nauka, Moscow, 480 p. (in Russian) [*Лучицкий И.В.* Основы полеовулканологии. Т. 1. М.: Наука, 1971. 480 с.].

Lunina O.V., Gladkov A.S., Nevedrova N.N., 2009. Rift Basins of Pribaikalie: Tectonic Structure and Development History. GEO, Novosibirsk, 316 p. (in Russian) [*Лунина О.В., Гладков А.С., Неведрова Н.Н.* Рифтовые впадины Прибайкалья: тектоническое строение и история развития. Новосибирск: ГЕО, 2009. 316 с.].

Magnitskii V.A., Mukhamediev S.A., Khasanov R., 1998. The possibility of rock melting in the Earth's crust during intense folding: evidence from the Pamirs. *Doklady Earth Sciences* 363A (9), 1292–1296.

McDonald G., 1975. Volcanoes. Mir, Moscow, 432 p. (in Russian) [*Макдональд Г.* Вулканы. М.: Мир, 1975. 432 с.].

Mulev S.N., Bondarev A.V., Panin S.F., 2013. The experience of the implementation of seismic monitoring systems in mines in Russia. In: Geodynamics and the state of stresses of the Earth interior. Proceedings of the 20th All-Russia Conference with participation of researchers from other countries (7–11 October 2013, Novosibirsk). Mining Institute SB RAS, Novosibirsk, p. 416–421 (in Russian) [*Мулев С.Н., Бондарев А.В., Панин С.Ф.* Опыт внедрения систем сейсмического мониторинга на шахтах и рудниках России // Геодинамика и напряженное состояние недр Земли: Труды XX Всероссийской конференции с участием иностранных ученых, Новосибирск, 7–11 октября 2013. Новосибирск: ИГД СО РАН, 2013. С. 416–421].

Nalivkin D.V., 1969. Hurricanes, Storms and Tornadoes. Nauka, Leningrad, 487 p. (in Russian) [*Наливкин Д.В.* Ураганы, бури и смерчи. Л.: Наука, 1969. 487 с.].

New Global Tectonics (*Plate Tectonics*)*,* 1974. Mir, Moscow. 472 p. (in Russian) [Новая глобальная тектоника (тектоника плит). М.: Мир, 1974. 472 с.].

Nikolaev A.V. (Ed.), 1987. Problems of Non-Linear Seismics. Nauka, Moscow, 228 p. (in Russian) [Проблемы нелинейной сейсмики / Ред. А.В. Николаев. М.: Наука, 1987. 228 с.].

Nikolaev A.V. (Ed.), 2003. Problems of Geophysics in the 21st Century. Two volumes. Nauka, Moscow, (in Russian) [Проблемы геофизики XXI века / Ред. А.В. Николаев. В 2-х кн. М.: Наука, 2003].

Nikolaevsky V.N., 1996. Geodynamics and Fluid Dynamics. Nedra, Moscow, 447 p. (in Russian) [*Николаевский В.Н.* Геодинамика и флюидодинамика. М.: Недра, 1996. 447 с.].

Oparin V.N., Annin B.D., Chugui Yu.V. et al., 2007. Methods and Measurement Equipment for Modelling and Field Studies of Non-Linear Strain and Wave Processes in Rock Blocks. SB RAS Publishing House, Novosibirsk, 320 p. (in Russian) [*Опарин В.Н., Аннин Б.Д., Чугуй Ю.В. и др.* Методы и измерительные приборы для моделирования и натурных исследований нелинейных деформационно-волновых процессов в блочных массивах горных пород. Новосибирск: Изд-во СО РАН, 2007. 320 с.].

Oparin V.N., Simonov B.F., Yushkin V.F. et al., 2010. Geomechanical and Technical Bases for Enhancement of Oil Recovery from Formations with Application of Vibration Wave Technology. Nauka, Novosibirsk, 404 p. (in Russian) [*Опарин В.Н., Симонов Б.Ф., Юшкин В.Ф. и др*. Геомеханические и технические основы увеличения нефтеотдачи пластов в виброволновых технологиях. Новосибирск: Наука, 2010. 404 с.].

Oparin V.N., Vostrikov V.I., 2010. The energy criterion of the volume destruction of focal zones, and oscillation waves. In: Methods and Systems for Monitoring of Seismic Deformation Caused by Technogenic Earthquakes and Rock Shocks. V. 2: Integration Projects of SB RAS. Issue 25. SB RAS Publishing House, Novosibirsk, p. 93–128 (in Russian) [*Опарин В.Н., Востриков В.И*. Энергетический критерий объемного разрушения очаговых зон и волны маятникового типа // Методы и системы сейсмодеформационного мониторинга техногенных землетрясений и горных ударов. Т. 2. Интеграционные проекты СО РАН. Вып. 25. Новосибирск: Изд-во СО РАН, 2010. С. 93–128].

Pamyatnykh E.A., Ursulov A.V., 2012. Nonlinear solitary waves in nonlocal elastic solids. *Acoustical Physics* 58 (2), 160–165. http://dx.doi.org/10.1134/S1063771012010162.

Pavlenkova N.I., 2013. The origin of the Moho according to geophysical data. In: Proceedings of the XLV Tectonic Meeting. GEOS, Moscow, p. 138–141 (in Russian) [*Павленкова Н.И*. Природа границы М по геофизическим данным // Материалы XLV Тектонического совещания. М.: ГЕОС, 2013. С. 138–141].

Peive A.V., 1961. Tectonics and magmatism. *Izvestia AN SSSR*. *Geological Series* (3), 36–54 (in Russian) [*Пейве А.В*. Тектоника и магматизм // *Известия АН СССР*. *Серия геологическая*. 1961. № 3. С. 36–54].

Ponomarev V.S., 2008. Energy Capacity of the Geological Medium. Nauka, Moscow, 379 p. (in Russian) [*Пономарев В.С*. Энергонасыщенность геологической среды. М.: Наука, 2008. 379 с.].

Prozorov A.G., 1978. On a lower probability of strong shocks in the space-and-time vicinity of strong global earthquakes. In: Issues of earthquake forecasting and the Earth structure. Computational Seismology. Issue 11. Nauka, Moscow, p. 35–41 (in Russian) [*Прозоров А.Г*. О пониженной вероятности сильных толчков в некоторой пространственно–временной окрестности сильных землетрясений мира // Вопросы прогноза землетрясений и строение Земли. Вычислительная сейсмология. Вып. 11. М.: Наука, 1978. С. 35–41].

Riznichenko Yu.V., 1985. Problems of Seismology. Selected Works. Nauka, Moscow. 408 p. (in Russian) [*Ризниченко Ю.В*. Проблемы сейсмологии. Избранные труды. М.: Наука, 1985. 408 с.].

Rudenko O.V., Sobisevich A.L., Sobisevich L.E., Hedberg C.M., Shamaev N.V., 2012. Nonlinear model of a granulated medium containing viscous fluid layers and gas cavities. *Acoustical Physics* 58 (1), 99–106. http://dx.doi.org/10.1134/S1063771012010198.

Rykunov L.N., Khavroshkin O.B., Tsiplakov V.V., 1979. Temporary variations of high-frequency seismic noise. *Izvestiya AN SSSR, Fizika Zemli* (11), 72–77 (in Russian) [*Рыкунов Л.Н., Хаврошкин О.Б., Циплаков В.В*. Временные вариации высокочастотных сейсмических шумов // *Известия АН СССР*. *Физика Земли*. 1979. № 11. С. 72–77].

Sadovsky M.A., 2004. Selected Works. Geophysics and Blast Physics. Nauka, Moscow, 440 p. (in Russian) [*Садовский М.А.* Избранные труды: Геофизика и физика взрыва. М.: Наука, 2004. 440 с.].

Sedov L.I., 1973. Solid Medium Mechanics. V. 1. Nauka, Moscow. 536 p. (in Russian) [*Седов Л.И.* Механика сплошной среды. Т. 1. М.: Наука, 1973. 536 с.].

Sherman S.I., 2009. A tectonophysical model of a seismic zone: experience of development based on the example of the Baikal rift system. *Izvestiya, Physics of the Solid Earth* 45 (11), 938–941. http://dx.doi.org/10.1134/S1069351309110020.

Sherman S.I., 2013. Deformation waves as a trigger mechanism of seismic activity in seismic zones of the continental lithosphere. *Geodynamics & Tectonophysics* 4 (2), 83–117 (in Russian) [*Шерман С.И*. Деформационные волны как триггерный механизм сейсмической активности в сейсмических зонах континентальной литосферы // *Геодинамика и тектонофизика*. 2013. Т. 4. № 2. С. 83–117]. http://dx.doi.org/10.5800/GT-2013-4-2-0093.

Sherman S.I., 2014. Seismic Process and the Forecast of Earthquakes: Tectonophysical Conception. Academic Publishing House “Geo”, Novosibirsk, 359 p. (in Russian) [*Шерман С.И.* Сейсмический процесс и прогноз землетрясений: тектонофизическая концепция. Новосибирск: Академическое издательство «Гео», 2014. 359 с.].

Sherman S.I., Cheremnykh A.V., Bornyakov S.A., Shishkina L.P., 2001. Modeling of large faults in zones of lithospheric extension and numerical constraints on deformation. *Geologiya i Geofizika* (*Russian geology and geophysics*) 42 (7), 1052–1057.

Sherman S.I., Gorbunova E.A., 2008. Wave origin of fault activation in Central Asia on the basis of seismic monitoring. *Fizicheskaya Mezomekhanika* 11 (1), 115–122 (in Russian) [*Шерман С.И., Горбунова Е.А*. Волновая природа активизации разломов Центральной Азии на базе сейсмического мониторинга // *Физическая мезомеханика*. 2008. Т 11. № 1. С. 115–122].

Sherman S.I., Seminsky K.Zh., Bornyakov S.A., Buddo V.Yu., Lobatskaya R.M., Adamovich A.N., Truskov V.A., Babichev A.A., 1992. Faulting in the Lithosphere. Tensile Stress Zones. Nauka, Siberian Branch, Novosibirsk, 227 p. (in Russian) [*Шерман С.И., Семинский К.Ж., Борняков С.А., Буддо В.Ю., Лобацкая Р.М., Адамович А.Н., Трусков В.А., Бабичев А.А.* Разломообразование в литосфере. Зоны растяжения. Новосибирск: Наука. Сибирское отделение, 1992. 227 с.].

Sherman S.I., Seminsky K.Zh., Bornyakov S.A., Buddo V.Yu., Lobatskaya R.M., Adamovich A.N., Truskov V.A., Babichev A.A., 1994. Faulting in the Lithosphere. Compression Zones. Nauka, Siberian Branch, Novosibirsk, 262 p. (in Russian)

[*Шерман С.И., Семинский К.Ж., Борняков С.А., Буддо В.Ю., Лобацкая Р.М., Адамович А.Н., Трусков В.А., Бабичев А.А*. Разломообразование в литосфере. Зоны сжатия. Новосибирск: Наука. Сибирское отделение, 1994. 262 с.].

Sherman S.I., Sorokin A.P., Sorokina A.T., Gorbunova E.A., Bormotov V.A., 2011. New data on the active faults and zones of modern lithosphere destruction in the Amur region. *Doklady Earth Sciences* 439 (2), 1146–1151. http://dx.doi.org/10.1134/S1028334X11080186.

Siebert L., *Simkin T., Kimberly P*., 2010. Volcanoes of the World. Third edition. Smithsonian Institution. Washington DC, University of California Press, 551 p.

Turcotte D., Schubert G., 1985. Geodynamics: Applications of Continuum Physics to Geological Problems. Part 1. Mir, Moscow, 376 p. (in Russian) [*Теркот Д., Шуберт Дж*. Геодинамика: Геологические приложения физики сплошных сред. Ч. 1. М.: Мир, 1985. 376 с.].

Tveritinova T.Yu., Vikulin A.V., 2014. The geomedium block concept and the problem of block boundaries. In: Faulting in the lithosphere and related processes: tectonophysical analysis. Abstracts of the All-Russia Conference with visiting researchers from other countries (11–16 August 2014, Irkutsk). IEC SB RAS, Irkutsk. P. 35–36 (in Russian) [*Тверитинова Т.Ю., Викулин А.В*. Концепция блоковой геосреды и проблема границ блоков // Разломообразование в литосфере и сопутствующие процессы: тектонофизический анализ: Тезисы докладов Всероссийского совещания с участием приглашенных исследователей из других стран. Иркутск, 11–16 августа, 2014. Иркутск: ИЗК СО РАН, 2014. С. 35–36].

Vikulin A.V., 2008. Vortex Motion World. KSTU, Petropavlovsk-Kamchatsky, 230 p. (in Russian) [*Викулин А.В*. Мир вихревых движений. Петропавловск-Камчатский: КГТУ, 2008. 230 с.].

Vikulin A.V., 2009. Physics of the Earth and Geodynamics. Textbook. Kamchatka State University, Petropavlovsk-Kamchatsky, 463 p. (in Russian) [*Викулин А.В*. Физика Земли и геодинамика: Учебное пособие. Петропавловск–Камчатский: КамГУ, 2009. 463 с.].

Vikulin A.V., 2010. New type of elastic rotational waves in geo-medium and vortex geodynamics. *Geodynamics & Tectonophysics* 1 (2), 119–141 (in Russian) [*Викулин А.В*. Новый тип упругих ротационных волн в геосреде и вихревая геодинамика // *Геодинамика и тектонофизика*. 2010. Т. 1. № 2. С. 119–141]. http://dx.doi.org/10.5800/GT-2010-1-2-0010.

Vikulin A.V., 2011. Seismicity. Volcanism. Geodynamics. Collection of Works. Kamchatka State University, Petropavlovsk-Kamchatsky, 407 p. (in Russian) [*Викулин А.В*. Сейсмичность. Вулканизм. Геодинамика: Сборник трудов. Петропавловск-Камчатский: КамГУ, 2011. 407 с.].

Vikulin A.V., 2013. Non-linearity–fractality or rheidity–power capacity: what categories are closer to geology? (Review of the article by N.V. Koronovsky and A.A. Naimark "Methods of dynamical geology at the threshold of applicability"). Vestnik KRAUNC (Kamchatka Regional Association Education–Science Centre). Earth Sciences (1), 152–157 (in Russian) [*Викулин А.В*. Нелинейность–фрактальность или реидность–энергонасыщенность: какие категории ближе геологии? (Отзыв на статью Н.В. Короновского, А.А. Наймарка «Методы динамической геологии на критическом рубеже применимости») // *Вестник КРАУНЦ. Науки о Земле*. 2013. № 1 (21). С. 152–157].

Vikulin A.V., 2014a. The Earth Acoustics. In: The system of Earth Planet. The 20th anniversary of the system of Earth Planet workshop. LENARD, Moscow, p. 202–242 (in Russian) [*Викулин А.В.* Акустика Земли // Система «Планета Земля»: XX лет семинару «Система “Планета Земля”». М.: ЛЕНАРД, 2014. С. 202–242].

Vikulin A.V., 2014b. The problem of vortex motions in geology (Review of the article by E.G. Mirlin and Yu.V. Mironov "The role of vortex motions in geodynamics of the Aegean sea (based on comparative analysis with the geodynamics of the Woodlark basin)". *Vestnik KRAUNC* (*Kamchatka Regional Association Education–Science Centre*). *Earth Sciences* (2), 186–190 (in Russian) [*Викулин А.В*. Проблема вихревых движений в геологии (Отзыв на статью Е.Г. Мирлина, Ю.В. Миронова «Роль вихревого движения в геодинамике Эгейского моря (на основе сравнительного анализа с геодинамикой котловины Вудларк)») // *Вестник КРАУНЦ. Науки о Земле*. 2014. № 2 (24). С. 186–190].

Vikulin A.V., Akmanova D.R., 2014. A magma focus as a property of the crust. *Vestnik KRAUNC* (*Kamchatka Regional Association Education–Science Centre*). *Earth Sciences* (1), 213–230 (in Russian) [*Викулин А.В., Акманова Д.Р.* Магматический очаг как свойство земной коры // *Вестник КРАУНЦ. Науки о Земле*. 2014. № 1 (23). С. 213–230].

Vikulin A.V., Akmanova D.R., Osipova N.A., 2010. Volcanism as an indicator of geodynamic processes. *Litosfera* (3), 5–11 (in Russian) [*Викулин А.В., Акманова Д.Р., Осипова Н.А*. Вулканизм как индикатор геодинамических процессов // *Литосфера*. 2010. № 3. С. 5–11].

Vikulin A.V., Akmanova D.P., Vikulina S.A., Dolgaya A.A., 2012a. Migration of seismic and volcanic activity as display of wave geodynamic process. *Geodynamics and Tectonophysics* 3 (1), 1–18. http://dx.doi.org/10.5800/GT-2012-3-1-0058.

Vikulin A.V., Ivanchin A.G., 2013a. Modern concept of block hierarchy in the structure of geomedium and its implications in geosciences. *Journal of Mining Science* 49 (3), 395–408. http://dx.doi.org/10.1134/S1062739149030076.

Vikulin A.V., Ivanchin A.G., 2013b. On the Moho origin as a phase boundary between the crust composed of blocks and the non-block upper mantle. In: Proceedings of the XLV Tectonic meeting. GEOS, Moscow, p. 38–42 (in Russian)

[*Викулин А.В., Ивнчин А.Г.* О природе Мохо как фазовой границе раздела между блоковой земной корой и неблоковой верхней мантией // Материалы XLV Тектонического совещания. М.: ГЕОС, 2013. С. 38–42].

Vikulin A.V., Ivanchin A.G., 2015. A new insight to the origin of a magma pocket. In: The system of Earth Planet. The 200th anniversary of the Holy Alliance (1815–2015). LENARD, Moscow, p. 293–321 (in Russian) [*Викулин А.В., Иванчин А.Г.* Новый взгляд на природу магматического очага // Система «Планета Земля»: 200 лет Священному союзу (1815–2015). М.: ЛЕНАРД, 2015. С. 293–321].

Vikulin A.V., Melekestsev I.V., Akmanova D.R., Ivanchin A.G., Vodinchar G.M., Dolgaya A.A., Gusyakov V.K., 2012b. The IT system for modelling of seismic and volcanic processes as a basis for studies of wave geodynamic phenomena. *Computational Technologies* 17 (3), 34–54 (in Russian) [*Викулин А.В., Мелекесцев И.В., Акманова Д.Р. и др*. Информационно-вычислительная система моделирования сейсмического и вулканического процессов как основа изучения волновых геодинамических явлений // *Вычислительные технологии*. 2012. Т. 17. № 3. С. 34–54].

Vikulin A.V., Tveritinova T.Yu., Ivanchin A.G., 2013. Wave moment geodynamics. *Acta Geophysica* 61 (2), 245–263. http://dx.doi.org/10.2478/s11600-012-0079-8.

Vlodavets V.I., 1984. Volcanology Guidebook. Nauka, Moscow, 340 p. (in Russian) [*Влодавец В.И*. Справочник по вулканологии. М.: Наука, 1984. 340 с.].

Zharkov V.N., 1983. The Interior Structure of the Earth and Other Planets. Nauka, Moscow, 416 p. (in Russian) [*Жарков В.Н*. Внутреннее строение Земли и планет. М.: Наука, 1983. 416 с.].

Ziman J.M., 1974. Principles of the Theory of Solids. Mir, Moscow, 472 p. (in Russian) [*Займан Дж.* Принципы твердого тела. М.: Мир, 1974. 472 с.].

Vikulin, Alexander V., Doctor of Physics and Mathematics, Lead Researcher
Institute of Volcanology and Seismology, Far East Branch of the Russian Academy of Sciences
9 Boulevard Piip, Petropavlovsk-Kamchatsky 683006, Russia
✉ e-mail: vik@kscnet.ru

Викулин Александр Васильевич, д.ф.-м.н, в.н.с.
Институт вулканологии и сейсмологии ДВО РАН
683006, Петропавловск-Камчатский, б-р Пийпа, 9, Россия
✉ e-mail: vik@kscnet.ru

GEODYNAMICS & TECTONOPHYSICS

PUBLISHED BY THE INSTITUTE OF THE EARTH'S CRUST
SIBERIAN BRANCH OF RUSSIAN ACADEMY OF SCIENCES

2015 VOLUME 6 ISSUE 3 PAGES 365–386 ISSN 2078-502X

http://dx.doi.org/10.5800/GT-2015-6-3-0186

Recent Geodynamics

AN OVERVIEW OF THE TECHNIQUE FOR SEISMICITY MICROZONATION MAPPING OF THE ULAN-UDE CITY TERRITORY

V. I. Dzhurik[1], Ts. A. Tubanov[2], S. P. Serebrennikov[1], A. F. Drennov[1], E. V. Bryzhak[1], A. Yu. Eskin[1]

[1] *Institute of the Earth's crust, Siberian Branch of RAS, Irkutsk, Russia*
[2] *Geological Institute, Siberian Branch of RAS, Ulan-Ude, Russia*

Abstract: For purposes of seismicity microzonation of the Ulan-Ude city territory, engineering geophysical studies are conducted to reveal which types of rocks and soils are dominant in the study area and to classify them by site-specific velocities of P- and S-waves and amplitude-frequency characteristics. The article describes a technique for establishing the baseline seismic signal corresponding to parameters of relatively strong earthquakes in potential earthquake foci (PEF) zones. It is shown that the established baseline signal is applicable. Presented are results of theoretical calculations based on seismicity-soil models providing reference parameters of bedrock, medium and water-saturated soils (soil categories 1, 2 and 3, respectively).

Seismic impacts are assessed for the zone with the baseline seismic intensity of 8 points, as per MSK-64 seismic intensity scale. The reference model is used to identify zones with seismic intensity from 7 to 9 points in the city territory, and it is established that such zones differ in thickness of water-saturated and non-water-saturated soil layers. As a result, a schematic map showing the main parameters of seismic impacts is constructed in the first approximation. The obtained data are useful for the development of recommendations concerning further engineering seismological studies and activities for the appropriate revision and upgrading of the seismic microzonation technique in order to complete seismic microzonation of the Ulan-Ude city territory.

Key words*:* Ulan-Ude, seismicity, seismic microzonation map, engineering seismological surveys, seismic waves velocity, accelerogram, spectra, frequency characteristics, maximum acceleration.

Recommended by V.S. Imaev

For citation: *Dzhurik V.I., Tubanov Ts.A., Serebrennikov S.P., Drennov A.F., Bryzhak E.V., Eskin A.Yu.* 2015. An overview of the technique for seismicity microzonation mapping of the Ulan-Ude city territory. *Geodynamics & Tectonophysics* 6 (3), 365–386. doi:10.5800/GT-2015-6-3-0186.

К ТЕХНОЛОГИИ ПОСТРОЕНИЯ КАРТЫ СЕЙСМИЧЕСКОГО МИКРОРАЙОНИРОВАНИЯ ТЕРРИТОРИИ Г. УЛАН-УДЭ

В. И. Джурик[1], Ц. А. Тубанов[2], С. П. Серебренников[1], А. Ф. Дреннов[1], Е. В. Брыжак[1], А. Ю. Ескин[1]

[1] *Институт земной коры СО РАН, Иркутск, Россия*
[2] *Геологический институт СО РАН, Улан-Удэ, Россия*

Аннотация: Город Улан-Удэ расположен в сейсмически активном районе и характеризуется сейсмической интенсивностью 8, 8 и 9 баллов для средних грунтовых условий [*The Map..., 1999*] и трех уровней сейсмической опасности – 10 % (A), 5 % (B) и 1 % (C). По результатам анализа макросейсмических данных отмечается, что максимальный сейсмический эффект от сильных землетрясений за исторический период для г. Улан-Удэ не превышает 7 баллов. Он вызван двумя событиями, произошедшими в Южном и Центральном Байкале: Цаганским (12.01.1862 г; M=7.5) и Среднебайкальским (29.08.1959 г; M=6.8) землетрясениями.

Для уточнения исходной сейсмичности территории г. Улан-Удэ за счет грунтовых условий проведены инженерно-геофизические работы, необходимые для характеристики преобладающих типов грунтов по скоростям распространения в них продольных и поперечных волн и по амплитудно-частотным характеристикам. При расчетах за эталон выбран скальный грунт с Vp=2200 м/с, Vs=1200 м/с и ρ=2.5 г/см^3 (средние значения скоростей в 10-метровом слое на участках выхода коренных пород на поверхность). Сейсмическая опасность участков с такими значениями скоростей оценивается на один балл меньше исходной. В этом случае средние грунты (неводонасыщенная толща песчаных и гравийно-галечных грунтов) будут иметь значения Vp=600 м/с, Vs=300 м/с и ρ=1.8 г/см^3. Сейсмическая опасность участков с такими значениями соответствует исходной сейсмичности.

Таким образом, проведенные измерения скоростей сейсмических волн на территории города и расчет приращений балльности (табл. 2) показывают, что относительно выбранного эталона (скальный грунт – 7 баллов) грунты, служащие основаниями сооружений города Улан-Удэ, будут иметь приращение балльности от +0.17 до +2.3 балла, а их сейсмическая опасность изменится от 7.17 до 9.3 балла.

Представлена методика формирования исходного сейсмического сигнала, отвечающего параметрам относительно сильных землетрясений из зон ВОЗ (вероятных очагов землетрясений). Отмечается, что выбранные акселерограммы относились к землетрясениям с различными магнитудами, поэтому была использована зависимость $\beta_M(f)$. Она показывает изменения уровня спектра ускорения с изменением магнитуды и зависит от частоты.

Используя эту зависимость, мы приводили амплитудные спектры к магнитуде рассматриваемой зоны ВОЗ. Завершающим шагом стало получение записей акселерограмм землетрясений из конкретных зон ВОЗ заданных магнитуд, являющихся характерными для каждой конкретной зоны (рис. 5). Это реализовано путем обратного преобразования Фурье среднего спектра ускорения данной зоны и фазового спектра наиболее сильного землетрясения, зарегистрированного из данной зоны ВОЗ.

В результате показана возможность использования полученного сигнала и проведены теоретические расчеты для сейсмогрунтовых моделей, характеризующих вероятностные параметры эталона для коренных пород (грунтов 1-й категории), средних грунтов (2-й категории) и водонасыщенных грунтов (3-й категории).

По результатам теоретических расчетов (раздел 2), данным экспериментальных измерений (раздел 1), имеющимся инженерно-геологическим и гидрогеологическим сведениям составлена в первом приближении схематическая карта (рис. 10) основных параметров сейсмических воздействий. На территории города выделены 7–9-балльные участки, характеризующиеся различной по мощности грунтовой толщей водонасыщенных и неводонасыщенных отложений. В каждой из зон по сейсмической опасности (рис. 10) при СМР могут быть выделены участки от 7 до 9 баллов. В этом случае они будут отвечать той или иной грунтовой модели (табл. 5) и требуют дальнейшего уточнения в соответствии с масштабом СМР территории города путем детализации расчетных моделей по предлагаемой нами методике.

Результаты исследований предполагается использовать для разработки рекомендаций по направлению, видам и очередности проведения дальнейших инженерно-сейсмологических исследований и для обновления технологии построения карты сейсмического микрорайонирования территории г. Улан-Удэ.

Таким образом, показано, что для конечного варианта карты СМР следует выявить и охарактеризовать на новом вероятностном уровне потенциальные сейсмические источники (локализацию деформаций и активных разломов, период повторяемости землетрясений, уровень сейсмичности, а также вероятность возникновения землетрясений), которые связаны с прогнозированием сильных сейсмических воздействий для г. Улан-Удэ. Необходимо определить параметры распространения сейсмических волн и их эффекты, обусловленные проявлением сейсмичности, на конкретных строительных площадках города. Затем необходим расчет спектров реакции и связанной с ними вероятности возникновения сильных землетрясений для составления карты сейсмического риска с указанием параметров, которые могут оказаться полезными в строительной политике региона.

Ключевые слова: Улан-Удэ, сейсмичность, карта сейсмического микрорайонирования, инженерно-сейсмологические исследования, скорости сейсмических волн, акселерограммы, спектры, частотные характеристики, максимальные ускорения.

1. Introduction

The city of Ulan-Ude is located in the seismically active region of Russia. According to [*The Map...*, *1999*], the city's territory with medium soil conditions is characterized by seismic intensity of 8, 8 and 9 points (as per MSK-64 seismic intensity scale) and three levels of seismic hazard with 10 % (A), 5 % (B), and 1 % (C) probabilities of exceedance in 50 years. Analyses of historical macroseismic data [*Solonenko, Treskov*, *1960*] show that the maximum seismic impact of the strongest earthquakes in Ulan-Ude did not exceed 7 points even with account of two major events which took place in the Southern and Central Baikal regions – the Tsagan (12 January 1862; M=7.5) and Middle Baikal earthquakes (29 August 1959; M=6.8).

Under the code of practice in the construction industry in the Russian Federation, the baseline seismic intensity was assessed according to the RF construction standards and rules specified in SNiP II-A.12-69* dated 01 July 1970, and for the Ulan-Ude territory with medium geological conditions, it was estimated at 7 points. Later on, SNiP II-A.12-69* was replaced by SNiP II-7-81 (in force since 01 January 1982), and the baseline seismic intensity for Ulan-Ude is now estimated at 8 points [*The USSR Seismic Zonation Map*, *1984*] which assumes the recurrence of a major seismic event every 1000 years, according to Map (B) under SNiP II-7-81* (updated revision) [*SNiP..., 2011*].

It is envisaged by the current construction regulations and standards that optimal locations must be selected for construction projects with account of seismic resistance calculations, which necessitates quantification of the main parameters of seismic impacts that may be imposed to foundations of building and facilities. In this regard, a seismicity microzonation (SMZ) map needs to be constructed for the Ulan-Ude city territory in scales 1:25000 and 1:5000 with account of new assumptions. The required mapping should be preceded by stages when a general seismic zonation map and a detailed seismic zonation map of the territory are constructed in larger scales.

Therefore, to achieve the objective of seismic microzonation mapping of the Ulan-Ude city, it is required to update the general seismicity zonation data and assess levels of seismic hazard for new construction project areas in the city. These tasks can be fulfilled by combining geotechnical, instrumentation and computational methods. For the purpose of seismicity microzonation, seismic intensity is estimated in points as per SNIP II-7-81* or determined as seismic loads shown by estimated or real accelerograms, i.e. curves showing how vibrations of soil layers are accelerated during strong earthquakes. To assess potential seismic hazard, it is needed to take into account the intensity and other parameters of elastic vibrations under the base structure of buildings and facilities and consider the manifestations of inelastic strain and residual deformation of soil layers. Ranges of elastic vibrations of the soil layers are recordable by direct instrumental observations conducted in the study area.

Comprehensive studies can provide source data for dividing the study area into zones which seismic intensity may differ by ±1–2 points, and forecasts for each zone can be adjusted with regard to site-specific tectonic, geological and geomorphological conditions. Calculations of incremental points against the baseline seismic intensity are significantly influenced by data on groundwater levels and lithological compositions of rocks and soils. Such calculations are also impacted by significant variations in the intensity of the seismic field due to heterogeneities in the bedrock to a depth comparable to the wavelength (up to 1 km). Should any sudden change take place in geological conditions while new construction activities are performed, the relevant seismic microzonation data should be revised and updated accordingly.

In this article, we present results of the initial stage of engineering seismological studies in the Ulan-Ude city territory and consider possibilities of zonation by the main parameters of seismic impacts of potential strong earthquakes in order to identify potential seismic hazard areas in compliance with the current regulatory requirements concerning urban construction. A technique for construction of a new seismicity microzonation map of the Ulan-Ude city territory is justified.

2. Results of engineering seismological studies with application of indirect seismicity microzonation methods

Generally, seismic hazard assessment is based on results of the acoustic (seismic) impedance method, data from catalogues of recorded earthquakes and microseisms, and data obtained by computational methods. Herein we briefly describe our technique of measurements, present estimations of seismic parameters and describe the rocks and soils that dominate in the study area.

The seismic impedance method [*Guidelines..., 1985, 1986; Medvedev, 1962; RSN 60-86, 1986; Pavlov, 1984*]. Incremental points are calculated from the equation published in [*Medvedev, 1962*]:

$$\Delta I=1.67Lg(\rho_э V_э/\rho_i V_i)+Re^{-0.04h*h}, \quad (1)$$

where ΔI is estimated value of incremental points; $\rho_э V_э$ and $\rho_i V_i$ is seismic impedance of the reference soil and the studied soil for P-/S-waves, Vp/Vs; h is groundwater level; coefficient R=1 is accepted for areas with dominant sandy and clayey soils, and R=0.5 for areas with dominant gravel-pebble and coarsely clastic rocks. If the groundwater level is at a depth below 10m from the ground surface, the correction coefficient is close to zero.

In order to calculate the seismic hazard in points and then to estimate it in terms of maximum acceleration, the following data are needed: rock and soil composition, velocity of seismic wave propagation in rocks and soils, thickness and composition of unconsolidated soil layers, and bulk weight of the reference rocks and soils and the studied rocks and soils [*Guidelines..., 2004; Pavlov..., 1988*].

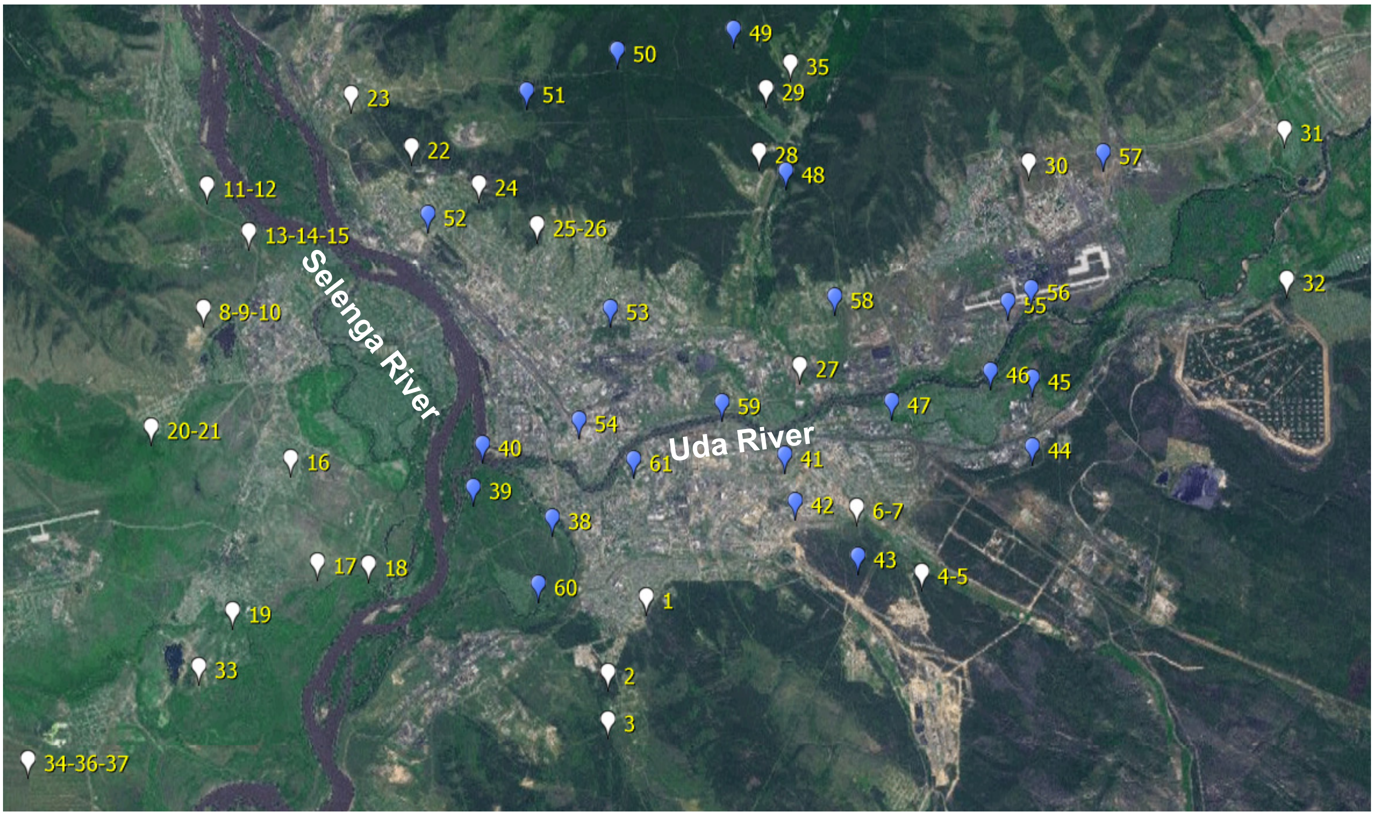

Fig. 1. The schematic map showing areas covered by seismic sounding studies in the Ulan-Ude city territory. 1–37 – locations where observations are conducted for seismic hazard assessment (UoM – point); 38–60 – locations where seismic wave velocities are measured for construction of seismicity-soil models.

Рис. 1. Схема сейсморазведочных зондирований на территории г. Улан-Удэ. 1–37 – пункты наблюдений для оценки сейсмической опасности в баллах; 38–60 – пункты измерения скоростей сейсмических волн для построения сейсмо-грунтовых моделей.

Therefore, the top section of the profile of rocks and soils to the bedrock needs to be characterised to correctly select locations of measurements and then to properly analyse the measurement results. A general description of the top section is presented herein at a level sufficient to support the first stage of our studies aimed at seismic microzonation mapping of the Ulan-Ude city territory.

In the regional Quaternary deposits, facies are diverse, and compositions of rocks and soils are variable. On the left-bank floodplain terrace of the Selenga River (Fig. 1), powdery fine-grained alluvial sands are alternating with small lenses of sandy loam and clay. The sand beds are 1.0 to 5.0 m thick and underlain by gravel. Groundwater occurs at depths ranging from 1 to 3 m. The left bank of the Uda River is composed of eolian fine-grained sand, and the sand beds vary in thickness from 10 to 15 m along the river and 50 to 80 m closer to the slope. Groundwater occurs at depths of 5–10 m and 50–60 m. Bedrocks are represented by the Jurassic-Cretaceous sandstone, argillite and granitic rocks.

The right bank of the Selenga River comprises a thick bed of conglomerates with sandstone interlayers that are overlain by either gravelly soil or fine-grained sands (1.5–3.0 m and 10–15 m thick beds, respectively). The groundwater table is deep-seated.

In terms of geomorphology, the terrain of the Ulan-Ude area is significantly rough. In the north, spurs of the Ulan Burgasy ridge are low, and hills are cut by ravines and gullies and located almost perpendicular to the valleys of the Uda and Selenga Rivers. In the south, spurs of the Tsagan-Daban ridge come to the Uda River valley.

Several terraces are recognized in the valleys of the Uda and Selenga Rivers: Terrace 1 is 2 to 4 m high (Ulan-Ude downtown), Terrace 2 is 10 to 20 m high (the Soviet and Oktyabrsky districts of the city), and Terrace 3 is 40 to 50 m high (the Zheleznodorozhny district and a part of the Oktyabrsky district).

Therefore, seismic sounding locations (Fig. 1) were selected with regard to data on the geological structure of the territory, composition of the unconsolidated Quaternary sediments, physical properties of rocks and

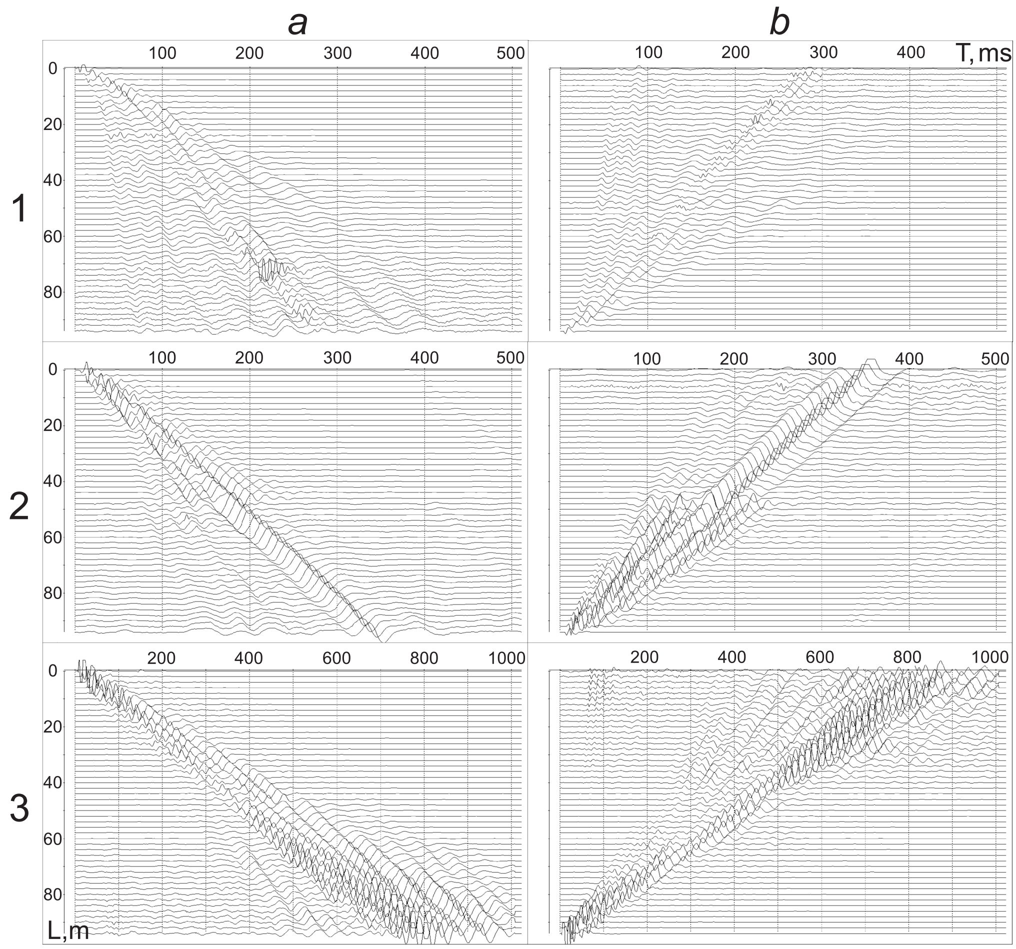

Fig. 2. An example of the direct (*a*) and impact (*b*) seismograms for rocky (1), medium (2) and water-saturated (3) soils, according to records in observation scheme YY.

Рис. 2. Пример прямой (*a*) и встречной (*b*) сейсмограмм для скальных (1), средних (2) и водонасыщенных (3) грунтов, зарегистрированных по системе наблюдений YY.

soils and dominating types of rocks and soils that are present on new construction sites. The GPS survey data were used to snap the locations to the grid.

Seismic wave velocities were measured by a LAKKOLIT digital 24-channel engineering seismic station made in Russia. The refraction method was applied as described in [*Seismic Surveying*, *1981*]. Measurements were carried out in separate sounding sessions, and reverse and catch-up time-distance plots (46, 92 and 150 m) were provided. Geophones were spaced by 2, 4 and 6 m (in the downtown, the distance was 12 m). Seismic waves were generated by shocks. Recording was done under observation schemes ZZ and YY corresponding to vertically oriented geophones and horizontal shocks perpendicular to the profile, with receivers oriented in the same direction. The selected measurement technique made it possible to obtain average values of seismic wave velocities for the top zone of the profile to depths from 10 to 30 m. It should be noted that the detection of 'useful' waves was challenging due to considerable background noise, and notwithstanding the accumulation of shocks, the detection of transverse waves was supported by data on surface waves.

In the city territory, velocities of P- and S-waves were measured at 37 locations assumed to cover all of the areas distinguished by the available geotechnical data. In the 'reference' bedrocks, Vp and Vs were measured in the city territory and in the vicinity of the city (measurements were taken in quarries and on sites where the bedrocks occur at shallow depths). At 23 locations (Nos. 38 to 60), special measurements were taken in order to design seismicity-soil models corresponding to zones in the city which may be subject to the highest and lowest seismic hazard. Such models also provided information complementing to the measurement statistics. Reflection seismic data processing was performed by the RadExPro software.

Examples of the recorded seismograms are given in Fig. 2. Time-distance plots of P- and S-waves and

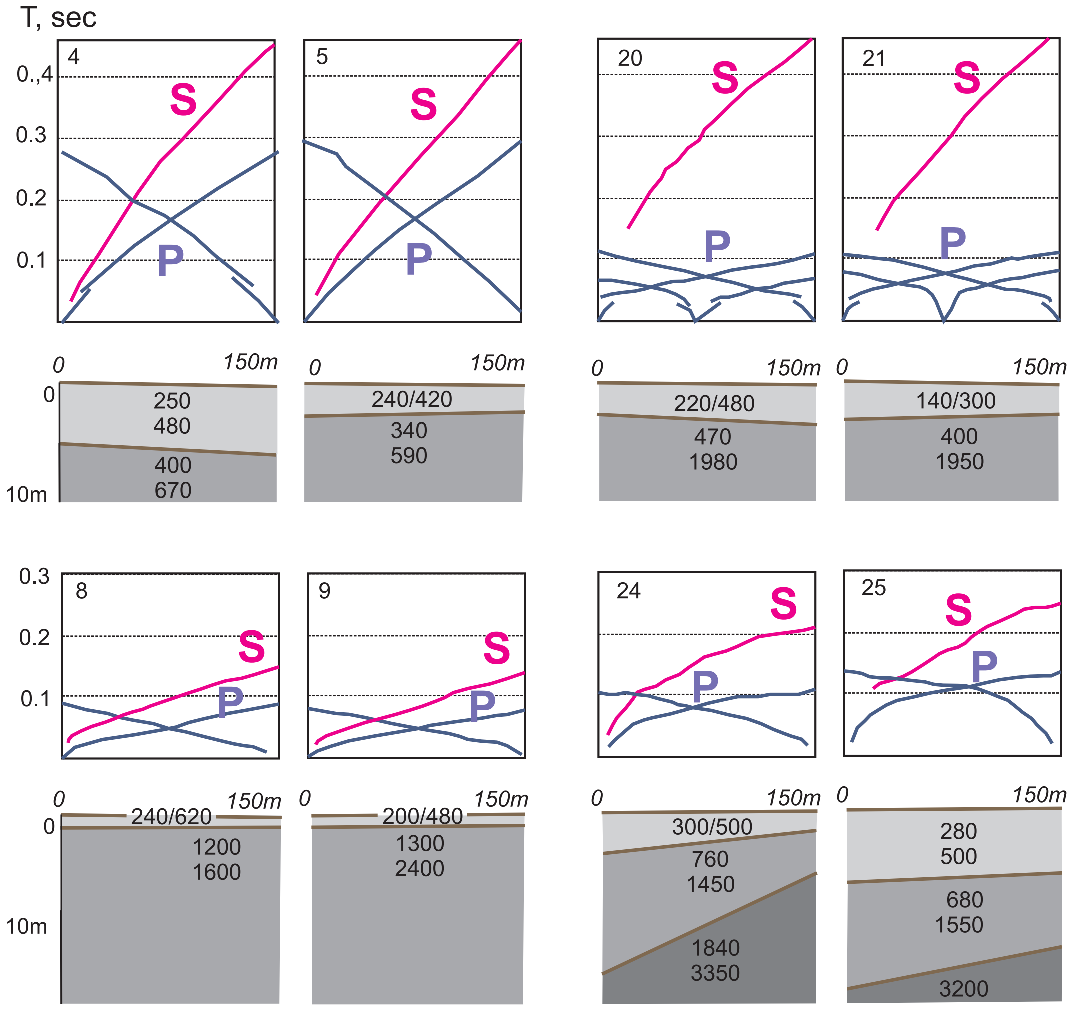

Fig. 3. Examples of travel-distance plots of P- and S-waves, and velocity profiles.

4–5 – unconsolidated none-water-saturated soil; 20–21 – water-saturated gravel-pebble sediments; 8–9 – strongly and weakly fractured rocky soils; 24–25 – unconsolidated, broken rocks and relatively intact bedrocks. Top and bottom numbers show velocities of P- and S-waves, respectively.

Рис. 3. Примеры годографов продольных и поперечных волн и скоростные разрезы.

4–5 – рыхлые неводонасыщенные грунты; 20–21 – водонасыщенные гравийно-галечные отложения; 8–9 – сильно- и слаботрещиноватые скальные грунты; 24–25 – рыхлые, разрушенные скальные и относительно сохранные коренные породы. Цифры сверху – скорости Р-волн, снизу – скорости S-волн.

seismic wave velocity profiles for sites that meet the specified seismicity-soil conditions are given in Fig. 3. The seismograms, plots and profiles give evidence that it is challenging to select 'useful' waves when seismic measurements are taken in urban areas, even if special attention is given to registration timelines, the amount of accumulated excitations and their intensity. Data from all the seismic measurement locations (see Fig. 1) were consolidated, and histograms were constructed to show the distribution of wave velocities and reveal most probable values (Fig. 4). However, the available histograms are limited in number, and additional measurements are required for each type of soil.

In general, it is evidenced by the seismic velocities recorded in the top zone of the profile near the city of Ulan-Ude that the seismic velocity values differ dramatically in ground conditions of three types – rocky, water-saturated soil and unconsolidated non-water-saturated soil.

The bedrocks are represented mainly by conglomerate, sandstone, argillite and granitic rocks. Velocities of P- and S-waves in these rocks are low in the top zone of the profile (to depth from 3 to 5m). In the uppermost zone, the P-wave velocity range from 1400 to 2000 m/sec. In less fractured rocks, Vp values range from 1500 to 3500 m/sec (Fig. 4, *a*) and Vs values range from 1000 to 2100 m/sec with increasing depth (Table 1). According to measurement in 50 bedrock samples

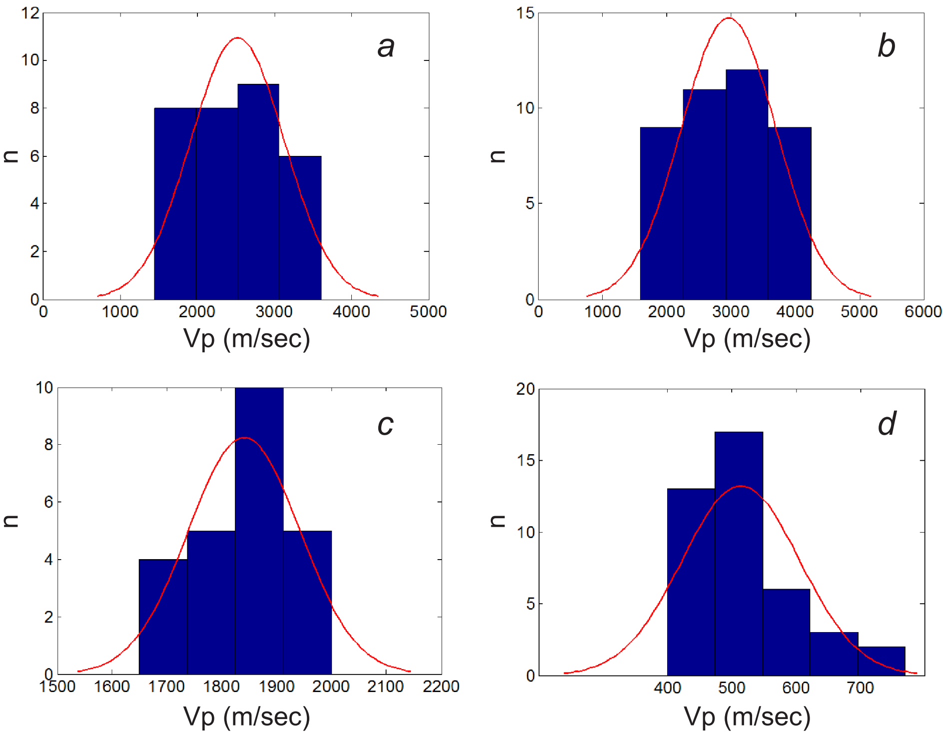

Fig. 4. Histograms of the distribution of P-wave velocities in the rocks and soils typical of the Ulan-Ude city territory: *a* – rocky soil; *b* –in the rock samples; *c* – flooded soil; *d* – air-dry soil.

Рис. 4. Гистограммы распределения скоростей продольных волн в грунтах района г. Улан-Удэ: *a* – для скальных грунтов; *b* –в образцах скальных пород; *c* – для обводненных грунтов; *d* – для воздушно-сухих грунтов.

taken from the outcrops, the range of ultrasound velocities shows an increase towards higher values of Vp (Fig. 4, *b*). The most probable P-wave velocities amount to almost 3000 m/sec, and the maximum velocity exceeds 4000 m/sec.

For water-saturated gravel-pebble and sandy soils, the typical velocities of P-waves range from 1650 to 2000 m/sec (Fig. 4, *c*), and the P/S-wave velocity ratio varies from 3.0 to 4.5 (Table 1). Measurements in soils of the same type but not water-saturated show P-wave velocities from 400–500 to 800 m/sec and S-wave velocities from 180 to 420 m/sec (note: the layer of seasonal freezing was excluded from the calculations) (Fig. 4, *d*). The available data on physical properties of soils which are required for further calculations are summarized in Table 1.

Data on soil composition, velocities of seismic wave propagation in soils of the specified types, thickness of unconsolidated sediments in the upper segment of the profile, and bulk weight of the reference and studied soils were collected as required for seismic hazard assessment, construction of the set of seismic models and application of the selected computational methods (see Section 2). Equation (1) was used to estimate values of incremental seismic intensity for each observation location. The average velocity value estimated for the top 10-meter thick zone was taken into account. Calculation results are given in Table 2.

Table 1. **Physical properties of rocks and soils**

Таблица 1. **Физические свойства грунтов**

Rocks and soils	Specific gravity, g/cm³	Bulk weight, g/cm³	Porosity, %	Water absorption, %
Granitic rock	2.73–2.86	2.53–2.57	2.1–3.3	0.10–0.79
Medium- and coarse-grained sandstone	2.62–2.81	2.15–2.74	2.8–9.1	0.09–7.30
Argillite	2.64	2.21	19.5	2.8
Conglomerate	2.71	2.40	12.0	0.6–3.4
Gravel	2.70–2.79	1.60–1.90	38–40	–
Sand	2.63–2.77	1.68–1.90	38–40	–

Table 2. **Seismic properties of rocks and soils in the Ulan-Ude city territory**

Таблица 2. **Результаты исследования сейсмических свойств грунтов на территории г. Улан-Удэ**

Item #	Rock and soil conditions	h, m	Vp, m/sec	Vs, m/sec	ρ, g/cm³	Vp/Vs	Average Vp, m/sec	Average Vs, m/sec	ΔIp, point	ΔIs, point
1	Powdery fine-grained sand	6	400 690	210 420	1.8 1.8	1.9 1.65	480	262	+1.34	+1.37
2	Powdery fine-grained sand Sandstone	20	440 2900	230 –	1.8 2.6	1.9 –	440	230	+1.40	+1.44
3	Powdery fine-grained sand Granitic rock	6	450 3000	210 1800	1.8 2.6	2.15 1.67	685	326	+0.93	+1.1
4	Powdery fine-grained sand Fine-grained sand	11	480 670	250 400	1.8 1.9	1.93 1.67	480	250	+1.40	+1.39
5	Powdery fine-grained sand Fine-grained sand	5	480 580	240 340	1.8 1.9	2.0 1.7	530	290	+1.29	+1.30
6	Fine-grained sand Water-saturated sand	10	350 1650	180 400	1.9 2.0	1.94 4.2	350	180	+1.50	+1.59
7	Sand, gravel Water-saturated sand	11	510 1890	210 520	1.9 2.0	2.4 3.6	510	510	+1.26	+1.45
8	Coarse-grained rocks Conglomerate	2	620 1900	240 1200	2.0 2.6	2.5 1.58	1350	670	+0.36	+0.46
9	Coarse-grained rocks Conglomerate	2.5	480 2400	200 1300	2.0 2.6	2.4 1.84	1200	550	+0.39	+0.42
10	Coarse-grained rocks Conglomerate	2.5	380 2400	160 1400	2.0 2.6	2.4 1.7	1030	480	+0.46	+0.69
11	Sand, gravel Water-saturated gravel	3	350 1900	170 420	1.8 2.0	2.1 4.5	350	170	+1.64	+1.83
12	Sand, gravel Water-saturated gravel	6	430 1880	140 430	2.0 2.0	3.0 4.4	430	140	+1.74	+2.14
13	Gruss, debris, sand Conglomerate	6	520 2400	280 1400	2.0 2.6	1.85 1.7	765	413	+0.86	+0.88
14	Debris, sand Conglomerate	2	440 2800	– 1680	2.0 2.6	– 1.68	1345	–	+0.36	–
15	Coarse-grained rocks Conglomerate	2	600 2700	320 1650	2.0 2.6	1.88 1.64	1590	900	+0.23	+0.23
16	Sand, gravel Water-saturated gravel	2	330 1800	160 500	2.0 2.6	2.05 3.6	330	160	+1.62	+1.65
17	Sand, gravel Water-saturated gravel	2,5	450 1960	180 480	2.0 2.0	2.6 4.1	450	180	+1.52	+1.67
18	Sand, gravel Water-saturated gravel	6	390 1840	180 460	2.0 2.0	2.2 4.0	390	180	+1.81	+1.95
19	Sand, gravel Water-saturated gravel	5	340 2000	150 400	2.0 2.0	2.26 5.0	480	220	+1.60	+1.79
20	Sand, gravel Water-saturated gravel	5	480 1980	220 470	2.0 2.0	2.18 4.2	480	220	+1.60	+1.79
21	Sand, gravel Conglomerate	5	300 1950	140 400	2.0 2.0	2.1 4.9	1125	270	+0.65	+1.28
22	Sand, coarse detrital rocks Conglomerate	4	550 2250	230 1300	2.0 2.6	2.4 1.74	1000	455	+0.60	+0.76
23	Debris, sand Conglomerate	6	500 2200	220 1300	2.6 2.6	2.25 1.68	725	330	+0.79	+0.94
24	Sand Coarse-grained rocks Conglomerate	5 12	500 1450 3350	300 760 1840	2.0 2.0 2.6	1.67 1.90 1.83	 975	 580	 +0.75	 +0.78
25	Sand Fractured rocks Conglomerate	12 15	500 1550 3200	280 680 –	2.0 2.6 2.0	1.80 2.30 –	 500	 280	 +1.26	 +1.23
26	Coarse-grained rocks Conglomerate	6	400 2050	180 1100	2.0 2.6	2.2 1.85	590	270	+1.06	+1.27
27	Sand, gravel Water-saturated gravel	2	400 1670	– –	2.0 2.0	– –	400	-	+1.7	1.8

End of Table 2

Окончание таблицы 2

Item #	Rock and soil conditions	h, m	Vp, m/sec	Vs, m/sec	ρ, g/cm3	Vp/Vs	Average Vp, m/sec	Average Vs, m/sec	ΔIp, point	ΔIs, point
28	Sand, gravel	13	500	260	2.0	1.94	500	260	+1.26	+1.37
	Conglomerate		2400	1650	2.6	1.45				
29	Coarse-grained rocks	2	520	280	1.8	1.85				
	Fractured rocks	14	1450	800	2.0	1.82	1070	574	+0.72	+0.74
	Conglomerate	–	3000	1600	2.6	1.88				
30	Fractured rocks	8	1560	920	2.2	1.70	1720	1000	+0.24	+0.24
	Conglomerate		2800	1500	2.6	1.87				
31	Sand, gravel	5	500	220	1.8	2.28	500	220	+1.79	+1.86
	Water-saturated gravel		1760	470	2.0	3.70				
32	Sand, gravel	7	310	180	1.8	1.74	310	180	+2.30	+2.34
	Water-saturated gravel		1700	550	2.0	3.10				
33	Fine-grained sand	25	420	200	2.0	2.10	420	200	+1.48	+1.47
	Granitic rock		3600	2100	2.6	1.70				
34	Fine-grained sand	17	510	220	1.8	2.30	510	220	+1.26	+1.45
	Water-saturated gravel	40	1900	480	2.0	3.90				
	Conglomerate		3400	–	2.6	–				
35	Fractured rocks	5	570	300	1.8	2.6	1975	1090	+0.17	+0.19
	Conglomerate		3380	1880	2.6	1.8				
36	Fine-grained sand	11	460	220	1.8	2.10	460	220	+1.40	+1.45
	Conglomerate		3200	1900	2.6	1.68				
37	Fractured rocks	3.0	480	–	1.8	–				
	Conglomerate		3050	–	2.6	–	1800	–	+0.2	–

In our calculations, the reference is the rocky soil with Vp=2200 m/sec, Vs=1200 m/sec and ρ=2.5 g/cm^3 (average velocities in the 10-metre thick layer on sites with bedrock outcrops). For sites with the above-mentioned values, the seismic hazard is assumed one point lower than the baseline level. In this case, the average soil type (i.e. non-water-saturated sand and gravel-pebble) is characterised by Vp=600 m/sec, Vs=300 m/sec and ρ=1.8 g/cm^3. In zones with the above-described soil, the seismic hazard corresponds to the baseline seismic intensity.

Our measurements of seismic wave velocities in the city of Ulan-Ude and calculations of incremental seismic intensity (Table 2) show that relative to the selected reference soil (rocky soil – 7 points), the rocky/soil foundations of buildings and facilities may be subject to an incremental seismic impact (+0.17 to +2.3 points), and the seismic hazard for the rocks and soils ranges from 7.17 to 9.3 points.

3. Results of the initial study stage to forecast how strong earthquakes may impact the rocky/soil foundations in the Ulan-Ude city territory

To solve the problem related to seismicity microzonation mapping in compliance with the current regulations concerning urban construction, the seismic hazard of rocky/soil foundations should be mapped with account of the maximum seismic wave acceleration, dominant periods of strong earthquakes, resonance frequencies of unconsolidated beds and other characteristics of the seismic impacts.

To provide a basis for seismicity microzonation mapping of the Ulan-Ude city territory, quantitative data on soil movements of ground are needed. In the current stage of our studies, we analyze dynamic characteristics of perceptible earthquakes that occurred in the study region, establish seismic signals corresponding to the baseline seismic intensity, develop the seismicity-soil models, try to forecast seismic impacts with regard to different construction conditions and classify zones in the Ulan-Ude city territory by the seismic impact parameters. To achieve the objectives, modeling and computer simulation methods are applied.

The priority task is to establish the baseline seismic signal for the Ulan-Ude city territory [*Dzhurik, 2014*]. Determining a ‘baseline’ seismic impact is challenging as a reference accelerogram cannot be unambiguously selected. The unambiguity is due to the fact that an earthquake can be manifested in different ways in particular local zones, depending on characteristics of the earthquake source, seismic signal propagation track, structures and compositions of rocky/soil foundations of buildings and facilities. Besides, it is needed to take into account a number of complicating factors, such as

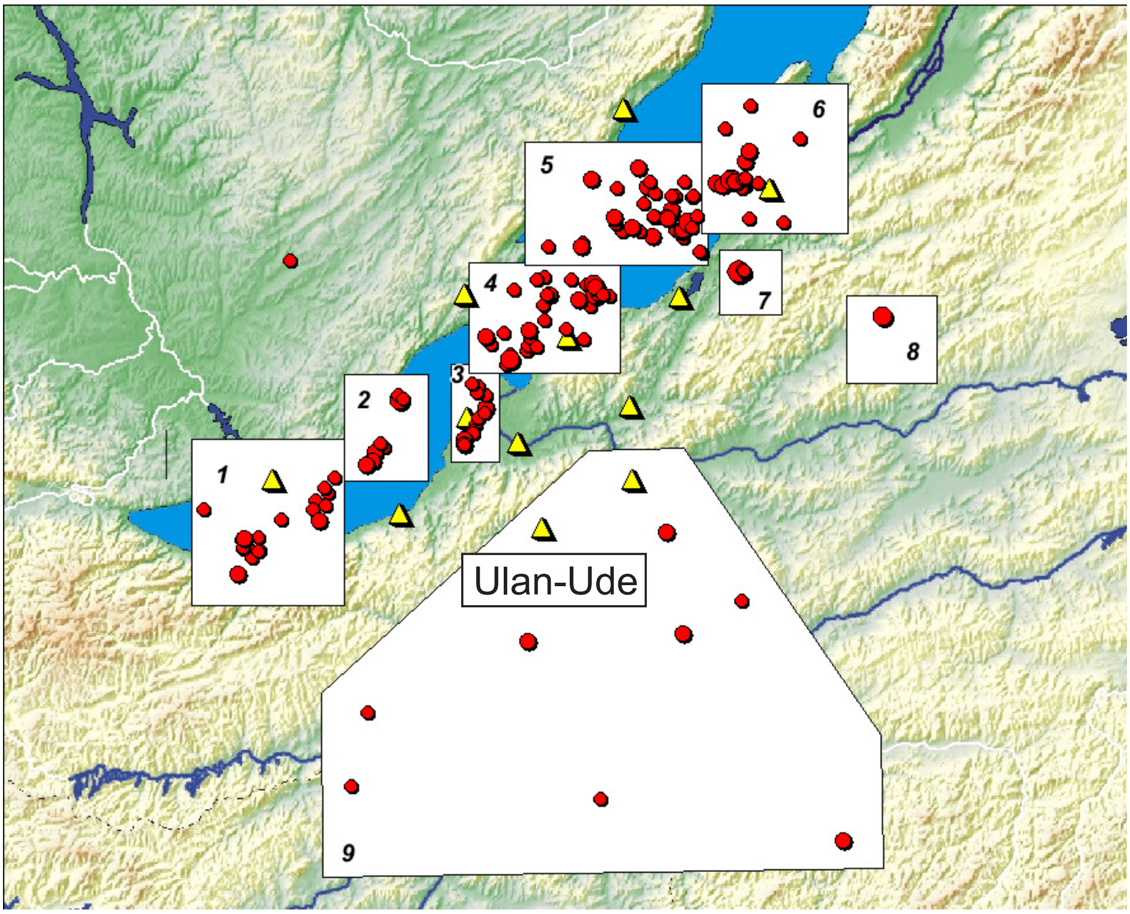

Fig. 5. Earthquake foci zones (Nos. 1 to 9, see Table 3) of potential danger for the Ulan-Ude city territory. Circles show earthquake epicentres selected for establishing the reference signals; triangles show locations of permanent seismic stations.

Рис. 5. Зоны очагов землетрясений (1–9, см. табл. 3), потенциально опасные для территории г. Улан-Удэ. Кружками обозначены эпицентры землетрясений, отобранные для задания исходных сигналов; треугольниками – постоянные сейсмические станции.

several potential earthquake foci zones (Fig. 5), physical and mechanical properties of rocks and soils, and types of displacement/movement in earthquake foci areas. Such factors predetermine whether an impulse-type seismic event may occur or an earthquake with a relatively slow increase and decrease of seismic intensity on the surface may take place.

Methods for selecting the baseline accelerograms are mainly oriented at the acquisition or calculation of peak accelerations and scaling [*Pavlov*, *1988*] in accordance with relevant seismic scales [*Nazarov, Shebalin*, *1975*]. Due to the fact that registered strong seismic events are not numerous in potential earthquake foci zones (and also in the vast regions under review), it becomes necessary to refer to data from catalogues of strong earthquakes registered by the global seismic network or use data on small earthquakes and establish phase characteristics [*RB-006-98*, *1998*].

In this study, we use only the earthquakes records by the regional network of seismic stations [*Drennov et al.*, *2011*]. Since the medium is considered as a form-generating factor of a focal pulse, the phase spectrum of local earthquakes, one way or another, takes into account the earthquake excitation and scattering properties of the inhomogeneous medium.

In engineering surveys for construction purposes, the earthquake resistance of buildings and facilities is typically calculated from accelerograms [*Ratnikova*, *1984*]. It is advisable to obtain accelerograms for each PEF zone that can be described by sets of average seismic characteristics.

In view of the above, our study has two main objectives: (1) Obtain potential earthquake accelerograms for each PEF zone with the reference to the available accelerograms of earthquakes that actually took place in the studied zones (for three components, NS, EW and Z); (2) Using the properly grounded models showing seismicity of the ‘reference’ rocks, correlate the obtained maximum acceleration rates with the seismic hazard scale specified in points.

In our study, to justify the seismic hazard of the Ulan-Ude city territory, we analyze accelerograms of actual earthquakes (M from 3.0 to 6.3) recorded by the Ulan-Ude seismic station. For each PEF zone, an average spectrum is calculated and taken as a characteristic of the entire zone. In total, the processed database includes records of 55 earthquakes from 2001 to 2011. Data on components NS, EW, and Z are processed separately. Some of the recorded accelerograms are rejected due to various reasons, such as an insignificant signal/noise ratio. For each earthquake, amplitude and phase spectra are calculated.

It should be noted that we select accelerograms of earthquakes differing in magnitudes and thus refer to relation $\beta_M(f)$ showing how the acceleration spectrum changes with magnitude variations and depends on frequency. In our study, we use the equation for the Baikal rift zone which was published in [*Drennov et al., 2013*]:

$\beta_M(f) = -0.31 log(f) + 0.93$ (0.78–20 Hz);
$\beta_M(f) = 0.96$ (<0.78 Hz) R^2=0.98,

where $\beta_M(f) = lg\Delta S/\Delta M$. It determines a spectrum logarithm incremental value at the *i*-th frequency with an earthquake magnitude increase by ΔM.

Based on the above relationship, the amplitude spectra are scaled to magnitudes of the PEF zones. Finally, earthquake accelerograms are obtained for the PEF zones characterized by their specific magnitudes (Fig. 5). This objective is met by using the inverse Fourier transform of the average acceleration spectrum for a specified PEF zone and the phase spectrum of the strongest earthquake recorded in the given PEF zone.

Based on the phase spectra of accelerations from various earthquakes, it is possible to obtain accelerograms of different durations, from accelerograms of the impulse type (when the released energy is concentrated in a small time window) to accelerograms of large time spans. In our study, phase spectra of accelerograms of the medium time span are mainly used.

The accelerograms and their spectra for all the studied PEF zones are shown in Fig. 6 and 7, and the corresponding spectral parameters are given in (Table 3).

According to Table 3, maximum and minimum acceleration rates for the rocks and soils under the Ulan-Ude seismic station can amount to 166 cm/sec^2 and 1.7 cm/sec^2, respectively (the three components are taken into account). The maximum acceleration rates are associated with frequencies from 1.2 to 8.3 Hz, the widths of the acceleration spectra for all the PEF zones range from 0.6 to 14.4 Hz at the level of 0.7S_m. Typically, for the PEF zones located closer and having larger potential magnitudes, the acceleration spectra are somewhat wider than those of the more remote PEF zone, and this expansion is due to higher frequencies. Besides, the maximum values of the spectra are widely variable (from 0.2 to 46 cm/sec) and correlate with the frequency range from 1 to 12.3 Hz.

It is revealed that ranges of maximum values of the studied parameters are widely variable for each component. Therefore, it is needed to conduct additional studies to eliminate the uncertainties. This problem can be solved by long-term recording of earthquakes on various sites in the city which have contrasting soil conditions, such as water-saturated or air-dry soils of specific compositions. In view of the above, at the current stage of our studies, we refer to relatively reliable analyses of seismic impacts by the frequency of their occurrence. Considering amplitudes, it is needed to scale the established baseline signals with regard to forecasted seismic impacts. Such objectives comply with requirement of the current construction regulations. However, a probability of establishing the maximum amplitudes can be properly justified by conducting the required comprehensive studies and consolidating the modeling and experimental data.

At the Ulan-Ude seismic station, geophones are located on soils of category 1. Such conditions may prove sufficient for seismological reconstructions; however, in order to solve problems of engineering seismology, we need quantitative data, including, in the first place, determinations of frequency response which (as a transfer function) are required to justify the baseline signals of the ‘reference’ rocks/medium soils represented in the seismicity-soil models. This objective can be achieved, as noted above, by direct and computational methods of seismicity microzonation [*Dzhurik et al., 2012*].

Thus, for further use of the accelerograms (see Fig. 6 and 7), they are assigned to the soils of category 1. For the Ulan-Ude city territory, a single baseline signal needs to be established. A mandatory condition is that it should take into account specific features of the spectral compositions of vibrations for each selected PEF zone (see Fig. 5). The vibration spectra are normalized and then averaged. A phase response of one of the earthquakes recorded is estimated, and normalized accelerograms are calculated by the inverse Fourier transform for the three components (Fig. 8, *a*). In its turn (Fig. 8, *b*), the amplitude spectrum of this signal reflects all the specific frequency characteristics of the accelerograms predicted for the PEF zones of the highest hazard (Nos. 3, 4 and 5). Its level exceeding 0.7 Smax is in the frequency range from 1.2 to 5.0 Hz. The main peaks of the spectra occur at frequencies from 1.6 to 2.2 Hz (Table 4).

For further theoretical calculations considering different soil conditions presented by the seismic models, it is required to correlate the background seismic

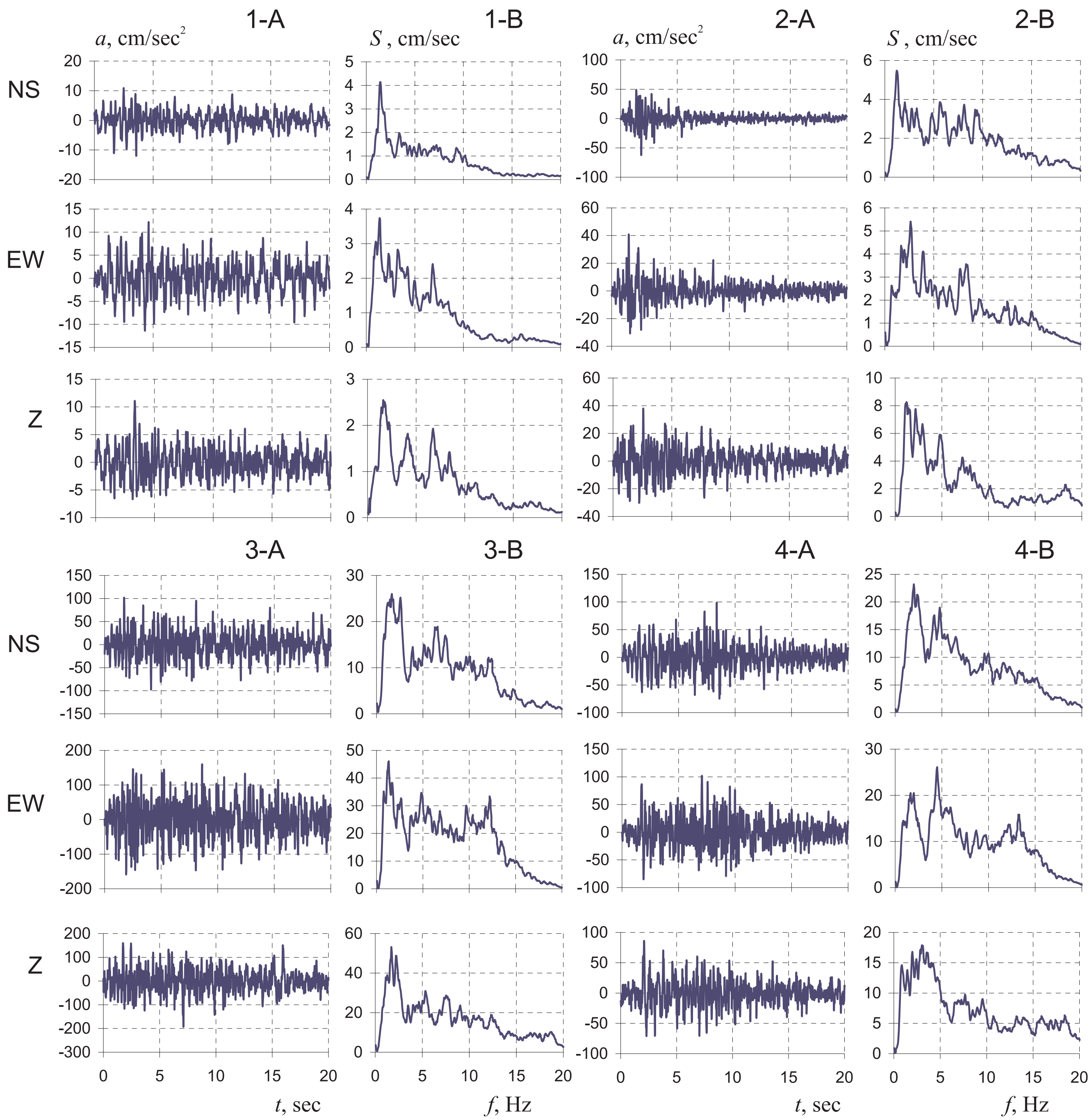

Fig. 6. Accelerograms (*A*) and their amplitude spectra (*B*) of components NS, EW and Z for potential earthquake foci zones (Nos. 1 to 4) (M=7.5, Δ=230 km; M=7, Δ=130 km; M=7.5, Δ=90 km; M=7.5, Δ=100 km).

Рис. 6. Акселерограммы (*А*) и их амплитудные спектры (*В*) для трех компонент (NS, EW, Z) для зон ВОЗ 1-4 (M=7.5, Δ=230 км; M=7, Δ=130 км; M=7.5, Δ=90 км; M=7.5, Δ=100 км).

signal with a reference soil/half-space, from which we can estimate changes in the signal by near-surface inhomogeneities. In further estimations, it is also reasonable to consider inhomogeneities located at depth.

To develop models that can characterize subsurface inhomogeneities, we use data on seismic wave velocities that are generalized with regard to soil compositions and conditions (see Table 2; Fig. 3 and 4) and also refer to the available file materials. Parameters of seismicity-soil reference models Nos. 1 and 2 (Table 5) are based on the above-mentioned data and correlated with predicted seismic impacts.

A set of the well-known methods and software packages [*Ratnikova, 1984; RB-006-98, 1998*] is used to carry out theoretical calculations.

Reference model No. 1 (see Fig. 9, *a–e*, and Table 5)

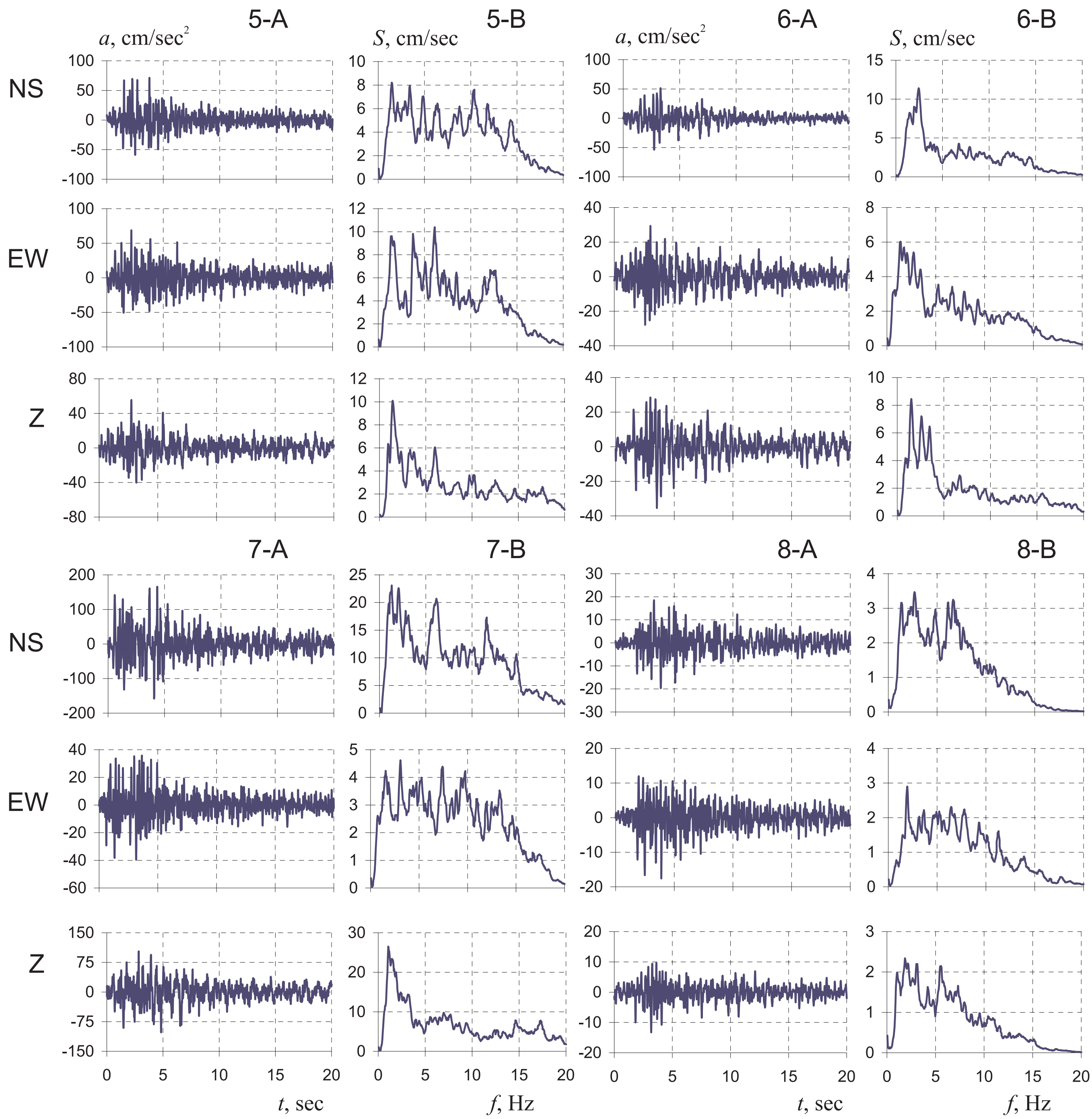

Fig. 7. Accelerograms (*A*) and their amplitude spectra (*B*) of components NS, EW, Z for potential earthquake foci zones (Nos. 5 to 8) (M=7.5, Δ=150 km; M=7, Δ=170 km; M=7, Δ=120 km; M=6.5, Δ=170 km).

Рис. 7. Акселерограммы (*A*) и их амплитудные спектры (*B*) для трех компонент (NS, EW, Z) для зон ВОЗ 5-8 (M=7.5, Δ=150 км; M=7, Δ=170 км; M=7, Δ=120 км; M=6.5, Δ=170 км).

represents the bedrock in the 8-points zone. Calculated acceleration rates correspond to the seismic hazard by one point lower than that for the medium soil. The maximum acceleration rates amount to 98 cm/sec^2 and 53 cm/sec^2 for the horizontal and vertical components, respectively. The acceleration spectrum has the maximum of 0.7 in the frequency range from 1.12 to 4.93 Hz and 1.17 to 2.34 Hz for the horizontal and vertical components, respectively.

Models Nos. 3 to 7 characterize dominating seismic risk areas of the city (see Fig. 1, and Tables 5 and 6). They are also applicable to areas with different soil conditions and reference bedrock depths from 10 to 80m. It should be noted that our models are substan-

Т a b l e 3. **Main parameters of estimated spectra for potential earthquake foci (REF) zones**

Т а б л и ц а 3. **Основные параметры расчетных спектров для землетрясений разных зон ВОЗ**

PEF M Δ	Component	a_m, cm/sec²	$f\,a_m$, Hz	S_m, cm/sec	$f\,S_m$, Hz	$(f_1–f_2)_{0.7Sm}$	$\delta f_{0.7Sm}$	$(f_1–f_2)_{0.5Sm}$	$\delta f_{0.5Sm}$
1 M=7.5 230 km	NS EW Z	11 12.2 11.1	3.6 2 2.2	4.2 3.7 2.5	1.5 1.4 1.8	1.3–1.9 0.8–3.4 1.3–6.9	0.6 2.6 5.6	1.2–2.0 0.7–4.9 1.2–7.1	0.8 4.2 5.9
2 M=7 130 km	NS EW Z	62.4 41 38	5.3 5.6 1.2	5.4 5.4 8.2	1.2 2.6 1.3	1–3.7 1.6–4 1–3.1	2.7 2.4 2.1	0.9–9.7 1.5–8.6 0.9–5.2	8.8 7.1 4.3
3 M=7.5 90 km	NS EW Z	102 160 138	3.1 2.8 2	26 46 53	1.7 1.3 1.7	1–2.7 0.6–13 1.5–2.4	1.7 12.4 0.9	0.7–7.7 0.7–12.7 1–7.9	7 12 6,9
4 M=7.5 100 km	NS EW Z	99 102 86.2	2.6 3.2 1.7	23 26 17.8	2 4.5 3.1	1.4–4.9 1.8–4.8 1–4.7	3.5 3 3.7	1.1–6.8 1.2–6.9 0.7–5.1	5.7 5.7 4.4
5 M=7.5 150 km	NS EW Z	69.5 68.8 55.5	4 3.8 4.2	8.2 10.4 10	1.5 6.1 1.5	1.3–12 1.3–6.4 1.3–1.8	10.7 5.1 0.5	0.9–14.6 1.1–12.8 1.1–6.2	13.7 11.7 5.1
6 M=7 170 km	NS EW Z	53.7 29.4 33.6	4 8.3 2.9	11.3 6 8.4	2.5 1.4 1.5	1.6–2.7 1.2–3.6 1.7–3.6	1.1 1.4 1.9	1.1–3 0.9–8 1.3–3.7	1.9 7.1 2.4
7 M=7 120 km	NS EW Z	166 40 102	3.1 4.2 2.8	23 4.6 26.5	1.3 3.1 1.1	0.8–6.4 1.3–10.3 0.9–2	5.6 9 1.1	0.7–12.7 1–14.7 0.8–3.3	12 13.7 2.5
8 M=6.5 170 km	NS EW Z	20 166 133	3.7 3.4 6.7	3.4 2.9 2.3	2.7 2.0 1.9	1.6–7.7 1.8–8.0 0.9–7.4	6.1 6.2 6.5	1–8.7 1.7–11.3 0.9–8.1	7.7 9.6 7.2
9 M=5.5 90 km	NS EW Z	1.2 2.7 1.7	6.2 4.2 5.6	0.2 0.4 0.2	12.8 12.3 10.2	7.9–14.1 6.4–14.4 1.0–20	6.2 8 19	5–14.8 4–15.9 1.5–20	9.8 11.9 18.5
9 M=6.5 130 км	NS EW Z	4.8 6.5 4	3.3 2.9 2.4	0.6 0.7 0.8	1 3.3 1.9	1.2–4 2.3–4.3 1.1–2.2	2.8 2 1.1	0.6–4 0.9–4.8 0.8–3.1	3.4 3.9 2.3

N o t e. M is magnitude; Δ is distance to epicentre; a_m is maximum amplitude of calculated acceleration; fa_m is frequency corresponding to a_m; S_m is maximum amplitude level of the spectrum; f_{Sm} is spectrum peak frequency; f_1 and f_2 are frequencies that limit acceleration spectra at levels 0.7 and 0.5 S_m; $\delta f_{0.7Sm}$ and $\delta f_{0.5Sm}$ are spectrum widths.

П р и м е ч а н и е. М – магнитуда; Δ – эпицентральное расстояние; a_m – максимальная амплитуда расчетного ускорения; fa_m – частота, соответствующая a_m; S_m – максимальный амплитудный уровень спектра; f_{Sm} – частота максимума спектра; f_1, f_2 – частоты, ограничивающие спектры ускорения на уровнях 0.7 и 0.5 S_m; $\delta f_{0.7Sm}$, $\delta f_{0.5Sm}$ – ширина спектра.

tiated also by other geotechnical and geophysical data providing for the zonation of the study area in the first approximation.

At the current stage of studies, for reference model No. 2 (see Table 5, Fig. 9) representing the 10-metre thick water-saturated soil of the medium composition, the acceleration rates are scaled with regard to the acceleration rates to 397 cm/sec² and 173 cm/sec² for the maximum and vertical components, respectively. This corresponds to the seismic hazard of 9 points, i.e. one point higher than the reference level for the non-water-saturated soil. The resonant frequency amounts to 12.79 Hz; the main peak of the spectrum is at the frequency of 1.56 and 1.51 Hz; the maximum spectral density amounts to 85.3 and 51.9 cm/sec for components EW and Z, respectively (Table 6).

It is noteworthy that in further studies, special attention should be paid to the justification of the potential seismic hazard of water-saturated soils [*Dzhurik et al., 2011*] based on records of the behaviour of such soils during earthquakes. As noted earlier, frequency characteristics need to be determined for the water-saturated soil layers varying in thickness, and such data can facilitate achieving more reliable results by the calculation methods.

In general, models Nos. 3, 4 and 6 represent the unconsolidated non-water-saturated soils varying in thickness. According to estimations by the seismic

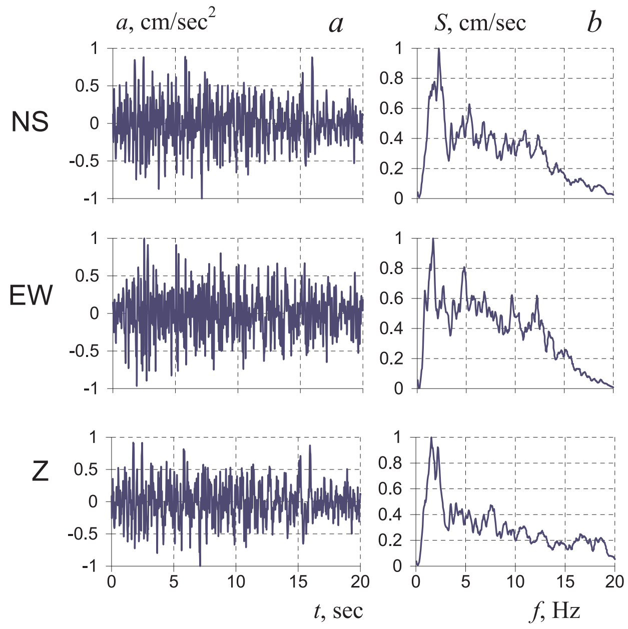

Fig. 8. Reference normalized accelerograms (*a*) and their amplitude spectra (*b*) (M=7.5, 90 km).

Рис. 8. Исходные нормированные акселерограммы (*a*) и их амплитудные спектры (*b*) (M=7.5, 90 км).

T a b l e 4. **Main parameters of normalized estimated spectra for earthquakes with M=7.5, Δ=90 km**

Т а б л и ц а 4. **Основные параметры нормированных расчетных спектров для землетрясения M=7.5, Δ=90 км**

Component	f_{am}, Hz	S_m, cm/sec	f_{Sm}, Hz	$(f_1–f_2)_{0.7Sm}$	$\delta f_{0.7Sm}$	$(f_1–f_2)_{0.5Sm}$	$\delta f_{0.5Sm}$
NS	3.3	1	2.2	1.5–2.6	1.1	1.1–6.8	5.7
EW	2.3	1	1.6	1.2–5.0	3.8	1.0–8.0	7.0
Z	2.3	1	1.6	1.2–2.4	1.2	1.0–2.7	1.7

T a b l e 5. **Parameters of standard seismicity-soil models**

Т а б л и ц а 5. **Параметры типовых сейсмогрунтовых моделей**

Model No., standard profile	h, m	Vp, m/sec	Vs, m/sec	ρ, t/m³	Average Vp, m/sec	Average Vs, m/sec	ΔI(Vp)	$\ddot{A}_{max}$, cm/sec² (point)
Reference model No. 1	10 12 ∞	2200 2600 3500	1240 1700 1900	2.5 2.6 2.7	2200	1240	0	98 (7)
Reference model No. 2 (water-saturated soil) h=10m	10 10 12 ∞	1600 2200 2600 3500	480 1240 1700 1900	1.9 2.5 2.6 2.7	600	300	2	396 (9)
Model No. 3 Unconsolidated and degraded, strongly fractured conglomerate	2 2 4 9 6 10 12 ∞	500 700 1000 1500 2000 2200 2600 3500	290 380 510 750 990 1240 1700 1900	1.6 1.9 2.0 2.2 2.4 2.5 2.6 2.7	820	441	0.76	171 (7.76)
Model No. 4 Gravel, sand (none-water-saturated), h=36m	4 2 12 12 6 14 16 ∞	400 600 900 1500 2000 2200 2600 3500	230 330 490 750 990 1240 1700 1900	1.6 1.8 2.0 2.2 2.4 2.5 2.6 2.7	570	316	1.16	186 (8.16)

End of Table 5

Окончание таблицы 5

Model No., standard profile	h, m	Vp, m/sec	Vs, m/sec	ρ, t/m3	Average Vp, m/sec	Average Vs, m/sec	ΔI(Vp)	Ämax, cm/sec² (point)
Model No. 5	10	1500	420	1.9	600	247	2.1	410
Loam, sandy loam, sand	12	2000	560	2.4				(9.1)
(water-saturated),	12	2200	1240	2.5				
h=22 m	16	2600	1700	2.6				
	∞	3500	1900	2.7				
Model No. 6	8	600	340	1.8	583	332	1.02	154
Medium-type soil, sand, gravel	16	800	440	1.9				(8.02)
(none-water-saturated),	24	1000	510	2.1				
h=80m	20	1500	750	2.2				
	12	2000	990	2.3				
	12	2200	1240	2.5				
	16	2600	1700	2.6				
	∞	3500	1900	2.7				
Model No. 7	8	1500	430	1.9	600	300	2.1	398
Sand, gravel (water-saturated),	16	1600	550	2.0				(9.1)
h=80m	24	1800	600	2.1				
	32	2000	700	2.2				
	12	2200	1240	2.5				
	16	2600	1700	2.6				
	∞	3500	1900	2.7				

N o t e. The seismic impedance method is applied to calculate seismic hazard levels (UoM – point) with respect to the bedrocks (baseline seismicity of 7 points). Average seismic wave velocities are estimated for the 10-metre thick layer. The watercut correction is +1 point.

П р и м е ч а н и е. Расчет сейсмической опасности в баллах проведен по методу сейсмических жесткостей относительно коренных пород (исходная сейсмичность 7 баллов); средние скорости рассчитаны для 10-метрового слоя; поправка за обводненность +1 балл.

impedance method, the seismic hazard of the sites with such soils ranges from 7.76 to 8.16 points. For the specified soil conditions (see Table 6; Fig. 9), the peak acceleration rates range from 154 to 186 cm/sec² (Fig. 9, *a, b*) and from 64 to 86 cm/sec² (Fig. 9, *c, d*) for components EW and Z, respectively.

Models No. 5 and No. 7 represent water-saturated soil layers (22 and 80 m thick). The peak acceleration rates range from 397 to 410 cm/sec² and 199 to 223 cm/sec² for components EW and Z, respectively (see Tables 5 and 6, and Fig. 9). The calculated acceleration rates correspond to the seismic hazard of 9 points, i.e. one point higher than the baseline for the medium non-water-saturated soil. For model No. 5 and 7, the resonant frequency amounts to 6.75 and 2.2 Hz, respectively. The calculated spectral density reaches its maximum in the frequency range from 1.51 to 4.74 Hz and varies from 99 to 130 cm/sec and 53.8 to 84.6 cm/sec for components EW and Z, respectively. With increasing thickness of the water-saturated layer from 22 to 80 m, its resonant frequency decreases from 6.79 Hz to 2.2 Hz (see Fig. 9, *d*).

Based on the theoretical calculation results (see Section 2), experimental measurements (see Section 1) and the available geotechnical and hydrogeological data, a schematic map is compiled in the first approximation (Fig. 10) to show zones differing in the basic seismic impact parameters.

The zone with the potential maximum seismic hazard of 9 points includes floodplain areas and the first above-floodplain terrace composed by alluvium (sand, clay soil and gravel) where groundwater occurs at shallow depths, less than 5m. It is possible that the weakened near-fault northern site will be also included. This zone can be represented by seismicity-soil models No. 2 and No. 7 (see Fig. 9 and Table 6). In this zone, the maximum acceleration rates are 410 cm/sec² and 223 cm/sec² for components NS and Z, respectively.

The zone with the relatively high seismic hazard (8 and 9 points, a transition zone) includes the left-bank terrace of the Uda River which is composed of silty fine-grained sand (models No. 4 and No. 5). In this zone, the maximum acceleration rates range from 154 to 410 cm/sec² and 64 to 223 cm/sec² for components NS and Z, respectively.

The seismic hazard of 8 points (models No. 3 and No. 4) may be expected at slightly sloped terraces of the Uda and Selenga Rivers where groundwater occurs at depths from 8 to 20 m. In this zone, the maximum acceleration rates are 186 cm/sec² and 86 cm/sec² for components NS and Z, respectively.

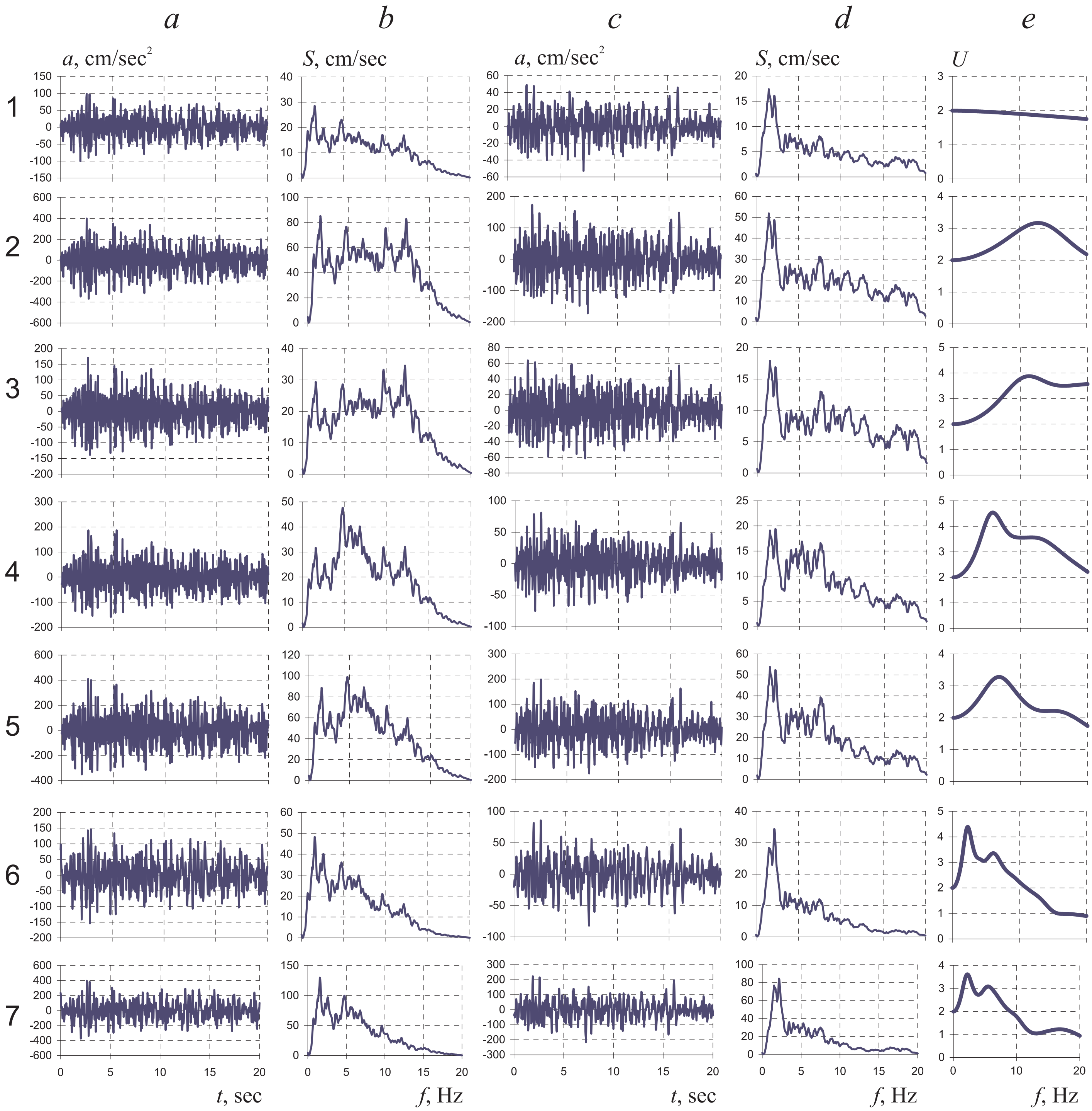

Fig. 9. Accelerograms (*a*) and their amplitude spectra (*b*) for the horizontal component; accelerograms (*c*) and their amplitude spectra (*d*) for the vertical component; frequency characteristics of unconsolidated soil layers (*e*).

Рис. 9. Акселерограммы (*a*) и их амплитудные спектры (*b*) для горизонтальной компоненты, акселерограммы (*c*) и их амплитудные спектры (*d*) для вертикальной компоненты, частотные характеристики рыхлых слоев (*e*).

The zone with the seismic hazard of 7 points includes sites composed of rocky and semi-rocky soils, except areas of tectonic fracturing (model no. 1). In this zone, the maximum acceleration rates are 98 cm/sec^2 and 53 cm/sec^2 for components NS and Z, respectively.

It should be noted that by applying the seismic microzonation method, it is possible to reveal sites with the seismic hazard from 7 to 9 points in each of the specified zones (Fig. 10). Such sites can be correlated with relevant soil models (see Table 5), and their locations can be further clarified and determined more precisely with regard to the scale of seismic microzona-

Т a b l e 6. **Main parameters of estimated accelerograms and corresponding spectra for models Nos. 1 to 7**

Т а б л и ц а 6. **Основные параметры расчетных акселерограмм и соответствующих им спектров для моделей 1–7**

Model No., standard profile	Maximum acceleration $\ddot{A}_{max}$, cm/sec^2	Peak spectrum value S_{max}, cm/sec	Frequency of main spectrum peak, Hz	Frequency range for $0.7{\cdot}S_{max}$ (f), Hz	Resonance frequency of unconsolidated layers, Hz
Horizontal component EW					
1	98	28.6	1.56	1.12–4.93	–
2	397	85.3	1.56	1.12–12.65	12.79
3	171	34.6	12.16	1.42–12.65	11.28
4	186	47.6	4.74	4.44–6.98	5.86
5	410	99	4.74	1.27–9.62	6.79
6	154	48.3	1.56	1.37–4.83	2.29
7	398	130	1.56	1.27–4.88	2.2
Vertical component Z					
1	53	17.4	1.51	1.17–2.34	–
2	173	51.9	1.51	1.22–2.34	12.79
3	64	17.9	1.51	1.22–7.67	11.28
4	81	19.4	2.15	1.27–7.86	5.86
5	199	53.8	1.51	1.22–7.62	6.79
6	86	34.4	2.15	1.42–2.39	2.29
7	223	84.6	2.15	1.32–2.34	2.2

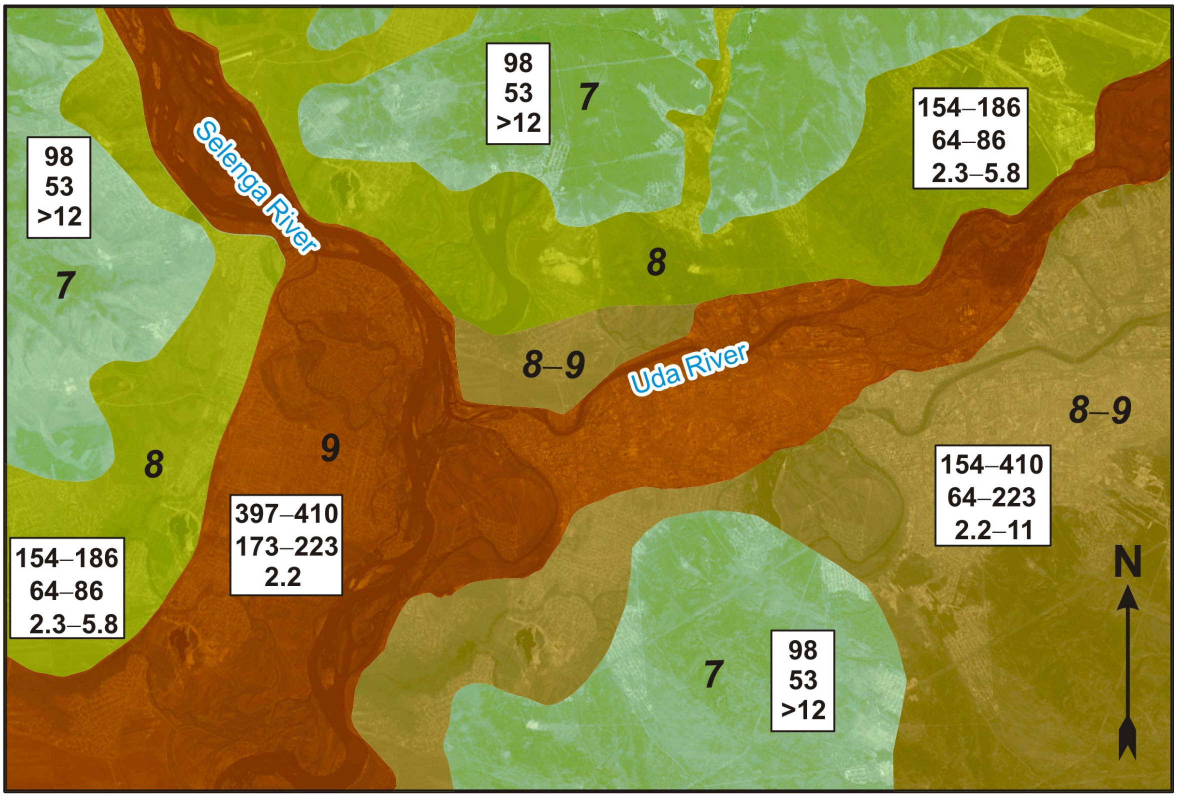

Fig. 10. The schematic map showing potential seismic hazard zones in the Ulan-Ude city territory. The map takes into account the soil and hydrogeological conditions of construction (reference seismic intensity – 8 points).

Numbers in boxes: top – maximum acceleration (cm/sec^2) for the horizontal component (NS); middle – maximum acceleration (cm/sec^2) for the vertical component (Z); bottom – resonant frequency (Hz) of the unconsolidated soil layer. 7–9 – potential maximum seismic intensity (UoM – point).

Рис. 10. Схематическая карта сейсмической опасности территории г. Улан-Удэ с учетом грунтовых и гидрогеологических условий строительства (исходная сейсмичность – 8 баллов).

В квадратах: верхнее значение – максимальные ускорения (см/с^2) для горизонтальной компоненты (NS), среднее значение – максимальные ускорения (см/с^2) для вертикальной компоненты (Z), нижнее значение – резонансные частоты (Гц) рыхлого слоя. 7–9 – вероятная максимальная интенсивность в баллах.

tion of the Ulan-Ude city territory by developing more detailed models with the application of the proposed technique.

4. Conclusion

The seismic hazard zonation of the Ulan-Ude city territory is a complex problem including studies by the seismic, seismotectonic, geotechnical and seismological methods. Each of the methods solves specific research problems, and their combination provides data for achieving the major objective to construct a seismic microzonation map of the territory.

At the current stage of studies, the indirect instrumental methods of seismic microzonation are used, and the types of rocks and soils prevailing in the studied territory are determined and classified by the propagation patterns of P- and S-waves. Using the acoustic impedance method, we estimate the incremental seismic intensity values for water-saturated and non-water-saturated sandy gravel-pebble sediments. The calculations are performed against parameters of the selected reference soil, i.e. the rocky soil with average seismic wave velocities in the upper 10-metre thick layer.

At the initial stage of forecasting how strong earthquakes can impact the rocks and soils under buildings and facilities in the Ulan-Ude city territory, we refer to the main parameters of significant ground movements that occurred in the Baikal rift zone in the past ten years. The established baseline seismic signal takes into account, in the first approximation, the main parameters of the potential earthquake occurrence zones and the previously established empirical relationships showing how the main dynamic characteristics of soil acceleration can vary depending on seismic event magnitudes and distances from earthquake foci. Based on such data, accelerograms can be forecasted for different epicentral distances and magnitudes and used for more reliable determinations of baseline seismic signals for the Ulan-Ude city territory with reference to the frequency characteristics.

It is shown that the established baseline signal is applicable, and the theoretical calculations are conducted on the basis of the seismicity-soil models characterizing bedrocks, medium soils and water-saturated soils (soil categories 1, 2 and 3, respectively). Based on the calculation results and the available geotechnical and hydrogeological data, and taking into account the soil and hydrogeological conditions for construction (the baseline seismic intensity of 8 points), a schematic map of seismic hazard is constructed for the Ulan-Ude territory in the scale sufficient for construction purposes. It shows that the seismic hazard is variable from 7 to 9 points through the studied territory. The map in the current format was used when we developed a detailed programme of studies aimed at seismic microzonation.

Obviously, the mapped data will be revised and updated in a more detail. Anyway, the obtained results can be useful today for planning possible construction sites in the Ulan-Ude city territory.

The technique of seismic microzonation mapping should be based on detailed measurements, and parameters for mapping the impact of seismic events should be determined at the precision level no less than that specified in requirements to engineering and design of earthquake-resistant buildings and facilities. It is recommended to apply GIS technologies and conduct more detailed engineering and seismic measurements in order to consolidate a database for construction of more detailed maps and schemes of the studied territory in smaller scales. In order to construct a digital map of seismic microzonation, the source materials should include topographical and special geotechnical and hydrogeological maps and schemes showing thickness of unconsolidated sediments, as well as various reference materials and data from other sources.

To complete seismic microzonation mapping, it is required to identify the potential seismic sources and characterize them at the new probabilistic level. It is thus needed to determine locations subject to deformation and active faulting, estimate the periods of earthquake recurrence, determine seismic intensity levels, and reveal probabilities of potential earthquake occurrence. Information on the potential seismic sources can facilitate forecasting of strong events for the Ulan-Ude city territory. Seismic wave propagation parameters and potential seismic impacts should be estimated for specific construction sites located in the city, and such estimations should be followed by calculations of response spectra and associated probabilities of the occurrence of strong earthquakes. Once the above-mentioned detailed data are consolidated, it will become possible to construct a map of seismic risks that can serve as a useful source of information for streamlining the regional construction policy.

This study was partially supported by the Russian Foundation for Basic Research (grants No. 14-45-04110 r_sibir_a and No. 14-05-31359 mol. a).

5. References

Drennov A.F., Dzhurik V.I., Serebrennikov S.P., Bryzhak E.V., Drennova N.N., 2013. Acceleration response spectra for the earthquakes of the southwestern flank of the Baikal Rift Zone. *Russian Geology and Geophysics* 54 (2), 223–230. http://dx.doi.org/10.1016/j.rgg.2013.01.008.

Drennov A.F., Dzhurik V.I., Serebrennikov S.P., Drennova N.N., 2011. Influence of the upper section on the amplitude-frequency content of a seismic signal by the example of seismic stations in the Baikal and the Transbaikal region. *Seismic Instruments* 47 (1), 57–65. http://dx.doi.org/10.3103/S0747923911010099.

Dzhurik V.I., 2014. Seismogeological, seismological and engineering seismological studies of the Laboratory of Engineering Seismology and Seismogeology of IEC RAS. *Geodynamics & Tectonophysics* 5 (1), 135–157 (in Russian) [*Джурик В.И.* Сейсмогеологические, сейсмологические и инженерно-сейсмологические исследования лаборатории инженерной сейсмологии и сейсмогеологии ИЗК СО РАН // *Геодинамика и тектонофизика*. 2014. Т. 5. № 1. С. 135–157]. http://dx.doi.org/10.5800/GT-2014-5-1-0121.

Dzhurik V.I., Serebrennikov S.P., Drennov A.F., Bryzhak E.V., Eskin A.Yu., 2012. Methodology of the establishment of a seismic signal for the seismic hazard zonation of urban agglomerations (a case of Irkutsk). *Izvestiya Irkutskogo gosudarstvennogo universiteta*, *Seriya* «*Nauki o Zemle*» (*The Bulletin of Irkutsk State University, Earth Sciences Series*) 5 (2), 96–110 (in Russian) [*Джурик В.И., Серебренников С.П., Дреннов А.Ф., Брыжак Е.В., Ескин А.Ю.* Методика формирования сейсмического сигнала с целью районирования сейсмической опасности городских агломераций (на примере г. Иркутска) // *Известия Иркутского государственного университета*. *Серия* «*Науки о Земле*». 2012. Т. 5. № 2. С. 96–110].

Dzhurik V.I., Serebrennikov S.P., Drennov A.F., Bryzhak E.V., Usynin L.A., Shagun A.N., Eskin A.Yu., 2011. On seismic hazard zonation of the city of Irkutsk. *Izvestiya Irkutskogo gosudarstvennogo universiteta*, *Seriya* «*Nauki o Zemle*» (*The Bulletin of Irkutsk State University, Earth Sciences Series*) 4 (2), 61–82 (in Russian) [*Джурик В.И., Серебренников С.П., Дреннов А.Ф., Брыжак Е.В., Усынин Л.А., Шагун А.Н., Ескин А.Ю.* К районированию сейсмической опасности территории г. Иркутска // *Известия Иркутского государственного университета*. *Серия* «*Науки о Земле*». 2011. Т. 4. № 2. С. 61–82].

Guidelines for Seismic Microzonation in Engineering Surveys for Construction, 1985. The USSR Gosstroy, Moscow, 73 p. (in Russian) [Рекомендации по сейсмическому микрорайонированию при инженерных изысканиях для строительства. М.: Госстрой СССР. 1985. 73 с.].

Guidelines for Seismic Microzonation in Engineering Surveys for Construction, 1986. The USSR Gosstroy, Moscow, 62 p. (in Russian) [Рекомендации по сейсмическому микрорайонированию при инженерных изысканиях для строительства. М.: Госстрой СССР, 1986. 62 с.].

Guidelines for Seismic Microzonation of Construction Sites for Transport Facilities, 2004. MDS 22-1. FGUP TsPP, Moscow, 48 p. (in Russian) [Методические рекомендации по сейсмическому микрорайонированию участков строительства транспортных сооружений. МДС 22-1. М.: ФГУП ЦПП, 2004. 48 с.].

Medvedev S.V., 1962. Engineering Seismology. Gosstroiizdat, Moscow, 260 p. (in Russian) [*Медведев С.В.* Инженерная сейсмология. М.: Госстройиздат, 1962. 260 с.].

Nazarov A.G., Shebalin N.V. (Eds.), 1975. The Seismic Scale and Seismic Intensity Measurement Methods. Nauka, Moscow, 279 p. (in Russian) [Сейсмическая шкала и методы измерения сейсмической интенсивности / Ред. А.Г. Назаров, Н.В. Шебалин. М.: Наука, 1975. 279 с.].

Pavlov O.V. (Ed.), 1984. Seismic Microzonation. Nauka, Moscow, 235 p. (in Russian) [Сейсмическое микрорайонирование / Ред. О.В. Павлов. М.: Наука, 1984. 235 с.].

Pavlov O.V. (Ed.), 1988. Assessment of Soil Conditions Impact on Seismic Hazard. Guidelines for Seismic Microzonation. Nauka, Moscow, 224 p. (in Russian) [Оценка влияния грунтовых условий на сейсмическую опасность. Методическое руководство по сейсмическому микрорайонированию / Ред. О.В. Павлов. М.: Наука, 1988. 224 с.].

Ratnikova L.I., 1984. Vibration calculations at the free surface at the points inside horizontally layered absorbent soil. In: O.V. Pavlov (Ed.), Seismic microzonation. Nauka, Moscow, p. 116–121 (in Russian) [*Ратникова Л.И.* Расчет колебаний на свободной поверхности во внутренних точках горизонтально-слоистого поглощающего грунта // Сейсмическое микрорайонирование / Ред. О.В. Павлов. М.: Наука, 1984. С. 116–121].

RB-006-98, 1998. Determination of Reference Seismic Vibrations of Soils for Design Basis. Gosatomnadzor of Russia, Moscow, 63 p. (in Russian) [*РБ-006-98*. Определение исходных сейсмических колебаний грунта для проектных основ. М.: Госатомнадзор России, 1998. 63 с.].

RSN 60-86, 1986. The RSFSR State Committee for Construction. The RSFSR Gosstroy, Moscow, 32 p. (in Russian) [РСН 60-86. Государственный комитет РСФСР по делам строительства: Госстрой РСФСР, 1986. 32 с.].

Seismic Surveying. Guidebook for Geophysicists. Nedra, Moscow, 462 p. (in Russian) [Сейсморазведка. Справочник геофизика. М.: Недра, 1981. 462 с.].

*SNiP II-7-81** (*Updated Revision*)*,* 2011. Construction in Seismic Regions. Ministry of Regional Development, Moscow, 71 p. (in Russian) [СНиП II-7-81*(Актуализированная редакция). Строительство в сейсмических районах. М.: Министерство регионального развития, 2011. 71 с.].

Solonenko V.P., Treskov A.A., 1960. The Middle Baikal Earthquake of 29 August 1959. Irkutsk Publishing House, Irkutsk, 36 p. (in Russian) [*Солоненко В.П., Тресков А.А.* Среднебайкальское землетрясение 29 августа 1959 года. Иркутск: Иркутское кн. изд-во, 1960. 36 с.].

The Map of General Seismic Zonation of the Russian Federation, 1999. Scale 1:8000000. The RF Ministry of Science and Technology, Schmidt UIPE, Moscow, 57 p. (in Russian) [Карта общего сейсмического районирования территории Российской Федерации. Масштаб 1:8000000. М.: Министерство науки и технологий РФ, ОИФЗ им. О.Ю. Шмидта, 1999. 57 с.].

The USSR Seismic Zonation Map, 1984. Scale 1:5000000. Explanatory Note. Nauka, Moscow, 32 p. (in Russian) [Карта сейсмического районирования СССР. М. 1:5000000. Объяснительная записка. М.: Наука, 1984. 32 с.].

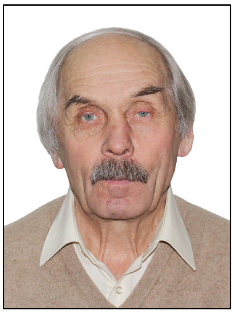

Dzhurik, Vasilii I., Doctor of Geology and Mineralogy, Head of Laboratory of Engineering Seismology and Seismogeology
Institute of the Earth's Crust, Siberian Branch of RAS
128 Lermontov street, Irkutsk 664033, Russia
✉ e-mail: dzhurik@crust.irk.ru

Джурик Василий Ионович, докт. геол.-мин. наук, зав. лаб. инженерной сейсмологии и сейсмогеологии
Институт земной коры СО РАН
664033, Иркутск, ул. Лермонтова, 128, Россия
✉ e-mail: dzhurik@crust.irk.ru

Tubanov, Tsyren A., Candidate of Geology and Mineralogy, Head of Laboratory of Earthquake Prediction
Geological Institute, Siberian Branch of RAS
6a Sakhyanova street, Ulan-Ude 670047, Russia
e-mail: geos@gin.bscnet.ru

Тубанов Цырен Алексеевич, канд. геол.-мин. наук, зав. лаб. методов сейсмопрогноза
Геологический институт СО РАН
670047, Улан-Удэ, ул. Сахьяновой, 6а, Россия
e-mail: geos@gin.bscnet.ru

Serebrennikov, Sergei P., Candidate of Geology and Mineralogy, Senior Researcher
Institute of the Earth's Crust, Siberian Branch of RAS
128 Lermontov street, Irkutsk 664033, Russia
e-mail: serebr@crust.irk.ru

Серебренников Сергей Петрович, канд. геол.-мин. наук, с.н.с.
Институт земной коры СО РАН
664033, Иркутск, ул. Лермонтова, 128, Россия
e-mail: serebr@crust.irk.ru

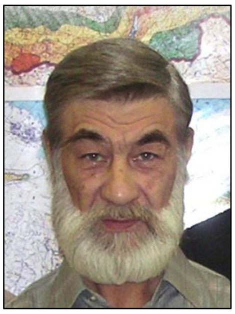

Drennov, Alexander F., Candidate of Geology and Mineralogy, Senior Researcher
Institute of the Earth's Crust, Siberian Branch of RAS
128 Lermontov street, Irkutsk 664033, Russia
e-mail: dzhurik@crust.irk.ru

Дреннов Александр Федорович, канд. геол.-мин. наук, с.н.с.
Институт земной коры СО РАН
664033, Иркутск, ул. Лермонтова, 128, Россия
e-mail: dzhurik@crust.irk.ru

Bryzhak, Evgenii V., Junior Researcher
Institute of the Earth's Crust, Siberian Branch of RAS
128 Lermontov street, Irkutsk 664033, Russia
e-mail: bryzhak@crust.irk.ru

Брыжак Евгений Вадимович, м.н.с.
Институт земной коры СО РАН
664033, Иркутск, ул. Лермонтова, 128, Россия
e-mail: bryzhak@crust.irk.ru

Eskin, Alexander Yu., Candidate of Geology and Mineralogy, Researcher
Institute of the Earth's Crust, Siberian Branch of RAS
128 Lermontov street, Irkutsk 664033, Russia
e-mail: eskin@crust.irk.ru

Ескин Александр Юрьевич, канд. геол.-мин. наук, н.с.
Институт земной коры СО РАН
664033, Иркутск, ул. Лермонтова, 128, Россия
e-mail: eskin@crust.irk.ru

GEODYNAMICS & TECTONOPHYSICS

PUBLISHED BY THE INSTITUTE OF THE EARTH'S CRUST
SIBERIAN BRANCH OF RUSSIAN ACADEMY OF SCIENCES

2015 VOLUME 6 ISSUE 3 PAGES 387–408 ISSN 2078-502X

http://dx.doi.org/10.5800/GT-2015-6-3-0187

Discussion

GENETIC SOURCES AND TECTONOPHYSICAL REGULARITIES OF DIVISIBILITY OF THE LITHOSPHERE INTO BLOCKS OF VARIOUS RANKS AT DIFFERENT STAGES OF ITS FORMATION: TECTONOPHYSICAL ANALYSIS

S. I. Sherman

Institute of the Earth's Crust, Siberian Branch of RAS, Irkutsk, Russia

Abstract: The paper presents the first tectonophysical reconstruction of initial divisibility of the protolithosphere as a result of convection in the cooling primitive mantle. Initial division of the protolithosphere into separate masses, i.e. prototypes of the blocks, and their size are predetermined by the emerging Rayleigh-Benard convection cells. In studies of geology and geodynamics, the Rayleigh-Benard convection cells were first referred to as a factor to explain the formation of initial continental cores. Considering the Rayleigh-Benard cells and their structural relics can help clarify initial divisibility of the protolithosphere and the origin of the major lithospheric plates, i.e. prototypes of continents. In our opinion, the initial mega-scale block structure of the protolithosphere and the emerging lithosphere were predetermined by the Rayleigh-Benard cells as they were preserved in the emerging lithosphere and their lower boundaries corresponded to the core-mantle boundary, i.e. one of the major discontinuities of the planet. Our theoretical estimations are in good agreement with the number and sizes of the Earth's theorized first supercontinents, Vaalbara and Ur.

In our tectonophysical discussion of the formation of the lithospheric block structure, we analyze in detail the map of modern lithospheric plates [*Bird*, *2003*] in combination with the materials from [*Sherman et al., 2000*]. In the hierarchy of the blocks comprising the contemporary lithosphere, which sizes are widely variable, two groups of blocks are clearly distinguished. The first group includes megablocks with the average geometric size above 6500 km. Their formation is related to convection in the Earth mantle at the present stage of the geodynamic evolution of the Earth, as well as at all the previous stages, including the earliest one, when the protolithosphere emerged. The second group includes medium-sized blocks with the average geometric size of less than 4500 km and those with minimum sizes, such as rock lumps. They reflect primarily the degradation of megablocks as a result of their destruction due to high stresses in excess of the tensile strength of the medium. This group may also include blocks which formation is related to convection in the upper mantle layer, asthenosphere. There are grounds to assume that through the vast intermediate interval of geologic time, including supercycles of Kenorlend, Rodin, and and partically Pangea, the formation of the large lithospheric blocks was controlled by convection, and later on, they were 'fragmented' under the physical laws of destruction of solid bodies. However, it is difficult to clearly distinguish between the processes that predetermine the hierarchy of formation of the block structures of various origins – sizes of ancient lithospheric blocks cannot be estimated unambiguously.

Thus, mantle convection is a genetic endogenous source of initial divisibility of the cooling upper cover of the Earth and megablock divisibility of the lithosphere in the subsequent and recent geodynamic development stages. At the present stage, regular patterns of the lithospheric block divisibility of various scales are observed at all the hierarchic levels. The areas of the lithospheric megaplates result from regular changes of convective processes in the mantle, which influenced the formation of plates and plate kinematics. Fragmentation of the megaplates into smaller ones is a result of destruction of the solid lithosphere under the physical laws of destruction of solid bodies under the impact of high stresses.

Key words: lithosphere, tectonic plates, blocks, convection, destruction, tectonophysics, divisibility of the lithosphere, Rayleigh-Benard cells, continents

Recommended by E.V. Sklyarov

For citation: *Sherman S.I.* 2015. Genetic sources and tectonophysical regularities of divisibility of the lithosphere into blocks of various ranks at different stages of its formation: tectonophysical analysis. *Geodynamics & Tectonophysics* 6 (3), 387–408. doi:10.5800/GT-2015-6-3-0187.

Генетические источники и тектонофизические закономерности разноранговой блоковой делимости литосферы на различных этапах ее формирования: тектонофизический анализ

С. И. Шерман

Институт земной коры СО РАН, Иркутск, Россия

Аннотация: Впервые проводится тектонофизическая реконструкция формирования первичной делимости протолитосферы в результате конвекции остывающей примитивной мантии. Формирующиеся в ней конвективные ячеи Рэлея-Бенара предопределяют размеры первичного разделения протолитосферы на отдельные массы – прообразы блоков. Ячеи Рэлея-Бенара не впервые используются в геологии и геодинамике. Первоначально на них ссылались для объяснения формирования первичных континентальных ядер. Обращение к ячеям Рэлея-Бенара и их структурным реликтам способствует пониманию того, как зарождается первичная делимость протолитосферы, которая трансформируется в крупные литосферные плиты – прообразы континентов. Именно консервирующиеся в формирующейся литосфере ячеи Рэлея-Бенара, нижняя граница которых корреспондировала с одним из главных разделов планеты – границей ядра, – предопределили первоначальную мегамасштабную блоковую структуру протолитосферы и формирующейся литосферы. Проведенные теоретические оценки сопоставлены и хорошо согласуются с количеством и размерами площадей первых гипотетических континентальных структур – суперконтинентов Ваальбара и Ура.

Продолжение тектонофизического разбора формирования блоковой структуры литосферы реализовано на детальном анализе карты современных литосферных плит [*Bird, 2003*] с привлечением фактических материалов [*Sherman et al., 2000*]. В широкой по размерам площадей иерархии блоков в современной литосфере Земли отчетливо выделяются две группы. Первая – мегаблоки, среднегеометрический размер которых превышает 6500 км. Их формирование на современном этапе геодинамического развития Земли, а также на всех предшествующих, в том числе и на самом раннем, при зарождении протолитосферы связано с конвекционными процессами в мантии Земли. Вторая группа – блоки со среднегеометрическим размером менее 4500 км, вплоть до минимального, соответствующего кусковатости горных пород, отражают, прежде всего, деструкцию мегаблоков в результате их разрушения под действием высоких внутренних напряжений, превышающих предел прочности среды. В этой же группе могут быть блоки, формирование которых также связано с конвекцией, охватывающей верхний мантийный уровень – астеносферу. Можно предполагать, что в громадном промежуточном интервале геологического времени, охватывающем суперциклы Кенорленд, Родинию и, частично, Пангею, формирование крупных литосферных блоков контролировалось конвекцией, а их дальнейшее «дробление» регулировалось физическими законами разрушения твердых тел. Однако четкую границу между процессами, определяющими иерархию формирования блоковых структур разного генезиса в прошедшие времена, провести трудно из-за неопределенности размеров литосферных блоков далекого прошлого.

Таким образом, конвекция в мантии является генетическим эндогенным источником первичной делимости остывающей верхней оболочки Земли, а также мегаблоковой делимости собственно литосферы в последующие этапы ее геодинамического развития. На современном этапе закономерности разномасштабной блоковой делимости литосферы прослеживаются на всех иерархических уровнях. Площади мегаплит литосферы – результат закономерных изменений конвективных процессов в мантии и их воздействия на формирование и кинематику плит; деструкция мегаплит на меньшие по площади блоки – результат закономерного дробления твердых тел литосферы при высоких напряжениях.

Ключевые слова: литосфера, тектонические плиты, блоки, конвекция, деструкция, тектонофизика, делимость литосферы, ячеи Релея-Бенара, континенты

> It is now evident that without understanding the Earth's evolution since the earliest stages when the covers of our planet and its continental crust were formed, it is difficult to determine locations where the major natural resources are accumulated and to reveal how various structural elements and a wide variety of igneous rocks were generated and continue their development.
>
> *Academician M.I. Kuz'min* [*2014*, p. 626]

1. Introduction

Initial divisibility of the Earth protolithosphere, i.e. the cooling outer hard cover of the planet, and its transformation with time into lithospheric blocks have not been properly studied yet in terms of the geodynamics of faulting, and tectonic regularities in divisibility of the lithospheric blocks of various ranks still need to be clarified. In the outer cover of the Earth, initial divisibility of the protolithosphere was due to cooling of the primitive mantle as a result of heat-gravitational convection manifested by Rayleigh–Bénard cells. In this study, we assess tectonophysical conditions for the generation of such cells and estimate potential sizes of the cells and amounts of primary proto-lithospheric cooling masses as prototypes of the blocks. Our estimations are consistent with the reconstructed first supercontinental cycles of the geodynamic evolution of the Earth. The block divisibility of the recent continental lithosphere is analysed in detail with reference to the map of present tectonic plates and blocks of the lithosphere and the cumulative plate count according to [*Bird, 2003*]. In addition to the data from [*Bird*, *2003*] which mainly cover megaplates and blocks of medium sizes, we analyse the parameters specified in [*Sherman et al., 2000*] for medium- and small-size blocks resulting from destruction of megaplates and blocks of the continental lithosphere. We propose regression equations describing divisibility of the continental lithosphere into blocks in a wide scale range, from medium- to small-sized blocks and rock fragments in outcrops. Such fragments result from destruction of medium- and small-sized blocks of the 'solid' lithosphere which takes place when internal stresses exceed the rock breakdown point, as described by exponential functions.

The occurrence of megablocks is related to mantle convection at the early stage of the evolution of the protolithosphere and subsequent stages of its transformation into the lithosphere through the global super-cycles of the geodynamic evolution of the Earth. The scale and organization of mantle convection are factors that predetermine divisibility of the lithosphere into megablocks through all the recent stages of its development, including the present stage.

2. The primary hot cover of the Earth, its composition and thickness

One of the most recent theoretical reviews of the early stages in the evolution of the Solar System and the geological history of the Earth was published by *M.I. Kuz'min* [*2014*] who rightly notes that the global academic geological community is challenged to estimate the time when the first continental crust was formed on the Earth. He develops the concepts co-authored with V.V. Yarmolyuk [*Yarmolyuk, Kuz'min, 2012*] on the formation of the outer and deep covers of the Earth, mantle processes and their impacts on the occurrence of surface structures, igneous rocks and ores.

The review [*Kuz'min*, *2014*] is based on the latest data on the origin of the Solar System and formation of the first continental rocks on the Earth, which contain zircon, the oldest mineral so far dated on the Earth. It is assumed that the Solar System formed from a gas-and-dust nebula 4.568 Ga ago. The continental crust was gradually growing from its recorded peak size (4.25 Ga) till 4.1 Ga, i.e. completion of the first eon in Earth's history, the Hadean. It seems to be a critical milestone in the early geological history of the Earth, followed by the Archaen history [*Kuz'min*, *2014*] – intensive cooling of the outer cover of the Earth commenced in this period. The heat flow was supported by the inner supply of heat generated due to gravitational compression of the planet while its solid body was formed [*Schubert et al., 2001*].

The estimated average temperatures of the mantle range from 1250–1350 °C to 1400 °C, and a roughly estimated temperature of the cooling Earth is 0 °C. In the present stage, the maximum temperature of the asthenosphere top is about 1350–1400 °C, and this temperature level is supported by various endogenous heat sources of the Earth and compensates heat losses caused by cooling. At the early stage of the Earth evolution, temperatures range from 0°C (or slightly above 0°C) at the Earth's surface to ~1350–1400 °C at the depth levels whereat temperature changes in the period of cooling are less significant due to heat influx. Under this assumption, the cover can be viewed as a gradually cooling low-viscous fluid body comprising the lower and upper layers which temperatures are significantly different. At the first stage when the outer cover of the Earth was formed, convection was the major mechanism of heat energy dissipation. It can be assumed that convection commenced in the pre-Katarchean eon and is underway until now, while the volumes and forms of convective flows have significantly changed with time. This time period agrees with the maximum age of about 4.1 Ga determined in [*Kuz'min, 2014*] for the start of the development of the protolithosphere that converted with time into the lithosphere which development is continued.

By its initial composition, the cooling upper cover of the Earth corresponds to the so-called primitive mantle, as evidenced by the composition of chondrites, i.e. stony (non-metallic) meteorites. The bulk composition of the primitive mantle is similar to the silicate cover of the Earth which was formed of the protoplanet material after the core had separated [*Hofmann*, *1997*]. It is noteworthy that variaitons in the composition of the primitive mantle do not influence estimations of temperatures at the lower boundaries of the primary mantle masses at the cooling surface of the Earth.

Physical parameters and the composition of the primitive mantle changed in the post-Archean period [*Vrevsky et al., 2010*] including several large cycles of the geodynamic development of the Earth, which were also related to mantle convection. By the Archean period, the Earth's crust was completely formed, and the upper boundary of the mantle convection processes went down into the Earth interior by dozens of kilometres [*Artemieva*, *2011*]. Responses of the upper solid part of the lithosphere as a rheological body to external impacts, especially external loading at different velocities, became different. In the former convective medium, convection in the cooling upper layer of the quasi-fluid was replaced by heat conduction/diffusion in the solid body. Studies of destruction of solid bodies and rank-variable fracturing and faulting are reported in many papers, including [*Peive*, *1990*; *Sherman et al.*, *1991, 1992, 1994*; *Seminsky*, *2003*; *Sherman*, *2002*, *2012*, *2014a*, *2014b;* and others], and it is established that physical laws of deformation and destruction of solid bodies are applicable.

A major challenge is to analyse, in a retrospective, the origin and initial formation of structures in the cooling protolithosphere which physical properties are assumed similar to those of the cooling low-viscous quasi-liquid mass. In such a medium, the maximum dissipation of energy was ensured by convection of various types, from structurally organized (Rayleigh–Bénard cells) to chaotic. This long-term process in the upper cover of the Earth had its regular features due to convective flows of the mega mass that was cooling it. The total thickness of the cooling mass of the primitive mantle can be assumed at 2900 km as the outer core boundary is located at this depth. Below we review hydrodynamic regularities in convection of cooling low-viscous materials and relic structures which are important for reconstructing the paleogeodynamic settings of the distant past and estimating probable dimensions of the primary blocks.

3. Key regularities in the formation of convective cells in cooling low-viscous materials and relic structures

It is most reasonable to believe that energy in the cooling low-viscous medium is dissipated by mantle convection that is most common manifested by Rayleigh–Bénard cells. The cooling surface of the Earth is assumed to behave as the cooling low-viscous medium much time before the Katarchean. Convection is generally reviewed below as a prerequisite for an assessment of conditions for initial divisibility of the outer cover of the protolithosphere.

General convection equation. The onset of convection occurs when the Rayleigh number reaches some critical value. The Rayleigh number, *Ra* is a dimensionless number predetermining the behaviour of gas, fluid or mass of a very low viscosity at a specified temperature gradient. When the Rayleigh number exceeds its critical value, the equilibrium of the cooling fluid is disturbed, which leads to the occurrence of convection flows and bifurcation. The bifurcation point is the critical value of the Rayleigh number:

$$\mathrm{Ra} = \frac{g\beta\Delta T L^3}{\upsilon\chi}, \tag{1}$$

where g is the gravity acceleration; L is the size of the fluid area; ΔT is the difference of temperatures at the surface and the lower layer of the fluid; υ is the kinematic viscosity of the fluid; χ is the heat conductivity of the fluid; β is the coefficient of thermal expansion of the fluid.

If the *Ra* value is small, convection does not start. If values of *Ra* are average, conditions are favourable for heat convection. Chaos occurs at high values of *Ra*. Values of *Ra* depend on combinations of all other parameters in equation 1. However, considering cooling of the primitive mantle in the model discussed here, the difference of temperatures and thickness of the cooling layer are the main parameters. It should be noted that patterns of convective cells are significantly dependent on dimensions of the cooling area. In such cases, an additional parameter needs to be introduced – aspect ratio, *G* [*Getling*, *1998*]:

$$G=L/h, \tag{2}$$

where L is horizontal size of an area (for a circular section, it corresponds to a radius); h is vertical size of the area.

The Grashof (*Gr*) and Prandtl (*Pr*) numbers are also widely used in studies of Rayleigh–Bénard cells, but not in this review.

In the below discussion of the natural conditions, we refer to cases with large values of *G*. Horizontal projections of cells are called planforms. The planforms may significantly vary depending on parameters of the medium. Planforms of the cells which are typical observed in the experimental and natural settings are reviewed below.

Planforms of convective cells, and physical conditions for their formation and stability. Three types of cell planforms are typically observed in the experiments [*Getling, 1998*]: two-dimensional bars, hexagonal cells and square/rectangular cells (Fig. 1).

As shown in Fig. 1a, 2D bars are oriented along axis X and parallel to axis *Y (x-bars)* or *vice versa,* and a cell is formed by a pair of neighbouring bars that occupy the entire spatial interval. In the bars, fluid circulates in vertical plane *X, Z* as well as in the opposite directions.

Hexagonal cells (Fig. 1, *b*) are composed by the superposition of three systems of bars which are located at angles 2π/3 to each other. Such cells are characterised by periodicity in directions of axes *X* and *Y* and invariant in case of rotation by an angle of 60°. A hexagonal cell is classified in l-type in liquid convection cases (Fig. 1, *b–l*) or g-type in gas convection cases (Fig. 1, *b–g*) with regard to a velocity vector, i.e. depending on whether the liquid is ascending in the central part of

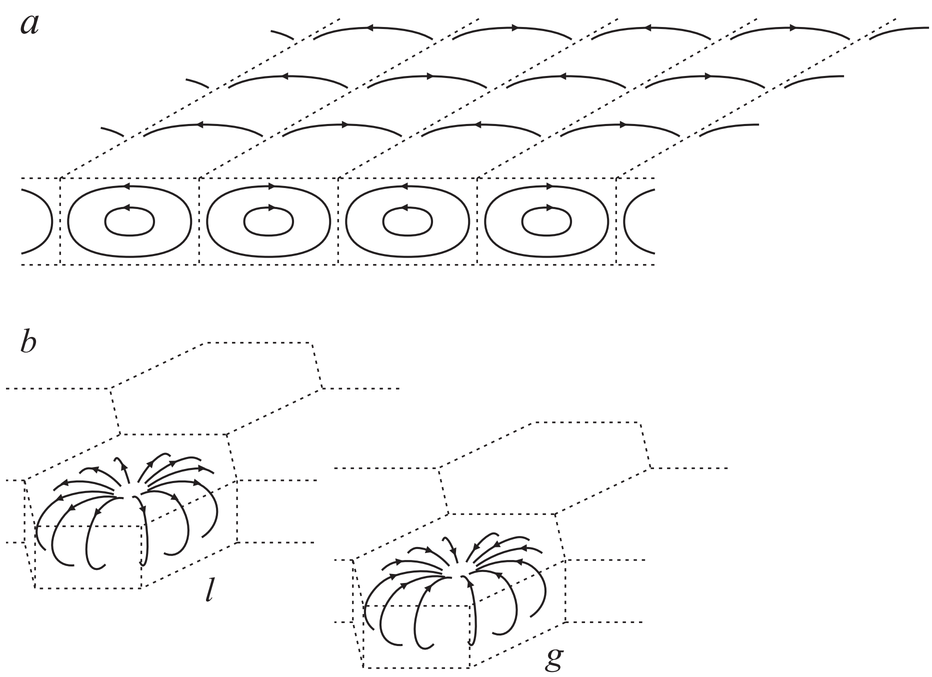

Fig. 1. Schematics of convective cells: *a* – 2D bars; *b* – hexagonal cells of l- and g-types (according to [*Getling, 1998*]).

Рис. 1. Схематическое изображение конвективных ячеек: *a* – двумерные валы; *b* – шестиугольные ячейки l- и g-типа (по [*Getling, 1998*]).

the cell or gas is descending, which, in its turn, is related to the temperature dependence from the viscosity of the medium. As known, with higher temperatures, viscosity of fluids decreases, while viscosity of gases increases. A velocity vector depends on a sign of derivative $d\gamma/dT$ which is negative for liquids and positive for gases. In the ascending convective flow, the material is always warmer than in the descending flow. Respectively, the liquid viscosity in the central parts of l-cells is lower, while the gas viscosity in the central parts of g-cells is higher. Circulation tends to follow the direction where the viscosity is lower in the centre of the cell. The stability of circulation trends, as well as the unchangeability of stationary flows of bars in relation to variations of defining parameters are estimated in a wide range of Rayleigh and Prandtl numbers, taking into account $k=2\pi/\lambda$, i.e. the number of waves of length λ per 2π radians, or the number of spatial intervals of waves per on 2π radians.

Square cells form systems which directions are rotated by a $\pi/4$ angle with respect to the coordinate system (*X, Y*).

Cell planforms are significantly influenced by even minor changes in the physical conditions of the medium and variations of its parameters included in the general equation of convection (see Equation 1). Two-dimensional bars are the main form of stationary convective structures produced by thermal-gravitational or thermocapillary convection mechanisms. In case of thermal-gravitational convection, the scale of flow can increase depending on ΔT and G (see Equations 1 and 2).

For the geological interpretation of the significance of cellular structures developing in cooling masses of the primitive mantle material, two facts are of importance: (1) relic structures, such as boundaries of cellular structures in the cooling protolithosphere, and subsequently, in the upper part of the lithosphere, and (2) relic masses of the deep mantle material, which were delivered into the Earth's upper horizons and cooled in zones of inter-cell boundaries, i.e. relic structures at the boundaries of the primary cellular formations. Specialists in the laws of Rayleigh–Bénard convection believe that two groups of boundaries in the Earth's upper horizons are of importance: boundaries between convective cells and border lines between orderly fragment-textures with different orientations of the bars, which comprise a more complex pattern (Fig. 2).

The most significant structural boundaries are lines bordering fragments-textures with different orientations of the bars [*Getling, 1998*]. The duration of their existence predetermines the stability of stationary convection flows and the geological significance of convection. According to [*Clever, Busse, 1996*], the hexagonal cells can be stable at $Pr \geq 1.2$ and $Ra \geq 3000$. If $Pr \leq 10$, the stability area of the hexagon cells looks like a band stretching from smaller to larger *Ra* values. If the

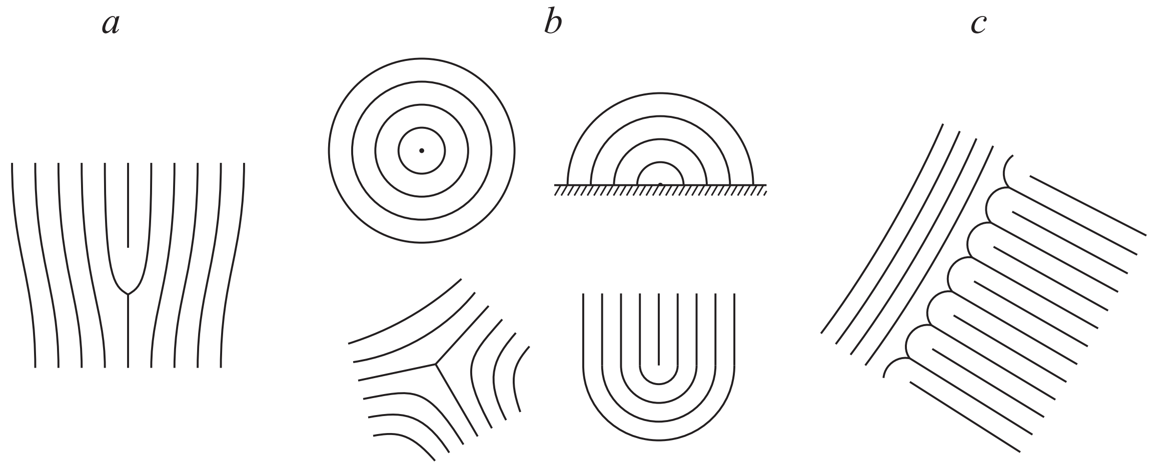

Fig. 2. Defects of bar structures (lines show boundaries of bars): *a* – dislocation; *b* – disclination (singularities of the focus type are below); *c* – structural boundary (according to [*Getling, 1998*]).

Рис. 2. Дефекты валиковых структур (линии соответствуют границам валов): *a* – дислокация; *b* – дисклинации (внизу сингулярности типа фокуса); *c* – структурная граница (по [*Getling, 1998*]).

Prandtl numbers are larger than 10, the area of stable hexagon cells is disturbed. In the experiments with *Ra* <3000, no stable hexagons are recorded.

The area of stable square cells is wider and covers the range of *Ra* from 4000 to 50000 with *Pr* varying from 2.5 to 16. When approaching the specified minimum value, the stability area narrows and becomes undetectable when *Pr*=2.5 [*Busse, Clever*, *1998*].

The material conveyed by the convective flows is hardening in places where the flows begin to move downward due to lower temperatures. Solidification takes place at the walls of thermal convection cells. Thus, when the vertical walls of the cells (i.e. surfaces of basalt prisms) are solidified, thermal convection continues inside the prisms until complete solidification of all the lava components. A photo in Fig. 3 shows the tops of basalt pillars with sagging centres of the columns which were the last to cool and solidify.

Based on the brief review of convective planforms and conditions of their formation, it is possible to reveal a common pattern of convection processes taking place during cooling of the homogeneous medium. In space and time, convection is manifested by a highly ordered flow of cooling quasi-liquid masses. The stability area is wide. As the area occupied by the flow is narrowing, stability is reduced as the characteristic scale of inhomogeneity of the structure is reducing [*Getling*, *1998*].

In standard experimental conditions, Rayleigh–Bénard convection cells occupy the entire thickness of the cooling layer, and their typical horizontal size is comparable to the vertical size or slightly exceeds it. In the majority of problems solved by geodynamics, it is assumed that convection cells occupy the entire mantle or partially occupy the layer or occur between the layers [*Kirdyashkin, Dobretsov*, *1991*; *Dobretsov et al.*, *2001*; *Trubitsyn V.P., Trubitsyn A.P.*, *2014*]. In such conditions, the main factor predetermining convection is viscosity of the medium, which is included in equations of interrelated Rayleigh, Grashof and Prandtl numbers. It can significantly increase or decrease their values and change the stability of convection accordingly. When viscosity varies by two or three orders (which may take place in the cooling upper part of the protolithosphere), the main viscosity gradient is in the topmost layer, wherein viscosity is increasing relatively faster than in the lower layers, and a hard cover is thus formed. Convection goes downward. Moreover, in the discussed cases of ascending convection, the cooling masses drift towards borders of the cells and subside due to gravity, which leads to simultaneous thickening of the emerging vertical border zone (i.e. a plane), which substance is more viscous. As the process develops further, such planes create favourable conditions for initial faulting of the lithosphere, and the lithospheric plates and large blocks are thus bordered by faults that are stable in time.

As a result of gradual cooling, a protective cap is formed over the cooling mass. As the process develops, the solid cap becomes thicker. The merger of the two descending cooling flows leads to further thickening of the emerging cap, and the partition between emerging blocks of the lithosphere is thus fixed.

Fig. 3. Solidified convection flows of basalt lava with 'sagging' surfaces in the centres of cells [*Shumilov, 2009*].

Рис. 3. Застывшие конвекционные потоки базальтовой лавы с «проседанием» поверхностей в центрах ячей [*Shumilov, 2009*].

Over time, the cap thickens and evolves into the brittle part of the lithosphere, while convection flows continue to function in the mantle and gradually drift to the lower hypsometric levels. The above-mentioned processes take place as the equilibrium of the convection system under the cap is disturbed due to changes of temperature and viscosity gradients. Conditions that are favourable for convection are now found at larger depths, and heat energy dissipation is facilitated. In this time period, the dominating convection occupying the entire mantle may be either replaced by convection in two layers or occur in a more complicated pattern.

Regardless of their planforms, the Rayleigh–Bénard cells give evidence that convection non-equilibrium can be a source of order. In comparison with the homogeneous hot mass, convective cells (regardless of their forms) can be regarded as highly organized structures facilitating the dissipation of energy and the formation of other, more stable forms in the cooling mantle. In this regard, the system remains open and continues to give the entropy.

Based on the above, cooling of the pre-Katarchean Earth's surface can be analysed with an assumption that the energy of the hot low-viscous body dissipated by thermal-gravitational convection. In this case, the Rayleigh–Bénard cells can be viewed as initial structures in the cooling mantle of the Earth, and boundaries between the cells were the first to get solidified and thus predetermined the contours of the future huge masses/blocks of the protolithosphere, which were the basis of Vaalbara and, may be, other theorized first supercontinents of the Earth.

4. The origin of the first largest local structures in the protolithosphere as viewed under the concept of convection in the cooling primitive mantle: a tectonophysical approach to paleogeodynamic reconstructions

In this study, a tectonophysical approach is proposed to analyse initial divisibility of the protolithosphere. The origin of the primary local structures / blocks is related to cooling of the Earth's surface layer composed by hot low-viscous masses of the primitive mantle. In such a medium, a relatively efficient way of heat dissipation is convection that is structurally arranged in Rayleigh–Bénard cells. Their relics, i.e. protocontinents, can be regarded as residual structures giving evidence of intitial atectonic divisibility of the protolithosphere. In this assumption, laws of their formation are determined by the laws of convection.

The cooling upper layer covered the entire primary surface of our planet. Its thickness was limited by the outer boundary of the almost completely formed core which was located at a depth of about 2900 km. It is known that the evolution of convection and its patterns are significantly influenced by dimensions (diameter and depth) of the area involved in convection (see Equation 2). For circular cross-sections in the experiments, the horizontal size of convection cells corresponds to the depth of the layer wherein convection takes place. Original convection experiments are described in the book by *N.L. Dobretsov et al.* [*2001*] who estimated the minimum horizontal size of convection cells in the lower mantle: "As follows from results of the experiments and the classical laws of convection, a cell can be stable if its transverse size is only by a factor of 1.8 times (or less) larger than its thickness" (p. 161).

Therefore, when convection takes place in a rather thick layer, a pattern of convection cells is compatible with the thickness of the layer. In our study of the mega-scale case, the horizontal size of the layer subject to convection is much larger than its vertical size, and the layer can thus be considered as a cooling flat body. The radius of the first round-shaped convective cells can amount to 2900–3000 km, and the distance between the emerging cooling boundaries of areas with descending masses (i.e. cell diameter) can be about 6000 km. In this case, the cell diameter can be numerically similar to the radius of the cooling Earth, and the cell area can be determined as the area of a spherical segment ($S_s=2\pi Rh$, where R is the Earth radius, and h is the thickness of the cooling layer, i.e. $R/2$). It amounts to πR^2 or about 3 steradians[1]. The total area of the Earth surface is $4\pi R^2$ (or $4\pi\ \Omega$). Under ideal conditions,

[1] Steradian, sr (Ω) a solid angle at the centre of a sphere subtending a section on the surface equal in area to the square of the radius of the sphere.

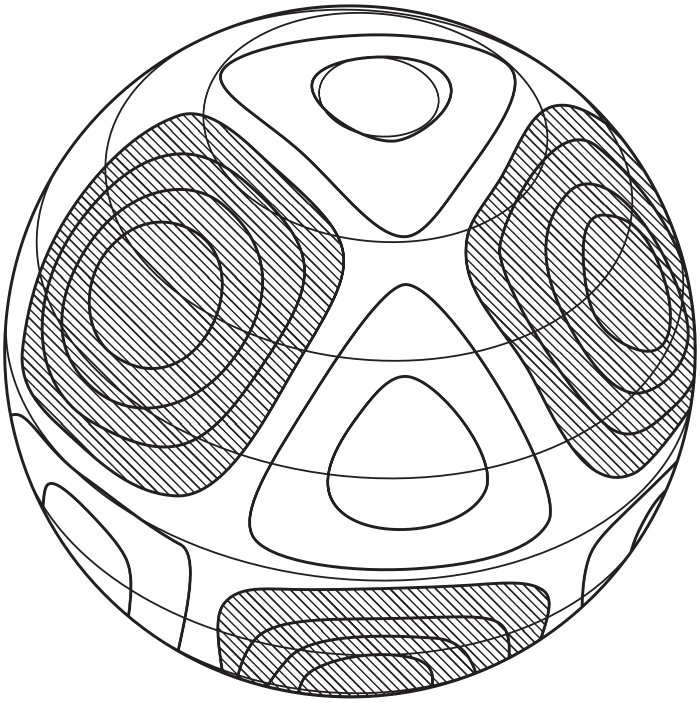

Fig. 4. Principal scheme of Rayleigh-Benard cells on the spherical surface.

Рис. 4. Принципиальная схема конвективных ячей Рэлея-Бенара на сфере.

as a maximum, four mega-large convective cells with an average area of about three steradians can form in the cooling upper cover of the Earth. It should be noted that the boundary of the bottom surfaces of the cells is the outer core of the Earth, which square area is four times smaller than that of the Earth surface. As the area of the bottom surfaces of the cells is restricted, the cells cannot achieve their potential maximum area on the surface. If a minimum surface area of a cell is one steradian, 12 cells as a maximum can form at the Earth surface. Therefore, the total number of the primary cells predetermining the initial divisibility of the emerging protolithosphere can range between 3–4 (minimum) to 12 (maximum) (Fig. 4).

Paleogeodynamic reconstructions shows that the first supercontinent Vaalbara (2.8–3.6 Ga) consisted of two major structures, i.e. protocontinents/cratons Kaapval and Pilbara [*Hazen, 2012*], which reflect the divisibility of the already solid protolithosphere and, may be, the divisibility of the emerging lithosphere. The concept that convection took place in the primitive mantle at the very early stages of the protolithosphere is not denied, although not widely discussed in the press [*Nebel et al., 2014*]. An acceptable argument is proposed by *I. Artemieva* and *B. Mooney* [*2001*] who consider the 'thermal' age of the Archean formations of the Earth.

There are grounds to state that convective processes in the Earth's mantle played the major role and were the basic criterion for the formation of the first largest block structures of the protolithosphere and also for subsequent transformations of such blocks into the lithospheric structures. According to the reconstructions, after Vaalbara supercontinent reconstructted Ura (about 3 Ga) and younger Kenorland (2100–2700 Ma), Columbia (1500–1800 Ma), Rodinia (750–1050 Ma) and Pangea (200–300 Ma) supercontinents [*Li et al., 2008*; *Lubnina, 2011*; *Hazen, 2012*]. About 200 mln years ago, Pangea broke apart to form Laurasia and Gondwana, i.e. groups of the southern and northern continents, respectively. The lithospheric megablocks have not been completely formed and destructed yet, and these processes are still ongoing at the present stage that is transitional to the formation of a new supercontinent. In the long-term geological history of the Earth, the number and dimensions of the lithospheric plates, which were actively involved in super cycles, were variable, but the blocks and plates *per se* have never disappeared completely (!). Since the Archean, these integral large bodies have been subject to many geodynamic catastrophes and reconstructions [*Li et al., 2008*], and their initial masses were partially 'lost' in some of the geodynamic cycles, regained in the others, converted into the six major lithospheric plates and survived! Strongly metamorphosed rocks of the Archaean age are observed in huge areas of the six continental lithospheric plates (Africa, Antarctica, North America, Eurasia, Australia and South America).

It is challenging to conduct a proper mathematical analysis of changes in the number of the lithospheric plates and their areas from one super cycle to another. The major cycles in the geodynamic evolution of the Earth and corresponding lithospheric plates of different shapes and kinematics are revealed by paleogeodynamic reconstructions. The lithospheric plates can provide for stable mantle convection at $Ra \leq 10^6$, but it becomes unsteady at $Ra \geq 10^7$ [*Getling, 1998*]. In response to changes in the convection pattern, the system of interacting lithospheric plates has to readjust itself. Numerical solutions of equations of energy, mass and momentum transfer suggest that mantle convection takes place while a set of plates is self-generated. According to [*Trubitsyn V.P., Trubitsyn A.P., 2014*], "the set of plates is inevitably generated, without requiring any additional boundary and initial conditions" (p. 146). The foregoing explains why the Earth has been subject to numerous transformations, including the catastrophic ones, in the natural course of its geodynamic evolution. Is this not a proof of the law of self-organized criticality which is discussed in [*Bak, 1996*]?

Obviously, mantle convection has been the major long-term genetic source providing for the cyclic geodynamic development of the entire lithosphere and its mega-block pattern.

In this regard, results of studies by P. Bird and co-authors [*Bird, 1988, 1998, 2003; Bird, Rosenstock, 1984; Bird et al., 2002*] are noteworthy – the hierarchy of the lithospheric plates and blocks is mathematically analyzed and the cumulative-number/area distribution is established. In our study, their results are complemented by experimental data published in [*Sherman et al., 2000*] (Table) and compared with other quantified information on the formation of plates and the fault-block structure of the lithosphere which vary in ranks at the present stage of development. We apply tectonophysical methods to analyse the hierarchy of the lithospheric plates and blocks with regard to their square areas at the present stage of the geodynamic evolution of the lithosphere. The analysis is aimed at identification of genetic sources and patterns of the lithosphere block divisibility at various hierarchical levels in different stages of the lithosphere evolution.

5. Recent hierarchic divisibility of the fault-block structure of the lithosphere: tectonophysical analysis

The subject of our analysis and the basis of further reconstructions is the map of lithospheric blocks of the Earth which is published in [*Bird, 2003*] (Fig. 5). Its main original features are (1) the pattern of the plates on the present surface of the Earth, and (2) calculations of plate areas in steradians (Table). To analyse ratios between areas and boundaries of the lithospheric plates, P. Bird showed them on the map close to each other in an arbitrary reconstruction (no more! – S. Sh.) of the 'intact' surface of the Earth. His map shows 52 plates of various ranks, including 'Manus microplate' which area is the smallest (0.0002 sr, see Table). Another specific feature of the map is the use of steradian, a dimensionless unit to estimate areas of plates and blocks, thus avoiding some skewing in quantitative comparisons of plates and blocks located at different latitudes of the sphere. Using this method, P. Bird presented in digital form a global set of boundaries of the present lithospheric plates and blocks of various sizes and ranks and estimated plate sizes. He established a mathematical regularity in the abrupt, non-uniform decrease of plate areas on the present Earth's sphere (columns 2 and 3 in Table). In Figure 6, the cumulative plate count as a function of plate areas in steradians is shown in the bilogarithmetic scale.

Based on Table (Nos. 1–52, column 3) supplemented by data from [*Bird, 1988, 1998, 2003; Bird, Rosenstock, 1984; Bird et al., 2002*], regression equations show that areas of the plates and blocks are decreasing with increasing numbers in the hierarchy, i.e. with transition from mega structures to regional and local ones (Fig. 6). The detailed interpretation of the plot is given in [*Bird, 2003*], and a brief is given in the figure caption (Fig. 6). The main regression line based on the data from Table has two bends.

According to *P. Bird* [*2003*], when plotted with logarithmic scales, the plates of areas between 0.002 and 1 steradian (from the relatively small Jian Fernandes plate, JZ to the large South America plate, SA) occur in numbers that roughly obey a power law:

$$\text{(cumulative count) } N\sim 7 \text{ (steradians)}^{-1/3} \text{ or } N\approx 7\Omega^{-1/3}. \quad (3)$$

This equation clearly reflects the scale relationship between the increase in the number of plates and a proportional reduction in their areas. This is characteristic of plates which areas are smaller than one steradian, i.e. plates with an average lateral size of about 4000 km (see Table).

For a more detailed tectonophysical analysis of the relationships between sizes of the lithospheric plates and blocks, the data published by P. Bird are supplemented by results of similar studies focused on intracontinental areas [*Sherman et al., 2000*]. The consolidated database provides for analyses of tectonophysical regularities in the block divisibility of the present 'solid' lithosphere. For now, seven major lithospheric plates (Nos. 1 to 7 in Table) are outside the scope of analysis and considered below in the closing statements. These major plates are viewed as original indicators of the initial and subsequent stages of lithosphere divisibility, and it seems more reasonable to consider them after reviewing and 'excluding' quantitative data on plates dominating in number in other hierarchic levels.

Table consolidates three data sets – [*Bird, 2003*] (Nos. 1 to 52, columns 1, 2 and 3), [*Cheremnykh, 1998*] and [*Sherman et al., 2000*] (Nos. 53 to 225) and thus provides for a more detailed consideration of the ratios of areas of medium- and small-sized lithospheric plates from [*Bird, 2003*] and the ratios of areas of continental lithospheric blocks from other publications. For an adequate comparison of plate areas in different hierarchical levels, the areas calculated in steradians are converted to measurement system SI and given in square kilometres and corresponding characteristic linear dimensions (columns 4 and 5, Table). In the recalculations, it is assumed that the Earth's radius is R=6371 km, and the equation from [*Sadovsky et al., 1987; Sadovsky, Pisarenko, 1991*] is used to calculate linear dimensions L_b and plate/block areas, S_b:

$$L_{\mathrm{b}} = \sqrt{S_{\mathrm{b}}}. \quad (4)$$

Regression equations are calculated for comparative analyses of the three above-mentioned data sets:

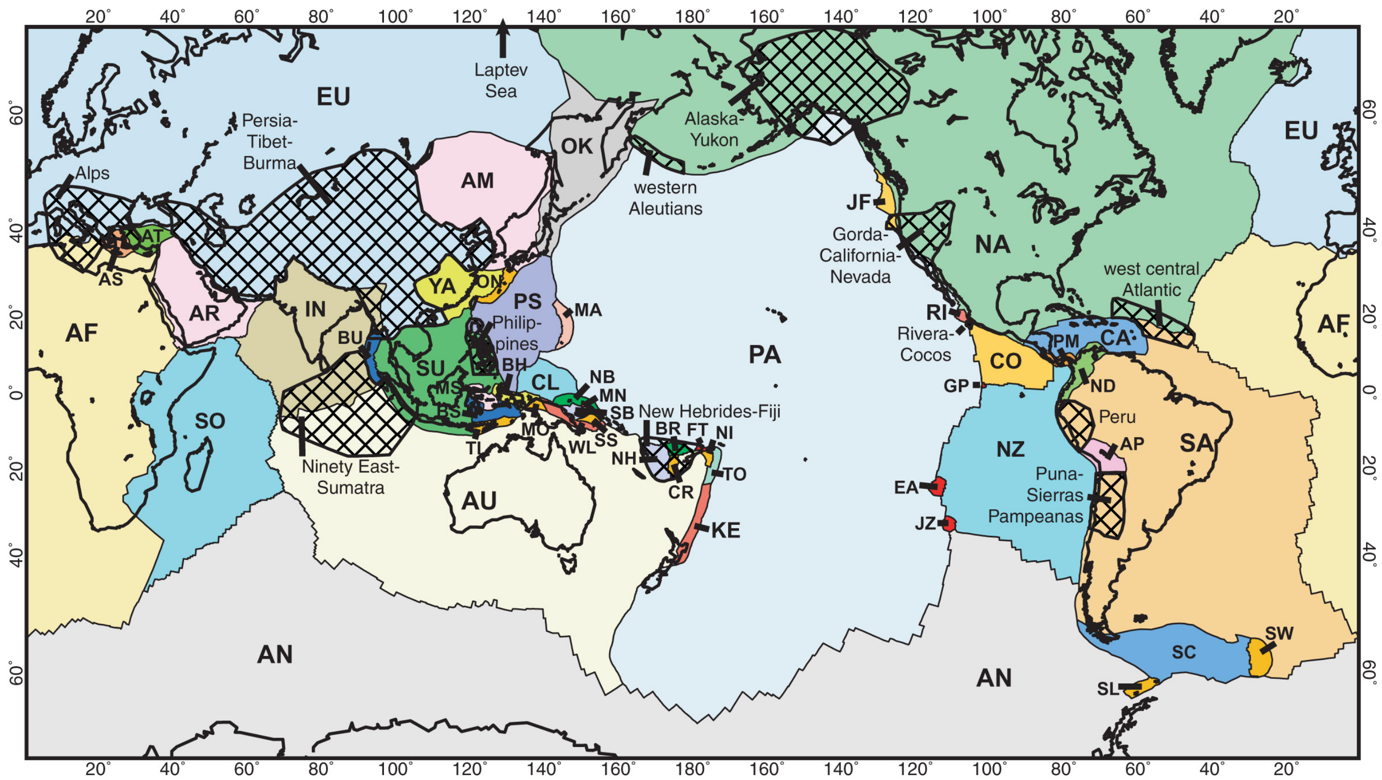

Fig. 5. Lithospheric plates mapped by P. Bird [*Bird, 2003*].

The 52 plates of his model PB2002 are shown with contrasting colours. Two-letter plate identifiers are explained in Table. The 13 cross-hatched areas are 'orogens' in which an Eulerian plate model is not expected to be accurate. Labels of small plates and orogens are offset (with leader lines) for clarity. Mercator projection.

Рис. 5. Карта литосферных плит по П. Бёрду [*Bird, 2003*].

Цветом выделены 52 плиты по модели PB2002. Наименование плит дано двойными буквами в соответствии с таблицей. Заштрихованные квадратной сеткой площади 13 районов соответствуют «орогенам», для которых модель вращения вокруг Эйлеровых полюсов не совсем точна. Двухбуквенное наименование мелких плит вынесено за их границы. Карта дана в проекции Меркатора.

(1) Regression by P. Bird, in its middle part showing areas from Jian Fernandes plate (JZ) to South America plate (SA), i.e. from mega- to medium-sized plates and blocks (Nos. 8 to 52, Table; equation 3 (in sr), and N_c=2259.3$L^{-0.67}$ (5) (symbol 1 in Fig. 7);

(2) Regression for the additional data on medium- and small-sized blocks (Nos. 53 to 225, Table; N_c=7049.1$L^{-0.91}$ (6) (symbol 2 in Fig. 7). An important indicator is an inclination angle of the regression curve. Equation 6 differs from Equation 5 by an increase of the inclination angle. Taking into account that Equation 6 is based on numerous data from geological and structural maps of continents in various scales, it can be noted that 'small-sized' blocks are more numerous that 'large' ones. This is a logical consequence following the ratio of data obtained by direct field observations that always record more small blocks on sites than large ones. The same is valid for even rock outcrops and evidenced by the plot from [*Bird*, *2003*] (see Fig. 6) at the second bend of the regression line;

(3) Regression for the consolidated data on plates and blocks of different characteristic sizes (No. 8 to 225, Table; N_c=3080.8$L^{-0.72}$ (7) (symbol 3 in Fig. 7). Regression (7) shows a significantly smoothed transition from small-sized lithospheric blocks to intra-continental blocks divisibility.

In general, equations 3, 5, 6 and 7 are similar, which suggests that the fragmentation of 'solid' rocks follows a physically uniform pattern, and, in more general terms, there is a tectonophysical law of the fault-block divisibility of the lithosphere which is valid for lithospheric blocks of a wide range of areas, from blocks which size is compatible with North and South America continents, i.e. nearly as big as lithospheric plates, to lump of rocks observed on small outcropped sites.

With account of our detailed studies of fault-block continental lithosphere structures of different ranks and in view of the identity of the physics of the process and the similarity of mathematical equations 5, 6 and 7, we construct a continuation of the regression curve

Areas and dimensions of lithospheric plates and blocks

Параметры площадей и размеров литосферных плит и блоков литосферы

#	Names of plates and blocks	Identifiers	Area, steradian	Area, km²	Average geometric size, km
1	**Pacific**	**PA**	2.57685	104593416	10227.09
2	**Africa**	**AF**	1.44065	58475466	7646.925
3	**Antarctica**	**AN**	1.43268	58151967	7625.744
4	**North America**	**NA**	1.36559	55428808	7445.053
5	**Eurasia**	**EU**	1.1963	48557388	6968.313
6	**Australia**	**AU**	1.13294	45985628	6781.27
7	**South America**	**SA**	1.03045	41825596	6467.271
8	Somalia	SO	0.47192	19155063	4376.65
9	Nazca	NC	0.39669	16101505	4012.668
10	India	IN	0.30637	12435448	3526.393
11	Sunda	SU	0.21967	8916326	2986.022
12	Philippine Sea	PS	0.13409	5442665	2332.952
13	Amur	AM	0.13066	5303442	2302.92
14	Arabia	AR	0.12082	4904040	2214.507
15	Okhotsk	OK	0.07482	3036917	1742.675
16	Caribbean	CA	0.07304	2964667	1721.821
17	Cocos	CO	0.07223	2931790	1712.247
18	Yangtze	YA	0.05425	2201988	1483.91
19	Scotia	SC	0.0419	1700706	1304.111
20	Caroline	CL	0.03765	1528200	1236.204
21	North Andes	ND	0.02394	971716	985.7566
22	Altiplano	AP	0.0205	832087.6	912.1884
23	Banda Sea	BS	0.01715	696112.3	834.3335
24	New Hebrides	NH	0.01585	643345.8	802.0884
25	Anatolia	AT	0.01418	575561.1	758.6574
26	Birds Head	BH	0.01295	525635.9	725.0075
27	Burma	BU	0.0127	515488.4	717.9752
28	Kermadec	KE	0.01245	505341	710.8734
29	Woodlark	WL	0.01116	452980.4	673.0382
30	Mariana	MA	0.01037	420914.6	648.7793
31	Molucca Sea	MS	0.0103	418073.3	646.5859
32	North Bismarck	NB	0.00956	388037	622.9261
33	Timor	TI	0.0087	353129.9	594.2473
34	Okinawa	ON	0.00802	325528.9	570.5514
35	Aegean Sea	AS	0.00793	321875.9	567.341
36	South Bismarck	SB	0.00762	309293.1	556.1412
37	Panama	PM	0.00674	273574.2	523.0432
38	Juan de Fuca	JF	0.00632	256526.5	506.4845
39	Tonga	TO	0.00625	253685.3	503.6718
40	Balmoral Reef	BR	0.00481	195236.2	441.8554
41	Sandwich	SW	0.00454	184277	429.2749
42	Easter	EA	0.00411	166823.4	408.4402
43	Conway Reef	CR	0.00356	144499.1	380.1304
44	Solomon Sea	SS	0.00317	128669.2	358.7048
45	Niuafo'ou	NI	0.00306	124204.3	352.4263
46	Maoke	MO	0.00284	115274.6	339.5211
47	Rivera	RI	0.00249	101068.2	317.9123
48	Juan Fernandez	JZ	0.00241	97821.03	312.7635
49	Shetland	SL	0.00178	72249.56	268.7928
50	Futuna	FT	0.00079	32065.82	179.0693
51	Galapagos	GP	0.00036	14612.27	120.8812
52	Manus	MN	0.0002	8117.928	90.09955
53	Angara-Ilim-9	IA_9		47520	218
54	Angara-Ilim-13	IA_{13}		34120	185
55	Angara-Ilim-3	IA_3		33620	183
56	Angara-Ilim-12	IA_{12}		31430	177
57	Prisayan-Enisei-2	IPE_2		28100	168
58	Baikal-Patom-3	$IIIBP_3$		27450	166
59	Angara-Ilim	IA_7		27380	165
60	Mirny	IM_1		25113	158
61	Stanovoy	IV_1		24000	155

Continuation of Table

Продолжение таблицы

#	Names of plates and blocks	Identifiers	Area, steradian	Area, km²	Average geometric size, km
62	Angara-Ilim	IA_{11}		23790	154
63	Angara-Ilim	IA_5		21770	148
64	Prisayan-Enisei	IPE_1		20700	144
65	Aldan	II_1		20680	144
66	Angara-Ilim	IA_{10}		18940	138
67	Selenga-Yablonovy	$IIISYa_{18}$		17730	133
68	Mirny	IM_{21}		17480	132
69	Mirny	IM_{25}		17300	131
70	Barguzin	$IIIB_3$		17060	131
71	Selenga-Yablonovy	$IIISYa_{15}$		16780	129
72	Angara-Ilim	IA_{15}		16380	128
73	Aldan	II_2		16370	128
74	Baikal-Patom	$IIIBP_1$		15700	125
75	Mirny	IM_{11}		15340	124
76	East Sayan	$IIIES_2$		15500	124
77	Selenga-Yablonovy	$IIISYa_5$		15200	123
78	Mirny	IM_7		14820	122
79	Selenga-Yablonovy	$IIISya_{21}$		14810	122
80	Stanovoy	IV_2		14580	121
81	Aldan	II_6		14360	119
82	Tunguska	IT_1		13900	118
83	Barguzin (IIIБ$_2$)	$IIIB_2$		13875	118
84	Mirny	IM_5		13800	117
85	Mirny	IM_{23}		13460	116
86	Aldan	II_5		13400	116
87	Selenga-Yablonovy	$IIISYa_{19}$		13470	116
88	Angara-Ilim	IA_1		13280	115
89	Aldan	II_{16}		13150	115
90	Baikal-Patom	$IIIBP_6$		13320	115
91	Selenga-Yablonovy	$IIISYa_{13}$		13200	115
92	Khentei-Dauria	$VKhD_2$		13260	115
93	Mirny	IM_2		13053	114
94	Barguzin	$IIIB_{13}$		12700	113
95	Angara-Ilim	IA_4		12470	112
96	East Sayan	$IIIES_{10}$		12400	111
97	East Transbaikalie	VET_3		12100	110
98	Barguzin	$IIIB_5$		11700	108
99	Selenga-Yablonovy	$IIISYa_4$		11600	108
100	Stanovoy	IV_{10}		11450	107
101	Mirny	IM_9		11170	106
102	Selenga-Yablonovy	$IIISYa_{20}$		11220	106
103	Angara-Ilim	IA_{16}		11020	105
104	Angara-Ilim	IA_8		10570	103
105	Sayan-Altai	$IIISA_3$		10320	101
106	Selenga-Yablonovy	$IIISYa_{16}$		10260	101
107	Stanovoy	IV_7		10300	101
108	Mirny	IM_3		9800	99
109	Mirny	IM_{14}		9730	99
110	Baikal-Patom	$IIIBP_4$		9800	99
111	Selenga-Yablonovy	$IIISYa_{23}$		9420	97
112	East Sayan	$IIIES_9$		9190	96
113	Selenga-Yablonovy	$IIISYa_{14}$		9200	96
114	Baikal-Patom	$IIIBP_{11}$		8900	94
115	Sayan-Altai	$IIISA_2$		8530	92
116	Barguzin	$IIIB_1$		8490	92
117	Barguzin	$IIIB_{11}$		8550	92
118	Baikal-Patom	$IIIBP_{12}$		8500	92
119	Stanovoy	IV_8		8530	92
120	East Transbaikalie	VET_1		8600	92
121	Mirny	IM_6		8250	91
122	Barguzin	$IIIB_{19}$		8100	90
123	Baikal-Patom	$IIIBP_2$		8100	90

Continuation of Table

Продолжение таблицы

#	Names of plates and blocks	Identifiers	Area, steradian	Area, km²	Average geometric size, km
124	Selenga-Yablonovy	$IIISYa_{24}$		8080	90
125	Selenga-Yablonovy	$IIISYa_{7}$		8000	89
126	Barguzin	$IIIB_{7}$		7700	88
127	Baikal-Patom	$IIIBP_{5}$		7600	87
128	Aldan	II_{9}		7315	86
129	Aldan	II_{18}		7400	86
130	Angara-Ilim	IA_{14}		7180	85
131	Barguzin	$IIIB_{21}$		7200	85
132	Baikal-Patom	$IIIBP_{15}$		7200	85
133	Selenga-Yablonovy	$IIISYa_{9}$		7300	85
134	Barguzin	$IIIB_{23}$		6850	83
135	East Sayan	$IIIES_{12}$		6750	82
136	Barguzin	$IIIB_{15}$		6750	82
137	Baikal-Patom	$IIIBP_{7}$		6700	82
138	East Transbaikalie	VET_{20}		6800	82
139	Dzhida	$(IIID_{1})$		6600	81
140	Khentei-Dauria	$(VKhD_{1})$		6500	81
141	East Transbaikalie	(VET_{16})		6500	81
142	East Transbaikalie	(VET_{17})		6500	81
143	Angara-Ilim	(IA_{2})		6400	80
144	Mirny	(IM_{24})		6400	80
145	Aldan	(II_{13})		6075	78
146	Barguzin	$(IIIB_{10})$		6000	77
147	Mirny	(IM_{4})		5800	76
148	Barguzin	$(IIIB_{14})$		5800	76
149	Baikal-Patom	$(IIIBP_{8})$		5850	76
150	Selenga-Yablonovy	$(IIISYa_{11})$		5800	76
151	Selenga-Yablonovy	$(IIISYa_{12})$		5800	76
152	Baikal-Patom	$(IIIBP_{9})$		5625	75
153	Dzhida	$(IIID_{2})$		5600	75
154	Mirny	(IM_{22})		5300	73
155	Stanovoy	(IV_{13})		5380	73
156	Stanovoy	(IV_{14})		5140	72
157	Barguzin	$(IIIB_{12})$		5100	71
158	Barguzin	$(IIIB_{22})$		5000	71
159	Stanovoy	(IV_{5})		5000	71
160	Angara-Ilim	(IA_{18})		4900	70
161	Aldan	(II_{8})		4855	69
162	Aldan	(II_{17})		4700	69
163	Stanovoy	(IV_{6})		4700	69
164	Mirny	(IM_{16})		4490	67
165	Pribaikalsky fault zone			4500	67
166	Stanovoy			4500	67
167	East Transbaikalie	VET_{8}		4500	67
168	Angara-Ilim	IA_{6}		4350	66
169	East Sayan	$IIIES_{8}$		4400	66
170	Baikal-Patom	$IIIBP_{13}$		4275	65
171	Mirny	IM_{13}		4040	64
172	Aldan	II_{12}		4050	64
173	Barguzin	$IIIB_{20}$		4150	64
174	Mirny	IM_{26}		4040	63
175	Baikal-Patom	$IIIBP_{10}$		4000	63
176	Selenga-Yablonovy	$IIISYa_{8}$		4000	63
177	East Transbaikalie	VET_{12}		4000	63
178	East Transbaikalie	VET_{15}		4000	63
179	Barguzin	$IIIB_{8}$		3800	62
180	Stanovoy	IV_{4}		3800	62
181	East Transbaikalie	VET_{13}		3800	62
182	Aldan	II_{10}		3740	61
183	Barguzin	$IIIB_{24}$		3600	60
184	Stanovoy	IV_{12}		3590	60
185	East Transbaikalie	VET_{7}		3590	60

E n d o f T a b l e

О к о н ч а н и е т а б л и ц ы

#	Names of plates and blocks	Identifiers	Area, steradian	Area, km^2	Average geometric size, km
186	Aldan (II$_{11}$)	II$_{11}$		3350	58
187	Baikal-Patom	IIIBP$_{14}$		3350	58
188	Aldan	II$_{15}$		3200	57
189	East Transbaikalie	VET$_4$		3300	57
190	East Transbaikalie	VET$_{21}$		3230	57
191	Aldan	II$_{14}$		3100	56
192	East Sayan	IIIES$_{11}$		3000	55
193	East Sayan	IIIES$_6$		2900	54
194	Barguzin	IIIB$_{16}$		2900	54
195	Stanovoy	IV$_{11}$		2900	54
196	Angara-Ilim	IA$_{17}$		2680	52
197	Mirny	IM$_{10}$		2690	52
198	Mirny	IM$_{15}$		2690	52
199	East Sayan	IIIES$_7$		2700	52
200	East Sayan	IIIES$_{13}$		2700	52
201	Barguzin	IIIB$_4$		2700	52
202	Selenga-Yablonovy	IIISYa$_{17}$		2700	52
203	Khentei-Dauria	VKhD$_4$		2690	52
204	East Transbaikalie	VET$_9$		2690	52
205	Mirny	IM$_{17}$		2470	50
206	East Sayan	IIIES$_3$		2475	50
207	Selenga-Yablonovy	IIISYa$_1$		2400	49
208	Khentei-Dauria	VKhD$_3$		2400	49
209	East Sayan	IIIES$_4$		2250	47
210	Selenga-Yablonovy	IIISYa$_{22}$		2240	47
211	Selenga-Yablonovy	IIISYa$_3$		2100	46
212	Mirny	IM$_{18}$		2000	45
213	Barguzin	IIIB$_9$		1800	42
214	East Sayan	IIIES$_5$		1700	41
215	Barguzin	IIIB$_{17}$		1600	40
216	Mirny	IM$_{27}$		1570	39
217	Selenga-Yablonovy	IIISYa$_{10}$		1500	39
218	Mirny	IM$_8$		1390	37
219	Barguzin	IIIB$_6$		1300	36
220	Barguzin	IIIB$_{18}$		1200	35
221	East Transbaikalie	VET$_5$		1100	33
222	East Transbaikalie	VET$_{11}$		1100	33
223	Mirny	IM$_{19}$		898	30
224	Mirny	IM$_{12}$		540	23
225	East Transbaikalie	VET$_{10}$		494	22

N o t e s. The table consolidates the following data: Nos. 1 to 52 – from [*Bird*, *2003*] with recalculation for area and linear sizes; Nos. 53 to 225 – according to [*Cheremnykh, 1998; Sherman et al., 2000*]. Names of the largest plates are bold printed; the general laws of destruction of solid bodies do not apply to such plates. Names and two-letter identifiers of megablocks correspond to [*Bird, 2003*]. Names of regional blocks are from the catalogue by A.V. Cheremnykh.

П р и м е ч а н и е. Данные с № 1 по 52 – по [*Bird*, *2003*] с пересчетом на площадные и линейные меры; с № 53–225 – по [*Cheremnykh, 1998; Sherman et al., 2000*]. Жирным шрифтом выделены самые крупные литосферные плиты, не вписывающиеся в общие закономерности деструкции твердого тела. Названия мегаблоков соответствуют карте [*Bird, 2003*], названия региональных блоков даны по авторскому каталогу А.В. Черемных.

derived from equation 3 (Fig. 7) in the direction that has been substantiated by P. Bird (see Fig. 6). The two regression lines based on equations 3 and 7 have the same physical meaning in bilogarithmical scales, and their middle parts are identical in Figure 6 and generally similar in Figure 7. The regression lines and the equations reflect destruction patterns of the 'solid' lithosphere in a wide variety of scales.

The area estimations obtained by different methods provide for well-reasoned general conclusions concerning regular patterns of the block destruction of the Earth's lithosphere at specified hierarchical levels. The reviewed results complement each other and extend our knowledge of destruction of the lithosphere as the solid cover of the Earth. It is now reasonable to briefly review the known laws of destruction of solid bodies, i.e. rocks.

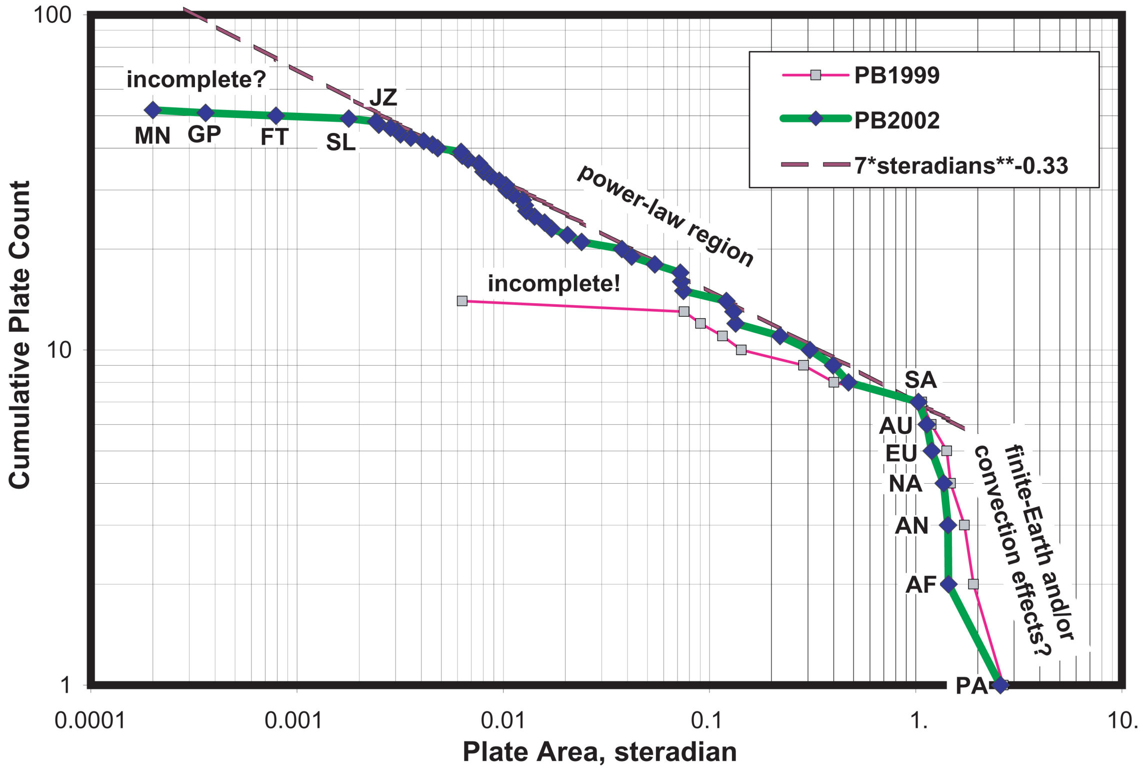

Fig. 6. Number of plates plotted as a function of area [*Bird, 2003*, fig. 19].

Curve PB2002 (green) refers to the model in Fig. 7. A relatively steady slope of the curve for plate areas between 0.002 and 1 steradian suggests a power law relationship between the number of plates and their minimum size. Flattening in the left segment of the curve is due to the model incompleteness, i.e. there are many plates of smaller sizes which are not included in model PB2002. An abrupt variation of the slope in the right segment of the curve suggests that very large plates are limited in their area because of the finite area of the Earth, and perhaps also by mantle convection tractions.

Рис. 6. График взаимосвязи количества плит как функции их площади (по [*Bird, 2003,* fig. 19]).

Кривая PB2002 (зеленый цвет) отражает ситуацию по данным рисунка 7. Относительно постоянный наклон кривой между границами площадей 0.002 и 1.000 стерадиан отражает взаимоотношения между числом плит и их минимальным размером. Изменение угла наклона в левой части графика отражает недостаточное число наблюдений, то есть имеются еще более мелкие, не учтенные в авторской модели блоки. Резкое изменение угла наклона в правой части графика показывает, что крупные плиты ограничены в своих размерах конечной площадью Земли, а также, возможно, конвекционными мантийными потоками.

6. Genetic sources of the lithosphere divisibility of various ranks

It can be stated that Equation 7 and its specific variants (see Fig. 7) are sufficient to fully describe relatively small lithospheric plates and intraplate blocks of the 'solid' lithosphere up to rock lumps. The experimental methods have yielded similar equations that mathematically reflect the physics of destruction of solid bodies in a wide range of scales (from a medium-size block which size amounts to a few thousand kilometres, to a rock fragment which diameter is a dozen centimetres), and there are ground to state that the block divisibility of the lithosphere follows laws of self-similarity. In the physics of destruction of solid and viscoelastic bodies, self-similarity patterns have been noted long ago at different scale levels. However, self-similarity in a very wide spectrum of hierarchical levels, from centimetres to mega sizes, has not been considered yet, and this paper is the first attempt in this respect.

Based on results of independent studies, *A.N. Kolmogorov* [*1941*] and *A.F. Filippov* [*1962*] established that rocks are subject to fragmentation according to the law of destruction of solid bodies, and the following exponential expression is linear in coordinates *lgN* and *lgL*:

$$lgN=f(lgL), \quad (8),$$

where *L* is the sample's arbitrary size, and *N* is the number of samples.

This conclusion includes the above-described empirical relationships that refer to large-size objects, such as lithosphere blocks of various ranks and, partly,

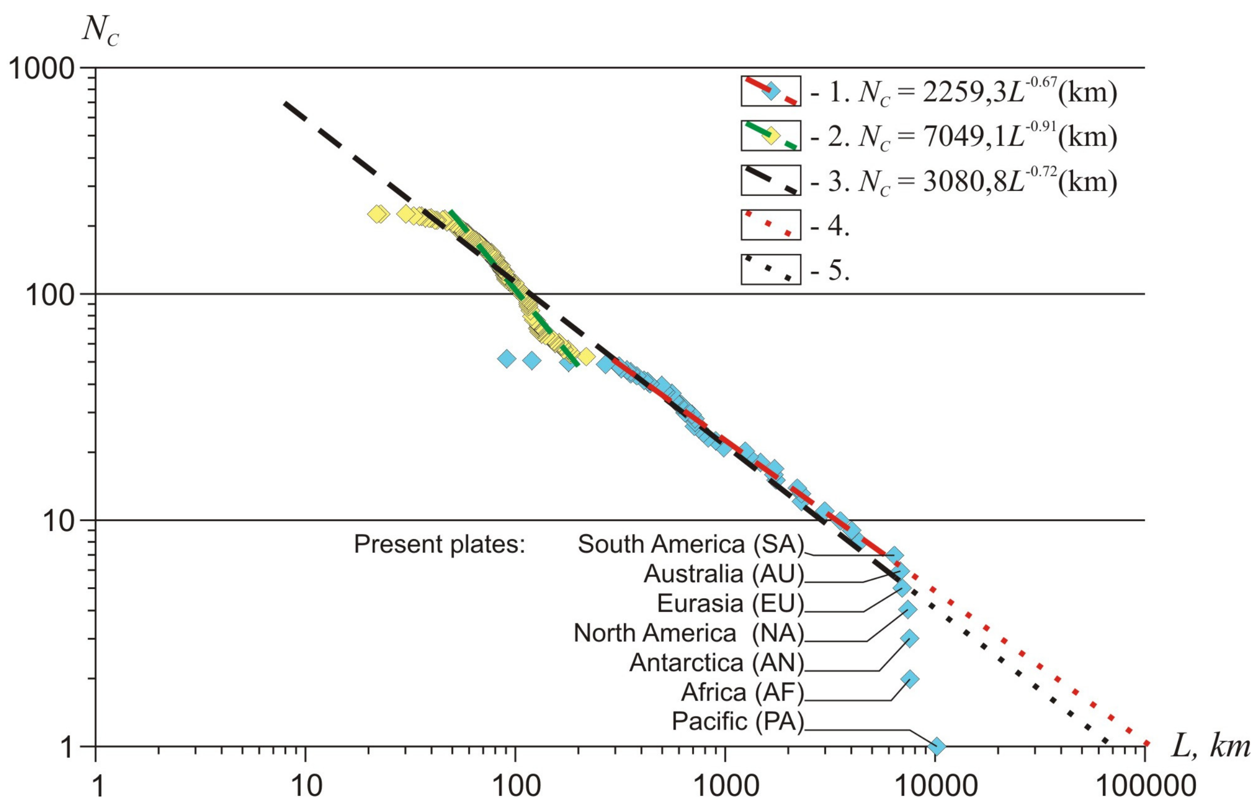

Fig. 7. Curves of relationships between medium lateral dimensions of lithospheric plates and blocks: 1 – according to [*Bird, 2003*]; 2 – according to [*Cheremnykh, 1998*; *Sherman et al., 2000*]; 3 – integrated regression line based on data (1) and (2); 4 – extrapolated regression line according to equation 1; 5 – extrapolated regression line according to equation 3. 3. N_c – row of lithospheric plates and blocks by average characteristic sizes L, km (analogues to reconstructions by P. Bird in steradians).

Рис. 7. Графики взаимосвязи средних поперечных размеров плит и блоков литосферы по: 1 – по данным [*Bird, 2003*]; 2 – по данным [*Cheremnykh, 1998*; *Sherman et al., 2000*]; 3 – совмещенная линия регрессии по данным [1 и 2]; 4 – экстраполяция линии регрессии по данным уравнения (1); 5 – экстраполяция линии регрессии по данным уравнения (3). N_c – последовательность литосферных плит и блоков в порядке увеличения усредненных характерных размеров L, км (по аналогии с построениями П. Бёрда в стерадианах).

faults in the upper brittle layer of the lithosphere, which cross each other to form the corresponding hierarchic group of the fault-block structures of the solid cover of the Earth [*Sherman*, *1977*; *Sherman et al., 2000, 2004; Seminsky, 2001, 2003*; and many others]. Obviously, this property mitigates issues related to 'buckling' of the regression lines at the boundaries of Juan Fernandez (JZ) and Shetland (SL) plates (0.00241 and 0.00178 sr, respectively). Buckling occurs due to the lack of quantitative data. In our study, this issue is completely eliminated after the additional data are supplemented (Table).

It can thus be stated that deformation and destruction of the Earth's solid cover under the influence of external loads take place according to a regular pattern. From certain hierarchical levels, residual destruction (in the form of blocks varying in ranks) is distributed in accordance with the characteristic sizes of the blocks and their number, as described by Equation 7. The regression is buckling at the transition from medium-sized plates to large ones (see Fig. 6 and 7) due to other reasons.

In terms of physics, buckling of the regression line showing the hierarchy of plate sizes versus plate areas (see Fig. 6 and 7) is related to sources of rank-variable destruction of the lithosphere as a solid body. The buckle occurs abruptly at the transition from a few very large lithospheric plates to medium-sized plates and small blocks that are statistically abundant. The regression curve is buckled from a very steep angle to a more gentle one at the boundary between South America (area of 1.03 sr) and Somali plates (area of 0.47 sr). A jump occurs when the square area is doubled. For six large plates (Africa, Antarctica, North America, Eurasia, Australia and South America; data on Pacific plate are not taken into account), the regression curve is a steep, almost vertical line. Their areas are nearly similar and almost unchangeable. Naturally, they are governed by another law of formation of solid lithospheric masses, which is not consistent with the laws of destruction of solid bodies. In this respect, *P. Bird* [*2003*] also notes that the fact that large plates are clearly established is indicative of a very weak dependence of plate areas from any quantitative parameters, except for the Earth radius. When the Earth radius is used as a natural independent unit to measure solid angles in steradians, it is clearly revealed that very large areas of the above-mentioned six plates (Pacific plate is an exception) are almost similar. According to *P. Bird* [*2003*], typical areas of the large lithospheric plates correlate with mantle convection: "....this characteristic size seems more consistent with whole mantle convection than with layered convection". Indeed, the formation of the largest blocks (i.e. primary lithospheric plates originating at the stage when the protolithosphere was formed and later periods) is more in line with mantle convection than destruction of the solid body. The author fully shares these assumptions by P. Bird as they are supported by all the above discussed data, arguments and tectonophysical calculations.

As shown by the analysis of areas of the rank-variable present lithospheric plates (see Table), the total area of the seven largest plates (less than 14 % of the total number of plates) is about 10.15 steradians, and they occupy almost 81 % of the entire surface of the Earth. The area of the six continental plates (Africa, Antarctica, North America, Eurasia, Australia and South America) is more than 60 % of the planet's surface area. They are well traced in the history of Pangea and less evidently in the more distant past. Through the history of the Earth, these huge integral bodies were subject to numerous geodynamic catastrophes and transformations. Some of them lost much of the initial mass, others completely 'disappeared' in the mantle, while some of the plates have grown in size. Therefore, from one super-continental cycle to another, the lithospheric blocks differ in number and kinematics. Based on the available data, it is impossible to state for sure which of them were formed before the Archaean and are still in place, and which of them were more or less transformed. It is challenging to restore the genesis of structural relics in the cooling medium of the protolithosphere and those in the lithosphere medium with reference to the very distant past. It is an inverse problem with unambiguous solutions. As a definite and indisputable conclusion cannot be drawn, one can only assume that convection is the most probable and better argumented physical process that took place when the low-viscous medium of the protolithosphere was cooling down to form large masses in the first hypothetical (?) supercycles of Vaalbara and Ur, and, finally, convection can be viewed as a mechanism predetermining the present shape of the Earth's continents. It is most probable that the megablocks were fragmented in the similar pattern in Kenorlend and later supercycles. However, based on the available materials, it is possible only to justify the block structure of the present stage.

It is reasonable here to quote the book by *N.L. Dobretsov et al.* [*2001*]: "In the history of the Earth, convection in two layers was replaced by convection in the entire mantle and vice versa, and this might have taken place several times... Therefore, it is most likely that in the Earth's history, convection in the entire mantle was replaced by two-layer convection. Another possible scenario is more complicated: about 2.5 Ga ago, two-layer convection was replaced by convection in the entire mantle [*Maruyama*, *1994*]; after a period of one billion years, two-layer convection occurred again [*Honda*, *1995*], and, finally, a transition back to convection in the entire mantle took place in the past 150-100 Ma [*Trubitsyn, Rykov, 2000*]" (p. 111). Convection predetermines the major cycles in the geodynamics of the Earth and fragmentation of the lithosphere into megablocks. The latter are destructed under the physical laws of destruction of solid rocks. Currently, destruction of the lithosphere is actively continued in seismic zones of the continental lithosphere and zones of subduction and spreading at the margins of the lithospheric blocks.

7. Discussion

Publications on convection in the Earth's mantle and its role in global geodynamic processes are quite numerous. In the majority of papers, recent geodynamic processes are considered with an assumption that the evolution of convection in the mantle and asthenosphere took place in two- or three-layer or more complicated patterns [*Lobkovsky, 1988; Lobkovsky, Kotelkin, 2000; Lobkovsky et al., 2004; Rykov, Trubitsyn, 1994a, 1994b; Trompert, Hansen, 1988; Trubitsyn, Rykov, 2002; Trubitsyn V.P., Trubitsyn A.P., 2014*]. Mantle convection was discussed in a number of publications many years ago, the most famous of which are [*Pekeris*, *1935*; *Molnar et al*., *1979*].

According to [*Molnar et al*., *1979*], large sizes of continental plates are related to convection in the entire mantle, and horizontal dimensions of the plate depend on the depth of the convective process. Their analysis is based on the proportional change in the length of the subduction zone on the surface and the velocity of its sinking which depends on heat assimilation in the absence of a barrier at the border with the lower mantle.

The two-layer convection in the Earth mantle is described by *L.P. Zonenshain* and *M.I. Kuz'min* [*1993*] and reconstructed in a world-known scheme by *S. Maruyama* [*1994*].

To sum up this very brief information on the two-layer models of convection in the Earth mantle, it is worthy to refer again to the book by *N.L. Dobretsov et al.* [*2001*] who give much attention to convection as an important component of geodynamic processes. In their book, prior to the geodynamic analysis of processes in the mantle, asthenosphere and lithosphere, they provide a comprehensive description of the two main models of thermal-gravitational convection which provide the basis for a variety of geodynamic reconstructions. In the first model, convection take place in the entire mantle, from boundaries of the lithosphere base (30 to 100km) to the upper limit of the core (about 2900 km). The second model shows convection in the upper and lower mantle without any significant mass transfer between the two layers. In [*Dobretsov et al*., 2001], the authors focus on the complexity of geodynamic processes in the mantle and discuss their evolution up to the present stage of the Earth development. The concept of two-layer mantle convection is convincingly proved by results of many original experiments conducted by the authors with the use of specially designed installations [*Kirdyashkin, Dobretsov, 1991; Dobretsov, Kirdyashkin, 1993*]. Besides, they estimated parameters of convection. Specifically, based on the video records, they revealed flow lines in the two-layer fluid convection system and estimated horizontal and vertical velocities of the flows. Their very important observation is that convection flows above and below the interface go in different directions, and this is an evidence that vector directions of horizontal convection flows in the layers located one upon another are not interrelated. According to [*Dobretsov et al*., *2001*], vectors of the vertical flows are similar, and this fact emphasises the major role of convection in the mantle which provides for dissipation of heat energy. Important are the digital parameters and vectors of flow velocities and cell sizes. In the bottom layer (which is thicker), cell sizes are proportional to the layer's thickness, and flow velocities are lower. In [*Dobretsov et al*., *2001*], the concept of the two-layer convection in the Earth's mantle is well established by the experimental and actual observation data. Nonetheless, the authors note: "In the majority of cases, the geochemical data support the two-layer convection model, while much geophysical data may be interpreted in favour of convection in the entire mantle" (p. 108).

In [*Trubitsyn V.P., Trubitsyn A.P., 2014*], a digital model is described in detail to show that the present set of the lithospheric plates is a result of the evolution of convection. It provides an insight into the possible mode of flows in the entire mantle, movements of the masses between the upper and lower mantle, as well as between the central and lateral limits of the convection cells. Using equations, V.P. Trubitsyn and A.P. Trubitsyn calculated temperature, viscosity and velocity of mantle convection flows generated by effective diffusion-dislocation creeping in the absence of pseudo-plastic deformation and in case of the very hard lithosphere. In particular, their temperature distribution pattern shows that small cold descending flows, i.e. small-scale convection, occur under the lithosphere. The estimated scheme of convection in the entire mantle in [*Trubitsyn V.P., Trubitsyn A.P., 2014*] is consistent with our ideas of the primary genetically emerging block divisibility of the protolithosphere. In the initial state, the protolithosphere remains uniform at the surface, has a roughly constant thickness and increased quasi-strength at the primary inter-cell boundaries whereat the viscosity of the medium is increasing due to cooling of the protolithosphere.

Regretfully, initial divisibility of the emerging upper solid cover of the Earth is taken into account by few researchers in their estimations, while such divisibility is one of the most likely results of convection in the cooling protolithosphere. This is obviously due to the absence of direct geological materials and the lack of appropriate paleo-reconstruction methods that can integrate geological, geophysical and geochemical databases. As shown by our study, computational methods are helpful, to a certain extent, in solving ill-conditioned inverse problems to reconstruct processes and structures of the distant past.

The concept of the single-layer convection, assuming that convection took place through the ½-radius depth at the initial stage when the Earth lithosphere was formed, is acceptable and seems quite realistic, even though the literature is still insufficient on this subject. This justifies the author's efforts to clarify the origin of divisibility of the primary non-solid, almost continuous cover of the Earth which evolution history includes periods of the Phanerozoic and contemporary faulting in the lithosphere and its fragmentation under the laws of destruction of solid bodies. It can be noted in general that the upper cover of the Earth is subject to destruction in a regular pattern, from larger to smaller masses.

8. Conclusion

This study is pioneering in tectonophysical reconstruction of initial divisibility of the protolithosphere as a result of convection in the cooling primitive mantle. Initial division of the protolithosphere into separate masses, i.e. prototypes of the blocks, and their size was predetermined by the emerging Rayleigh–Bénard convection cells. In studies of geology and geodynamics, the Rayleigh–Bénard convection cells were first referred to as a factor to explain the formation of initial continental cores. Considering the Rayleigh–Bénard cells and their structural relics can help clarify initial divisibility of the protolithosphere and the origin of the major lithospheric plates, i.e. prototypes of continents.

In our opinion, the initial mega-scale block structure of the protolithosphere and the emerging lithosphere were predetermined by the Rayleigh–Bénard cells as they were preserved in the emerging lithosphere and their lower boundaries corresponded to the core-mantle boundary, i.e. one of the major discontinuities of the planet. Our theoretical estimations are in good agreement with the number and sizes of the Earth's theorized first supercontinents, Vaalbara and Ur.

In our tectonophysical discussion of the formation of the lithospheric block structure, we analyse in detail the map of modern lithospheric plates [*Bird*, *2003*] in combination with the materials from [*Sherman et al., 2000*]. In the hierarchy of the blocks comprising the present lithosphere, which sizes are widely variable, two groups of blocks are clearly distinguished. The first group includes megablocks with the average geometric size above 6500 km. Their formation is related to convection in the Earth mantle at the present stage of the geodynamic evolution of the Earth, as well as at all the previous stages, including the earliest one, when the protolithosphere emerged. The second group includes medium-sized blocks with the average geometric size of less than 4500 km and those with minimum sizes, such as rock lumps. They reflect primarily the degradation of the megablocks as a result of their destruction due to high internal stresses in excess of the tensile strength of the medium. This group may also include blocks which formation is related to convection in the upper mantle layer, asthenosphere. There are grounds to assume that through the vast intermediate interval of geologic time, including supercycles of Kenorlend, Rodin, and Pangea, the formation of the large lithospheric blocks was controlled by convection, and later on, they were 'fragmented' under the physical laws of destruction of solid bodies. However, it is difficult to clearly distinguish between the processes that predetermine the hierarchy of formation of the block structures of various origins – sizes of ancient lithospheric blocks cannot be estimated unambiguously.

Thus, mantle convection is a genetic endogenous source of initial divisibility of the cooling upper cover of the Earth and megablock divisibility of the lithosphere in the subsequent and recent geodynamic development stages. In the present stage, regular patterns of the lithospheric block divisibility of various scales are observed at all the hierarchic levels. The areas of the lithospheric megaplates result from regular changes of convection processes in the mantle, which influenced the formation of plates and plate kinematics. Fragmentation of the megaplates into smaller ones is primarily a result of destruction of the solid lithosphere under the physical laws of destruction of solid bodies under the impact of high stresses.

9. Acknowledgements

The author wishes to express his sincere gratitude to his colleagues: M.I. Kuz'min, Academician of RAS, E.V. Sklyarov, Corresponding Member of RAS, V.A. San'kov, Head of the Laboratory of Recent Geodynamics, IEC SB RAS, professor R.M. Lobatskaya and Ph.D. A.I. Kiselev for constructive scientific discussions that were helpful for improving the paper. The author appreciates the help provided by A.V. Cheremnykh in consolidating the input data and measurements of continental lithospheric blocks varying in hierarchic levels.

The study was conducted under the Research Plan of the Laboratory of Tectonophysics, IEC SB RAS with a partial financial support by the Russian Foundation for Basic Research (Grant No. 15-55-53023).

10. References

Artemieva I.M., 2011. The lithosphere: An interdisciplinary approach. Cambridge University Press, Cambridge, 794 p.

*Artemieva I.M., Mooney W.*D., 2001. Thermal thickness and evolution of Precambrian lithosphere; a global study. *Journal of Geophysical Research* 106 (B8), 16387–16414. http://dx.doi.org/10.1029/2000JB900439.

Bak P., 1996. How Nature Works: The Science of Self-Organised Criticality. Copernicus Press, New York, 212 p.

Bird P., 1988. Formation of the Rocky Mountains, western United States: A continuum computer model. *Science* 239 (4847), 1501–1507. http://dx.doi.org/10.1126/science.239.4847.1501.

Bird P., 1998. Kinematic history of the Laramide orogeny in latitudes 35°–49°N, Western United States. *Tectonics* 17 (5), 780–801. http://dx.doi.org/10.1029/98TC02698.

Bird P., 2003. An updated digital model of plate boundaries. *Geochemistry Geophysics Geosystems* 4 (3), 1027. http://dx.doi.org/10.1029/2001GC000252.

Bird P., Kagan Y.Y., Jackson D.D., 2002. Plate tectonics and earthquake potential of spreading ridges and oceanic transform faults. In: S. Stein, J.T. Freymueller (Eds.), Plate Boundary Zones. AGU Geodynamics Series, vol. 30. AGU, Washington, D.C., p. 203–218. http://dx.doi.org/10.1029/GD030p0203.

Bird P., Rosenstock R.W., 1984. Kinematics of present crust and mantle flow in southern California. *Geological Society of America Bulletin* 95 (8), 946–957. http://dx.doi.org/10.1130/0016-7606(1984)95<946:KOPCAM>2.0.CO;2.

Busse F.H., Clever F.M., 1998. Asymmetric squares as an attracting set in Rayleigh-Benard convection. *Physical Review Letters* 81 (2), 341–344. http://dx.doi.org/10.1103/PhysRevLett.81.341.

Cheremnykh A.V., 1998. Tectonophysical Analysis of Fault-Block Divisibility of the Lithosphere in Southern Region of East Siberia. Thesis, PhD in Geology and Mineralogy. IEC SB RAS, Irkutsk, 206 p. (in Russian) [*Черемных А.В.* Тектонофизический анализ разломно-блоковой делимости литосферы юга Восточной Сибири: Дис. … канд. геол.-мин. наук. Иркутск: ИЗК СО РАН, 1998. 206 с.].

Clever R.M., Busse F.H., 1996. Hexagonal convection cells under conditions of vertical symmetry. *Physical Review E* 53 (3), R2037–R2040. http://dx.doi.org/10.1103/PhysRevE.53.R2037.

Dobretsov N.L., Kirdyashkin A.G., 1993. Experimental modeling of two-layer mantle convection. *Ofioliti* 18 (1), 61–81.

Dobretsov N.L., Kirdyashkin A.G., Kirdyashkin A.A., 2001. Deep Geodynamics. Second edition. GEO Branch, Publishing House of SB RAS, Novosibirsk, 409 p. (in Russian) [*Добрецов Н.Л., Кирдяшкин А.Г., Кирдяшкин А.А.* Глубинная геодинамика. 2-е дополн. изд. Новосибирск: Изд-во СО РАН, филиал «ГЕО», 2001. 409 с.].

Filippov A.F., 1962. On the scatter of particle sizes during fragmentation. In: The theory of probability and its application. Vol. VI, Iss. 3. Publishing House of the USSR Acad. Sci., Moscow, p. 14–19 (in Russian) [*Филиппов А.Ф.* О распределении размеров частиц при дроблении // Теория вероятностей и ее применения. М.: Изд-во АН СССР, 1962. Т. VI. Вып. 3. С. 14–19].

Getling A.V., 1998. Rayleigh–Bénard Convection: Structures and Dynamics. World Scientific, Singapore – New Jersey – Hong Kong, 245 p.

Hazen R.M., 2012. The Story of Earth: The First 4.5 Billion Years, from Stardust to Living Planet. Penguin Group, New York, 320 p.

Hofmann A.W., 1997. Mantle geochemistry: the message from oceanic volcanism. *Nature* 385 (6613), 219–229. http://dx.doi.org/10.1038/385219a0.

Honda S.A., 1995. Simple parameterized model of Earth's thermal history with the transition from layered to whole mantle convection. *Earth and Planetary Science Letters* 131 (3–4), 357–369. http://dx.doi.org/10.1016/0012-821X(95)00034-A.

Kirdyashkin A.G., Dobretsov N.L., 1991. Modeling of the double-layered mantle convection. *Doklady AN SSSR* 318 (4), 946–949 (in Russian) [*Кирдяшкин А.Г., Добрецов Н.Л.* Моделирование двухслойной мантийной конвекции // *Доклады АН СССР*. 1991. Т. 318. № 4. С. 946–949].

Kolmogorov A.N., 1941. On the log-normal law of distribution of particles during fragmentation. *Doklady AN SSSR* 31 (2), 99–101 (in Russian) [Колмогоров А.Н. О логарифмически-нормальном законе распределения частиц при дроблении // *Доклады АН СССР*. 1941. Т. 31. № 2. С. 99–101].

Kuz'min M.I., 2014. The Precambrian history of the origin and evolution of the Solar System and Earth. Part 1. *Geodynamics & Tectonophysics* 5 (3), 625–640 (in Russian) [*Кузьмин М.И.* Докембрийская история зарождения и эволюции Солнечной системы и Земли. Статья I // *Геодинамика и тектонофизика*. 2014. Т. 5. № 3. С. 625–640]. http://dx.doi.org/10.5800/GT-2014-5-3-0146.

Li Z.X., Bogdanova S.V., Collins A.S., Davidson A.B., Waele D., Ernst R.E., Fitzsimons I.C.W., Fuck R.A., Gladkochub D.P., Jacobs J., Karlstrom K.E., Lul S., Natapov L.M., Pease V., Pisarevsky S.A., Thrane K., Vernikovsky V., 2008. Assembly, configuration, and break-up history of Rodinia: A synthesis. *Precambrian Research* 160 (1–2), 179–210. http://dx.doi.org/10.1016/j.precamres.2007.04.021.

Lobkovsky L.I., 1988. Geodynamics of zones of spreading, subduction and double-layered plate tectonics. Nauka, Moscow, 252 p. (in Russian) [*Лобковский Л.И.* Геодинамика зон спрединга, субдукции и двухъярусная тектоника плит. М.: Наука, 1988. 252 с.].

Lobkovsky L.I., Kotelkin V.D., 2000. Double-layered thermo-chemical model of convection in the mantle and its geodynamic consequences. In: Problems of Global Geodynamics. GEOS, Moscow, p. 29–53 (in Russian) [*Лобковский Л.И., Котелкин В.Д.* Двухъярусная термохимическая модель конвекции в мантии и ее геодинамические следствия // Проблемы глобальной геодинамики. М.: ГЕОС, 2000. С. 29–53].

Lobkovsky L.I., Nikishin A.M., Khain V.E., 2004. Modern Problems of Geotectonics and Geodynamics. Nauchny Mir, Moscow, 610 p. (in Russian) [*Лобковский Л.И., Никишин А.М., Хаин В.Е.* Современные проблемы геотектоники и геодинамики. М.: Научный мир, 2004. 610 с.].

Lubnina N.V., 2011. Supercontinents in the Earth's history (in Russian) [*Лубнина Н.В.* Суперконтиненты в истории Земли. 2011]. Available from: http://www.ises.su/2011/pdf_lectures/lubnina-lecture.pdf (last accessed June 22, 2015).

Maruyama S., 1994. Plume tectonics. *The Journal of the Geological Society of Japan* 100 (1), 24–49.

Molnar P., Freedmann D., Shih J.S.F., 1979. Length of intermediate and deep seismic zones and temperature in down going slabs of lithosphere. *Geophysical Journal of the Royal Astronomical Society* 56 (1), 41–54. http://dx.doi.org/10.1111/j.1365-246X.1979.tb04766.x.

Nebel O., Campbell I.H., Sossi P.A., Van Kranendonk M.J., 2014. Hafnium and iron isotopes in early Archean komatiites record a plume-driven convection cycle in the Hadean Earth. *Earth and Planetary Science Letters* 397, 111–120. http://dx.doi.org/10.1016/j.epsl.2014.04.028.

Peive A.V., 1990. Selected Works. Deep Faults and Their Role in Construction and Development of the Earth's Crust. Nauka, Moscow, 352 p. (in Russian) [*Пейве А.В.* Избранные труды. Глубинные разломы и их роль в строении и развитии земной коры. М.: Наука, 1990. 352 с.].

Pekeris G.L., 1935. Thermal convection in the interior of the Earth. *Monthly Notices of the Royal Astronomical Society, Geophysical Supplements* 3 (suppl. 8), 343–367. http://dx.doi.org/10.1111/j.1365-246X.1935.tb01742.x.

Rykov V.V., Trubitsyn V.P., 1994a. Digital modeling of mantle convection and tectonics of continental plates. In: Geodynamics and earthquake prediction. Computational Seismology, vol. 26. Nauka, Moscow, p. 94–102 (in Russian) [*Рыков В.В., Трубицын В.П.* Численное моделирование мантийной конвекции и тектоники континентальных плит // Геодинамика и прогноз землетрясений. Вычислительная сейсмология. Вып. 26. М.: Наука, 1994. С. 94–102].

Rykov V.V., Trubitsyn V.P., 1994b. A three-dimensional model of mantle convection with mobile continents. In: Theoretical problems of geodynamics and seismicity. Computational Seismology, vol. 27. Nauka, Moscow, p. 21–41 (in Russian) [*Рыков В.В., Трубицын В.П.* Трехмерная модель мантийной конвекции с движущимися континентами // Теоретические проблемы геодинамики и сейсмологии. Вычислительная сейсмология. Вып. 27. М.: Наука, 1994. С. 21–41].

Sadovsky M.A., Bolkhovitinov L.G., Pisarenko V.F., 1987. Deformation of Geophysical Medium and Seismic Process. Nauka, Moscow, 100 p. (in Russian) [*Садовский М.А.*, *Болховитинов Л.Г., Писаренко В.Ф.* Деформирование геофизической среды и сейсмический процесс. М.: Наука, 1987. 100 с.].

Sadovsky M.A., Pisarenko V.F., 1991. Seismic process in the block environment. Nauka, Moscow, 96 p.

Schubert G., Turcotte D.L., Olson P., 2001. Mantle convection in the Earth and Planets. Cambridge University Press, Cambridge, 940 p.

Seminsky K.Zh., 2001. Tectonophysical regularities of destruction of the lithosphere as exemplified by the Himalayan compression zone. *Tikhookeanskaya geologiya* 20 (6), 17–30 (in Russian) [*Семинский К.Ж.* Тектонофизические закономерности деструкции литосферы на примере Гималайской зоны сжатия // *Тихоокеанская геология*. 2001. Т. 20. № 6. С. 17–30].

Seminsky K.Zh., 2003. The Internal Structure of Continental Fault Zones. Tectonophysical Aspect. GEO Branch, Publishing House of SB RAS, Novosibirsk, 244 p. (in Russian) [*Семинский К.Ж.* Внутренняя структура континентальных разломных зон. Тектонофизический аспект. Новосибирск: Изд-во СО РАН, филиал «ГЕО», 2003. 244 с.].

Sherman S.I., 1977. Physical Regularities of Faulting in the Earth's Crust. Nauka, Moscow, 102 c. (in Russian) [*Шерман С.И.* Физические закономерности развития разломов земной коры. Новосибирск: Наука, 1977. 102 с.].

Sherman S.I., 2002. Development of M.V. Gzovsky's concepts in recent tectonophysical studies of faulting and seismicity in the lithosphere. In: Tectonophysics today (to the Jubilee of M.V. Gzovsky). Institute of Physics of the Earth, Moscow, p. 49–59 (in Russian) [*Шерман С.И.* Развитие представлений М.В. Гзовского в современных тектонофизических исследованиях разломообразования и сейсмичности в литосфере // Тектонофизика сегодня (к юбилею М.В. Гзовского). М.: Институт физики Земли РАН, 2002. С. 49–59].

Sherman S.I., 2012. Destruction of the lithosphere: Fault-block divisibility and its tectonophysical regularities. *Geodynamics & Tectonophysics* 3 (4), 315–344 (in Russian) [*Шерман С.И.* Деструкция литосферы: разломно-блоковая делимость и ее тектонофизические закономерности // *Геодинамика и тектонофизика*. 2012. Т. 3. № 4. С. 315–344]. http://dx.doi.org/10.5800/GT-2012-3-4-0077.

Sherman S.I., 2014a. Seismic Process and the Forecast of Earthquakes: Tectonophysical Conception. Academic Publishing House “Geo”, Novosibirsk, 359 p. (in Russian) [*Шерман С.И.* Сейсмический процесс и прогноз землетрясений: тектонофизическая концепция. Новосибирск: Академическое издательство «Гео», 2014. 359 с.].

Sherman S.I., 2014b. Tectonophysical regularities of destruction of the continental lithosphere of the Earth. In: Geodynamic evolution of the lithosphere in the Central Asian mobile belt: from ocean to continent. Issue 12. Institute of the Earth’s crust SB RAS, Irkutsk, p. 333–336 (in Russian) [*Шерман С.И.* Тектонофизические закономерности деструкции континентальной литосферы Земли // Геодинамическая эволюция литосферы Центрально-Азиатского подвижного пояса: от океана к континенту. Вып. 12. Иркутск: ИЗК СО РАН, 2014. С. 333–336].

Sherman S.I., Lysak S.V., Dem’yanovich V.M., 2004. Active faults, seismicity and recent fracturing in the lithosphere of the Baikal rift system. *Tectonophysics* 380 (3–4), 261–272. http://dx.doi.org/10.1016/j.tecto.2003.09.023.

Sherman S.I., Seminsky K.Zh., Bornyakov S.A., Buddo V.Yu., Lobatskaya R.M., Adamovich A.N., Truskov V.A., Babichev A.A., 1991. Faulting in the Lithosphere. Shear Zones. Nauka, Siberian Branch, Novosibirsk, 261 p. (in Russian) [*Шерман С.И., Семинский К.Ж., Борняков С.А., Буддо В.Ю., Лобацкая Р.М., Адамович А.Н., Трусков В.А., Бабичев А.А.* Разломообразование в литосфере. Зоны сдвига. Новосибирск: Наука. Сибирское отделение, 1991. 261 с.].

Sherman S.I., Seminsky K.Zh., Bornyakov S.A., Buddo V.Yu., Lobatskaya R.M., Adamovich A.N., Truskov V.A., Babichev A.A., 1992. Faulting in the Lithosphere. Tensile Stress Zones. Nauka, Siberian Branch, Novosibirsk, 227 p. (in Russian) [*Шерман С.И., Семинский К.Ж., Борняков С.А., Буддо В.Ю., Лобацкая Р.М., Адамович А.Н., Трусков В.А., Бабичев А.А.* Разломообразование в литосфере. Зоны растяжения. Новосибирск: Наука. Сибирское отделение, 1992. 227 с.].

Sherman S.I., Seminsky K.Zh., Bornyakov S.A., Buddo V.Yu., Lobatskaya R.M., Adamovich A.N., Truskov V.A., Babichev A.A., 1994. Faulting in the Lithosphere. Compression Zones. Nauka, Siberian Branch, Novosibirsk, 262 p. (in Russian)

[*Шерман С.И., Семинский К.Ж., Борняков С.А., Буддо В.Ю., Лобацкая Р.М., Адамович А.Н., Трусков В.А., Бабичев А.А.* Разломообразование в литосфере. Зоны сжатия. Новосибирск: Наука. Сибирское отделение, 1994. 262 с.].

Sherman S.I., Seminsky K.Zh., Cheremnykh A.V., 2000. Destructive zones and fault-produced block structures of Central Asia. *Geology of Pacific Ocean* 16, 231–252.

Shumilov V., 2009. The origin of the basalt pillars (in Russian) [*Шумилов В.* Происхождение базальтовых столбов. 2009]. Available from: http://shumilov.kiev.ua/geofizika/proisxozhdenie-bazaltovyx-stolbov.html (last accessed June 22, 2015).

Trompert R., Hansen U., 1988. Mantle convection simulations with rheologies that generate platelike behaviour. *Nature* 395 (6703), 686–689. http://dx.doi.org/10.1038/27185.

Trubitsyn V.P., Rykov V.V., 2000. Mantle convection with mobile continents. In: Problems of global geodynamics. GEOS, Moscow, p. 7–28 (in Russian) [*Трубицын В.П., Рыков В.В.* Мантийная конвекция с плавающими континентами // Проблемы глобальной геодинамики. М.: ГЕОС, 2000. С. 7–28].

Trubitsyn V.P., Rykov V.V., 2002. Digital models of the evolution of mantle convection. In: N.L. Dobretsov (Ed.), Global changes of environment. V. 3, Ch. 2, p. 42–56 (in Russian) [*Трубицын В.П., Рыков В.В.* Численные модели эволюции мантийной конвекции // Глобальные изменения природной среды / Ред. Н.Л. Добрецов. Новосибирск: Наука, 2002. Т. 3, гл. 2. С. 42–56].

Trubitsyn V.P., Trubitsyn A.P., 2014. Numerical model for the generation of the ensemble of lithospheric plates and their penetration through the 660-km boundary. *Izvestiya, Physics of the Solid Earth* 50 (6), 853–864. http://dx.doi.org/10.1134/S106935131406010X.

Vrevsky A.B., Glebovitsky V.A., Goncharov A.G., Nikitina L.P., Pushkarev Yu.D., D., 2010. The continental lithospheric mantle beneath Early Precambrian and Late Proterozoic – Phanerozoic structures of the Earth crust: chemical composition, thermal state, evolution. *Vestnik ONZ RAN* 2, NZ6009, 65–75. (in Russian) [*Вревский А.Б., Глебовицкий В.А., Гончаров А.Г., Никитина Л.П., Пушкарев Ю.Д.* Континентальная литосферная мантия под разновозрастными структурами земной коры: химический состав, термальное состояние, эволюция // *Вестник ОНЗ РАН.* 2010. № 2. NZ6009. С. 65–75. http://dx.doi.org/10.2205/2010NZ000027.

Yarmolyuk V.V., Kuzmin M.I., 2012. Late Paleozoic and Early Mesozoic rare-metal magmatism of Central Asia: Stages, provinces, and formation settings. *Geology of Ore Deposits* 54 (5), 313–333. http://dx.doi.org/10.1134/S1075701512050054.

Zonenshain L.P., Kuz'min M.I., 1993. Deep geodynamics of the Earth. *Geologiya i Geofizika* (*Russian Geology and Geophysics*) 34 (4), 3–13 (in Russian) [*Зоненшайн Л.П., Кузьмин М.И.* Глубинная геодинамика Земли // *Геология и геофизика.* 1993. Т. 34. № 4. С. 3–13].

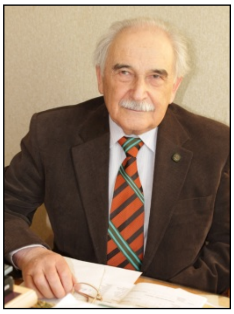

Sherman, Semen I., Academician of the Russian Academy of Natural Sciences,
Doctor of Geology and Mineralogy, Professor, Chief Researcher
Institute of the Earth's Crust, Siberian Branch of RAS
128 Lermontov street, Irkutsk 664033, Russia
Tel.: (3952)428261; ✉ e-mail: ssherman@crust.irk.ru

Шерман Семен Иойнович, академик Российской академии естественных наук,
докт. геол.-мин. наук, профессор, г.н.с.
Институт земной коры СО РАН
664033, Иркутск, ул. Лермонтова, 128, Россия
Тел.: (3952)428261; ✉ e-mail: ssherman@crust.irk.ru